AD-A107 964 AIR FORCE INST OF TECH WRIGHT-PATTERSON AFB OH F/G 9/2
AN INVESTIGATION OF THE INTERACTION, EVOLUTION AND MAINTENANCE --ETC(U)
MAR 79 J L HATCH
UNCLASSIFIED AFIT-CI-79-2930-S NL

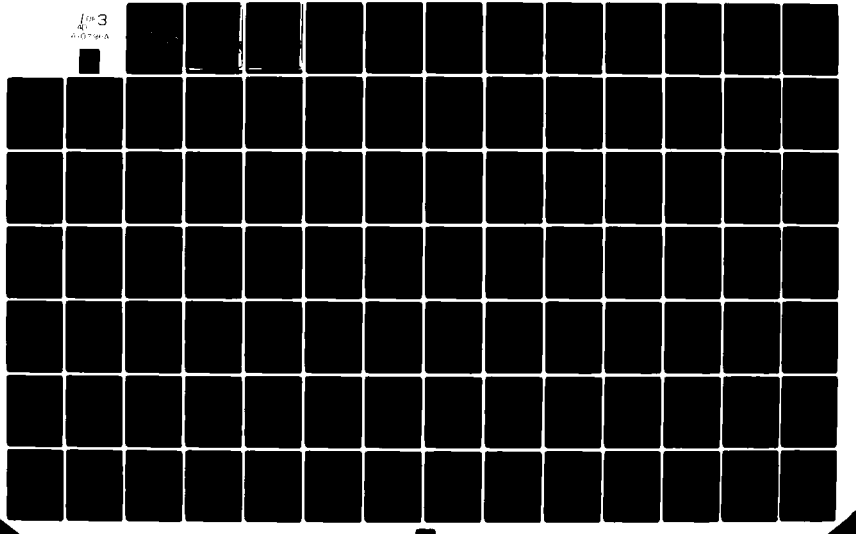

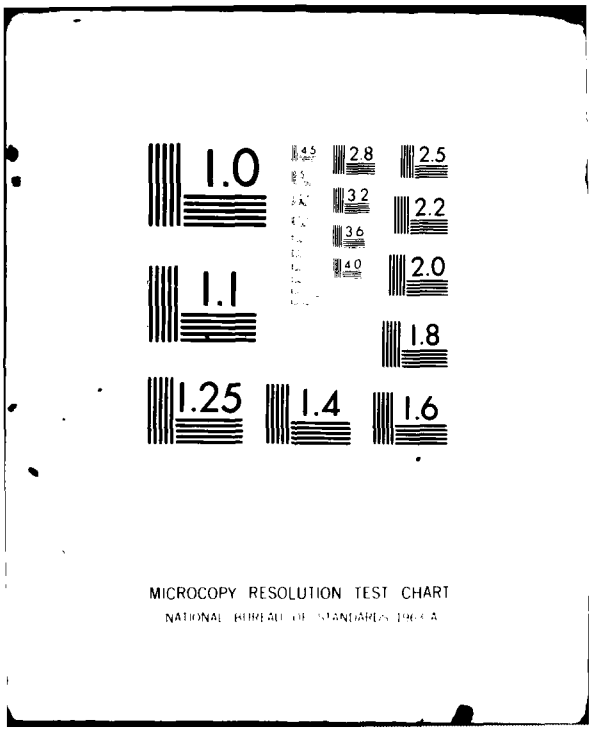
1.0
1.1
1.25
1.4
1.6
1.8
2.0
2.2
2.5
2.8
3.2
3.6
4.0
MICROCOPY RESOLUTION TEST CHART
NATIONAL BUREAU OF STANDARDS 1963-A

UNCLASS
SECURITY CLASSIFICATION OF THIS PAGE (When Data Entered)

## REPORT DOCUMENTATION PAGE

READ INSTRUCTIONS BEFORE COMPLETING FORM

1 REPORT NUMBER: 79-293D-S

2 GOVT ACCESSION NO: AD-A107 964

3 RECIPIENT'S CATALOG NUMBER:

4 TITLE (and Subtitle): An Investigation of the Interaction, Evolution and Maintenance of the Large-Scale Waves in the Stratosphere and Troposhere

5 TYPE OF REPORT & PERIOD COVERED: ~~THESIS~~/DISSERTATION

6 PERFORMING ORG. REPORT NUMBER:

7 AUTHOR(s): James Larrien Hatch

8 CONTRACT OR GRANT NUMBER(s):

9 PERFORMING ORGANIZATION NAME AND ADDRESS: AFIT STUDENT AT: Univ of Utah

10 PROGRAM ELEMENT, PROJECT, TASK AREA & WORK UNIT NUMBERS:

11 CONTROLLING OFFICE NAME AND ADDRESS: AFIT/NR, WPAFB OH 45433

12 REPORT DATE: Mar 1979

13 NUMBER OF PAGES: 215

14 MONITORING AGENCY NAME & ADDRESS (if different from Controlling Office):

15 SECURITY CLASS (of this report): UNCLASS

15a DECLASSIFICATION/DOWNGRADING SCHEDULE:

LEVEL II

16 DISTRIBUTION STATEMENT (of this Report)

APPROVED FOR PUBLIC RELEASE; DISTRIBUTION UNLIMITED

DTIC ELECTE DEC 1 1981 S D

17 DISTRIBUTION STATEMENT (of the abstract entered in Block 20, if different from Report)

DEC 1 1981

18 SUPPLEMENTARY NOTES

APPROVED FOR PUBLIC RELEASE: IAW AFR 190-17

Fredric C. Lynch

FREDRIC C. LYNCH, Major, USAF
Director of Public Affairs
Air Force Institute of Technology (ATC)
Wright-Patterson AFB, OH 45433

19 KEY WORDS (Continue on reverse side if necessary and identify by block number)

20 ABSTRACT (Continue on reverse side if necessary and identify by block number)

ATTACHED

DD FORM 1 JAN 73 1473 EDITION OF 1 NOV 65 IS OBSOLETE

UNCLASS

## ABSTRACT

Based on National Meteorological Center and Air Force gridded analysis data over the Northern Hemisphere and tropical regions, an analysis of the interaction, evolution, and maintenance of available potential and kinetic energy was carried out. This analysis indicated that the maintenance of the energetics in the winter, middle latitudes followed a definite cycle. Diabatic heating supplied energy to the mean stratospheric available potential energy, which then converted to mean stratospheric kinetic energy and was subsequently removed from the system by Reynolds and molecular stresses. Energy input to the mean tropospheric available potential energy by nonadiabatic process was seen to transfer to, in turn, tropospheric eddy available potential energy, tropospheric eddy kinetic energy, stratospheric eddy kinetic energy, stratospheric eddy available potential energy, and finally, was transferred out of the system by diabatic cooling and sub-scale interactions.

Analysis of energy transfer at boundaries indicated that boundary terms act principally to decrease centers of high kinetic and available potential energy or to increase energy in areas of relative minimum kinetic or available potential energy. Of all boundary terms, the vertical geopotential flux was seen as the most important, transferring energy upward over most of the Northern Hemisphere for all wave numbers and converging energy in

the region of the tropical tropopause for wave number 2. It suggests that stratospheric warmings may be an effect of energy transfer at boundaries.

An analysis of the mechanism for the evolution of the large scale atmospheric waves in the mid-latitudes, winter 1975-76, indicates that vertical convergence of geopotential flux provides a substantial mechanism for kinetic energy evolution in both the mid-latitude troposphere and stratosphere. While nonlinear interaction provides a more effective mechanism for wave evolution in the troposphere, the vertical convergence of geopotential flux is effective in affecting wave evolution in the stratosphere. The vertical convergence of geopotential flux, which is found generally in phase with the rate of change in kinetic energy, would enhance the wave growth; whereas the meridional convergence of geopotential flux, which is generally out of phase from the rate of kinetic energy change, would act as an energy sink. The evolution of kinetic energy is found generally to preceed that of available potential energy associated with the waves. Summer tropical wave evolution was found to be far more variable and less well defined than for the middle latitudes in winter.

# AN INVESTIGATION OF THE INTERACTION, EVOLUTION AND MAINTENANCE OF THE LARGE-SCALE WAVES IN THE STRATOSPHERE AND TROPOSPHERE

by

James Larrien Hatch

A dissertation submitted to the faculty of The University of Utah in partial fulfillment of the requirements for the degree of

Doctor of Philosophy

Department of Meteorology

University of Utah

March 1979

THE UNIVERSITY OF UTAH GRADUATE SCHOOL

# SUPERVISORY COMMITTEE APPROVAL

of a dissertation submitted by

JAMES LARRIEN HATCH

I have read this dissertation and have found it to be of satisfactory quality for a doctoral degree.

12/8/78
Date

S. K. Kao
Chairman, Supervisory Committee

I have read this dissertation and have found it to be of satisfactory quality for a doctoral degree.

12/8/78
Date

Kuo-Nan Liou
Member, Supervisory Committee

I have read this dissertation and have found it to be of satisfactory quality for a doctoral degree.

12/8/78
Date

Jan Paegle
Member, Supervisory Committee

I have read this dissertation and have found it to be of satisfactory quality for a doctoral degree.

8 Dec 1978
Date

Robert E. Stephenson
Member, Supervisory Committee

THE UNIVERSITY OF UTAH GRADUATE SCHOOL

# FINAL READING APPROVAL

To the Graduate Council of The University of Utah:

I have read the dissertation of James Larrien Hatch in its final form and have found that (1) its format, citations, and bibliographic style are consistent and acceptable; (2) its illustrative materials including figures, tables, and charts are in place; and (3) the final manuscript is satisfactory to the Supervisory Committee and is ready for submission to the Graduate School.

January 24, 1979
Date

S. K. Kao
Member, Supervisory Committee

Approved for the Major Department

S. K. Kao
Chairman Dean

Approved for the Graduate Council

James L. Clayton
Dean of The Graduate School

ABSTRACT

Based on National Meteorological Center and Air Force gridded analysis data over the Northern Hemisphere and tropical regions, an analysis of the interaction, evolution, and maintenance of available potential and kinetic energy was carried out. This analysis indicated that the maintenance of the energetics in the winter, middle latitudes followed a definite cycle. Diabatic heating supplied energy to the mean stratospheric available potential energy, which then converted to mean stratospheric kinetic energy and was subsequently removed from the system by Reynolds and molecular stresses. Energy input to the mean tropospheric available potential energy by nonadiabatic process was seen to transfer to, in turn, tropospheric eddy available potential energy, tropospheric eddy kinetic energy, stratospheric eddy kinetic energy, stratospheric eddy available potential energy, and finally, was transferred out of the system by diabatic cooling and sub-scale interactions.

Analysis of energy transfer at boundaries indicated that boundary terms act principally to decrease centers of high kinetic and available potential energy or to increase energy in areas of relative minimum kinetic or available potential energy. Of all boundary terms, the vertical geopotential flux was seen as the most important, transferring energy upward over most of the Northern Hemisphere for all wave numbers and converging energy in

the region of the tropical tropopause for wave number 2. It suggests that stratospheric warmings may be an effect of energy transfer at boundaries.

An analysis of the mechanism for the evolution of the large scale atmospheric waves in the mid-latitudes, winter 1975-76, indicates that vertical convergence of geopotential flux provides a substantial mechanism for kinetic energy evolution in both the mid-latitude troposphere and stratosphere. While nonlinear interaction provides a more effective mechanism for wave evolution in the troposphere, the vertical convergence of geopotential flux is effective in affecting wave evolution in the stratosphere. The vertical convergence of geopotential flux, which is found generally in phase with the rate of change in kinetic energy, would enhance the wave growth; whereas the meridional convergence of geopotential flux, which is generally out of phase from the rate of kinetic energy change, would act as an energy sink. The evolution of kinetic energy is found generally to preceed that of available potential energy associated with the waves. Summer tropical wave evolution was found to be far more variable and less well defined than for the middle latitudes in winter.

ACKNOWLEDGMENTS

To Dr. Shih-Kung Kao, my committee chairman, I extend my deepest respect and most sincere appreciation. Without his forceful guidance, patience, and encouragement, this research would have been impossible. I also wish to thank Dr. Jan Paegle for his interest and extremely valuable advice regarding the tropical data analysis used in this study. It has been a rare privilege and a great honor to have worked with these men.

Great amounts of computer time and considerable moral support was extended to this project by the Ogden ALC, Data Automation Branch, Comptroller, Hill AFB, Utah. I would particularly like to thank Mr. Max Peterson, Mr. Earl Rose, Mr. Parley Jeffs, and the many computer operators for their assistance in providing the highest quality computer support possible.

I would like to acknowledge the Air Force Global Weather Center, and especially Captain Gregory Logan, for computer support during the early stages of this research. I am additionally indebted to the people at USAF/ETAC, Scott AFB, Illinois and OL-A, Asheville, North Carolina, for their prompt action in supplying the tropical data used in this study.

I also want to express my gratitude to the National Center for Atmospheric Research for supplying the fast Fourier transform package and the Northern Hemisphere gridded National Meteorological

Center analysis used in this research.

My salary and tuition during the course of this work was supplied by the United States Air Force through the Air Force Institute of Technology, Wright-Patterson AFB, Ohio.

Printing expenses for this paper were paid by the Air Force Office of Scientific Research under grant AFOSR 78-3576. Computer supplies were purchased by NASA contract NAS 5-25373.

TABLE OF CONTENTS

TABLE OF CONTENTS (continued)

LIST OF ILLUSTRATIONS

Tables



Figures

LIST OF ILLUSTRATIONS (continued)

LIST OF ILLUSTRATIONS (continued)

LIST OF ILLUSTRATIONS (continued)

LIST OF ILLUSTRATIONS (continued)

LIST OF ILLUSTRATIONS (continued)

LIST OF ILLUSTRATIONS (continued)

LIST OF ILLUSTRATIONS (continued)

LIST OF ILLUSTRATIONS (continued)

LIST OF ILLUSTRATIONS (continued)

LIST OF ILLUSTRATIONS (continued)

# CHAPTER 1

## INTRODUCTION

One of the effective ways of studying atmospheric dynamics is to analyze the generation, transfer, conversion and dissipation of available potential and kinetic energy in the atmosphere. It is known that in a barotropic fluid unstable waves of small amplitude would amplify by drawing kinetic energy from the mean flow, whereas in a baroclinic atmosphere an amplifying wave would receive kinetic energy through the conversion of available potential energy of the mean flow.

For waves of finite amplitude, however, interactions of two-dimensional waves would transfer a large portion of the kinetic energy to waves of larger scale and a small fraction of the energy to waves of smaller scale (Fjørtoft, 1953); and the exchanges of kinetic energy between a zonal flow and two waves lead to a porcess similar to the index cycle in the atmosphere (Lorenz, 1960). Recent studies of the energetics in the mid-latitude troposphere indicate that the nonlinear interactions of waves provide a major mechanism for the evolution of the available potential and kinetic energy (Kao, 1977; Kao and Chi, 1978; Tsay, and Kao, 1978) and therefore for the development of weather.

In regard to the energetics in the atmosphere, studies of its maintenance have been made and valuable results have been obtained

by many researchers. In wavenumber domain investigations have been made by Saltzman (1957, 1970), Van Mieghen (1961), Wiin-Nielsen (1959, 1968), Saltzman and Fleisher (1960, 1961, 1962), Reed et al. (1963), Teweles (1963), Oort (1964), Dutton and Johnson (1967), Kung (1967), Lorenz (1967), Yang (1967), Steinberg et al. (1971). In the wavenumber frequency space, research has been done by Kao (1968, 1970), Wendell (1969), Kao and Wendell (1970), Kao et al. (1970), Gruber (1975), Pratt (1976), Tenenbaum (1976), Burrows (1976) and Kao and Lee (1977). However, these studies have been confined mostly to the maintenance of the seasonal or yearly mean state of the waves at particular pressure levels or in the whole Northern Hemisphere. In so doing, little insight can be gained regarding the interactions between the troposphere and the stratosphere, tropics and mid-latitudes, and between hemispheres; and these interactions provide an important mechanism for the transfer and conversion of available potential and kinetic energy. To investigate these interactions and the maintenance and evolution of the available potential and kinetic energy in the troposphere and stratosphere is the purpose of this study.

# CHAPTER 2

# THEORETICAL CONSIDERATIONS

## 2.1 Introduction

To analyze the maintenance and evolution of the kinetic and available potential energy associated with atmospheric waves of various wavelengths, we first transformed the governing equations from physical space to the wave number domain, then to wave number frequency space.

## 2.2 Equations from the Large-Scale Atmospheric Motion and Transports in the Physical Space

In the longitude ($\lambda$), latitude ($\phi$), pressure (p) coordinate system, the equations of motion, the hydrostatic equation, the continuity equation, and the thermodynamic energy equation may be written as

$$\left( \frac{\partial}{\partial t} + \frac{u}{a \cos \phi} \frac{\partial}{\partial \lambda} + \frac{v}{a} \frac{\partial}{\partial \phi} + \omega \frac{\partial}{\partial p} \right) u - \left( f + u \frac{\tan \phi}{a} \right) v = - \frac{g}{a \cos \phi} \frac{\partial z}{\partial \lambda} + F_1 \quad , \tag{2.1}$$

$$\left( \frac{\partial}{\partial t} + \frac{u}{a \cos \phi} \frac{\partial}{\partial \lambda} + \frac{v}{a} \frac{\partial}{\partial \phi} + \omega \frac{\partial}{\partial p} \right) v + \left( f + u \frac{\tan \phi}{a} \right) u = - \frac{g}{a} \frac{\partial z}{\partial \phi} + F_2 \quad , \tag{2.2}$$

$$\frac{\partial z}{\partial p} + \frac{R}{g}\frac{T}{p} = 0 \quad , \tag{2.3}$$

$$\frac{\partial \omega}{\partial p} + \frac{1}{a \cos \phi}\left\{\frac{\partial u}{\partial \lambda} + \frac{\partial v \cos \phi}{\partial \phi}\right\} = 0 \quad , \tag{2.4}$$

$$c_p\left\{\frac{\partial}{\partial t} + \frac{u}{a \cos \phi}\frac{\partial}{\partial \lambda} + \frac{v}{a}\frac{\partial}{\partial \phi} + \omega\frac{\partial}{\partial p}\right\}T = R\frac{\omega T}{p} + h \quad . \tag{2.5}$$

In (2.1) through (2.5), a is the radial distance from the center of the earth, f is the Coriolis parameter, g is the gravity acceleration, z is the height of isobaric surfaces, $\omega$ is the individual rate of change of pressure (dp/dt), T is the temperature, R is the gas constant, h is the rate of heat addition per unit mass, u and v are respectively the longitudinal and meridional component of the velocity, and $F_1$ and $F_2$ are respectively the longitudinal and meridional component of the Reynolds and molecular stresses. For large-scale atmospheric motion, $F_1$ and $F_2$ represent the sum of molecular frictional force and the Reynolds stress force due to eddies of high frequencies.

## 2.3 Power and Cross Spectra in Wave Number Frequency Space

Let $q(\lambda,t)$ be a real, single-valued function, which is piecewise differentiable in a normalized domain, $0 \leq \lambda$, $t \leq 2\pi$, where $\lambda$ and t stand, respectively, for the longitude and time. The Fourier transform of $q(\lambda,t)$ may be written as

$$Q(k,t) = \frac{1}{2\pi}\int_0^{2\pi} q(\lambda,t)e^{-ik\lambda}d\lambda \quad , \tag{2.6}$$

where Q is the Fourier coefficient and k is the wave number. The inverse transform of (2.6) gives $q(\lambda,t)$ expressed in terms of its Fourier coefficient as

$$q(\lambda,t) = \sum_{k=-\infty}^{\infty} Q(k,t)e^{ik\lambda} \quad . \tag{2.7}$$

Here the summation of the Fourier coefficient Q with respect to the integer wave numbers is the consequence of the cyclic distribution of $q(\lambda,t)$ along latitude circles.

Consider the same conditions for another scaler function $m(\lambda,t)$ with a Fourier transform $M(k,t)$. It can be shown that for functions $m(\lambda,t)$ and $q(\lambda,t)$ we have

$$\frac{1}{2\pi}\int_0^{2\pi} m(\lambda,t)\ q(\lambda,t)\ e^{-ik\lambda}d\lambda = \sum_{j=-\infty}^{\infty} M(j,t)\ Q(k-j,t) \quad . \tag{2.8}$$

Letting $k \to 0$, then $j = k$, we obtain

$$\frac{1}{2\pi}\int_0^{2\pi} m(\lambda,t)\ q(\lambda,t)\ d\lambda = \sum_{k=-\infty}^{\infty} M(k,t)\ Q^*(k,t)$$

$$= \frac{1}{2}\sum_{k=-\infty}^{\infty} [M(k,t)\ Q^*(k,t) + M^*(k,t)\ Q(k,t)] \quad ,$$

where $Q^*(k,t)$ is the conjugate of $Q(k,t)$.

## 2.4 Energy and Transport Equations in the Wave Number Frequency Space

To analyze the evolution of the kinetic and available

potential energy associated with waves of various wavelengths, we shall express the kinetic and available potential energy equations in the wave number frequency space. To do so, we shall first express the governing equations (2.1) to (2.5) in the wave number domain. This can be accomplished by applying (2.6) and (2.8) to (2.1) thru (2.5). The governing equations in the wave number domain become

$$\frac{\partial}{\partial t} U(k,t) = - \sum_{j=-\infty}^{\infty} \{ \frac{ik}{a \cos} [U(j,t)U(k-j,t)] + \frac{1}{a \cos\phi} [U(j,t)V(k-j,t)\cos\phi]_\phi + [U(j,t)W(k-j,t)]_p - \frac{1}{a} \tan\phi V(j,t)U(k-j,t) \} + fV(k,t) - \frac{ik}{a \cos\phi} gZ(k,t) + G_1(k,t) , \quad (2.9)$$

$$\frac{\partial}{\partial t} V(k,t) = - \sum_{j=-\infty}^{\infty} \{ \frac{ik}{a \cos\phi} V(j,t)U(k-j,t) + \frac{1}{a \cos\phi} [V(j,t)V(k-j,t)\cos\phi]_\phi + [V(j,t)W(k-j,t)]_p + \frac{1}{a} \tan\phi U(j,t)U(k-j,t) \} - fU(k,t) - \frac{g}{a} Z_\phi(k,t) + G_2(k,t) , \quad (2.10)$$

$$Z_p(k,t) = - \frac{R}{gp} \theta(k,t) , \quad (2.11)$$

$$W_p(k,t) = - \frac{1}{a \cos\phi} \{ ik\, U(k,t) + [V(k,t)\cos\phi]_\phi \} , \quad (2.12)$$

$$\frac{\partial}{\partial t}\theta(k,t) = -\sum_{j=-\infty}^{\infty}\left\{\frac{ik}{a\cos\phi}\left[\theta(j,t)U(k-j,t)\right]\right.$$

$$+\frac{1}{a\cos\phi}\left[\theta(j,t)V(k-j,t)\cos\phi\right]_{\phi}+\left[\theta(j,t)W(k-j,t)\right]_{p}$$

$$\left.-\frac{R}{c_p p}\theta(j,t)W(k-j,t)\right\}+\frac{1}{c_p}H(k,t) \quad . \qquad (2.13)$$

Subscripts $\phi$ and p denote partial differentiation with respect to $\phi$ and p respectively, and the Fourier coefficients of physical variables are listed as follows:

| q | u | v | ω | z | T | h | $F_1$ | $F_2$ |
|---|---|---|---|---|---|---|---|---|
| Q | U | V | W | Z | θ | H | $G_1$ | $G_2$ |

Let the kinetic and available potential energy per unit mass of waves in the wave number domain be respectively denoted by

$$EK(k,t) = \left\{|U(k,t)|^2 + |V(k,t)|^2\right\} , \qquad (2.14)$$

$$EA(k,t) = c_p\gamma|\theta(k,t)|^2 , \qquad (2.15)$$

where $\gamma = (\overline{T} - c_p R^{-1} p\ \partial\overline{T}/\partial p)^{-1}$ and $\overline{T}$ is the mean zonal temperature.

The kinetic and available potential energy equations in the wave number domain can be shown to take the form

$$\frac{\partial EK(k,t)}{\partial t} = NK(k,t) + MK(k,t) + AK(k,t) + NKB(k,t)$$

$$+ AKB(k,t) + GK(k,t) , \qquad (2.16)$$

$$\frac{\partial EA(k,t)}{\partial t} = NA(k,t) + MA(k,t) + KA(k,t) + NAB(k,t) + HA(k,t) \quad , \tag{2.17}$$

where

$$NK(k,t) = NK1(k,t) + NK2(k,t) + NK3(k,t)$$

$$= -\sum_{\substack{j=-\infty \\ \neq 0}}^{\infty} \left\{ \frac{ik}{a\cos\phi} \{U(j,t)[U(-k,t)U(k-j,t) - U(k,t)U(-k-j,t)] + V(j,t)[V(-k,t)U(k-j,t) - V(k,t)U(-k-j,t)]\} \right.$$

$$+ \sum_{\substack{j=-\infty \\ \neq 0}}^{\infty} \left( \frac{1}{a} \{U(j,t)[U_\phi(-k,t)V(k-j,t) + U_\phi(k,t)V(-k-j,t)] + V(j,t)[V_\phi(-k,t)V(k-j,t) + V_\phi(k,t)V(-k-j,t)]\} \right.$$

$$\left. + \frac{\tan\phi}{a} \{V(j,t)[U(-k,t)U(k-j,t) + U(k,t)U(-k-j,t)] - U(j,t)[V(-k,t)U(k-j,t) + V(k,t)U(-k-j,t)]\} \right)$$

$$+ \sum_{\substack{j=-\infty \\ \neq 0}}^{\infty} \left( U(j,t)[U_p(-k,t)W(k-j,t) + U_p(k,t)W(-k-j,t)] + V(j,t)[V_p(-k,t)W(k-j,t) + V_p(k,t)W(-k-j,t)] \right) \quad , \tag{2.18}$$

is the contribution of the nonlinear wave interaction to the rate of change in the kinetic energy of waves of wave number k; NK1, NK2, and NK3 are respectively the nonlinear interaction associated with the longitudinal, meridional, and vertical gradients of the velocity;

$$MK(k,t) = MK1(k,t) + MK2(k,t)$$

$$= \{-[U(k,t)V(-k,t) + U(-k,t)V(k,t)]\frac{\cos\phi}{a}\left(\frac{\bar{u}}{\cos\phi}\right)_\phi$$

$$+ 2|U(k,t)|^2\bar{v}\frac{\tan\phi}{a} - \frac{2}{a}|V(k,t)|^2\bar{v}_\phi\}$$

$$- \{[U(k,t)W(-k,t) + U(-k,t)W(k,t)]\bar{u}_p$$

$$+ [V(k,t)W(-k,t) + V(-k,t)W(k,t)]\bar{v}_p\} \qquad (2.19)$$

is the contribution of the interactions involving waves and the zonal mean flow; MK1 and MK2 are respectively the interactions associated with the meridional and vertical gradients of the zonal mean velocities;

$$AK(k,t) = -\frac{R}{p}[W(k,t)\theta(-k,t) + W(-k,t)\theta(k,t)] \qquad (2.20)$$

is the contribution through the conversion of available potential energy to the kinetic energy;

$$NKB(k,t) = NKB1(k,t) + NKB2(k,t)$$

$$= -\sum_{\substack{j=-\infty \\ \neq 0}}^{\infty}\frac{1}{a\cos\phi}\{U(j,t)[U(-k,t)V(k-j,t)+U(k,t)V(-k-j,t)]\cos$$

$$+ V(j,t)[V(-k,t)V(k-j,t) + V(k,t)V(-k-j,t)]\cos\phi\}_\phi$$

$$-\sum_{\substack{j=-\infty \\ \neq 0}}^{\infty}\{U(j,t)[U(-k,t)W(k-j,t) + U(k,t)W(-k-j,t)]$$

$$+ V(j,t)[V(-k,t)W(k-j,t) + V(k,t)W(-k-j,t)]\}_p \qquad (2.21)$$

is the contribution of the meridional and vertical convergence of the nonlinear wave interactions;

$$AKB(k,t) = AKB1(k,t) + AKB2(k,t)$$

$$= -\frac{g}{a\cos\phi}\left\{[V(k,t)Z(-k,t) + V(-k,t)Z(k,t)]\cos\phi\right\}_\Phi$$

$$- g\left\{W(k,t)Z(-k,t) + W(-k,t)Z(k,t)\right\}_p \qquad (2.22)$$

is the contribution of the meridional and vertical convergence of geopotential flux;

$$GK(k,t) = U(k,t)G_1(-k,t) + U(-k,t)G_1(k,t)$$

$$+ V(k,t)\,G_2(-k,t) + V(-k,t)G_2(k,t) \qquad (2.23)$$

is the contribution of the Reynolds and molecular stresses.

$$NA(k,t) = NA1(k,t) + NA2(k,t) + NA3(k,t)$$

$$= \sum_{\substack{j=-\infty \\ \neq 0}}^{\infty}\left\{-\frac{ikc_p\gamma}{a\cos\Phi}\,\theta(j,t)[\theta(-k,t)U(k-j,t) - \theta(k,t)V(-k-j,t)]\right.$$

$$+ \frac{c_p\gamma}{a}\,\theta(j,t)[V(k-j,t)\theta_\phi(-k,t) + V(-k-j,t)\theta_\phi(k,t)]$$

$$+ c_p\gamma\,\theta(j,t)\left\{W(k-j,t)\left[\frac{R}{c_p p}\,\theta(-k,t) + \theta_p(-k,t)\right]\right.$$

$$\left.\left. + W(-k-j,t)\left[\frac{R}{c_p p}\,\theta(k,t) + \theta_p(k,t)\right]\right\}\right\} \qquad (2.24)$$

is the contribution of the interactions of temperature and velocity waves to rate of change of the available potential energy associated with waves of wave number k; NA1, NA2, and NA3 are respectively associated with the longitudinal, meridional, and vertical gradients of temperature;

$$MA(k,t) = -\frac{c_p\gamma}{a}\,[V(k,t)\theta(-k,t) + V(-k,t)\theta(k,t)]\,\bar{T}_\phi \qquad (2.25)$$

is the contribution assocaited with the meridional gradient of the zonal mean temperature;

$$NAB(k,t) = NAB1(k,t) + NAB2(k,t)$$

$$= \sum_{\substack{j=-\infty \\ \neq 0}}^{\infty} \left\{ \frac{c_p\gamma}{a\cos\phi} \left\{ [\theta(-k,t)V(k-j,t) + \theta(k,t)V(-k-j,t)]\theta(j,t)\cos\phi \right\}_\phi \right.$$

$$\left. + c_p\gamma\left\{\theta(j,t)[\theta(-k,t)W(k-j,t) + \theta(k,t)W(-k-j,t)]\right\}_p \right\} \qquad (2.26)$$

is the contribution of the meridional and vertical convergence of flux of available potential energy;

$$HA(k,t) = \gamma\{\theta(-k,t)H(k,t) + \theta(k,t)H(-k,t)\} \qquad (2.27)$$

is the contribution of the diabatic heating or cooling and eddy flux of available potential energy in the atmosphere; and

$$KA(k,t) = -AK(k,t) \quad . \qquad (2.28)$$

Since we are interested in the evolution of kinetic and available potential energy, let us apply the Fourier time transform to energy spectrum EQ(k,t) and obtain EQ(k,n). The inverse transform of EQ(k,n) may be written as

$$EQ(k,t) = \int_{-\infty}^{\infty} |EQ(k,n)|\, e^{i[nt + \alpha_{EQ}(k,n)]}\, dn \qquad (2.29)$$

where n is frequency.

It can be shown, by expressing each term in (2.16) in the

form of (2.29), that (Kao, 1977)

$$\frac{\partial}{\partial t}\left[|EK(k,n)|\sin(nt-\pi/2)\right] = n|EK(k,n)|\sin nt$$

$$= |NK(k,n)|\sin[nt+\alpha_{NK}(k,n)-\alpha_{EK}(k,n)-\pi/2]$$

$$+ |MK(k,n)|\sin[nt+\alpha_{MK}(k,n)-\alpha_{EK}(k,n)-\pi/2]$$

$$+ |AK(k,n)|\sin[nt+\alpha_{AK}(k,n)-\alpha_{EK}(k,n)-\pi/2]$$

$$+ |NKB(k,n)|\sin[nt+\alpha_{NKB}(k,n)-\alpha_{EK}(k,n)-\pi/2]$$

$$+ |AKB(k,n)|\sin[nt+\alpha_{AKB}(k,n)-\alpha_{EK}(k,n)-\pi/2]$$

$$+ |GK(k,n)|\sin[nt+\alpha_{GK}(k,n)-\alpha_{EK}(k,n)-\pi/2], k,n\neq 0. \quad (2.30)$$

Equation (2.30), which shows the phase shift between the rate of change of kinetic energy of wave number k, frequency n, and NK(k,n), MK(k,n), AK(k,n), etc., provides valuable information regarding the contributions of various mechanisms to the rate of change of waves with amplitude $|EK(k,n)|$.

Similarly, it can be shown by expressing each term in (2.17) in the form of (2.29) that

$$\frac{\partial}{\partial t}\left[|EA(k,n)|\sin(nt-\pi/2)\right] = n|EA(k,n)|\sin nt$$

$$= |NA(k,n)|\sin[nt+\alpha_{NA}(k,n)-\alpha_{EA}(k,n)-\pi/2]$$

$$+ |MA(k,n)|\sin[nt+\alpha_{MA}(k,n)-\alpha_{EA}(k,n)-\pi/2]$$

$$+ |KA(k,n)|\sin[nt+\alpha_{KA}(k,n)-\alpha_{EA}(k,n)-\pi/2]$$

$$+ |NAB(k,n)|\sin[nt+\alpha_{NAB}(k,n)-\alpha_{EA}(k,n)-\pi/2]$$

$$+ |HA(k,n)|\sin[nt+\alpha_{HA}(k,n)-\alpha_{EA}(k,n)-\pi/2], k,n\neq 0. \quad (2.31)$$

It can be shown by eliminating KA and AK from (2.30) and (2.31) that there is a phase shift of $(\alpha_{EA} - \alpha_{EK})$ between the evolution of the kinetic and available potential energy of the transient waves.

For the zonal mean flow, we have the following equations for kinetic and available potential energy

$$\frac{\partial EK(0,t)}{\partial t} = MK(0,t) + AK(0,t) + AKB(0,t) + GK(0,t) \quad , \quad (2.32)$$

$$\frac{\partial EA(0,t)}{\partial t} = MA(0,t) + KA(0,t) + HA(0,t) \quad , \quad (2.33)$$

where

$$MK(0,t) = - \sum_{k=1}^{\infty} MK(k,t) \quad , \quad (2.34)$$

$$MA(0,t) = - \sum_{k=1}^{\infty} MK(k,t) \quad . \quad (2.35)$$

It can be shown by expressing each term in (2.32) and (2.33) in the form of (2.29) that

$$\begin{aligned} \frac{\partial}{\partial t} |EK(0,n)| \sin(nt - \pi/2) &= n|EK(0,n)| \sin nt \\ &= |MK(0,n)| \sin[nt + \alpha_{MK}(0,n) - \alpha_{EK}(0,n) - \pi/2] \\ &+ |AK(0,n)| \sin[nt + \alpha_{AK}(0,n) - \alpha_{EK}(0,n) - \pi/2] \\ &+ |AKB(0,n)| \sin[nt + \alpha_{AKB}(0,n) - \alpha_{EK}(0,n) - \pi/2] \\ &+ |GK(0,n)| \sin[nt + \alpha_{GK}(0,n) - \alpha_{EK}(0,n) - \pi/2], \; n \neq 0 \quad , \quad (2.36) \end{aligned}$$

$$\frac{\partial}{\partial t}\left[|EA(0,n)|\sin(nt-\pi/2)\right] = n|EA(0,n)|\sin nt$$

$$= |MA(0,n)|\sin[nt+\alpha_{MA}(0,n)-\alpha_{EA}(0,n)-\pi/2]$$

$$+ |KA(0,n)|\sin[nt+\alpha_{KA}(0,n)-\alpha_{EA}(0,n)-\pi/2]$$

$$+ |HA(0,n)|\sin[nt+\alpha_{HA}(0,n)-\alpha_{EA}(0,n)-\pi/2], \quad n\neq 0. \tag{2.37}$$

For $k \neq 0$, $n = 0$, i.e., for stationary amplitude waves, (2.30) and (2.31) reduce to

$$NK(k,0) + MK(k,0) + AK(k,0) + NKB(k,0) + AKB(k,0) + GK(k,0) = 0, \quad k \neq 0, \tag{2.38}$$

$$NA(k,0) + MA(k,0) + KA(k,0) + NAB(k,0) + HA(k,0) = 0, \quad k \neq 0 . \tag{2.39}$$

For $k = n = 0$, i.e., for stationary mean flow, (2.32) and (2.33) reduce to

$$MK(0,0) + AK(0,0) + AKB(0,0) + GK(0,0) = 0 , \tag{2.40}$$

$$MA(0,0) + KA(0,0) + HA(0,0) = 0 . \tag{2.41}$$

The above four equations show that the mechanism for the maintenance of kinetic and available potential energy of stationary amplitude waves and stationary mean zonal flow depends on the balance of wave interactions (NK, NA), interactions between waves and mean velocity and temperature fields (MK, MA), conversion of energy (AK, KA), effects of eddy and molecular stresses (GK), diabatic heating (HA), and fluxes of kinetic and available

potential energy at boundaries (AKB, NKB).

It may be pointed out that, when GK and HA are determined as the residue of (2.16) and (2.17), these terms also contain the sub-scale wave interactions, and therefore can act either as energy sources or energy sinks.

# CHAPTER 3

# DATA AND COMPUTATIONAL METHODS

## 3.1 Data Sources

Twelve hourly National Meteorological Center (NMC) and Air Force (AF) gridded anlayses of meteorological data were used in this study. The single data source for all computations carried out between 20°N and 85°N was the NMC analysis, while all computations done between 35°S and 15°N relied completely on AF data. Since the NMC data were gridded on a polar stereographic projection and the AF data were gridded on a Mercator projection, a Bessel interpolation scheme was applied to both to arrive at a common spherical grid with data existing at each 5° latitude and longitude intersection. The U-component and V-component of the wind derived from NMC data were then rotated so that the U-component was positive to the east and the V-component was positive to the north. The AF winds were also rotated in this sense.

Before beginning actual computations, our first objective was to secure a complete data base, free of all missing data, for each 0Z and 12Z data period. Isolated missing fields of height and temperature were constructed by linear interpolation in time. Missing wind fields in NMC data were either constructed geostrophically from observed height data, or were linearly interpolated in

time if the height field was also linearly interpolated in time. Since NMC wind fields were not available on the 12Z cycle at 50 mb and 10 mb, these winds were always obtained geostrophically. For the Air Force tropical grid, winds were not available at 1000 mb or at 10 mb. In these cases, the 850 mb and 20 mb wind was used, respectively. Height fields were also not available at 1000 mb in the Air Force data. These fields were constructed hydrostatically from the 1000 mb temperature and the 850 mb height and temperature fields. All other missing Air Force data was obtained using linear interpolation in time.

Applying the above operations produced a complete data base of temperature, U-component of the wind, V-component of the wind, and height for each 0Z and 12Z period at 1000 mb, 850 mb, 700 mb, 500 mb, 300 mb, 200 mb, 100 mb, 50 mb, and 10 mb levels. Data coverage in time included 1 DEC 1973 through 28 FEB 1974 and 1 DEC 1975 through 28 FEB 1977 for NMC data and 1 DEC 1975 through 29 FEB 1976 and 1 JUN 1976 through 31 AUG 1976 for Air Force data.

## 3.2 Omega Computation

In order to proceed with the computation of the individual terms of (2.16) and (2.17), omega fields for all data periods and levels were required. Our first attempt involved the computation of "adiabatic" omegas as done by Reed et al. (1963) and Muench (1965), among others. Neglecting heat sources in (2.5) and solving for $\omega$ gives

$$\omega = \frac{\left(\frac{\partial}{\partial t} + \frac{u}{a\cos\phi}\frac{\partial}{\partial\lambda} + \frac{v}{a}\frac{\partial}{\partial\phi}\right)T}{\left(\frac{R}{c_p}\frac{T}{P} - \frac{\partial T}{\partial P}\right)} \quad . \tag{3.1}$$

As pointed out by Miyakoda (1963), the results generated by this equation are unreliable, due to the adiabatic assumption. Under some conditions, it is possible to generate $\omega$ values of order $10^3$ mb/day using (3.1). In addition to these extreme values, large average values also result.

An alternate method of computing omega values from the divergence of the wind field using (2.4) was suggested by O'Brien (1970). However, it must be pointed out that most wind fields used in this study were produced by Flattery's Method (1967). These wind fields are essentially horizontally non-divergent, and are not suitable for computations based on divergence. Instead, a method similar to that recommended by Perry (1967) was used.

Following Perry, the quasi-geostrophic vorticity equation,

$$\frac{\partial\omega}{\partial P} = \frac{1}{f}\left\{\frac{\partial\eta}{\partial t} + \frac{u}{a\cos\phi}\frac{\partial\eta}{\partial\lambda} + \frac{v}{a}\frac{\partial\eta}{\partial\phi}\right\} \quad , \tag{3.2}$$

was solved for $\partial\omega/\partial P$ at all latitudes north of 5°N and south of 5°S and at all pressure levels listed in section 3.1. In (3.2), $\eta = \zeta + f$, $f = 2\,\Omega\sin\phi$, $\Omega$ is the earth angular velocity, and

$$\zeta = \frac{1}{a\cos\phi}\frac{\partial v}{\partial\lambda} - \frac{1}{a}\frac{\partial u}{\partial\phi} - \frac{u\tan\phi}{a} \quad . \tag{3.3}$$

A smoother to eliminate $2\Delta X$ waves was passed once over the computed $\eta$ fields before computation of $\partial\omega/\partial P$ and once over the $\partial\omega/\partial P$ fields

themselves. Values of $\partial\omega/\partial P$ at 5°N, Equator, and 5°S were obtained by linear interpolation in latitude. Using the algorithm of Conte and deBoor (1972), a cubic spline was then passed through all nine pressure levels and anchored at P = 0 mb and P = 1010 mb by boundary conditions of $\partial\omega/\partial P = 0$ and $\partial^2\omega/\partial P^2 = 0$. It should be pointed out that the choice of boundary values in these computations is rather arbitrary, since the computed values of $\partial\omega/\partial P$ at P = 0 mb, P = 1000 mb, and all other intermediate levels tend to produce nearly the same cubic spline for any reasonable boundary values selected. To verify this, two different sets of boundary values were tested.

These were

$$\left.\frac{\partial\omega}{\partial P}\right)_{\substack{P=0\\P=1010}} = \left.\frac{\partial^2\omega}{\partial P^2}\right)_{\substack{P=0\\P=1010}} = 0 \qquad (3.4)$$

and

$$\left.\frac{\partial\omega}{\partial P}\right)_{\substack{P=0\\P=1010}} = \left.\frac{\partial\omega}{\partial P}\right)_{\substack{P=10\\P=1000}}$$

$$\left.\frac{\partial^2\omega}{\partial P^2}\right)_{\substack{P=0\\P=1010}} = \left.\frac{\partial\omega}{\partial P}\right)_{\substack{P=10\\P=1000}} \times .10 \quad . \qquad (3.5)$$

Table 1 shows two examples of results obtained at 50°North latitude by application of (3.4) and (3.5). At 55°East, the column of omega values produced using (3.4) shows smaller omega values near the boundaries, and larger values near the middle troposphere while

Table 1. Values of omega (mb/sec × $10^3$) resulting from application of boundary conditions given by Equations (3.4) and (3.5).

| Location: | 50°N/55°E | | 50°N/170°W | |
|---|---|---|---|---|
| Boundary Equation: | (3.4) | (3.5) | (3.4) | (3.5) |
| 10 mb | -.44 | -1.10 | .27 | .15 |
| 50 mb | -.21 | -.65 | .30 | .14 |
| 100 mb | -.60 | -.90 | .39 | .18 |
| 200 mb | -.08 | -.63 | .39 | .19 |
| 300 mb | .67 | .29 | .46 | .29 |
| 500 mb | 2.20 | 1.80 | .52 | .36 |
| 700 mb | 2.30 | 2.00 | .46 | .35 |
| 850 mb | 2.60 | 2.30 | .63 | .38 |
| 1000 mb | .66 | 1.50 | -.26 | -.12 |

applying (3.5) produced these features at 170°W. In spite of typical magnitude differences, as shown in Table 1, application of (3.4) and (3.5) nearly always produced the same general vertical velocity structure with regard to sign and order of magnitude. Overall, however, the 55°E case shown in Table 1 was most typical, and (3.4) was selected for use in this study because it generally gave smaller omega values near the boundaries and slightly larger values near the middle troposphere.

After application of (3.4) and passage of the cubic spline through all levels, values of $\partial\omega/\partial P$ were then obtained directly from the spline at increments of 10 mb from P = 0 mb to P = 1010 mb. To determine values of $\omega$ from the values of $\partial\omega/\partial P$ a modified "shooting" technique as follows was used.

Let the derivative, $\partial\omega/\partial P$, to be represented in finite difference form by the leap frog approximation,

$$\partial\omega/\partial P = \frac{\omega_{i+1} - \omega_{i-1}}{2\Delta P} \quad , \tag{3.6}$$

so

$$\omega_{i+1} = A(P_i)2\Delta P + \omega_{i-1} \quad , \tag{3.7}$$

where $A(P) = (\partial\omega/\partial P)_p$. Two sequences of $\omega_{i+1}$ were then generated using (3.7) by beginning with two different approximations to the derivative at 10 mb. In generating these sequences, we also specified $\omega = 0$ at P = 0 mb. Our goal was to construct a column of $\omega$ values such that the $\partial\omega/\partial P$ values at each level were not violated and which would be zero at both P = 0 mb and

P = 1010 mb. Note that requiring $\omega = 0$ at P = 0 mb and P = 1010 mb appears to be an overspecification of (3.2); however, this will be seen to be possible due to the use of the three point recurrence relation (3.6) to approximate $\partial\omega/\partial P$. Let the first approximation to the derivative at 10 mb, which is used to generate the first sequence, be

$$\left(\omega_1^{(1)} - \omega_o^{(1)}\right)/\Delta P = A\left(P_{1_2}\right) , \tag{3.8}$$

where the superscript represents sequence one. From (3.8) we have

$$\omega_1^{(1)} = \Delta P \; A\left(P_{1_2}\right) + \omega_o^{(1)} , \tag{3.9}$$

or

$$\omega_1^{(1)} = \Delta P \; A\left(P_{1_2}\right) , \tag{3.10}$$

since $\omega_1^{(1)} = 0$. The second approximation to the derivative is

$$\left(\omega_1^{(2)} - \omega_o^{(2)}\right)/\Delta P = A\left(P_1\right) \tag{3.11}$$

from which

$$\omega_1^{(2)} = \Delta P \; A\left(P_1\right) . \tag{3.12}$$

From (3.11) and (3.12) we may now write

$$\omega_2^{(1)} = 2\Delta P\ A(P_1) + \omega_o^{(1)} \quad ; \quad \omega_2^{(2)} = 2\Delta P\ A(P_1) + \omega_o^{(2)}$$

$$\omega_3^{(1)} = 2\Delta P\ A(P_2) + \omega_1^{(1)} \quad ; \quad \omega_3^{(2)} = 2\Delta P\ A(P_2) + \omega_1^{(2)}$$

$$\vdots \qquad\qquad\qquad \vdots$$

$$\omega_n^{(1)} = 2\Delta P\ A(P_{n-1}) + \omega_{n-2}^{(1)} \quad ; \quad \omega_n^{(2)} = 2\Delta P\ A(P_{n-1}) + \omega_{n-2}^{(2)}$$

$$\omega_{n+1}^{(1)} = 2\Delta P\ A(P_n) + \omega_{n-1}^{(1)} \quad ; \quad \omega_{n+1}^{(2)} = 2\Delta P\ A(P_n) + \omega_{n-1}^{(2)} \quad . \qquad (3.13)$$

Since both sequences of (3.13) will satisfy (3.2), a linear combination of these sequences will also satisfy (3.2). The linear combination we choose will be the one which will force $\omega = 0$ at P = 1010 mb. That is, let

$$\lambda\, \omega_{n+1}^{(1)} + (1-\lambda)\ \omega_{n+1}^{(2)} = 0 \qquad (3.14)$$

or,

$$\lambda = \frac{-\ \omega_{n+1}^{(2)}}{\omega_{n+1}^{(1)} - \omega_{n+1}^{(2)}} \quad . \qquad (3.15)$$

Substituting from (3.13), $\lambda$ is solved from (3.15) and a third sequence is generated as

$$\left\{\omega_i^{(3)}\right\}_{i=0}^{i=n+1} = \left\{\lambda\, \omega_i^{(1)} + (1-\lambda)\ \omega_i^{(2)}\right\}_{i=0}^{i=n+1} \quad . \qquad (3.16)$$

Solving (3.14) gives $\omega$ values at all levels which are consistent

with the $\partial\omega/\partial P$ values produced by the spline and which are exactly zero at P = 0 mb and P = 1010 mb.

Since the current study is more concerned with the general condition than the individual condition at a specific layer, the $\omega$ values produced by (3.16) were layer averaged as

$$\omega_{10\,mb} = \left(\sum_{i=o}^{2} \omega_{10\,i}\right)/3 \quad ,$$

$$\omega_{50\,mb} = \left(\sum_{i=2}^{8} \omega_{10\,i}\right)/7 \quad , \quad \omega_{100\,mb} = \left(\sum_{i=5}^{15} \omega_{10\,i}\right)/11 \quad ,$$

$$\omega_{200\,mb} = \left(\sum_{i=15}^{25} \omega_{10\,i}\right)/11 \quad , \quad \omega_{300\,mb} = \left(\sum_{i=25}^{30} \omega_{10\,i}\right)/11 \quad , \quad . \quad . \quad .$$

$$\omega_{850\,mb} = \left(\sum_{i=80}^{90} \omega_{10\,i}\right)/11 \quad , \quad \omega_{1000\,mb} = \left(\sum_{i=99}^{101} \omega_{10\,i}\right)/3 \quad . \quad (3.17)$$

The $\omega$ values produced by (3.17) are those used in the current study and are shown for the 1975 winter season in Figure 1 along with the corresponding omegas compiled using the adiabatic assumption over the same data. It is seen that the quasi-geostrophic omegas are smaller than the theromodynamic omegas at all wavelengths, and this is especially true at very short and very long wavelengths. The maximum at k = 7 is common, indicating that synoptic scale systems produce the greatest vertical velocities. Note that the mean value over the season for the quasi-geostrophic omegas is nearly an order of magnitude smaller than the mean value for the adiabatic omegas.

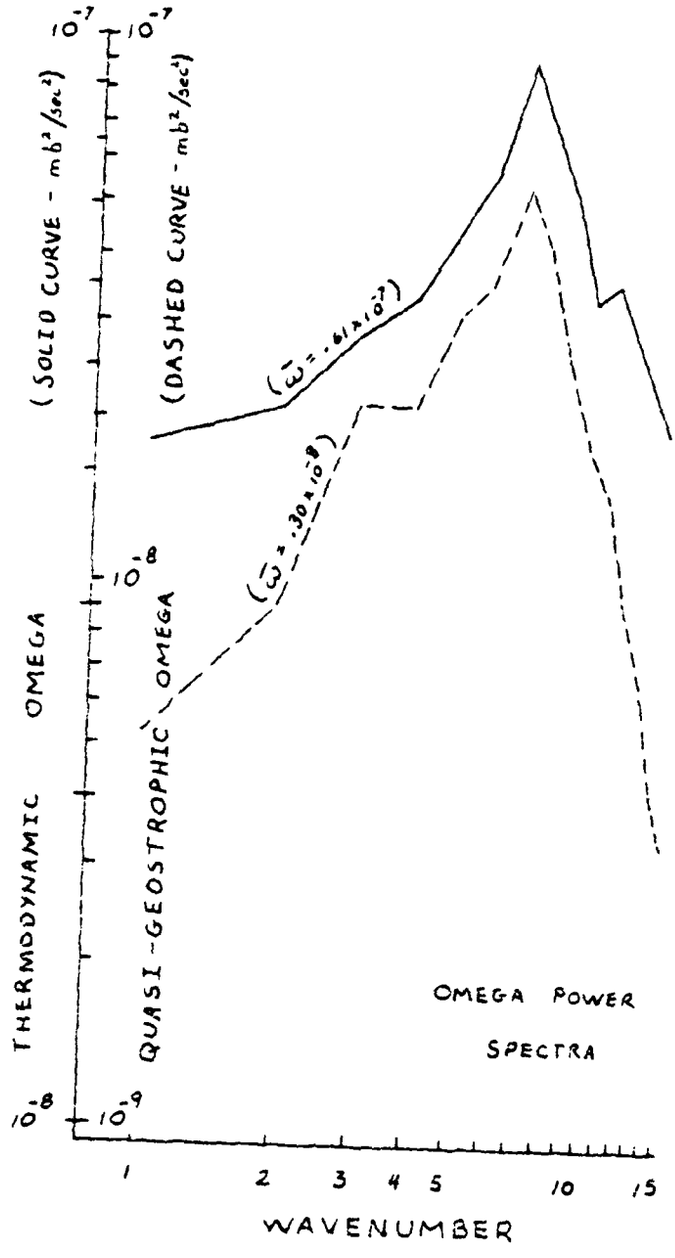


Figure 1. Omega power spectra determined with the use of the thermodynamic and vorticity equations and averaged over 30°N to 60°N for the 1975-76 winter season at 500 mb.

## 3.3 Fast Fourier Transform Computations

After the complete data set of ω, T, U, V, and Z at all levels and for all time periods was determined, the data were then transformed in wave number domain using the standard fast Fourier transform package supplied to us by the National Center for Atmospheric Research (NCAR) software distribution service. Transforms in time also used this package, but the data were modified by removing both linear trends in time and by application of a cosine bell tapering window, recommended by Bingham et al. (1967). In all time transformations, time is normalized as $t = 2\pi/t'$, where t is normalized time, T is in the period over which the transformation is done and t' is real time. Note that as t' ranges from zero to T, t ranges from 0 to $2\pi$, giving the cyclic order required of data to be transformed.

## 3.4 Miscellaneous Computational Techniques

All numerical quadrature in latitude was accomplished using the Cote's formulation presented by Fröberg (1969), whereas vertical integration was accomplished by passing a cubic spline through all levels and then integrating the resulting cubic spline exactly between the levels desired.

Finite difference approximations to derivatives in latitude were centered except at 85°N and 35°S, where one-sided differences were used. Centered differencing in pressure was also used throughout, where all term values at P = 0 mb and P = 1010 mb were assumed to be zero.

# CHAPTER 4

# SEASONAL MEAN FLOW, TEMPERATURE, SPECTRA, BOUNDARY TRANSFER, AND ENERGETICS

## 4.1 Distribution of Mean Flow and Temperature

Figure 2 shows the mean zonal wind for the winter of Dec 1975 through Feb 1976. The maximum average U-component of the wind appeared at 60°N at 10 mb. A secondary maximum, the winter middle latitude jet stream, was seen at 30°N centered at 200 mb. A minor westerly maximum was also observed near 20°N at 10 mb. The major easterly maximum was seen near 10 mb at 35°S, and a minor easterly maximum was found near 1000 mb at 10°N.

The sudden stratospheric warming that occurred during the winter season described above was classified as a minor warming, while the warmings that occurred during the 1973-74 and 1976-77 winter seasons available in our data base were classified as major. Since we hope to derive general conclusions concerning the energy exchanges in the atmosphere, we have chosen the 1975-76 winter season, our least perturbed winter season, to be the primary season for our study. In all diagrams and discussion to follow, then, winter will always refer to the Dec 1975 through Feb 1976 season unless otherwise specifically stated.

Figure 3 presents the mean meridional flow for the winter season. The diagram was constructed by first plotting omega

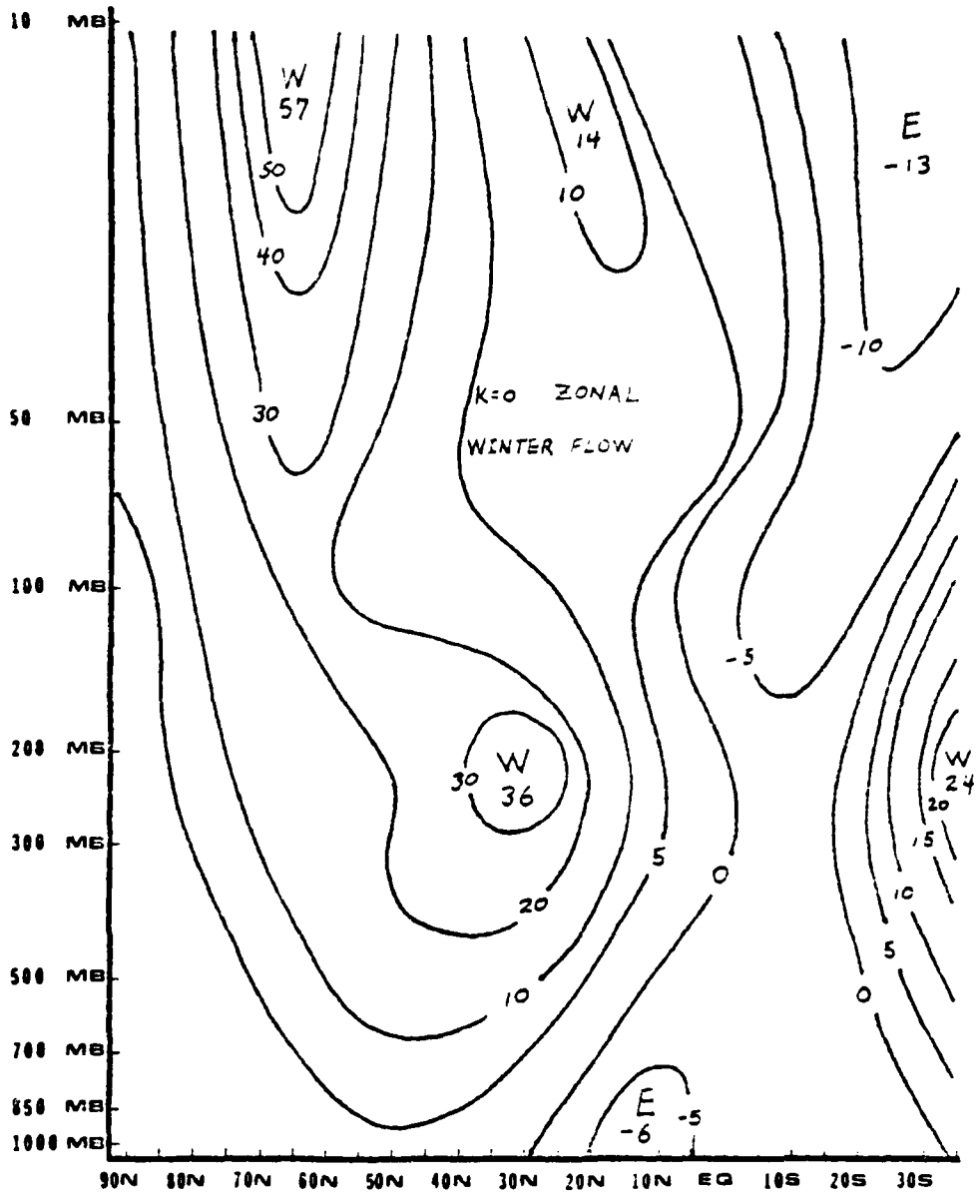


Figure 2. Cross section of the mean zonal wind distribution in m/sec for the 1975-76 winter season.

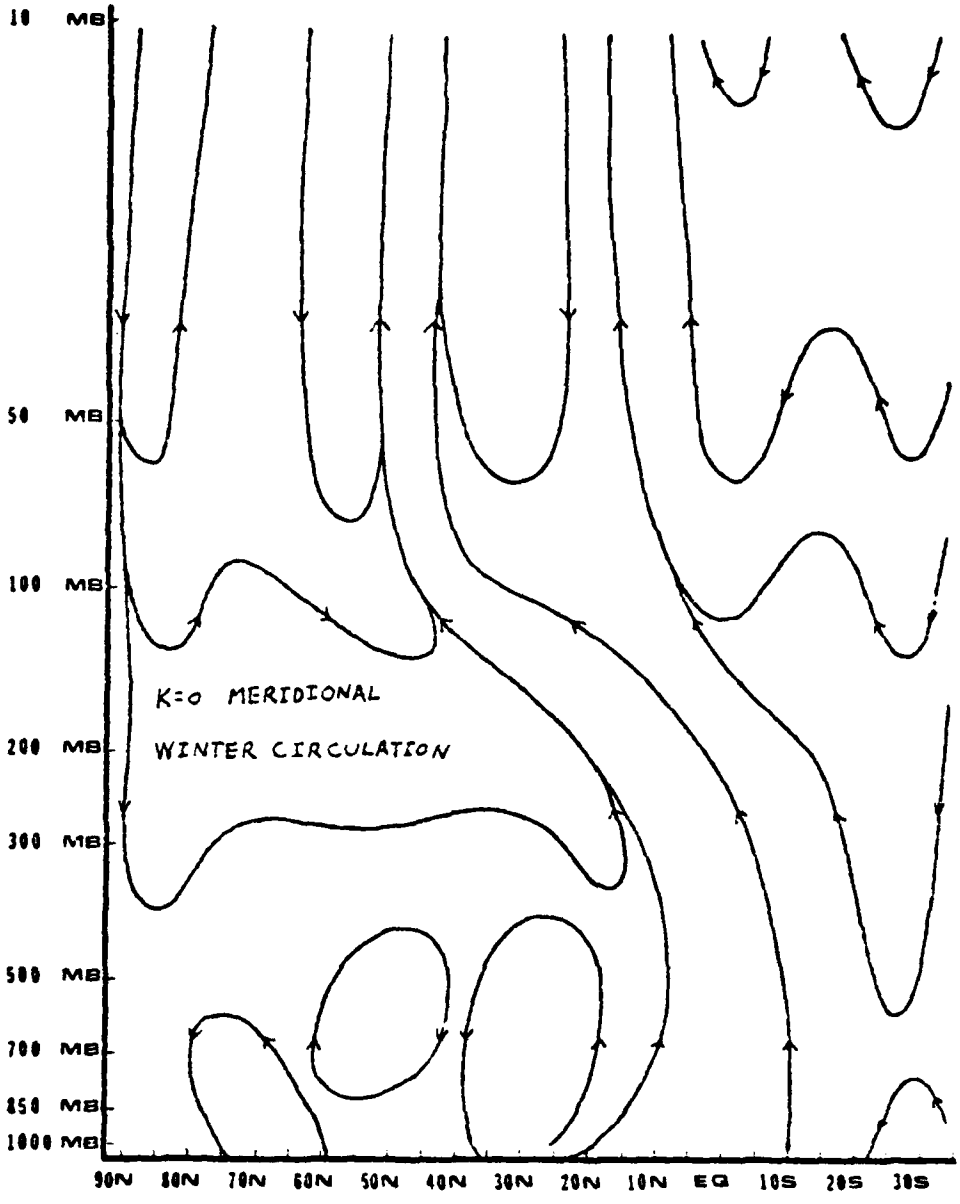


Figure 3. Cross section of the mean meridional circulation for the 1975-76 winter season.

values in mb/sec ($X\ 10^4$) as a vertical vector and the V-component of the wind in m/sec ($X\ 10^2$) as a horizontal vector. In the current scale of the diagram, $1 \times 10^{-4}$ mb/sec or $1 \times 10^{-2}$ m/sec is equivalent to 2/3 cm. A "vector sum" field was then constructed, and this was streamlined to produce the flow shown on Figure 3. While at first glance it may seem improper to construct a vector sum of two vectors with different units, it should be pointed out that dividing omega in mb/sec by the product of density and gravity gives the corresponding vertical velocity in m/sec. These values would be considerably smaller than the values of the V-component of the wind, and still more scaling would have to be done to produce a reasonable picture of the circulation. Essentially, the diagram was constructed directly from the mb/sec values because it required less work to do so and because the end results would be the same if the mb/sec values had been converted to m/sec.

In Figure 3, the Northern Hemisphere troposphere is characterized by two direct circulation cells appearing between 20°N and 40°N and between 60°N and 80°N, and an indirect cell between 45°N and 60°N. Another major feature shown in this diagram is the apparent flow from low levels in the tropical regions upward and northward into the middle latitude stratosphere. This major feature will be discussed in detail in section 4.3.2.

Figure 4 shows a cross section plot of the mean omega computed from the quasi-geographic vorticity equation (3.2). The dashed curves in this figure are lines connecting the terminal points of the omega vectors with starting points located on each pressure

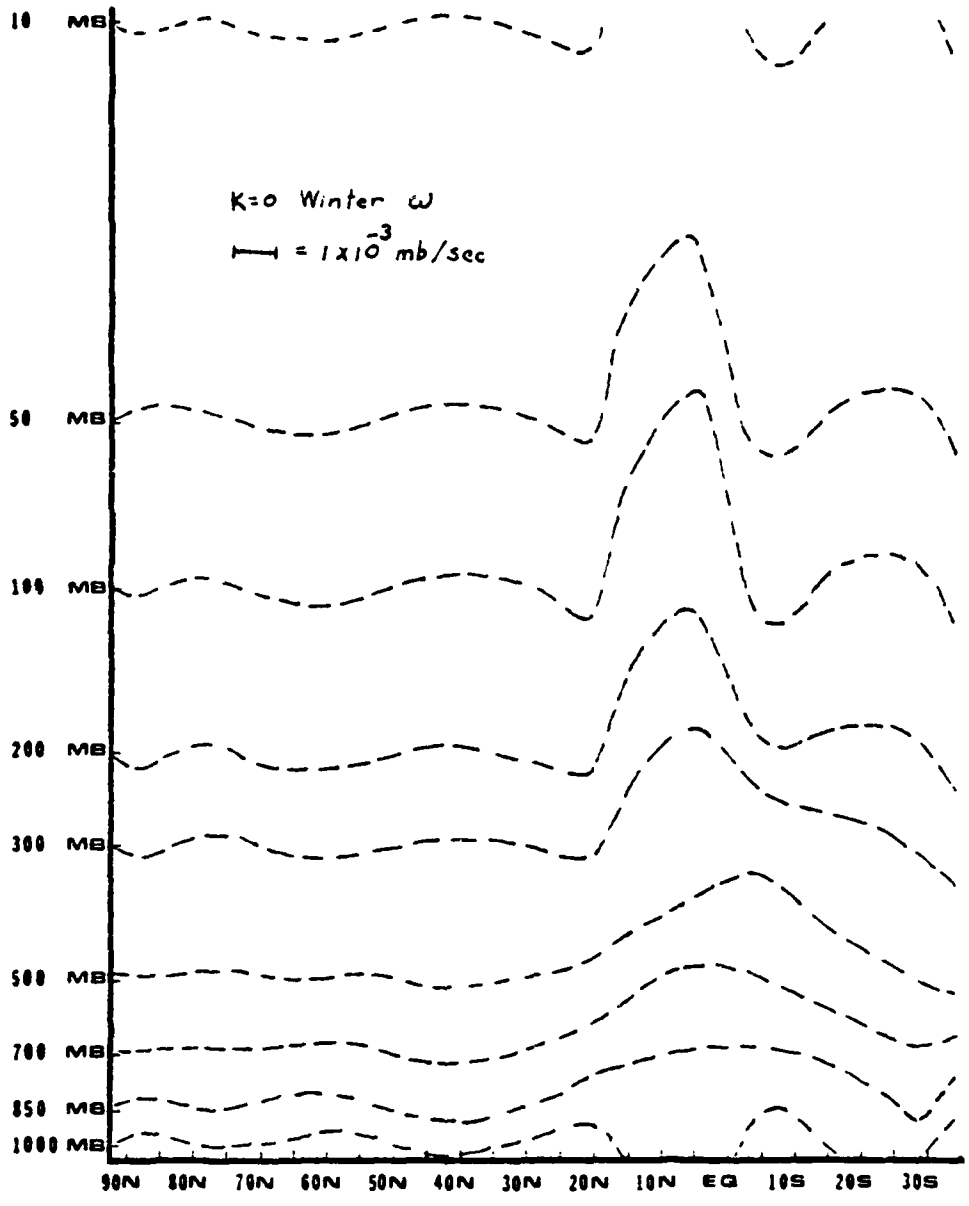


Figure 4. Cross section of the mean omega distribution for the 1975-76 winter season.

level. Since these curves represent the seasonal mean flow, they appear to indicate the presence of standing waves generated in the area of maximum vertical velocity at 5°N. Perhaps tropical regions impose a greater dynamic effect on the mean circulation in the middle and high latitudes beyond the Hadley cell? In addition to the primary maximum at 5°N, Figure 3 also shows a secondary vertical velocity maxima about 500 mb near 25°S. Comparing these two upward vertical velocity maxima with the mean zonal flow shown in Figure 2, it is seen that vertical velocity maxima occur between westerly and easterly jet streams, and are not necessarily associated with areas of maximum heating. This appears to be a feature generated by use of the quasi-geostrophic vorticity equation, and will also be seen for the summer season discussed below.

Figure 5 depicts the mean temperatures observed during the winter season. Note the extremely cold temperatures centered at 100 mb in the region of the high tropical tropopause. These cold temperatures are found directly over the area of maximum vertical velocity shown in Figure 4. The region where the upward vertical velocity maximum intersects the extremely cold temperatures will be seen to be an area of strong conversion of kinetic energy to available potential energy.

In addition to the winter season discussed above, we also collected and processed all data continuing through the following winter season. We have chosen to present the 1976 summer season, consisting of June, July, and August, for reasons similar to those given above for selecting the winter season. That is, these

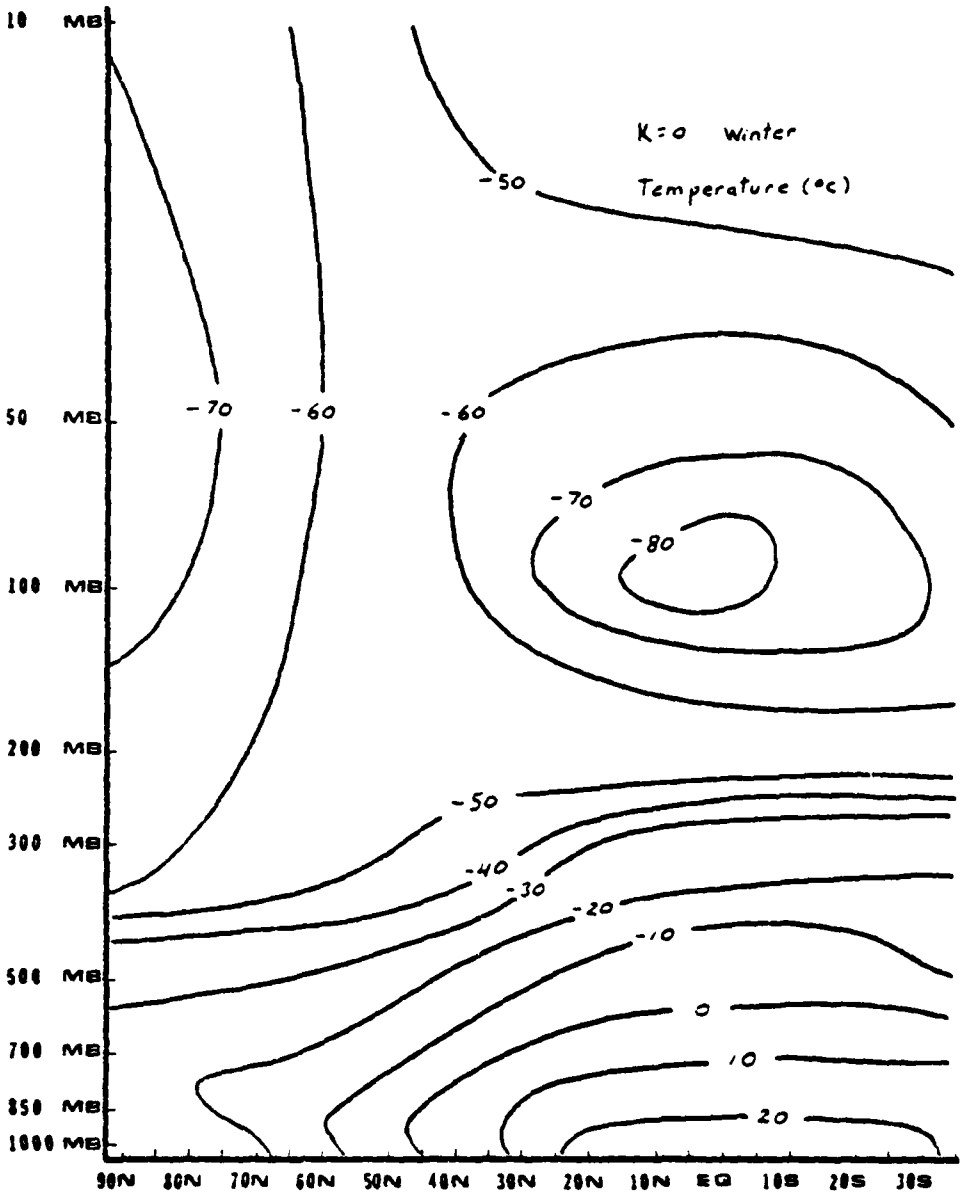


Figure 5. Cross section of the mean temperature distribution for the 1975-76 winter season.

summer months were in a quasi-stationary state, free of the continually increasing temperature and decreasing wind intensity of March, April, and May, and of the decreasing temperature and increasing wind intensity of September, October, and November.

Figure 6 depicts the mean zonal wind for the summer season. Two major westerly jets are seen at 35°S and 45°N centered at 200 mb. The greatest westerly intensity is again found in the winter hemisphere. A major easterly maximum was observed at 10 mb near 15°N, and extended southward and downward into the middle troposphere over the equator.

The mean meridional flow for summer was constructed exactly as it was for the winter season and is presented in Figure 7. Again, the Northern Hemisphere troposphere was characterized by three cells. The Hadley cell remained essentially as it was during winter, but the northern two cells were much weaker and in the reverse sense of that observed for winter. A strong direct circulation cell between 10°S and 30°S was also seen. A strong flow emanating from low levels just south of the equator was seen to move upward and southward into the Southern Hemisphere stratosphere. This flow is essentially the mirror image of that observed during winter.

The mean cross section plot of omegas for summer is given in Figure 8. As for the winter season, the major upward vertical velocity maximum at 5°S falls between the major westerly and easterly zonal jets shown in Figure 6. A minor upward vertical velocity maximum was also seen at 20 N.

Figure 9 shows the mean summer temperature cross section.

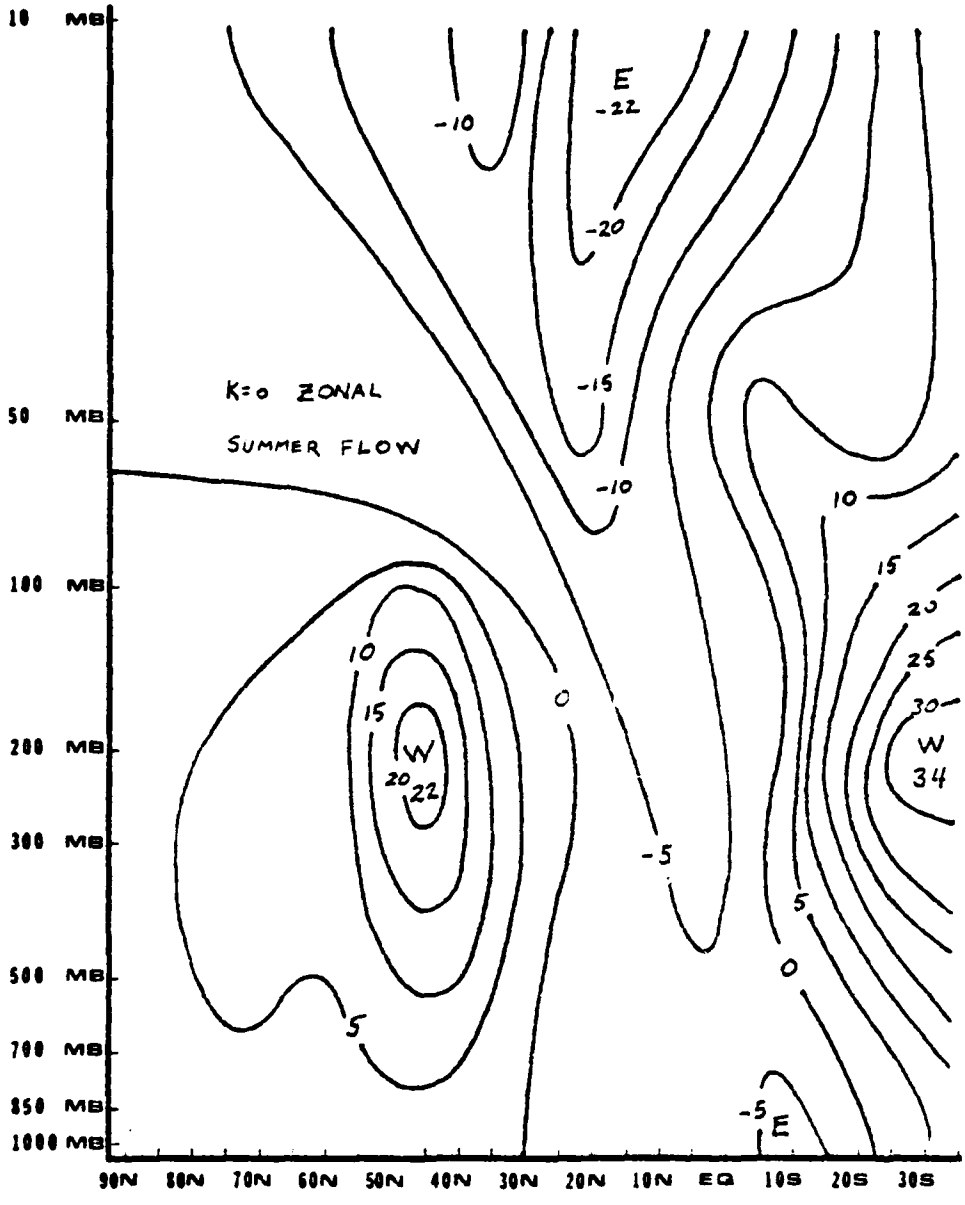


Figure 6. Cross section of the mean zonal wind distribution in m/sec for the 1976 summer season.

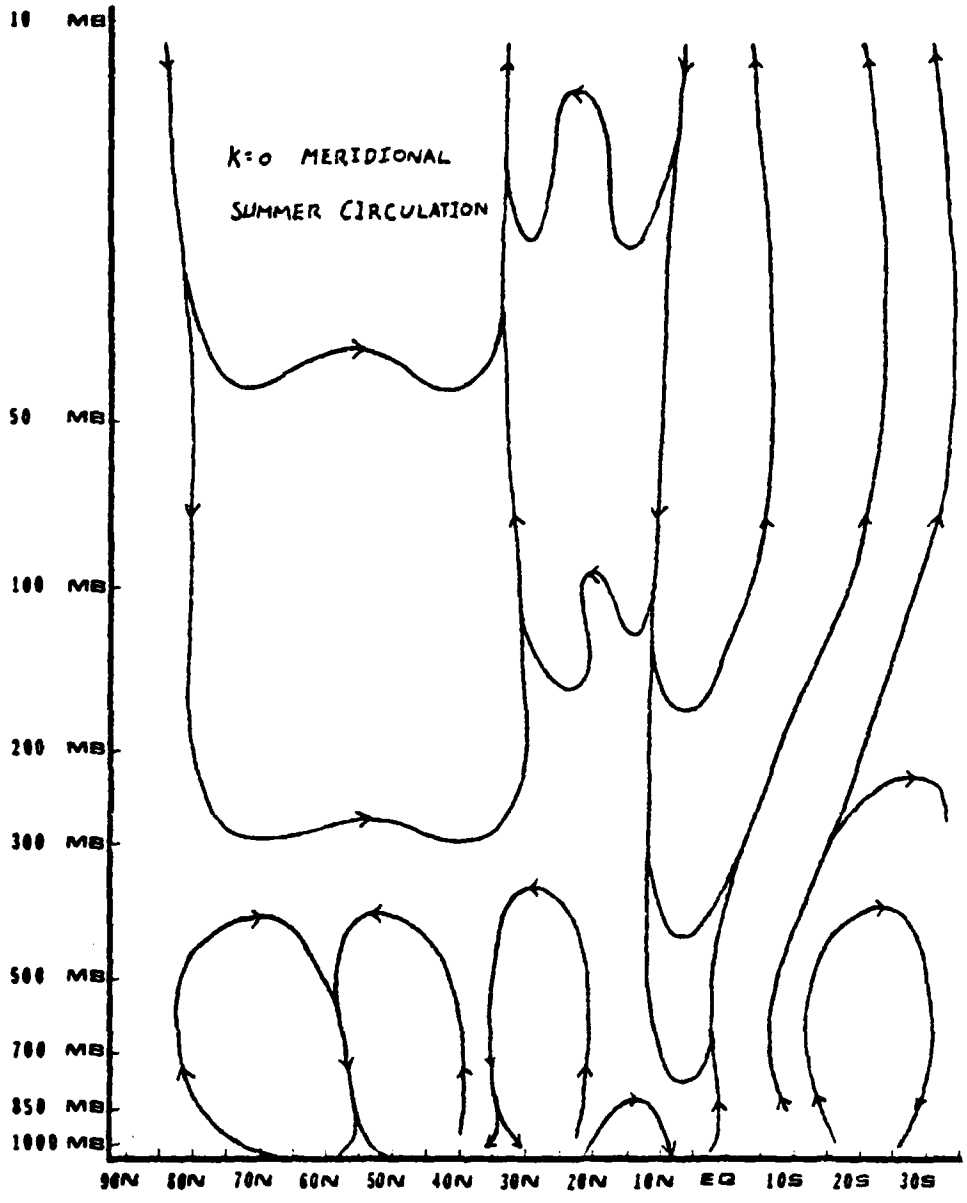


Figure 7. Cross section of the mean meridional circulation for the 1976 summer season.

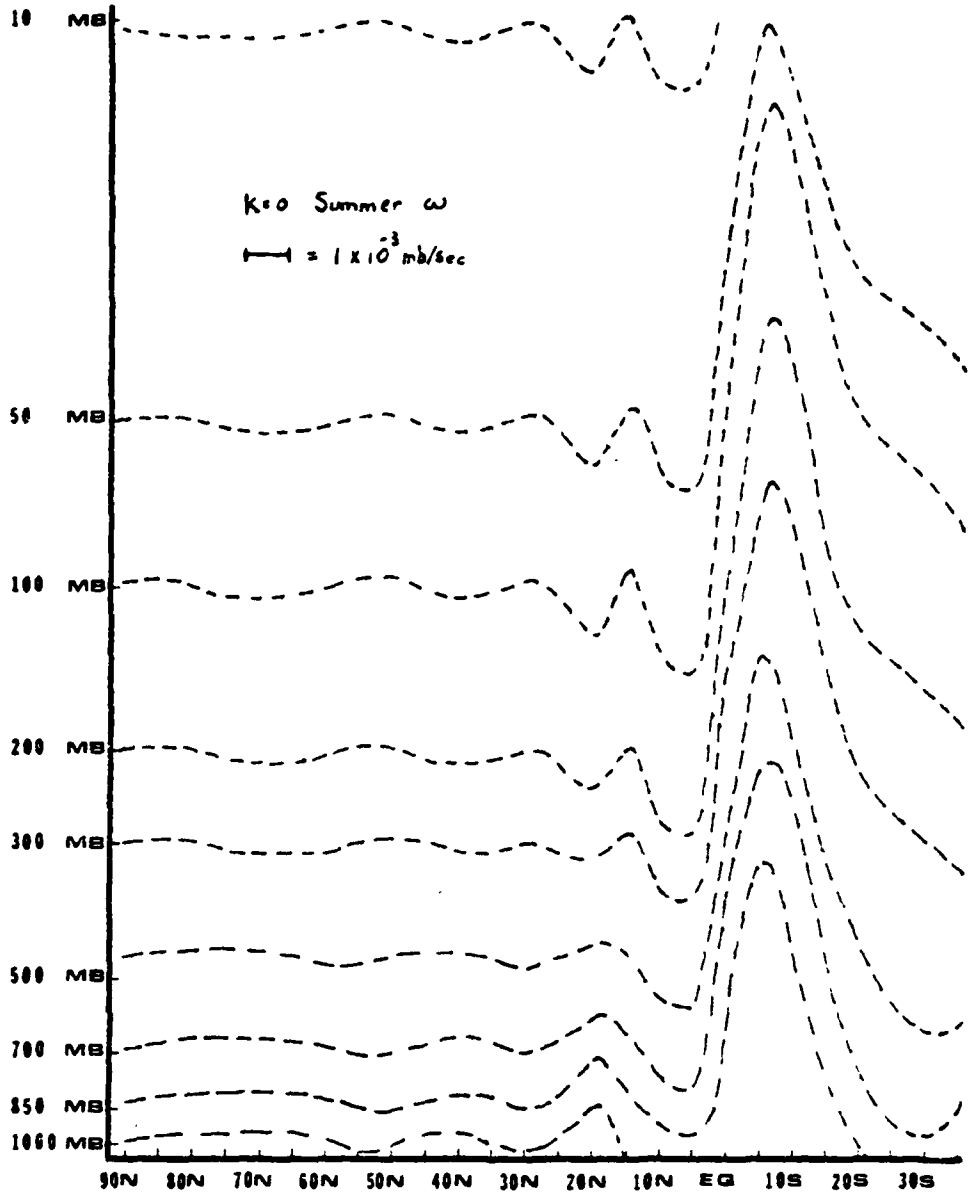


Figure 8. Cross section of the mean omega distribution for the 1976 summer season.

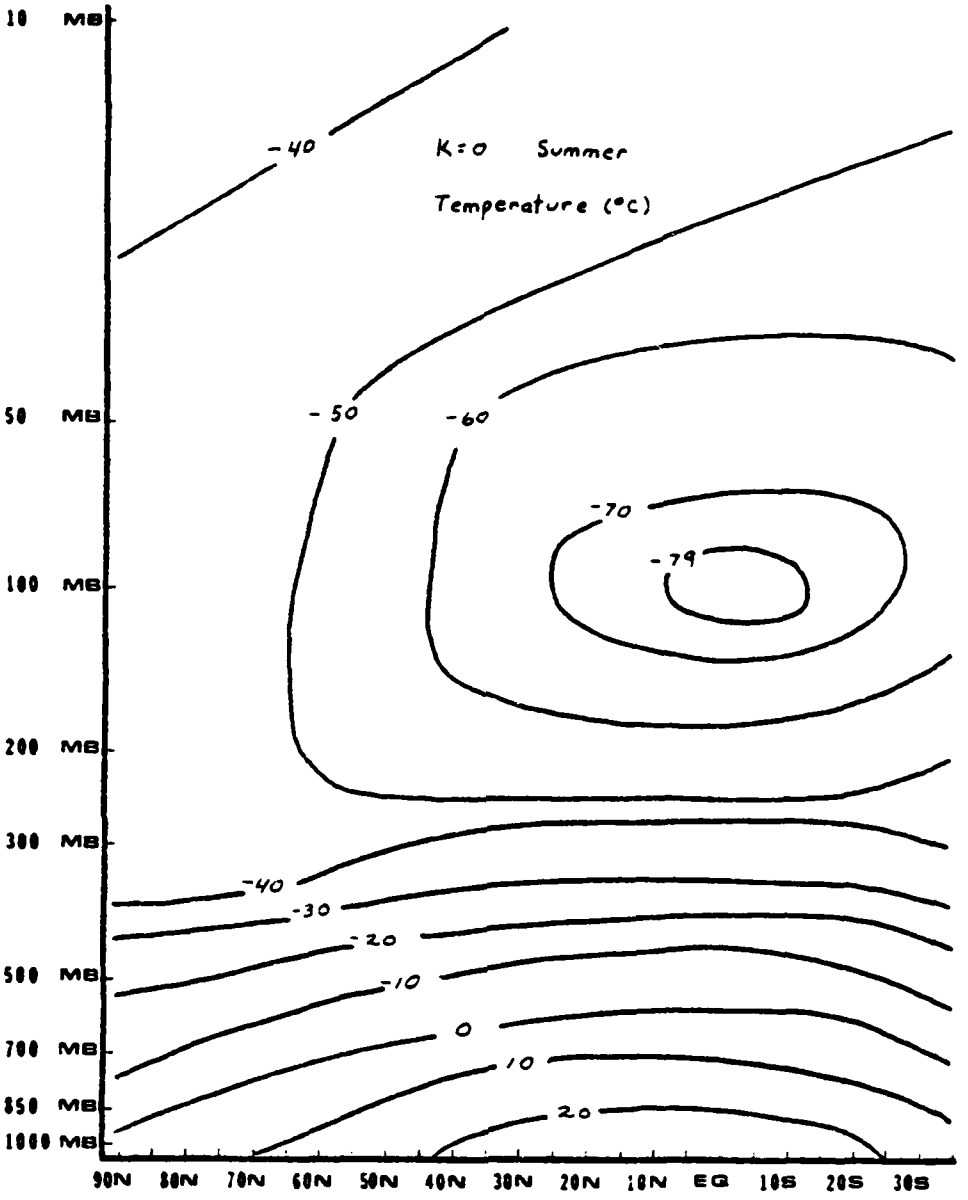


Figure 9. Cross section of the mean temperature for the 1976 summer season.

Again, the coldest temperatures observed in our region of study was at 100 mb above the equator, directly over the area of maximum upward vertical velocity. This will also be seen to be a region of strong mean conversion of kinetic energy to available potential energy.

## 4.2 Seasonal Mean Spectra

### 4.2.1 Mean power spectra distribution

Figures 10 through 17 show the distribution of the seasonal mean power spectra of omega, height, U-component of the wind, V-component of the wind, kinetic energy, and available potential energy denoted, respectively, by $\overline{E}_\omega$, $\overline{E}_z$, $\overline{E}_u$, $\overline{E}_v$, $\overline{EK}$, and $\overline{EA}$. Temperature spectra are not included, since they have a similar distribution as $\overline{EA}$. Winter spectra are given for the 30°N to 60°N latitude band because these are of greater intensity than corresponding spectra for the summer season. Similarly, summer spectra over the 15°S to 15°N latitude band are chosen because they demonstrate greater intensities than the corresponding winter spectra over the same band. The 500 mb level has been selected to be representative of the troposphere, and the 50 mb and 10 mb levels have been chosen to represent the stratosphere.

Area average of a quantity over the latitude bands selected was accomplied by applying

$$\frac{\int_A ( ) \, dA}{\int_A dA} , \qquad (4.1)$$

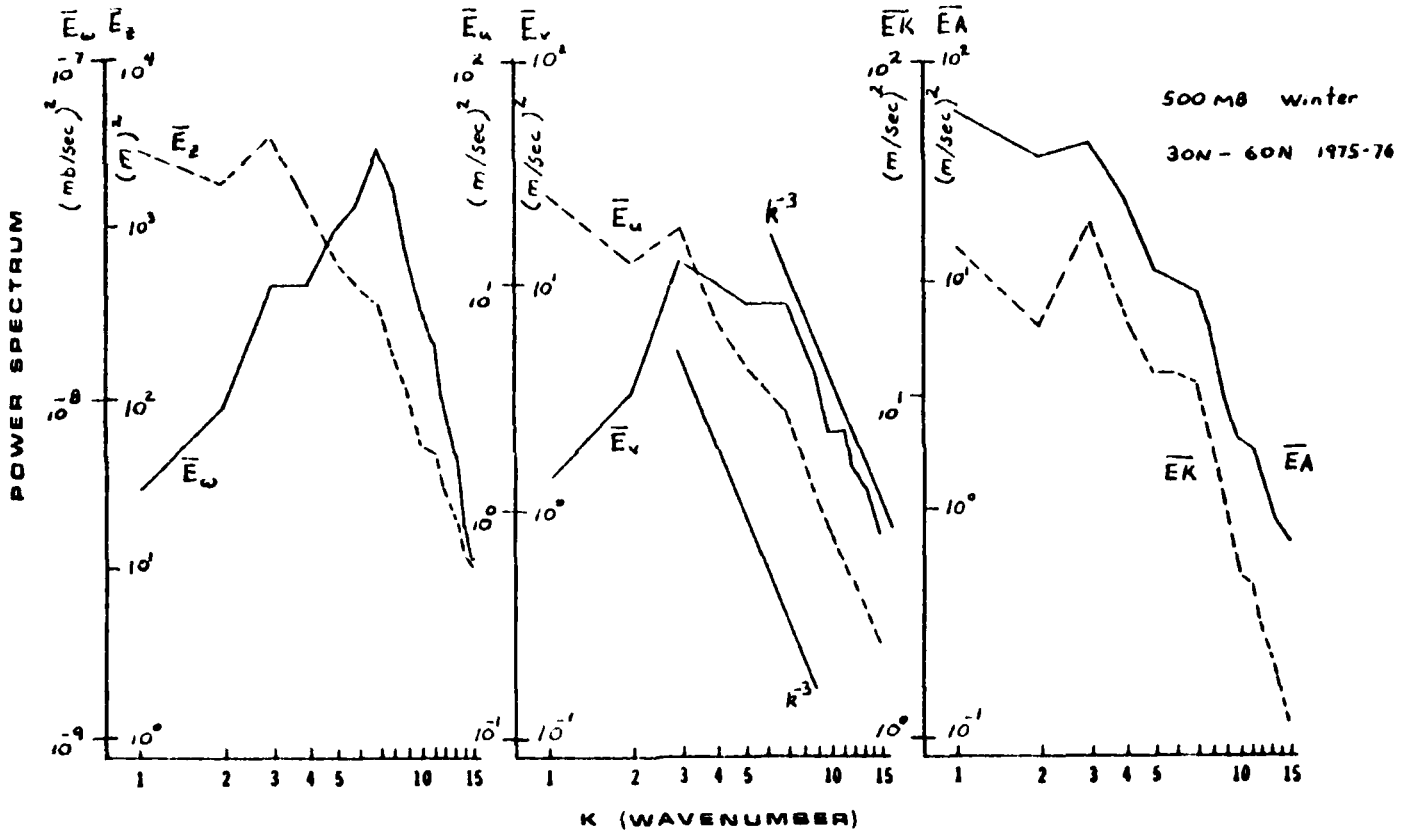


Figure 10. Distribution of seasonal mean power spectra for the 1975-76 winter season at 500 mb.

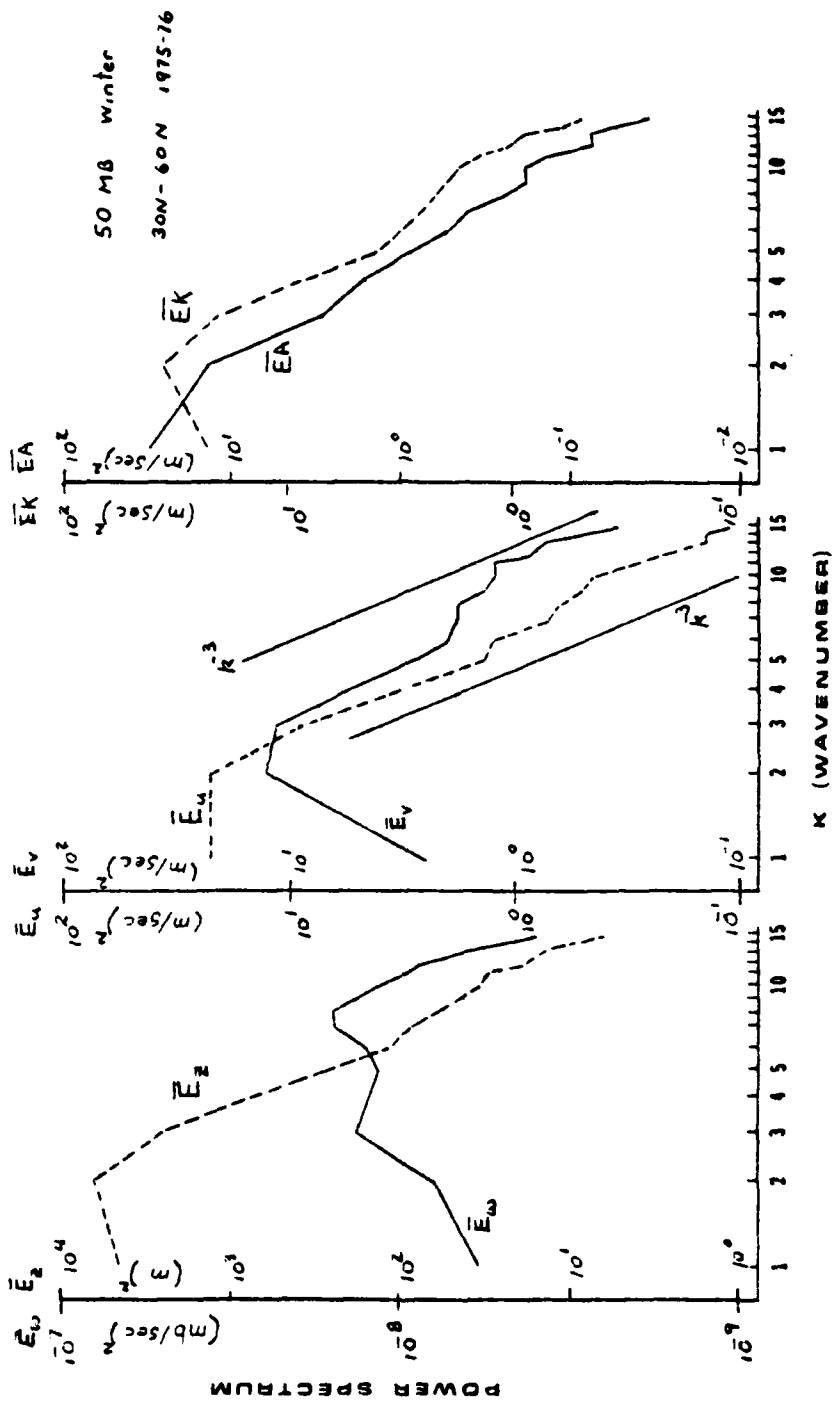


Figure 11. Distribution of seasonal mean power spectra for the 1975-76 winter season at 50 mb.

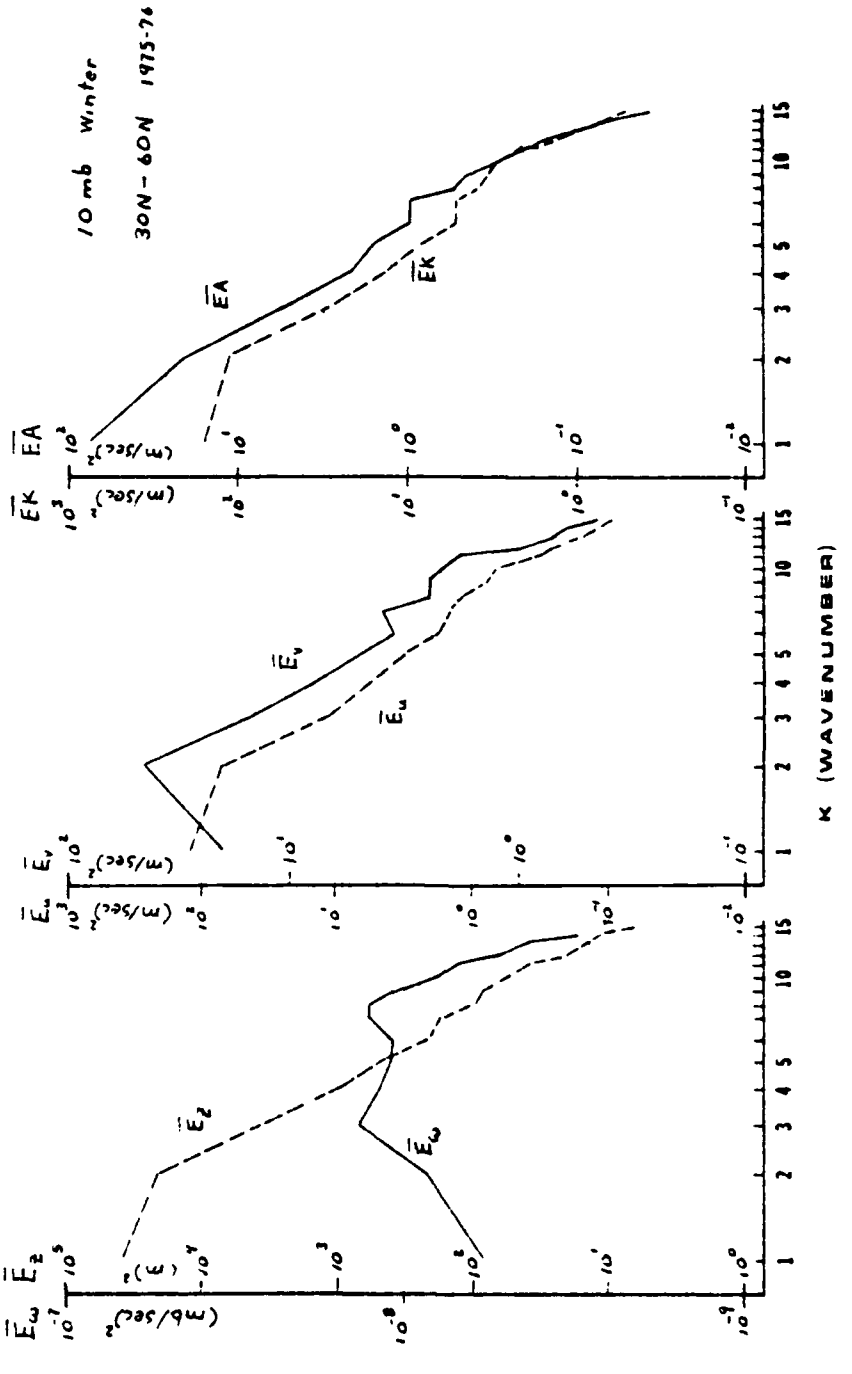


Figure 12. Distribution of seasonal mean power spectra for the 1975-76 winter season at 10 mb.

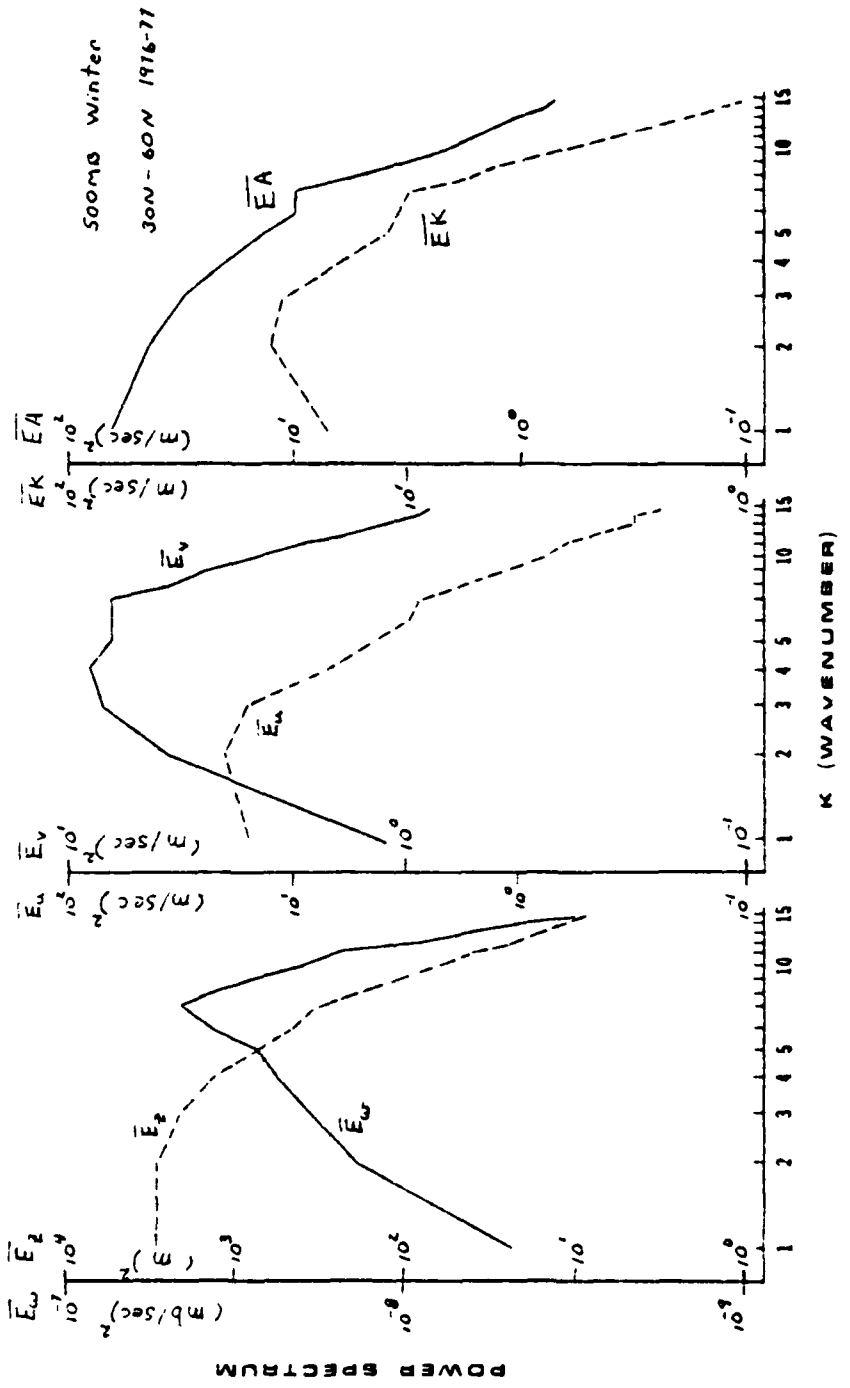


Figure 13. Distribution of seasonal mean power spectra for the 1976-77 winter season at 500 mb.

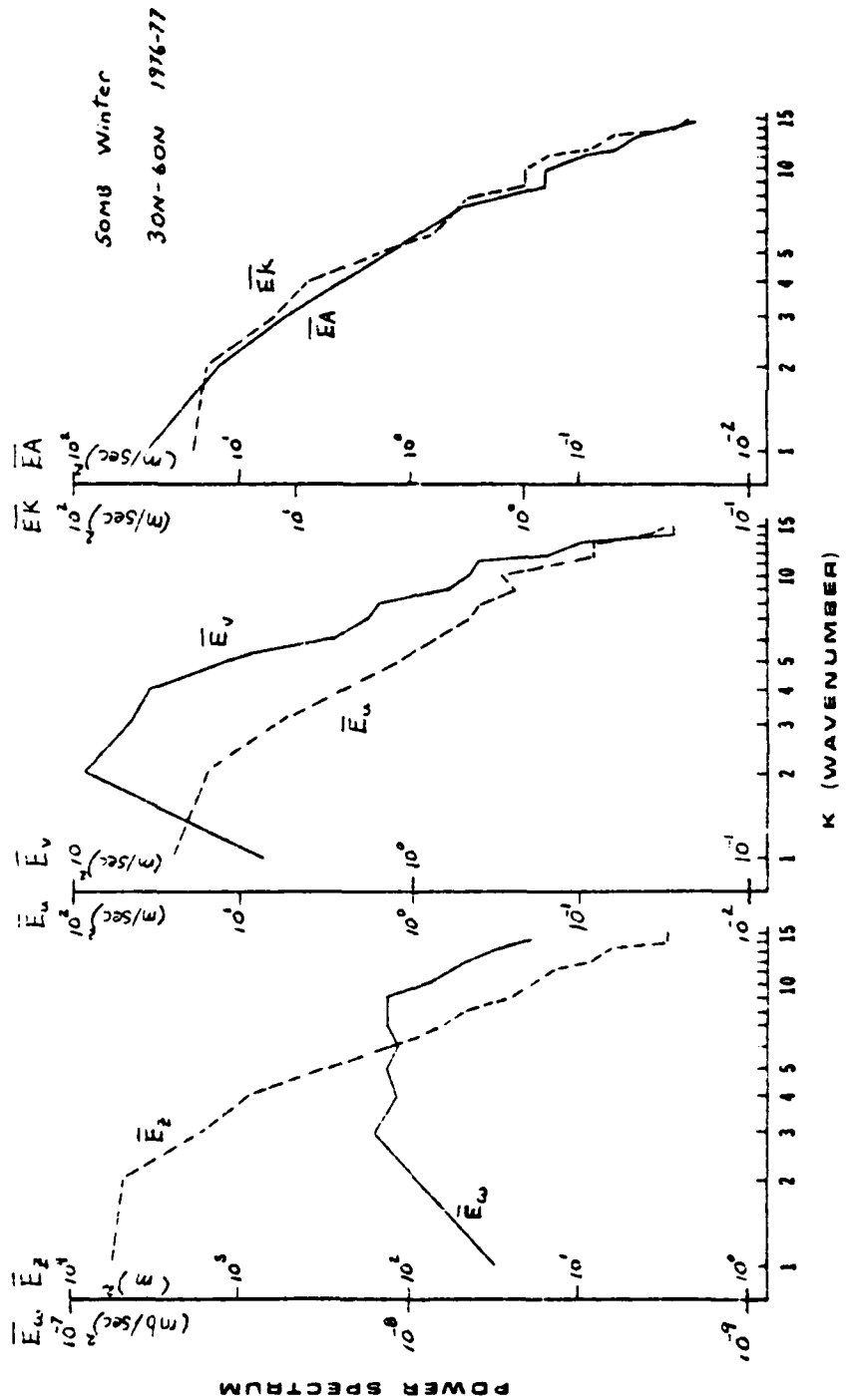


Figure 14. Distribution of seasonal mean power spectra for the 1976-77 winter season at 50 mb.

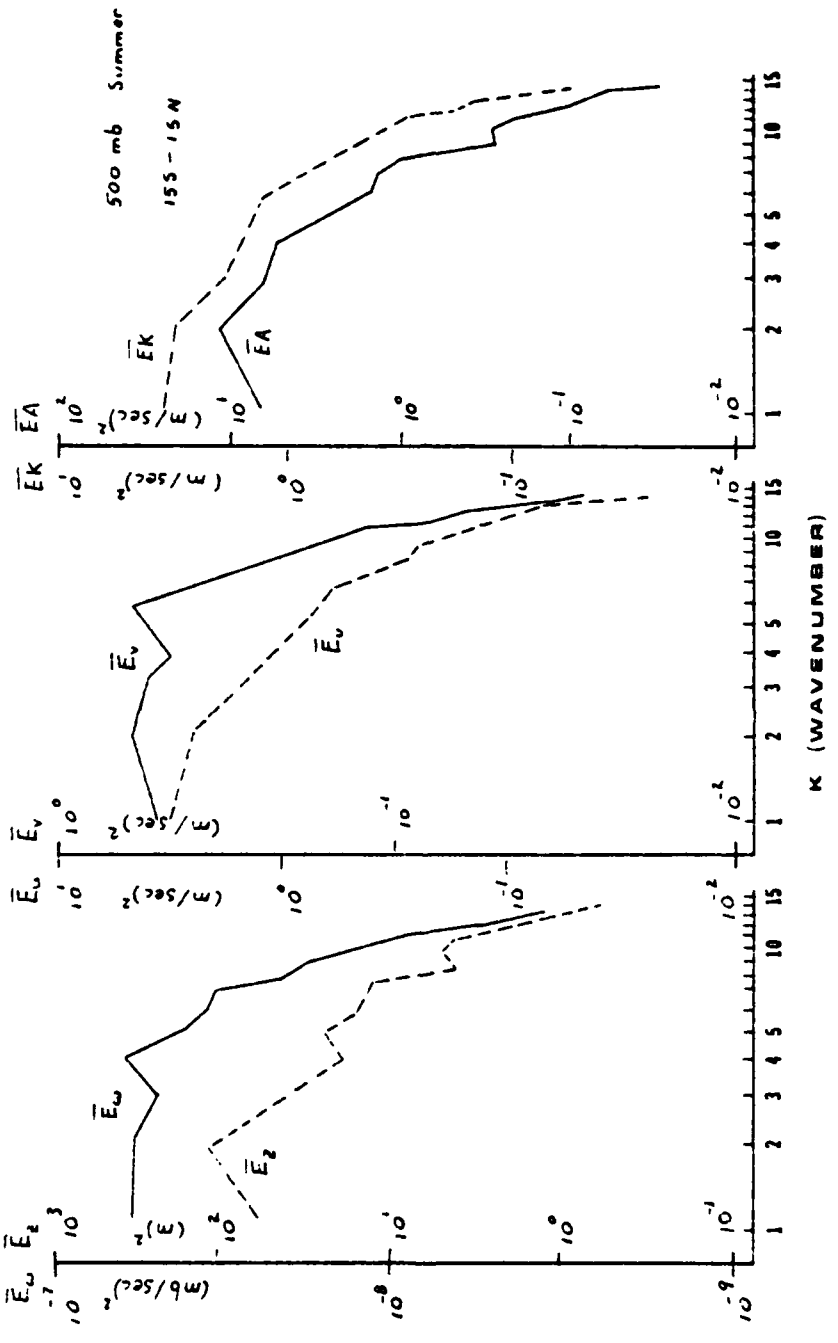


Figure 15. Distribution of seasonal mean power spectra for the 1976 summer season at 500 mb.

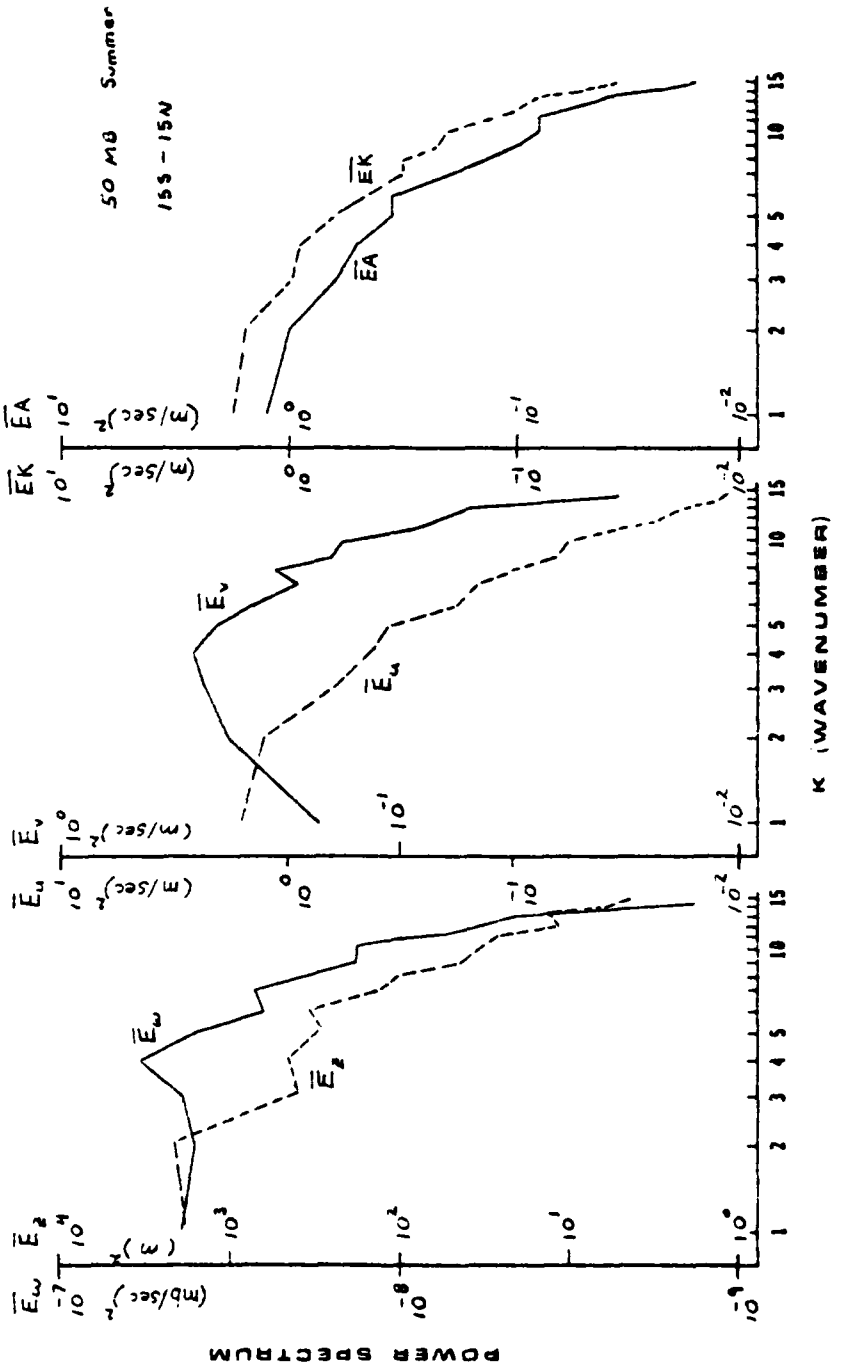


Figure 16. Distribution of seasonal mean power spectra for the 1976 summer season at 50 mb.

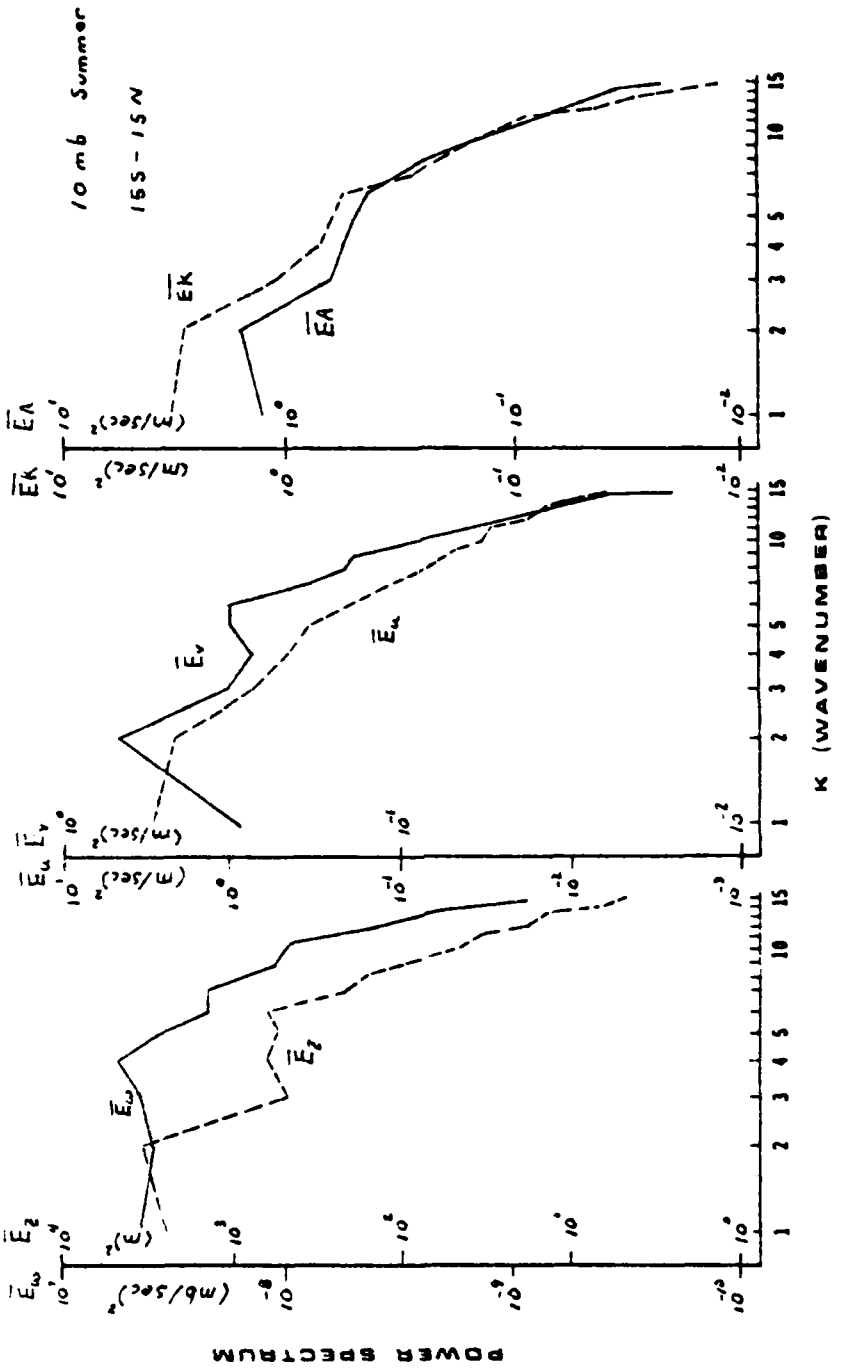


Figure 17. Distribution or seasonal mean power spectra for the 1976 summer season at 10 mb.

where ( ) represents the parameter to be averaged. Equation (4.1) may be expanded as

$$\frac{\int_{\phi_1}^{\phi_2}\int_{0}^{2\pi}(\,)\,(a\cos\phi\,d\lambda)(a\,d\phi)}{\int_{\phi_1}^{\phi_2}\int_{0}^{2\pi}(a\cos\phi\,d\lambda)(a\,d\phi)} \tag{4.2}$$

$$= \frac{1}{(\sin\phi_2 - \sin\phi_1)}\int_{\phi_1}^{\phi_2}(\,)\cos\phi\,d\phi\ , \tag{4.3}$$

since the quantity in parenthesis is a function of wave number and, therefore, independent of longitude $\lambda$. That is, numbers plotted in Figures 10 through 17 are per unit area values, not values of total energy.

Figures 10, 11, and 12 show the mean power spectra observed at 500, 50, and 10 mbs during the winter of 1975-76. A striking feature seen in Figure 10 is the relative minimum value of wave number 2 appearing in the power spectra for $\overline{E}_\omega$, $\overline{E}_u$, $\overline{EA}$, and $\overline{EK}$. For comparison of this feature, we have included the corresponding spectra for the 1976-77 winter season (Figure 13). Note that a relative minimum value does not occur for the power spectra presented in Figure 13. In fact, a relative maximum value is seen instead. Power spectra for 1973-74 $\overline{E}_u$ demonstrate a strong "dip" at wave number 2, although a relative minimum there is not actually achieved. When the behavior of the power spectra at wave number 2 is compared with the strengths of the sudden stratospheric warmings that occurred during the three winter seasons discussed above, we see that weak warmings correspond with relative small

values of 500 mb kinetic energy at wave number 2, and that strong warmings correspond with intense values at wave number 2. To better understand this feature, consider the cross section plot of wave number 2 kinetic energy presented in Figure 25 of section 4.2.2. In this figure, a tongue of maximum kinetic energy is seen to extend downward from the stratosphere over all latitudes north of 30°N. Maximum or minimum values of the middle latitude kinetic energy power spectrum at 500 mb may well be determined by the extent to which the tongue of maximum kinetic energy shown in Figure 25 extends into the troposphere. Therefore, we assume the wave number 2 minimum observed for 1975-76 winter season to be real and more typical of the atmosphere not being affected by extremes.

Figure 10 and 13 show middle latitude 500 mb mean spectral distributions for the 1975-76 and 1976-77 winter seasons. The distribution of $\overline{E}_z$ in these figures is similar to that of $\overline{EA}$, as required by the hydrostatic relation between height and temperature. It is also seen that $\overline{EK}$ is similar to $\overline{E}_u$ for low wave numbers, but more closely related to $\overline{E}_v$ for higher wave numbers. This is also required, since $\overline{E}_u$ contains more energy than $\overline{E}_v$ at low wave numbers, and the reverse is true at higher wave numbers. It may also be noted in Figures 10 and 11 that $\overline{E}_u$ and $\overline{E}_v$ are proportional to $k^{-3}$ in the wave number range 7 to 15, demonstrating a characteristic of two dimentional turbulence of large scale atmospheric motion.

The middle latitude tropospheric distributions of $\overline{E}_\omega$, shown in Figures 10 and 13 are characteristic, showing maximum values at

or near wave number 7. This indicates that the maximum vertical motion in the troposphere is primarily associated with synoptic scale waves (weather systems). The middle latitude stratospheric distribution of $\overline{E}_\omega$ shown in Figures 11, 12, and 14 show rather characteristic flat profiles between wave number 3 and 7, with relative maxima generally occurring at both wave number 3 and wave number 7. This indicates that stratospheric vertical velocity is associated with both planetary and synoptic scale disturbances. In the tropics, however, the maximum $\overline{E}_\omega$ is at wave number 4 in both the stratosphere and the troposphere (Figures 15 through 17). This implies that vertical motion in the tropics is primarily associated with the planetary waves rather than synoptic waves. Also note that tropical spectra of $\overline{E}_\omega$ demonstrate considerably more energy in wave numbers 1 through 6 than seen in the middle latitudes. It may also be pointed out that the distribution of $\overline{E}_u$ and $\overline{E}_z$ in the tropics are quite dissimilar, since the geostrophic relation does not hold near the equator.

The distributions of $\overline{E}_v$ are quite variable, but the energy peak in these figures always falls inclusively between wave number 2 and wave number 7.

4.2.2 Spatial distribution of mean energy spectra

Figures 18 through 28 show cross section plots of average values of kinetic energy and available potential energy for wave nubmers 0, 1, 2, 3, and the sum of wave numbers 1 through 20 for the winter season. The kinetic energy plot for wave number 4 is

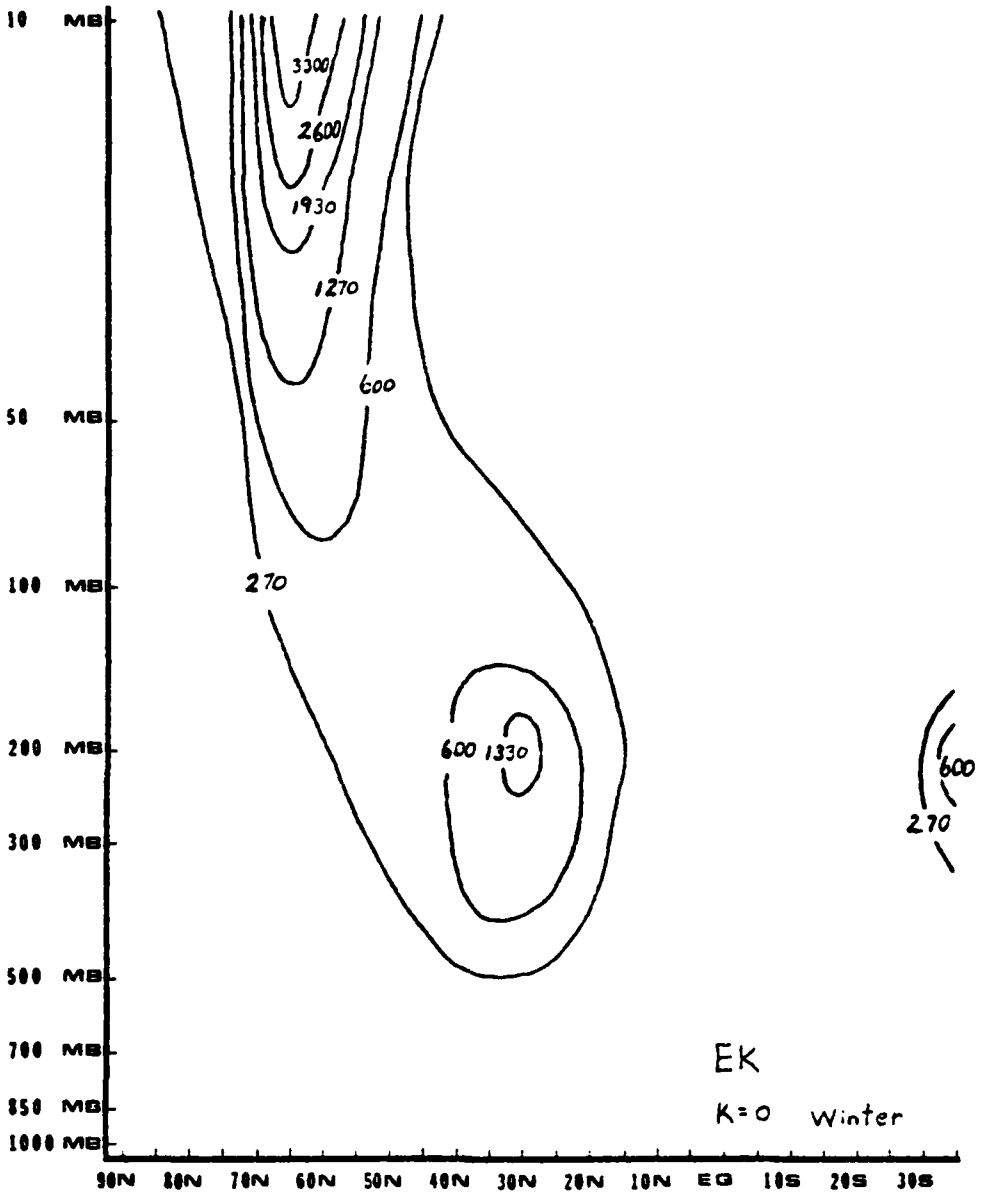


Figure 18. Cross section of the distribution of the mean kinetic energy of the zonal flow for winter ($m^2/sec^2$).

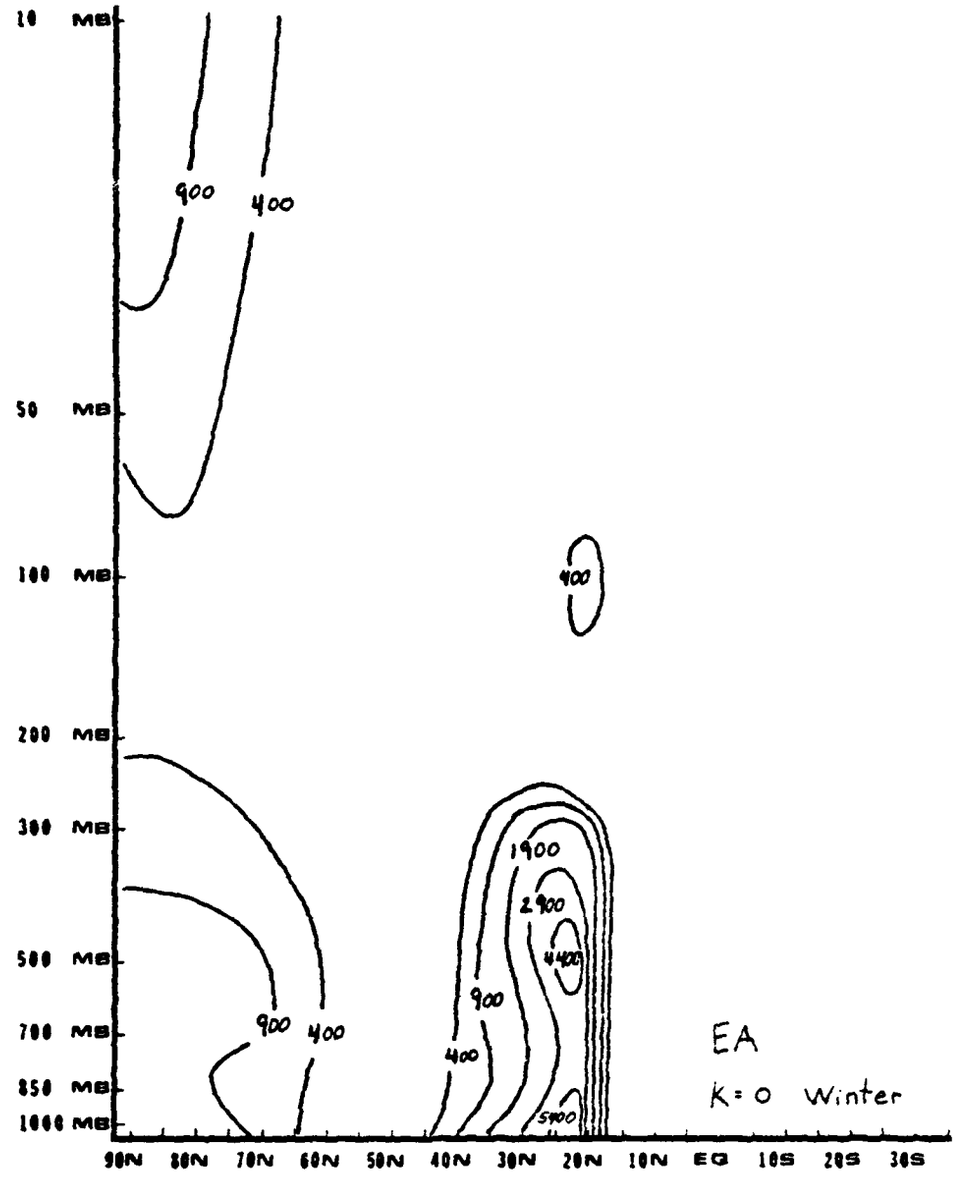


Figure 19. Cross section of the distribution of the mean available potnetial energy of the zonal flow for winter ($m^2/sec^2$).

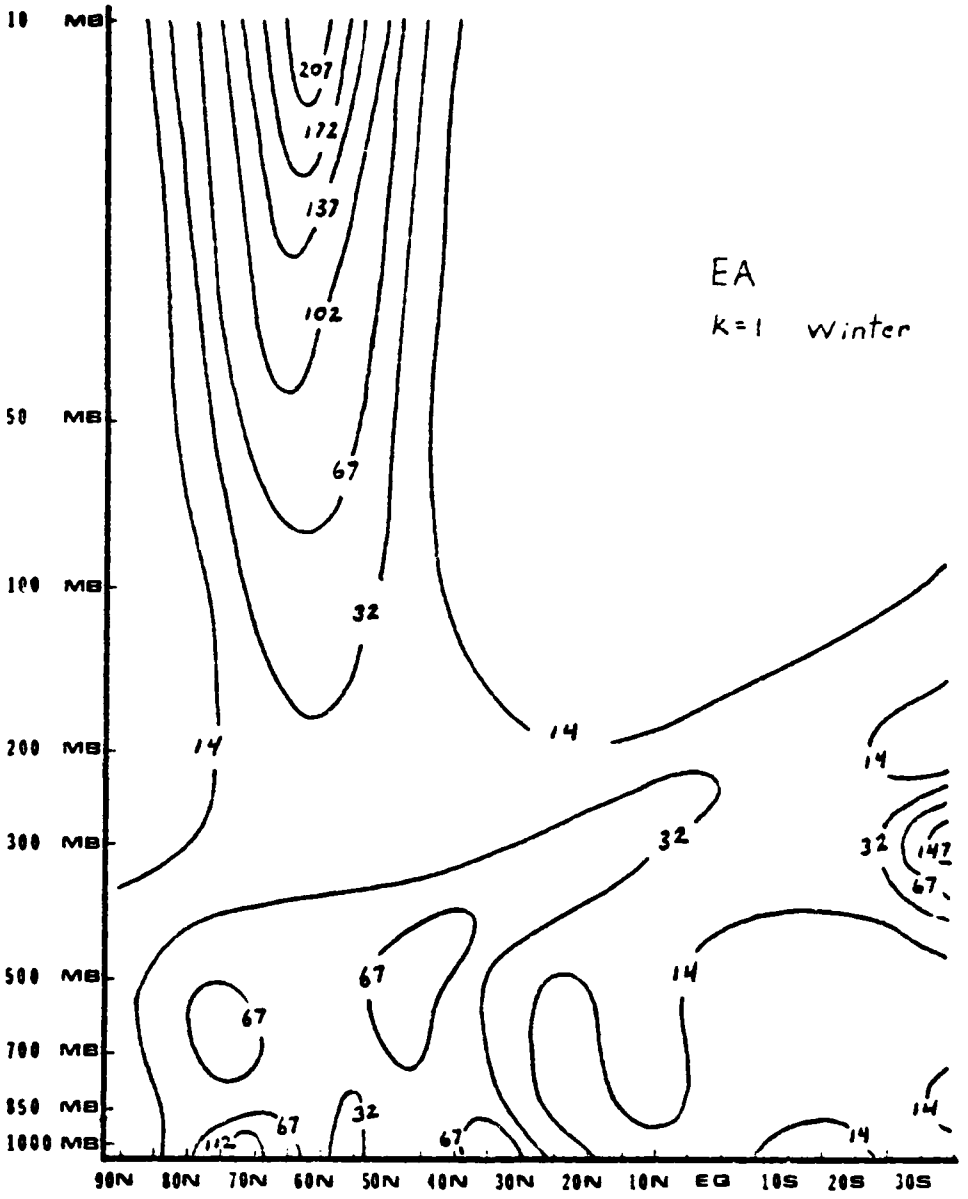


Figure 20. Cross section of the available potential energy distribution for wave number 1 during winter ($m^2/sec^2$).

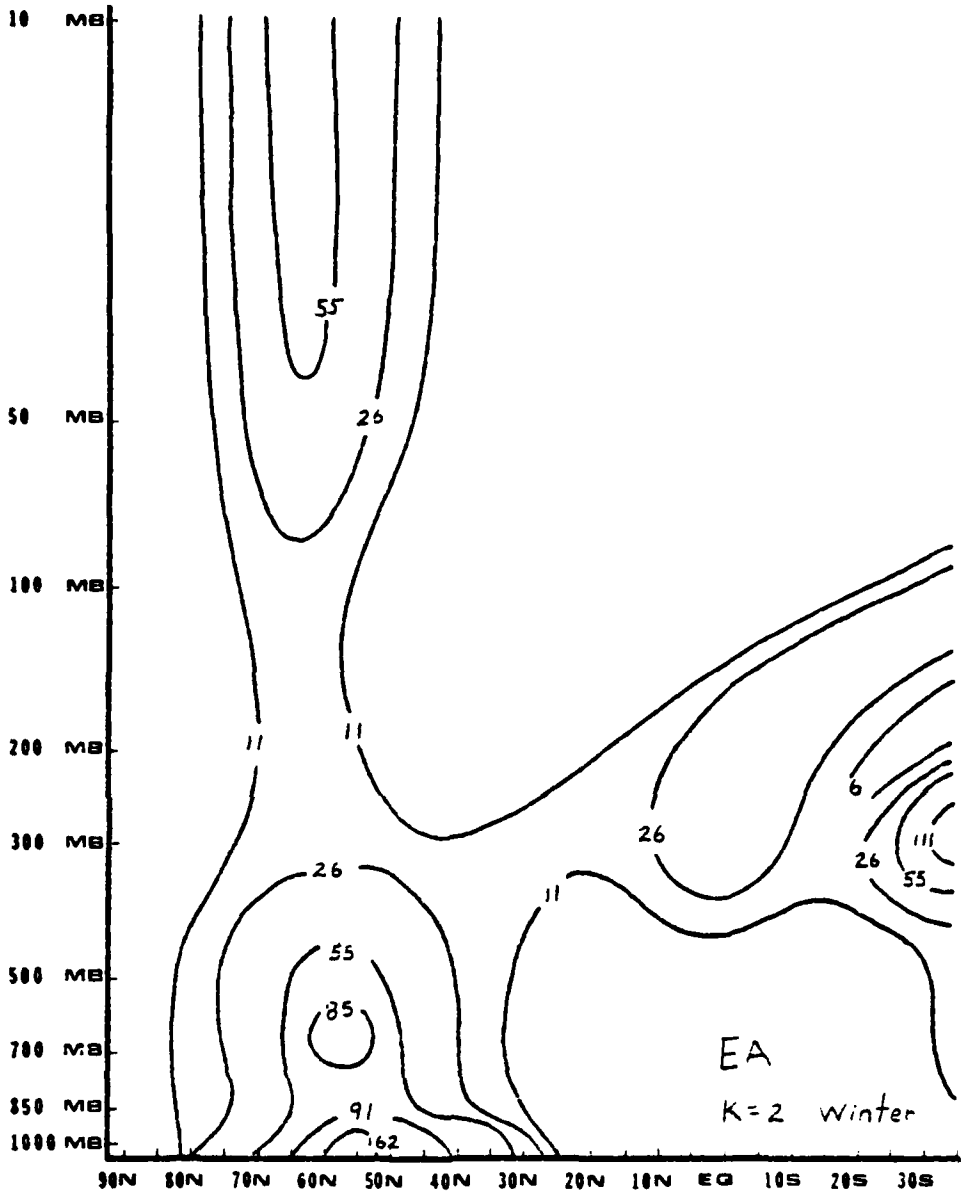


Figure 21. Cross section of the available potential energy distribution for wave number 2 during winter ($m^2/sec^2$).

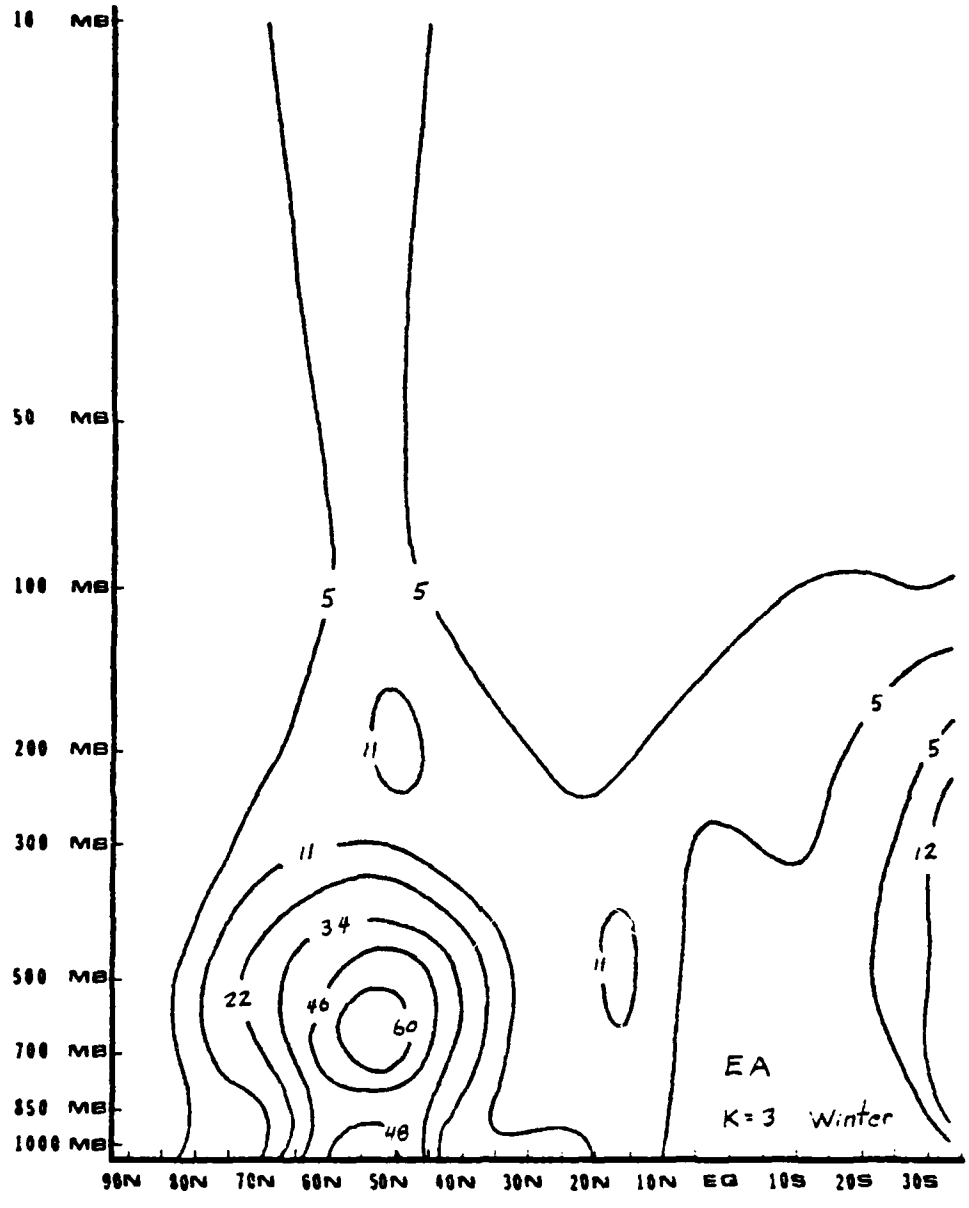


Figure 22. Cross section of the available potential energy distribution for wave number 3 during winter ($m^2/sec^2$).

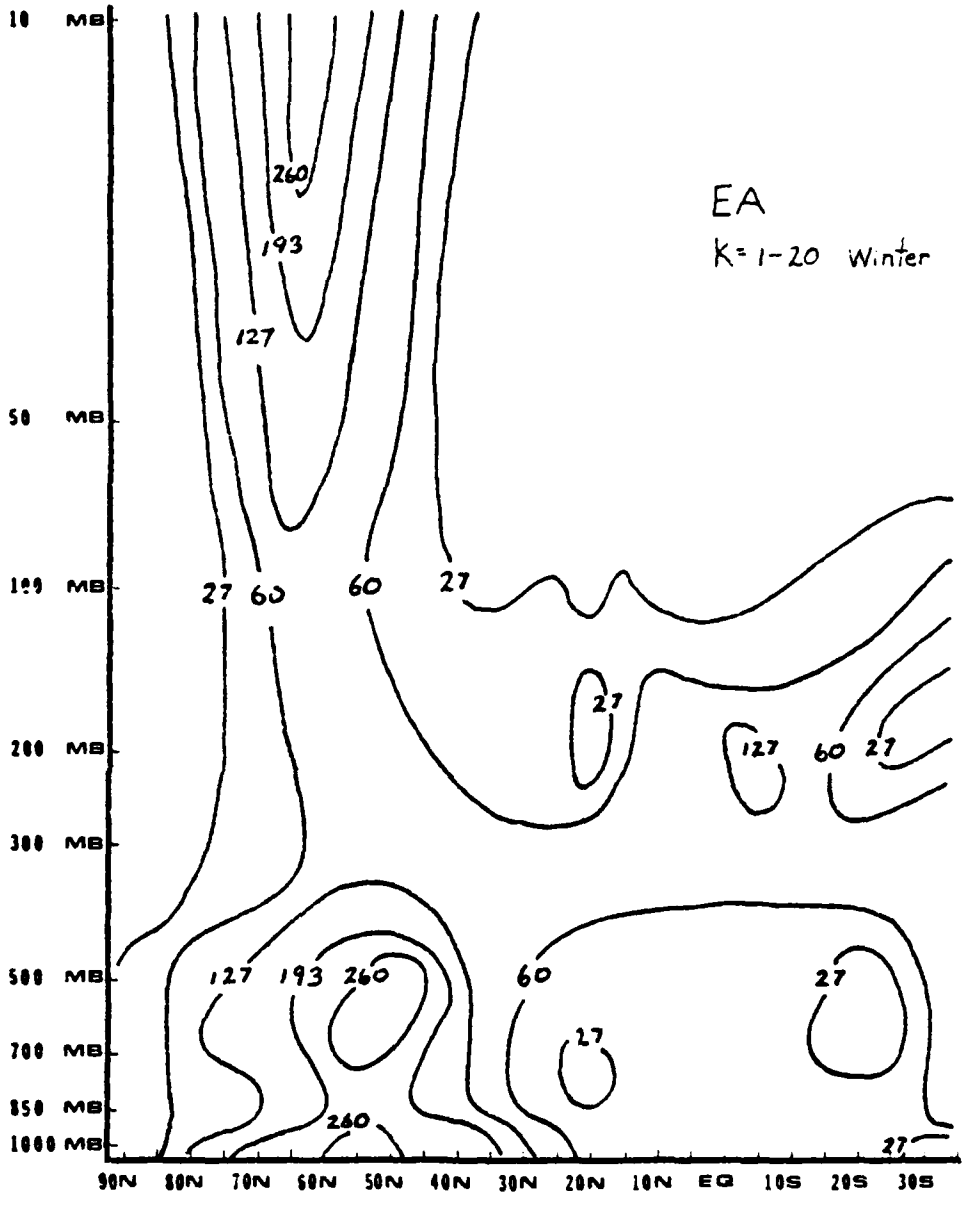


Figure 23. Cross section of the available potential energy distribution for wave numbers 1 - 20 during winter ($m^2/sec^2$).

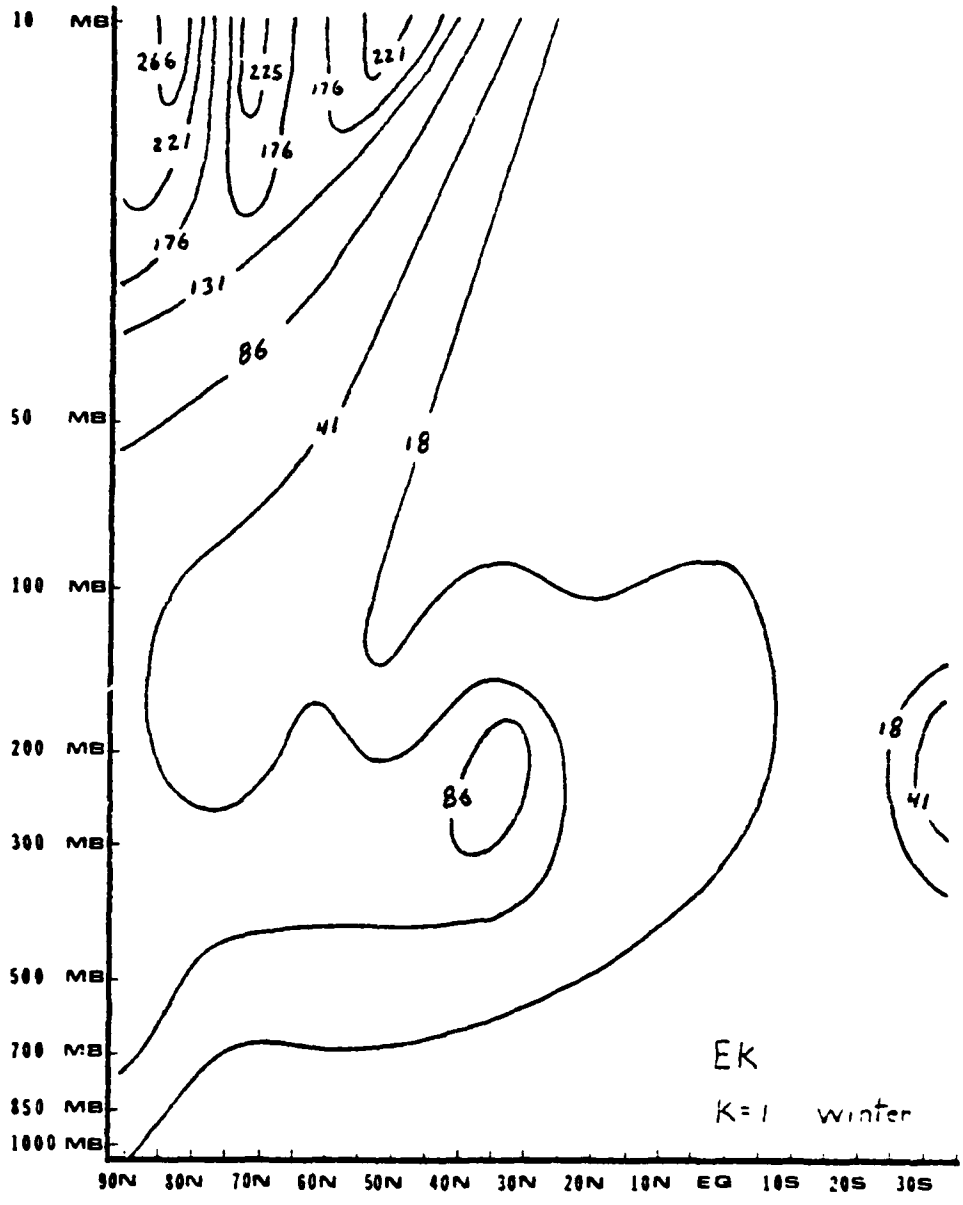


Figure 24. Cross section of the kinetic energy distribution for wave number 1 during winter ($m^2/sec^2$).

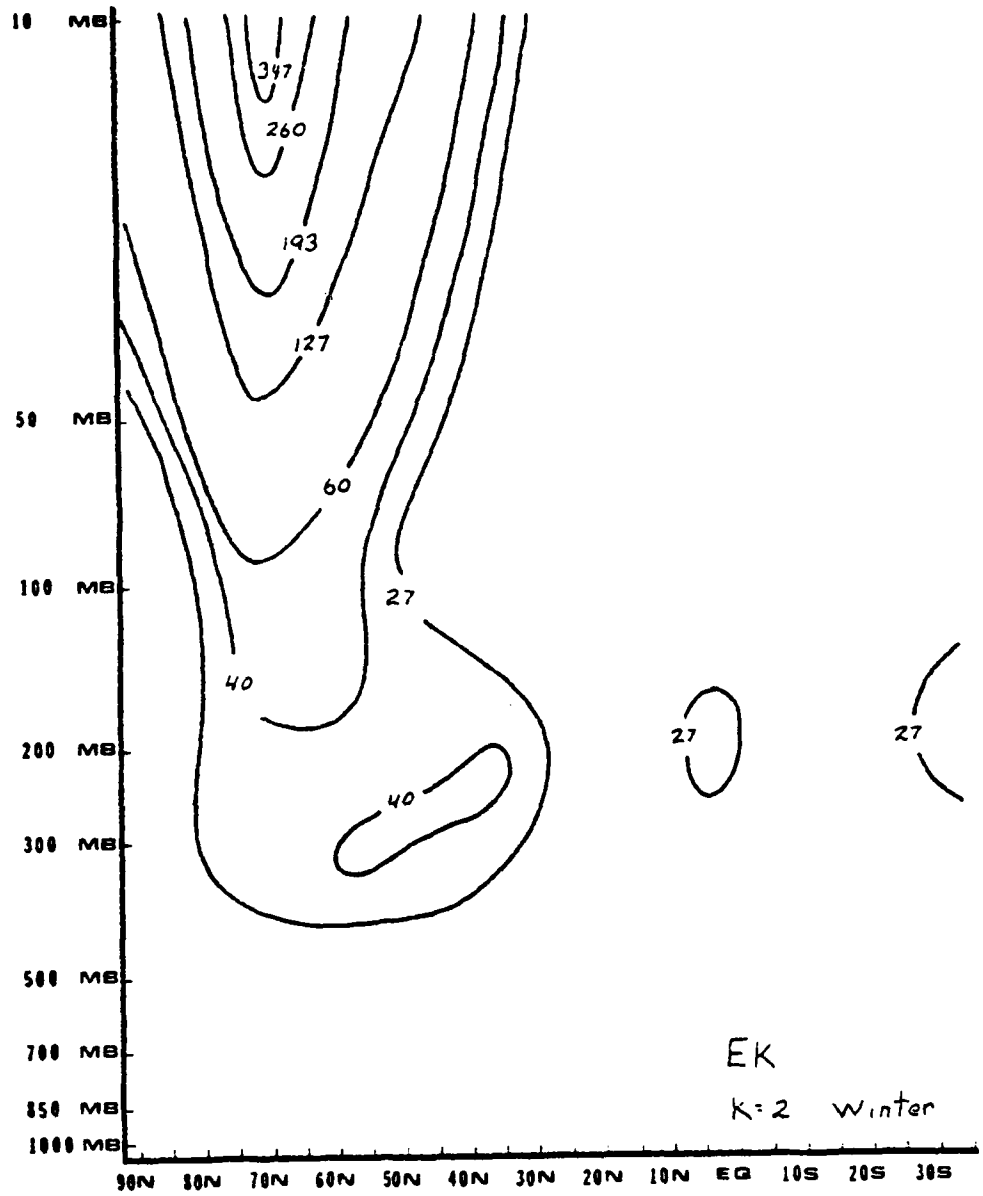


Figure 25. Cross section of the kinetic energy distribution for wave number 2 during winter ($m^2/sec^2$).

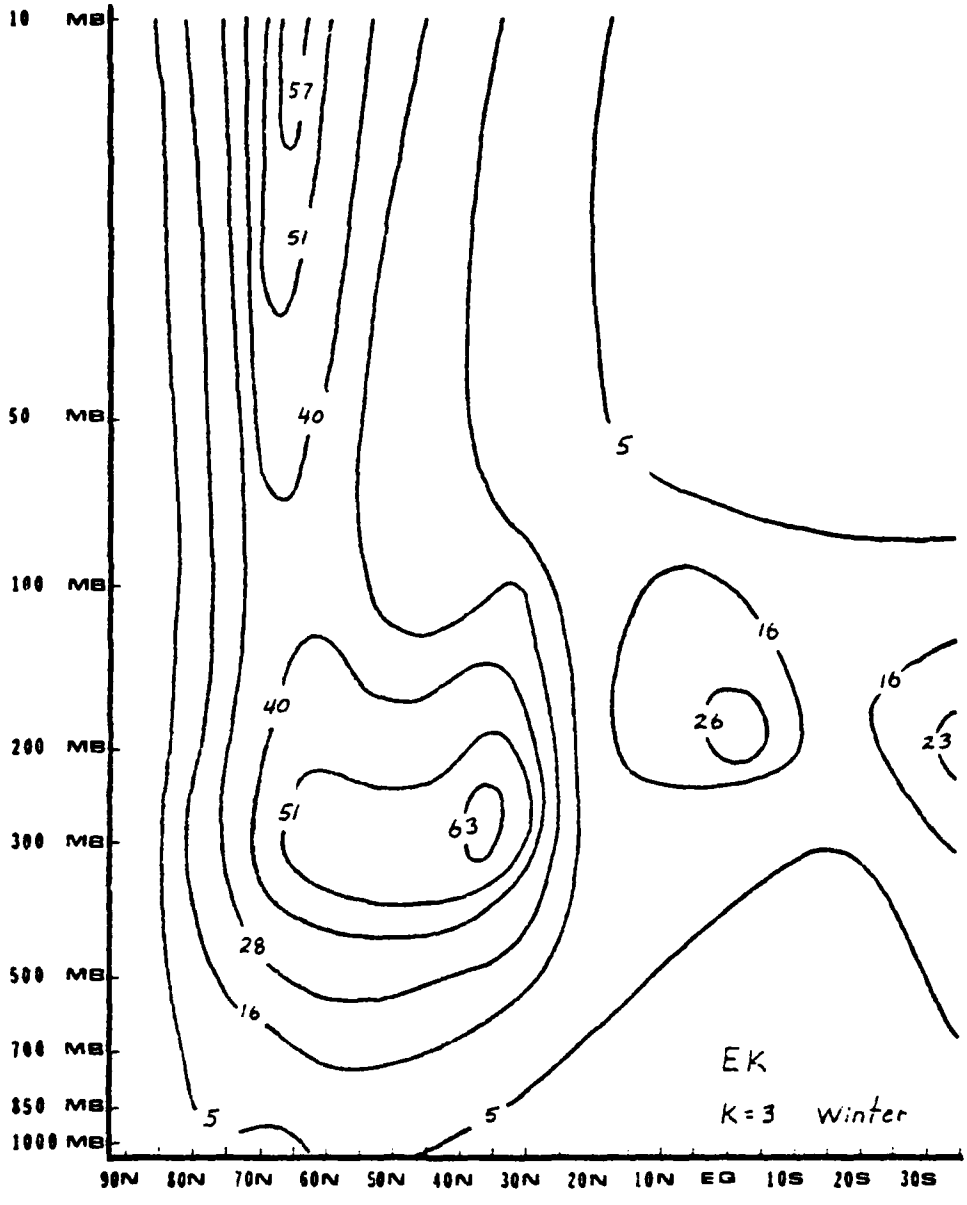


Figure 26. Cross section of the kinetic energy distribution for wave number 3 during winter ($m^2/sec^2$).

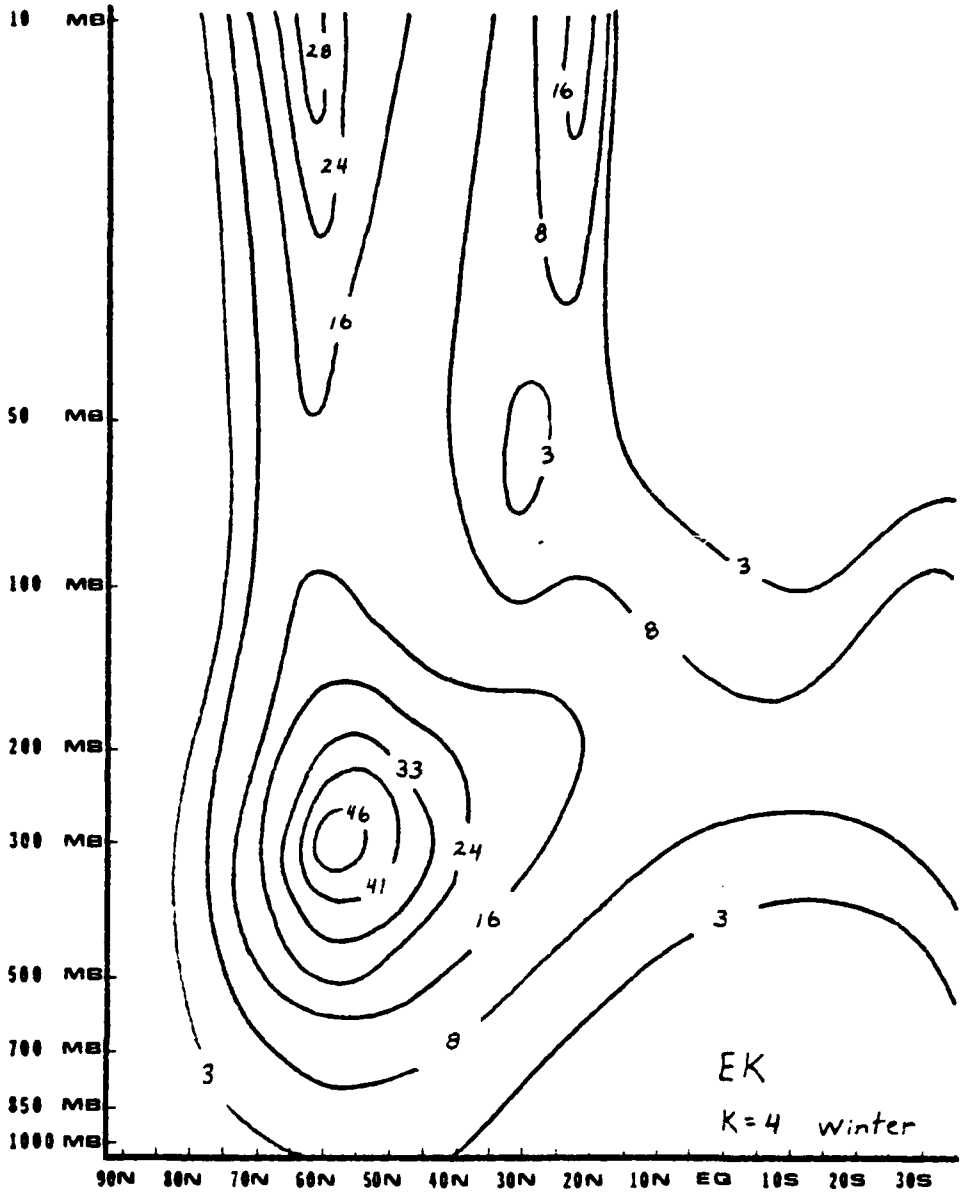


Figure 27. Cross section of the kinetic energy distribution for wave number 4 during winter ($m^2/sec^2$).

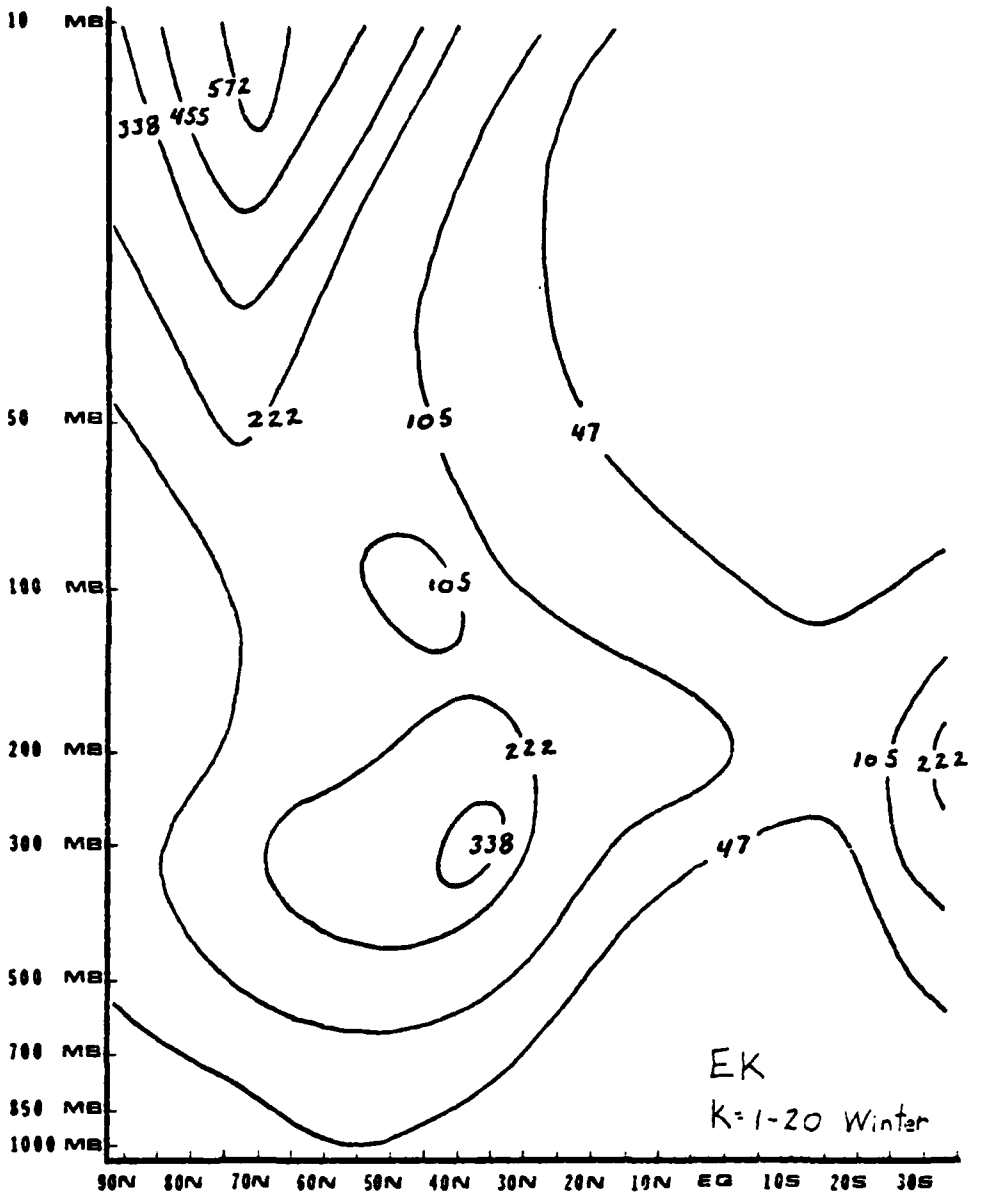


Figure 28. Cross section of the kinetic energy distribution for wave numbers 1 - 20 during winter ($m^2/sec^2$).

also presented. Our discussion here will concern only the winter season, since the intensities of kinetic energy and available potential energy are greater for this season, and the dynamics at work are more interesting.

Figures 18 and 19 present cross sectional distributions of kinetic energy and available potential energy associated with the mean zonal flow, i.e., wave number zero. The kinetic energy distribution is exactly as expected from our earlier discussion of seasonal mean U-component of the wind, and centers of maximum kinetic energy correspond exactly with centers of maximum mean zonal wind velocity shown in Figure 2. However, the bimodal distribution of tropospheric available potential energy may be somewhat unexpected. The bimodal distribution of available potential energy is strongly associated with the method of computation used for wave number zero. The distribution can be understood clearly by considering the mean winter temperature cross section (Figure 5) and the following discussion. The mean values of available potential energy plotted for wave number zero are not computed directly from the mean temperatures around each latitude circle, but are computed using temperature deviations defined by

$$T' = \overline{T}_L - \overline{T}_A \quad , \tag{4.4}$$

where $T'$ is the deviation from the area averaged temperature, $\overline{T}_L$ is the mean temperature around a latitude circle, and $\overline{T}_A$ is the area averaged temperature given by (4.3). In this study there were two computational areas, determined by our two data sources.

The northern region, where only NMC data were used, consisted of 20°N to 85°N, while data for remaining area form 15°N to 35°S were supplied by the Air Force. Applying (4.4) to the northern region temperatures seen in Figure 5 will produce fairly large values of T' at the extremities of the region, and therefore large values of available potential energy. The same effect will not be seen for the southern region, due to the relatively constant temperatures observed south of 20°N. Does this mean the results presented in Figure 19 may be somewhat artificial? Probably not, as the concept of available potential energy itself requires definition of an area over which computation is to be done (Lorenz, 1955). One can only choose his area in a meaningful way. In the current study, the 20°N southern limit is probably a reasonable one independent of data source, since the southern edge of the Hadley cell (Figure 3) is also at 20°N.

Some extremely interesting features may be seen in Figures 20 through 28. Consider first Figures 20 through 23, representing spatial distribution of available potential energy for wave numbers 1, 2, 3, and the summation of wave numbers 1 through 20. For wave number 1 (Figure 20), a strong maximum of available potential energy appears at 10 mb near 65°N, with relatively weak values generally scattered about the troposphere. Figure 21, for wave number 2, appears to show a transition feature, with the stratospheric maximum greatly reduced and the appearance of a very well defined, moderately strong, tropospheric maximum near 55°N. Wave number 3, shown in Figure 22, gives a reversed picture of

Figure 20, and now a strong tropospheric maximum of available potential energy exists at 600 mb near 53°N. The stratospheric maximum has completely disappeared. Figure 23 indicates that total eddy available potential energy fluctuation has two maxima of equal strength, one located near 65°N, 10 mb, and the other near 50°N below 500 mb.

The meaning of the sequence above is clear. Wave number 1 is of paramount importance in northern latitude stratospheric dynamics, wave number 2 has nearly equal effect in the northern latitude stratosphere as it does in the northern latitude troposphere, and the wave number 3 is almost exclusively of great importance in the dynamics of available potential energy in the northern latitude troposphere.

The sequence of Figures 24 through 28 show similar features, except for kinetic energy rather than for available potential energy. In Figure 24, representing the distribution of the kinetic energy spectrum for wave number 1, very large values are noted in the northern stratosphere, with a secondary maximum near the middle latitude tropospheric jet stream. Wave number 2 (Figure 25) shows a marked tendency to extend the stratospheric maximum into the troposphere, although the extreme maximum values remain in the stratosphere. Recall in the discussion of Figure 10, we assumed that the extent of the transition into the troposphere was responsible for the tropospheric minimum energy spectra values observed for wave number 2. Figure 26, for wave number 3, shows the transition continuing, with nearly equal values for both stratospheric

and tropospheric maximum values of kinetic energy. Figure 27, the cross section for wave number 4, shows a continuation of this process, with the tropospheric maximum at 300 mb near 55°N obtaining twice the value of the major stratospheric maximum at 10 mb and 60°N. As in the case of available potential energy, the summation over all wave numbers for kinetic energy also indicates a composite of features just described. Again the interpretation is clear. Wave numbers 1 and 2 are vitally important to stratospheric kinetic energy dynamics, but show considerably smaller magnitude in the troposphere. It is also of interest to note that the stratospheric warming itself is essentially a wave number 1 phenomena. Wave number 3 has about equal influence on the stratosphere and troposphere, but wave number 4 operates primarily in tropospheric kinetic energy dynamics.

It may be noted that the eddy kinetic energy in the stratosphere is essentially the contribution of the extra-long waves ($k = 1, 2, 3, 4$), whereas that in the troposphere is the contribution of both the planetary and synoptic scale waves. The eddy available potential energy is essentially contributed by the extra-long planetary waves in both the stratosphere and troposphere.

## 4.3 Maintenance of Energetics of the Large Scale Waves in the Stratosphere and Troposphere

### 4.3.1 Hemispheric averaging

To analyze the major mechanisms of energy transfer within the atmosphere, all terms of (2.16) and (2.17) were first averaged in

time over the appropriate season. The time averaged distributions of kinetic energy and available potential energy were discussed in section 4.2.2 and are presented in Figures 18 through 28. All other time averaged distributions for the winter season which are not specifically discussed in this paper, with exceptions of time averaged boundary terms, are presented for completeness in Appendix A. The time averaged distributions were then averaged over the mass of the Northern Hemisphere stratosphere and troposphere by applying

$$\frac{\int_M Q \, dM}{\int_M dM} , \tag{4.5}$$

where Q is any terms of (2.16) or (2.17). Expanding (4.5) we have

$$\frac{\int_{P_2}^{P_1} \int_{\phi_1}^{\phi_2} \int_0^{2\pi} \frac{Q}{g} (a \cos\phi \, d\lambda)(a \, d\phi) \, dp}{\int_{P_2}^{P_1} \int_{\phi_1}^{\phi_2} \int_0^{2\pi} \frac{1}{g} (a \cos\phi \, d\lambda)(a \, d\phi) \, dp} , \tag{4.6}$$

or, in final form,

$$\frac{1}{(P_1 - P_2)(\sin\phi_2 - \sin\phi_1)} \int_{P_2}^{P_1} \int_{\phi_1}^{\phi_2} Q \cos\phi \, d\phi \, dp . \tag{4.7}$$

The stratosphere was defined between 0 mb and 200 mb, while the troposphere integration limits were 200 mb and 1010 mb. All averaged values were then plotted as shown in Figure 29. In dia-

grams to follow, the averaged value of a given term of (2.16) or (2.17) will be placed in the same location as the name of the term as plotted in Figure 29. Terms of the kinetic energy equation (2.16) appear on the right hand side of Figure 29, while terms of the available potential energy equation occur on the left hand side. All terms appearing in the upper portion of Figure 29 have been integrated over the stratosphere for a given wave number, while terms in the lower portion of the figure were integrated over the troposphere. Dashed lines represent energy transfer in the stratosphere and solid lines represent energy transfer in the troposphere. Note that two locations are reserved for each of NAB2, NKB2, and AKB2. These are vertical transfer terms and give the flux of energy between the stratosphere and the troposphere. The upper location is for the energy transfer value per unit mass of the stratosphere, whereas the lower location is for the energy transfer value per unit mass of the troposphere. While the same amount of flux leaving the troposphere enters the stratosphere, the per unit mass value of flux averaged over the troposphere differs from the per unit mass value averaged over the stratosphere. The numerical values appearing in the two locations will not be the same, but they do represent the same amount of energy (the stratosphere value may be obtained from the troposphere value by multiplying the latter by 310/200). Also, the two plotted vertical flux values will not be of the same sign, since one area (stratosphere or troposphere) is losing energy while the other is gaining energy. The wave number for which integration

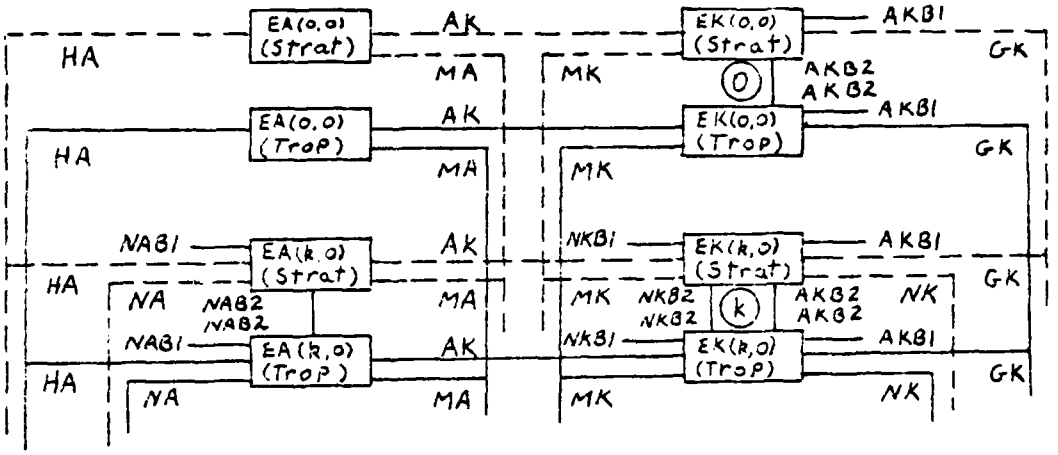


Figure 29. Plot model showing the location of averaged terms of the available potential and kinetic energy equations.

was carried out will replace the "k" appearing within the circle on the right hand side of Figure 29. A brief description of each term appearing in Figure 29 is given in Table 2. In discussions to follow, the terms defined in Table 2 will frequently be used by themselves without further explanation.

### 4.3.2 Mean energy transfer

Figures 30 and 31 show the results obtained for Northern Hemisphere integration over the winter season. Note again that terms GK and HA were determined as the residual of (2.16) and (2.17), and therefore contain sub-scale wave interactions. Because of this, these terms can act as energy sources or as energy sinks.

The large amount of data presented in Figures 30 and 31 is essential for detailed study of energy exchanges occurring in and between the stratosphere and the troposphere, but makes the extraction of important general conclusions difficult. For this reason, we have summarized these complex figures in the simplified model presented in Figure 32. Two types of arrows appear in this model. External arrows are outside of the small boxes representing available potential energy and kinetic energy. Each external arrow is associated with an averaged term of (2.16) and (2.17) and corresponds to the locations specified in Figure 29. Each external arrow points in the direction of predominant energy flow associated with the term represented by the arrow. When numbers appear above an external arrow, they represent wave numbers for which observed energy flow direction is not the same as that indicated by the arrow. Internal arrows, appearing within the kinetic and available

Table 2. Definition of terms contributing to the rates of change of kinetic and available potential energy.

| Term | Definition |
|---|---|
| EK | Kinetic energy |
| $EK_t$ | Rate of change of EK with time |
| NK | Contribution of the nonlinear wave interactions to $EK_t$ |
| MK | Contribution to $EK_t$ of interactions involving waves and the mean flow |
| AK | Contribution to $EK_t$ through conversion of EA to EK |
| NKB1, NKB2 | Contribution to $EK_t$ by meridional and vertical convergence, respectively, of the nonlinear wave interactions |
| AKB1, AKB2 | Contribution to $EK_t$ by meridional and vertical convergence, respectively, of geopotential flux |
| GK | Contribution to $EK_t$ of the Reynolds and molecular stresses and sub-scale interactions |
| EA | Available potential energy |
| $EA_t$ | Rate of change of EA with time |
| NA | Contribution of nonlinear interactions of temperature and velocity waves to $EA_t$ |
| MA | Contribution to $EA_t$ of interactins involving waves and the meridional gradient of the zonal mean temperature |
| NAB1, NAB2 | Contribution to $EA_t$ by the nonlinear meridional and vertical convergence, respectively, of flux of EA |
| KA | Contribution to $EA_t$ through conversion of EK to EA |
| HA | Contribution of diabatic heating or cooling and of sub-scale wave interactions to $EA_t$ |

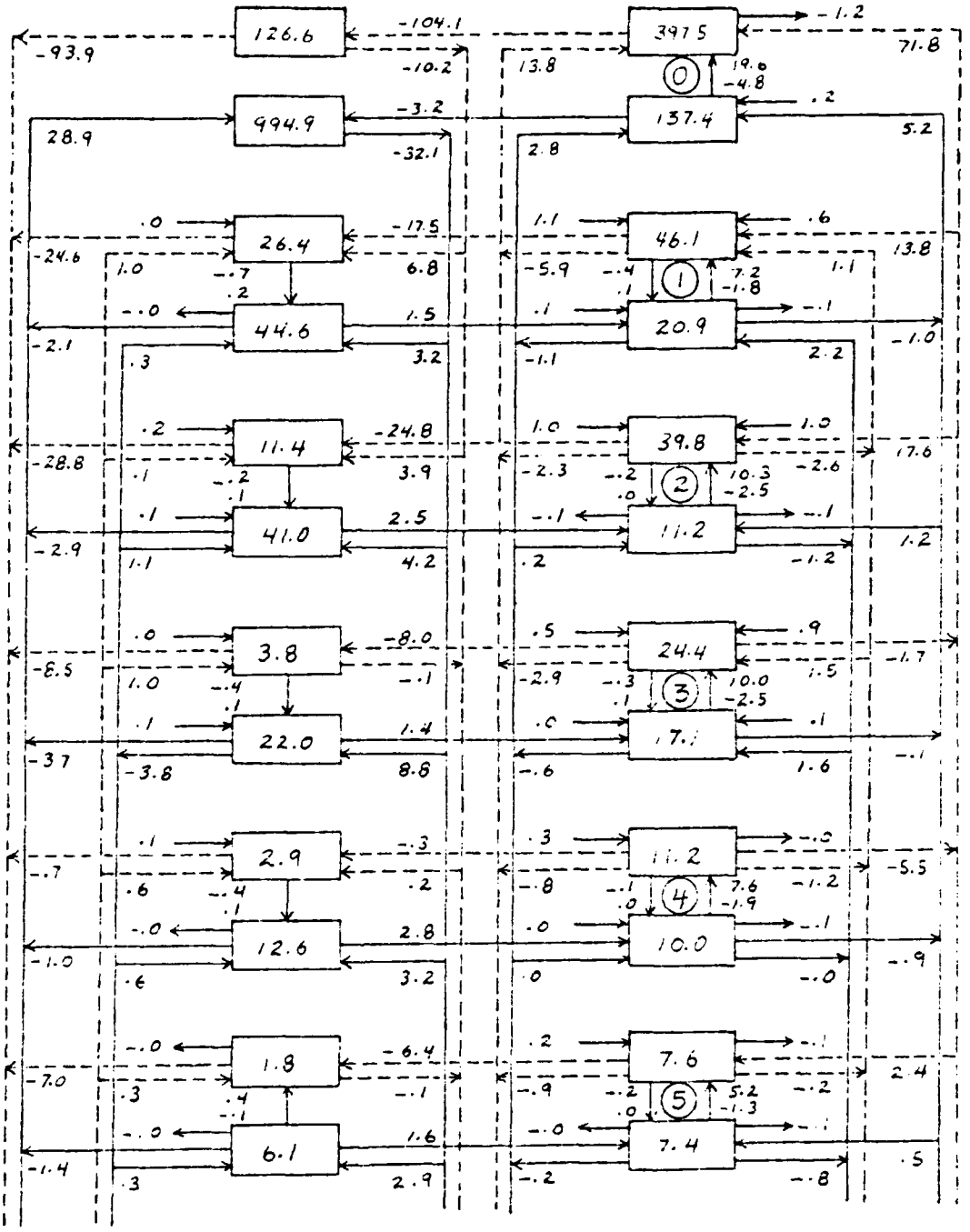


Figure 30. Transfer diagram of atmospheric energy for winter average conditions for wave numbers 0 - 5 over the Northern Hemisphere. Energy fluxes are in $m^2/sec^2/day$, while EK and EA within the boxes are $m^2/sec^2$.

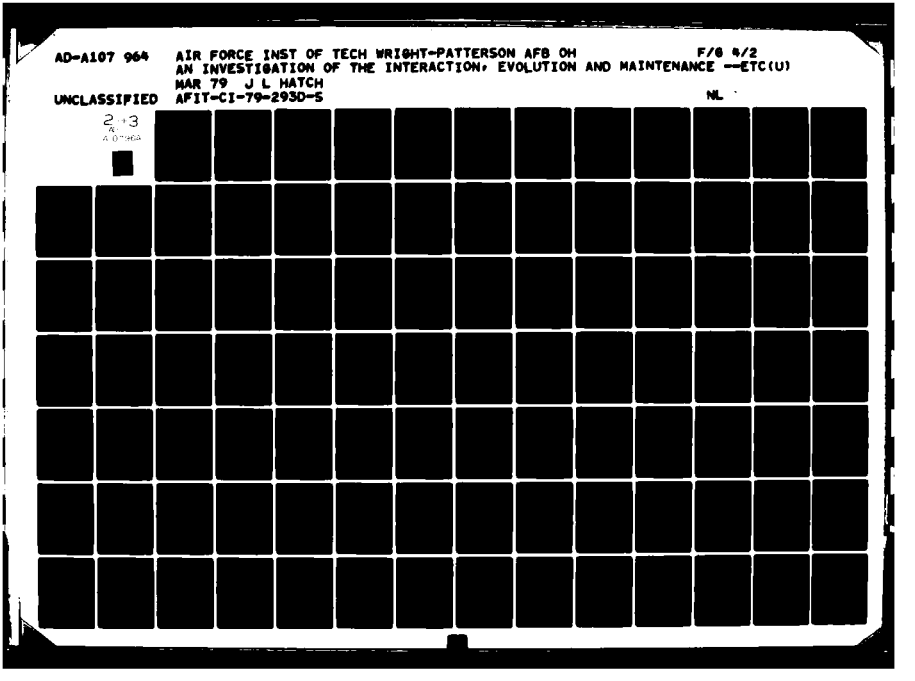
AD-A107 964
AIR FORCE INST OF TECH WRIGHT-PATTERSON AFB OH
F/G 9/2
AN INVESTIGATION OF THE INTERACTION, EVOLUTION AND MAINTENANCE --ETC(U)
MAR 79 J L HATCH
UNCLASSIFIED
AFIT-CI-79-293D-5
NL
2 +3
A
A07964

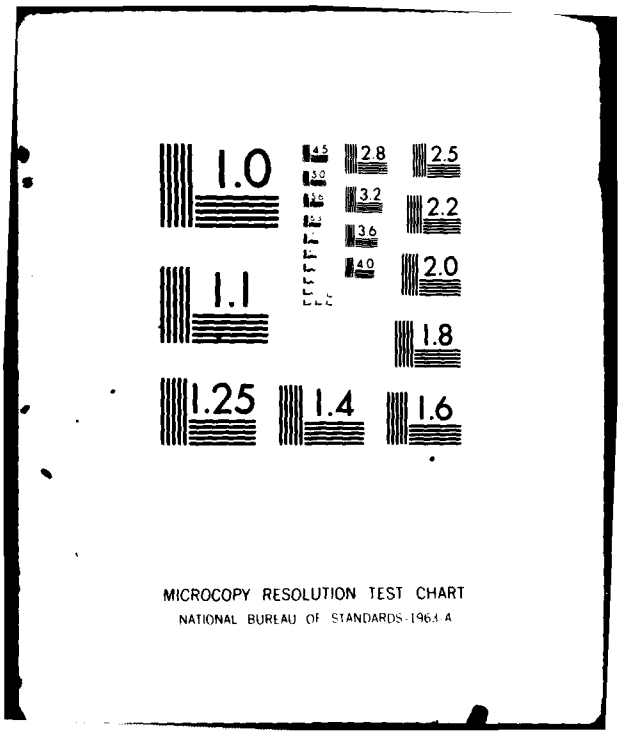
1.0
1.1
1.25
1.4
1.6
1.8
2.0
2.2
2.5
2.8
3.2
3.6
4.0
4.5
MICROCOPY RESOLUTION TEST CHART
NATIONAL BUREAU OF STANDARDS-1963-A

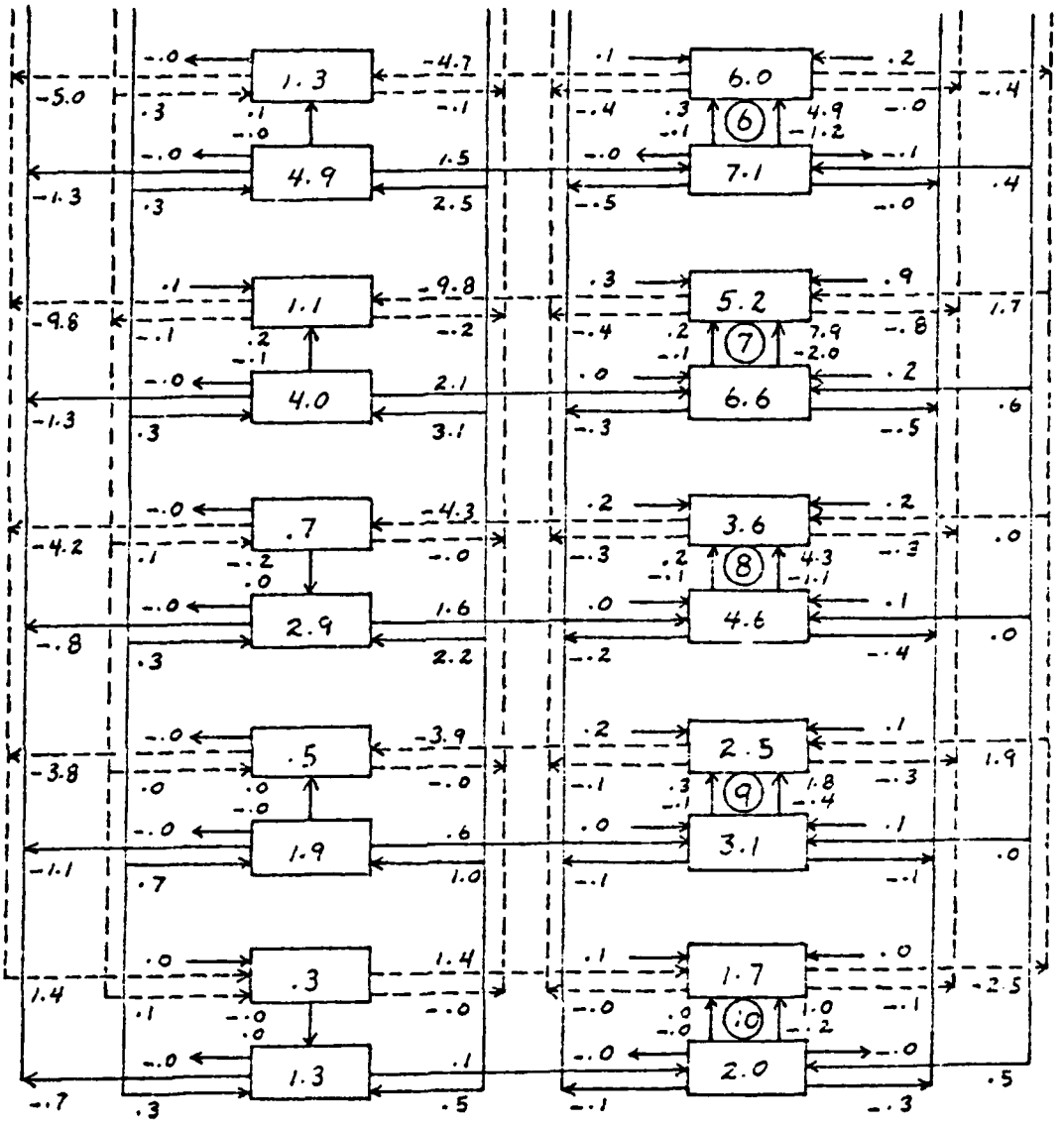


Figure 31. Transfer diagram of atmospheric energy for winter average conditions for wave numbers 6 - 10 over the Northern Hemisphere. Energy fluxes are in $m^2/sec^2/day$, while EK and EA within the boxes are $m^2/sec^2$.

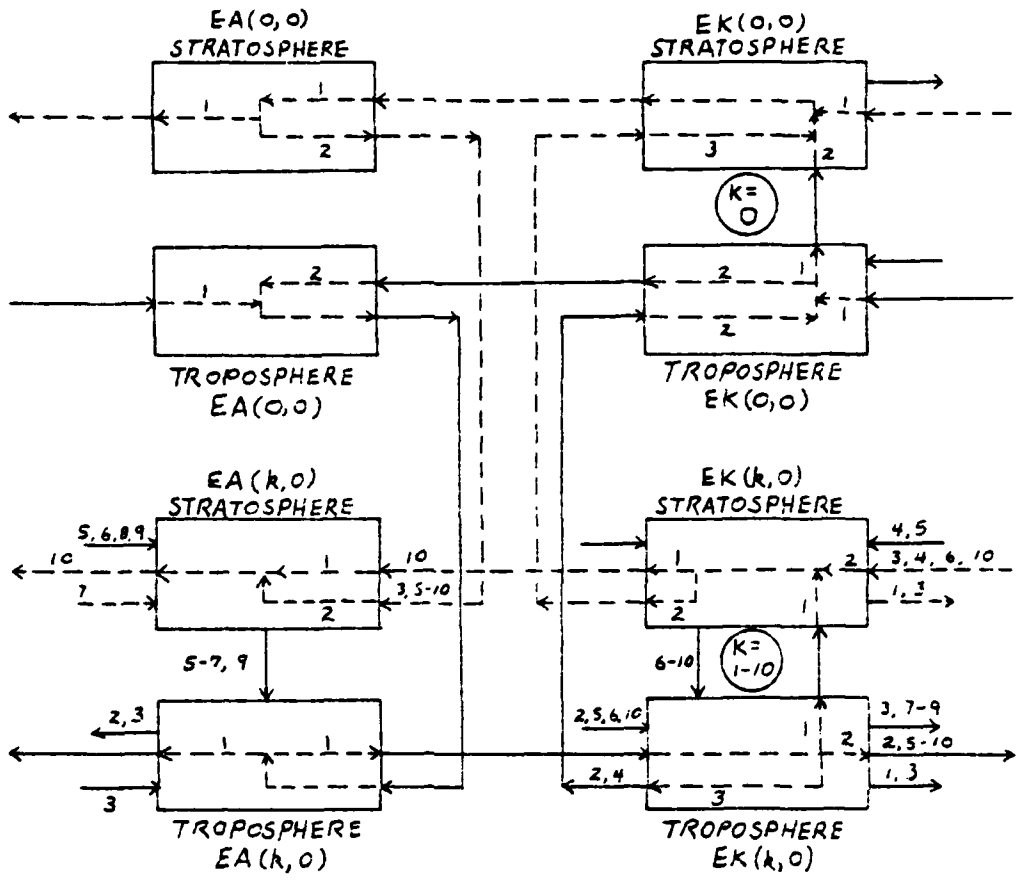


Figure 32. Model showing major average energy flow through the stratosphere and troposphere for the Northern Hemisphere during the winter season.

potential energy boxes, represent the direction of major energy flow into and out of the available potential energy and kinetic energy of the atmosphere. The numbers associated with internal arrows indicate the relative strength of the energy input or output. The most intense source or sink is labeled as "1", the second most intense as "2", and so on. When two sources or sinks of energy are labeled with the same number, both are of the same intensity.

Before discussing the major energy flow depicted in Figure 32, some comments on wave number 0 are required. In striking contrast to the wave number 0 data collected by Saltzman (1970), Figure 32 shows that energy is primarily supplied through sub-scale interactions (GK) in both the stratosphere and the troposphere. The reason for this difference may be found in the area of integration used in the current study opposed to the area actually integrated by authors summarized by Saltzman. Nearly all authors referenced by Saltzman performed integration between 20°N and 80°N, only six referenced papers contained data above 100 mb, and only two contained the 10 mb level. It should be pointed out that Flattery analysis data, used exclusively in this study, was not available in 1970. With the above in mind, consider again the wave number 0 cross sections for omega and temperature (Figures 4 and 5). Note that the intersection of maximum upward vertical motion with the coldest observed temperatures occurs at 100 mb and 5°N, outside the area of any of the integrations included in Satlzman's paper. In the region where this intersection takes place, strong

conversion of kinetic energy to available potential energy must take place (cold air rising). This feature is seen clearly in Figure 33, a cross section display of the winter mean energy conversion values. Also note, in Figure 33, that tropospheric values of AK south of about 15°N are negative. Inclusion of this additional block of negative AK in hemispheric integration, as was done in the current study, is all that is required to reverse the sense of energy conversion for the whole hemisphere.

To demonstrate the above, we carried out integration from 90°N to 20°N. These results are presented in Figures 34 and 35. A model was also constructed from these figures, and is presented as Figure 36. Note that by simply changing the area of integration, we have essentially reversed the sense of energy flow through both the stratosphere and the troposphere for wave number 0. That is, in the stratosphere, the major energy input to the mean EA is now seen to be the diabatic heating term HA. Some energy is transferred into the stratospheric eddy EA through action of MA, but most of the mean available potential energy is converted to mean kinetic energy by way of AK. The mean stratospheric kinetic energy also recieves energy from the stratospheric eddy EK through MK and through the vertical convergence of geopotential flux, AKB2. The mean stratospheric EK thus obtained, is now seen to transfer out of the system through GK. In the troposphere, the mean EA also receives energy from HA; however, the majority of tropospheric mean available potential energy transfers to tropospheric wave EA through MA. The remainder of tropospheric mean EA becomes a secondary source of tropospheric mean EK through the

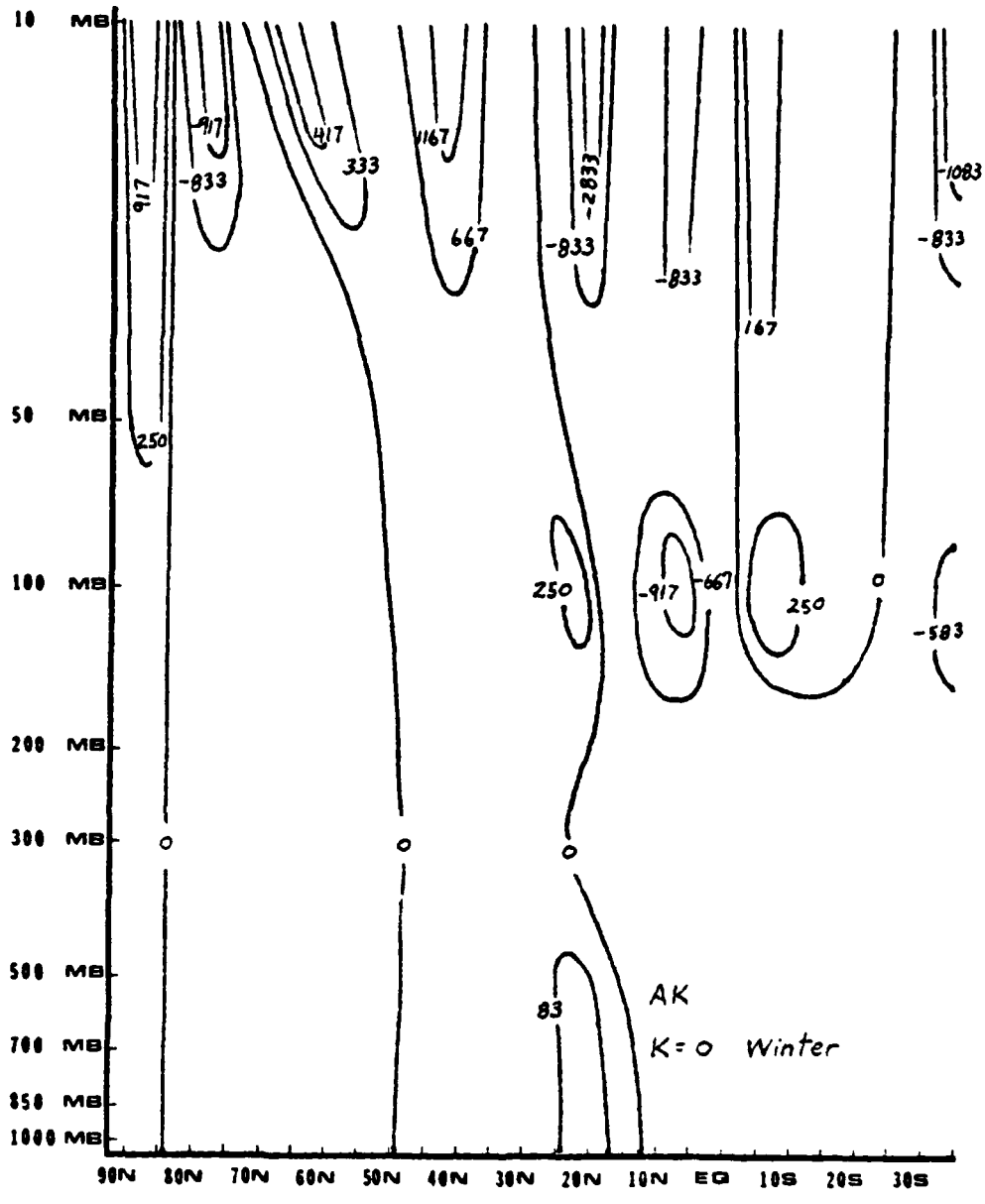


Figure 33. Distribution of mean energy conversion from available potential energy to kinetic energy for the winter season ($m^2/sec^2/day$).

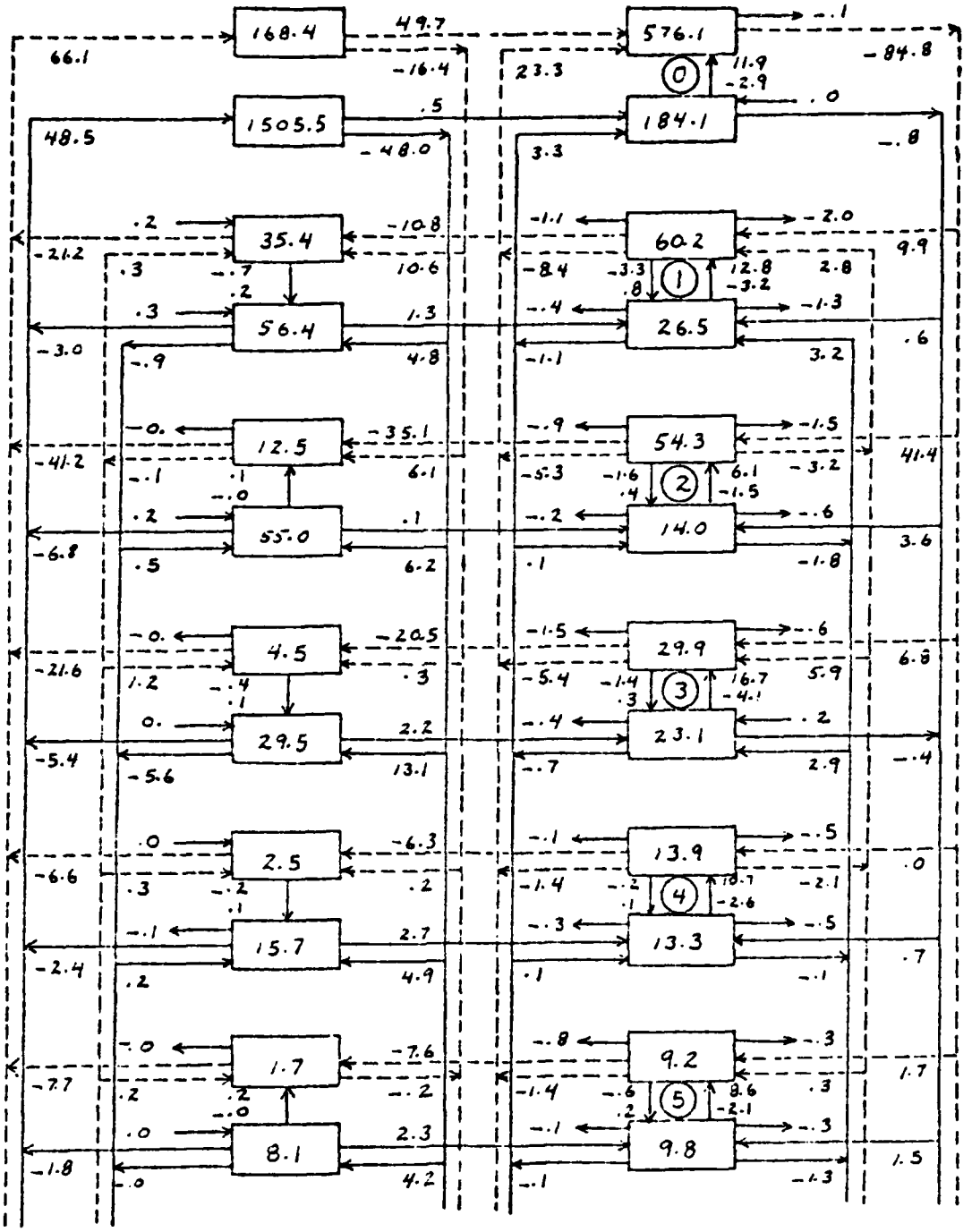


Figure 34. Transfer diagram of atmospheric energy for winter average conditions for wave numbers 0 - 5 over 90°N to 20°N. Energy fluxes are in $m^2/sec^2/day$, while EK and EA within the boxes are $m^2/sec^2$.

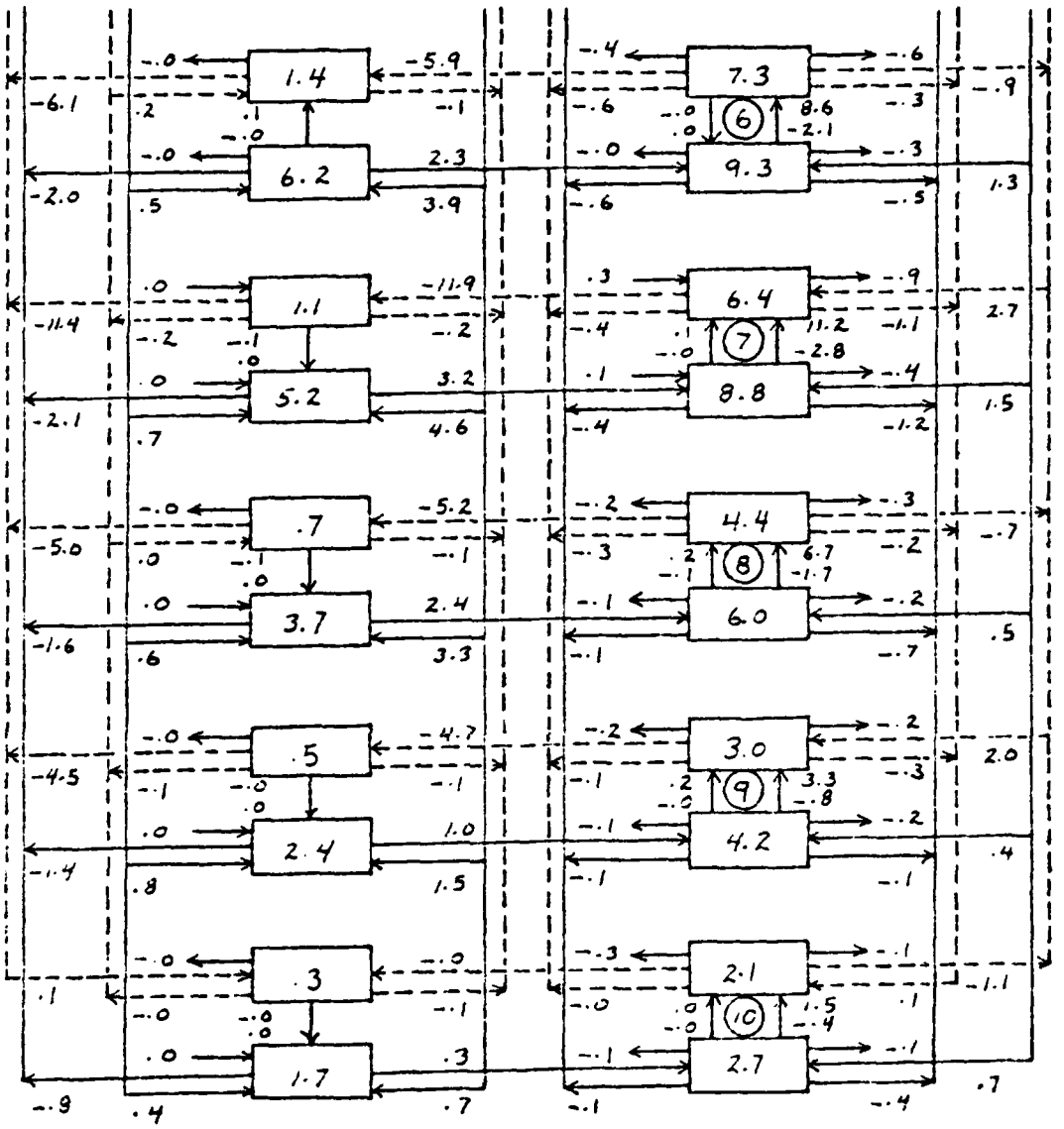


Figure 35. Transfer diagram of atmospheric energy for winter average conditions for wave numbers 6 - 10 over 90°N to 20°N. Energy fluxes are in $m^2/sec^2/day$, while EK and EA within the boxes are $m^2/sec^2$.

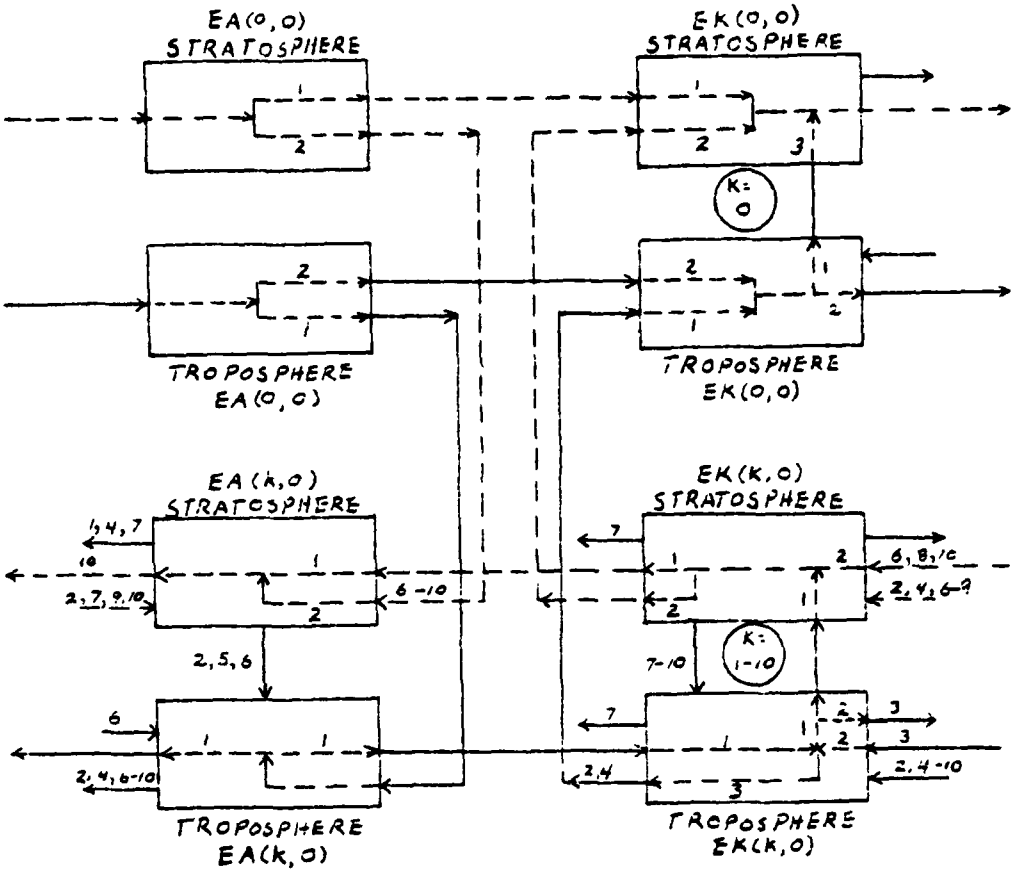


Figure 36. Model showing major average energy flow through the stratosphere and troposphere for 90°N to 20°N during the winter season.

conversion term AK. The primary source of tropospheric mean EK is seen to be energy transfer from tropospheric eddy kinetic energy. The mean tropospheric EK now transfers into the stratospheric mean EK through AKE2, or transfers out of the system by action of the Reynolds and molecular stresses (GK).

While Figure 36 agrees completely with Satlzman's work for wave number 0, we note a major departure from his results in the lower half of the diagram representing the major energy transfer summer over wave numbers 1 through 10. In this portion of Figure 36, for both stratosphere and troposphere, GK is seen to be an energy source, rather than a sink. For all wave numbers, except wave number 2, Saltzman showed this term as removing energy from the system. The reason for this difference is partly due to the difference in the area of integration and partly due to the inclusion of the boundary transfer terms, AKB1, AKB2, NKB1, and NKB2 in this study. In Figure 36, note that meridional boundary terms almost always transfer energy out of the system. More importantly, however, note that AKB2 always transfers considerable energy upward. If the stratosphere and troposphere were lumped together with an upper limit of vertical integration at around 50 mb, as was done by Saltzman, and if all boundary terms were included as part of the residual term (GK), then the current study would give results in almost complete agreement with those of Saltzman. All major paths of energy flow for wave numbers 1 through 10 shown in Figure 36 are the same as those shown in Figure 32, and are discussed below.

With the above differences from past work in mind, let us now consider Figure 32, and follow the energy flow through the most important path observed during the winter season. In the stratosphere, most energy is supplied through subscale interactions (GK) to the mean kinetic energy (EK). Additional energy inputs are seen to be the vertical convergence of geopotential flux (AKB2) and transfer of energy from kinetic energy waves (MK). The mean EK is subsequently converted to mean available potential energy (EA) through KA and is then primarily transferred out of the system by diabatic cooling (HA). Additional mean available potential energy is transferred to waves of available potential energy in the stratosphere through temperature, velocity interactions (MA), where it is subsequently transferred out of the waves through diabatic cooling.

In the troposphere, the mean kinetic energy receives energy through sub-scale interactions (such as thunderstorms) and transfer of energy from tropospheric waves of EK. The majority of the tropospheric mean kinetic energy is then transferred to stratospheric mean kinetic energy through vertical convergence of geopotential flux. Conversion to mean tropospheric available potential energy through KA is seen as a secondary mechanism of moving energy out of the mean kinetic energy. While some mean tropospheric EA is supplied by conversion from mean tropospheric EK, the contribution to the mean tropospheric EA through diabatic heating is far more important. In fact, this energy input will become the primary energy source driving major energy transfers in both stratospheric and tropospheric waves of kinetic energy and

available potential energy. The process begins by transfer of the mean tropospheric EA through MA to all tropospheric waves of available potential energy. This transfer from the mean EA is the major energy source driving tropospheric EA wave dynamics. Energy input to eddies of EA in this way is transferred out either through diabatic cooling and sub-scale wave interactions or is converted to kinetic energy in waves of the same wave number through AK, becoming the major energy source for tropospheric EK waves. Some of the tropospheric eddy EK now contributes to the tropospheric mean flow, and some is transferred out of the system through GK. Most of the eddy EK, however, is transferred to stratospheric eddy EK through AKB2, where it becomes the primary energy input for stratospheric EK waves. Some of the stratospheric EK transfers to the stratospheric mean flow by action of MK, but the majority of the energy is converted to stratospheric eddy EA through KA. Finally, the stratospheric eddy EA is transferred out of the system by diabatic cooling and sub-scale wave interactions.

Results obtained from integration over the Northern Hemisphere during the summer season are presented in Figures 37 and 38. Figure 39 gives the model for the summer season general energy flow, and is discussed below.

In contrast to winter, the energy flow associated with the mean EA had been completely reversed. Now diabatic heating becomes the major energy input to the stratospheric mean EA, and stratospheric waves of EA become a secondary source. The mean EA is then converted through AK to mean stratospheric EK. Energy from

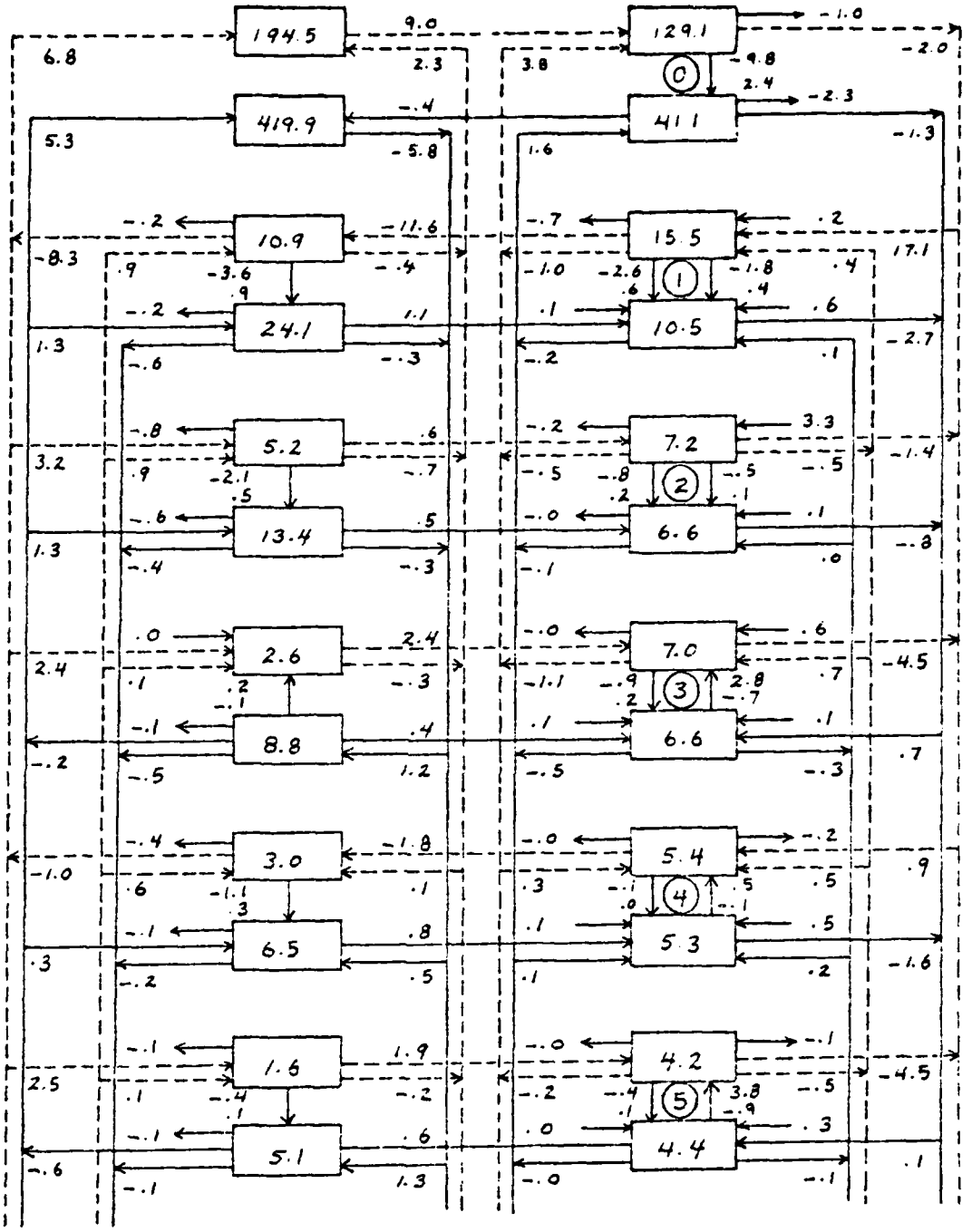


Figure 37. Transfer diagram of atmospheric energy for summer average conditions for wave numbers 0 - 5 over the Northern Hemisphere. Energy fluxes are in $m^2/sec^2/day$, while EK and EA within the boxes are $m^2/sec^2$.

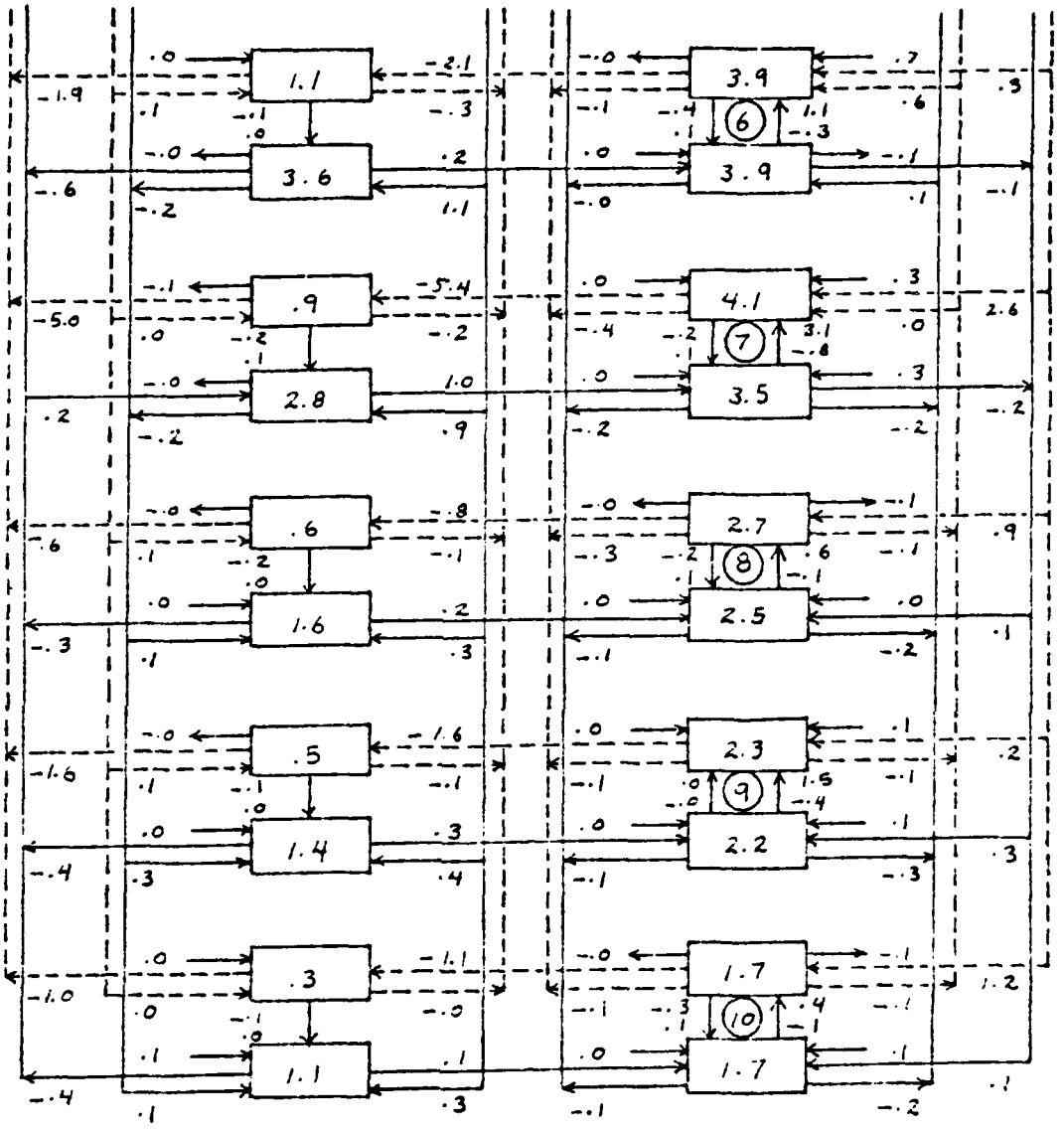


Figure 38. Transfer diagram of atmospheric energy for summer average conditions for wave numbers 6 - 10 over the Northern Hemisphere. Energy fluxes are in $m^2/sec^2/day$, while EK and EA within the boxes are $m^2/sec^2$.

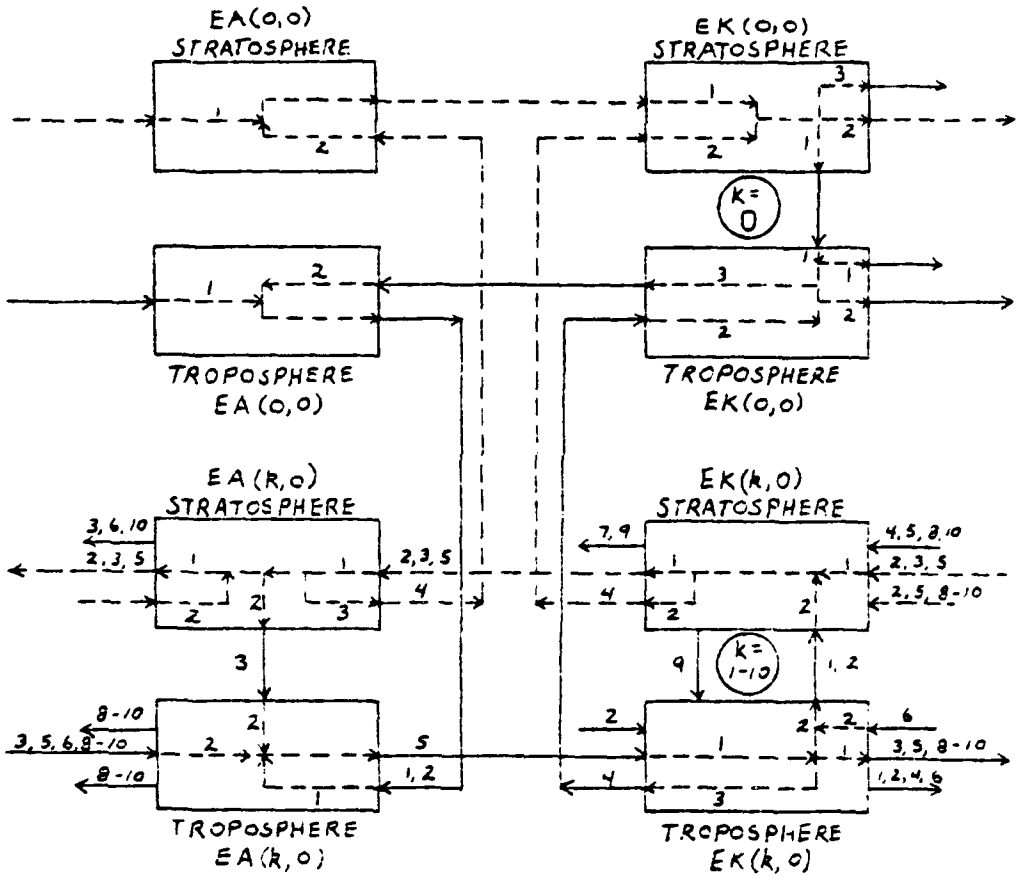


Figure 39. Model showing major average energy flow through the stratosphere and troposphere for the Northern Hemisphere during the summer season.

stratospheric waves of EK is also transferred into the mean flow. Some of the mean stratospheric EK is now removed from the system through GK and southward meridional energy transfer by the pressure work term AKB1; however, most of the energy is transferred through AKB2 into tropospheric mean kinetic energy. Some of the mean tropospheric EK is also transferred from tropospheric eddy EK through MA. In stark contrast to the winter situation, most of the tropospheric mean EK is now removed from the system through action of AKB1 transferring energy to the south and through GK, and only a small amount of the mean EK is converted through KA into mean tropospheric available potential energy. As for the winter case discussed earlier, diabatic heating is still the primary source of mean tropospheric EA; however, unlike the winter case, this energy input will not become the major energy source for all wave energy transfers. Rather, other energy sources will be seen to become dominant as we trace the path of major energy flow through the system.

At this point, we also encounter another type of division of energy not seen along the major path of energy flow discussed for winter. The entire path of major energy flow for winter (Figure 32), starting from input of energy by HA to the mean tropospheric EA, was characteristic of all waves of wave number 1 through 10, except in the very last step, where wave number 10 was an exception. For summer this is not the case, as waves of wave number 1 and 2 do not act in the same sense as waves of wave number 3 through 10 along the major energy paths in the troposphere, and

waves of wave numbers 2, 3, and 5 operate in the reversed sense of waves of other wave numbers along the major energy transfer path in the stratosphere. Despite these differences, the arrows drawn in Figure 39 still represent the direction of major energy flow through the composite system of wave numbers 1 through 10. The reader should be aware of the differences above, however, if more specific conclusions from Figure 39 are desired.

Returning again to the general path of major energy flow shown in Figure 39, we see that the tropospheric mean EA obtained by contributions from HA and KA transfers to tropospheric eddy EA through eddy heat transfer (MA), becoming the major energy source of tropospheric eddy available potential energy. Two other sources of tropospheric wave EA are seen to be HA and nonlinear downward energy transfer by NAB2. Tropospheric eddy available potential energy now becomes the major source of tropospheric eddy kinetic energy through the conversion term AK. An additional source of tropospheric eddy EK is the meridional convergence of geopotential flux (AKB1). Some of the tropospheric eddy EK is transferred to stratospheric eddy EK through AKB2 and some is transferred into the mean flow by MK, but most of the tropospheric eddy EK is removed from the system through GK. Whereas AKB2 was the primary source of stratospheric eddy EK in winter, AKB2 is the secondary source in summer, with the stratospheric sub-scale interactions embodied in GK becoming the most important energy input. Most stratospheric eddy kinetic energy is converted through KA to stratospheric eddy available potential energy; however, some of the

wave EK is transferred to the mean flow EK through MK. Finally, stratospheric eddy EA is primarily removed from the system by diabatic cooling and sub-scale wave interactions.

Winter and summer integrations were not only carried out for the whole Northern Hemisphere, but were also done for four latitude bands. Southern hemisphere, tropical, middle latitude, and polar bands were selected, and are given for completeness in Appendix B.

## 4.4 Energy Transfer at Boundaries

### 4.4.1 Development of linear boundary terms for the pressure gradient force

Applying (2.14) to (2.9) and (2.10), one arrives at (2.16). An important intermediate step in this computation involves the pressure gradient force of (2.9) and (2.10). When (2.14) is applied to these pressure forces alone, the result is

$$-\left\{\frac{g}{a}\left[V(-k,t)\,Z_{\phi}(k,t)+V(k,t)\,Z_{\phi}(-k,t)\right]\right.$$

$$\left.+\frac{igk}{a\cos\phi}\left[U(-k,t)\,Z(k,t)-U(k,t)\,Z(-k,t)\right]\right\} \qquad (4.8)$$

Substituting from (2.11) and (2.12) leads to

$$-\frac{g}{a\cos\phi}\left\{ik[U(-k,t)\,Z(k,t)-U(k,t)\,Z(-k,t)]\right.$$

$$+\frac{\partial}{\partial\phi}\left[\{Z(k,t)\,V(-k,t)+V(k,t)\,Z(-k,t)\}\cos\phi\right]$$

$$\left.-Z(-k,t)\,\frac{\partial}{\partial\phi}\left[V(k,t)\cos\phi\right]-Z(k,t)\,\frac{\partial}{\partial\phi}\left[V(-k,t)\cos\phi\right]\right\} \qquad (4.9)$$

$$= - g \left\{ [Z(-k,t)\ \Omega_p(k,t) + Z(k,t)\ \Omega_p(-k,t)] \right.$$

$$\left. + \frac{1}{a \cos\phi} \frac{\partial}{\partial\phi} [\{Z(k,t)\ V(-k,t) + Z(-k,t)\ V(k,t)\} \cos\phi] \right\} \quad (4.10)$$

$$= - g \left\{ \frac{1}{a \cos\phi} \frac{\partial}{\partial\phi} [\{Z(k,t)\ V(-k,t) + Z(-k,t)\ V(k,t)\} \cos\phi] \right.$$

$$\left. + \frac{\partial}{\partial P} [Z(k,t)\ \Omega(-k,t) + Z(-k,t)\ \Omega(k,t)] \right\}$$

$$- \frac{R}{P} [\Omega(-k,t)\ \theta(k,t) + \Omega(k,t)\ \theta(-k,t)] \quad (4.11)$$

$$= AKB1 + AKB2 + AK \quad . \quad (4.12)$$

That is, the effect of the pressure gradient force has been decomposed into a meridional pressure work term, a vertical pressure work term, and a term representing conversion of available potential energy to kinetic energy. These terms are of great importance in the atmosphere because the pressure gradient force generates energy. AKB1 and AKB2 will be discussed in detail later in this section.

4.4.2 Integration of boundary terms

Boundary terms are given by (2.22), (2.26), and (2.21). To arrive at the meridional energy transfer from these terms, we apply

$$\int_{\phi}^{\pi/2} \int_{0}^{2\pi} \frac{1}{\cos\phi} \frac{\partial B}{\partial\phi} (a \cos\phi\, d\lambda)(a\, d\phi) = - 2\pi a^2 B \quad , \quad (4.13)$$

where $1/\cos\phi \ \partial B/\partial\phi$ is AKB1, NKB1, or NAB1, and values of these terms at the north pole are assumed equal to zero. To produce the vertical transfer values, apply

$$\int_0^P \int_0^{2\pi} \frac{\partial C}{\partial P} (a \cos\phi \, d\lambda) \, dP = 2\pi a \, C \cos\phi \quad , \tag{4.14}$$

where $\partial C/\partial P$ is AKB2, NKB2, or NAB2, and all values at P = 0 mb are assumed to be zero. Values produced by application of (4.13) and (4.14) are total energy values, and therefore differ considerably from the per unit mass values discussed to this point. All figures representing this type of integration are so marked by appending an "I" to the appropriate term as, for example, AKB2I.

### 4.4.3 Characteristics of vertical and meridional energy transfer in the atmosphere

Figures 40 through 44 show cross section plots of the vertical transfer that is the integrated value of AKB2I for wave numbers 1 through 20 summed together, and for wave numbers 0, 1, 2, and 3. The dominant feature on Figure 40, the total eddy energy plot, is a giant positive area over most of the Northern Hemisphere troposphere and stratosphere with strong maximum upward forcing at 250 mb near 45°N. A secondary maximum positive center is seen near 35°S at 100 mb, and four smaller negative centers appear at 100 mb, 10°S; 600 mb, 35°S; 10 mb, 80°N; and 300 mb, 15°N. This diagram demonstrates two important features of vertical transport. The giant positive center in the Northern Hemisphere and the large positive center at 35°S are both located just above maximum

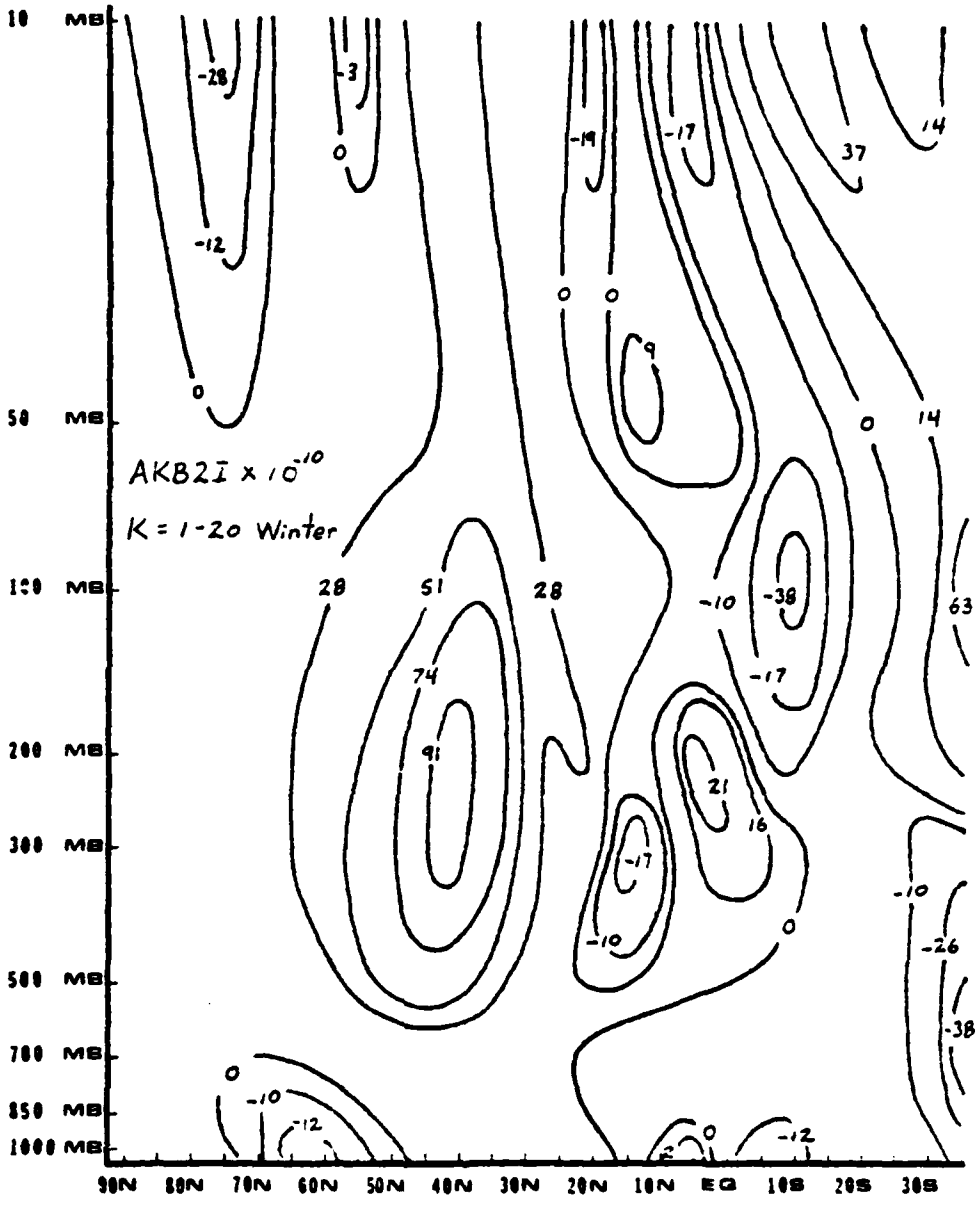


Figure 40. Distribution of vertical geopotential flux summed over wave numbers 1 - 20 and averaged over the winter season ($m^2/sec^2/day$).

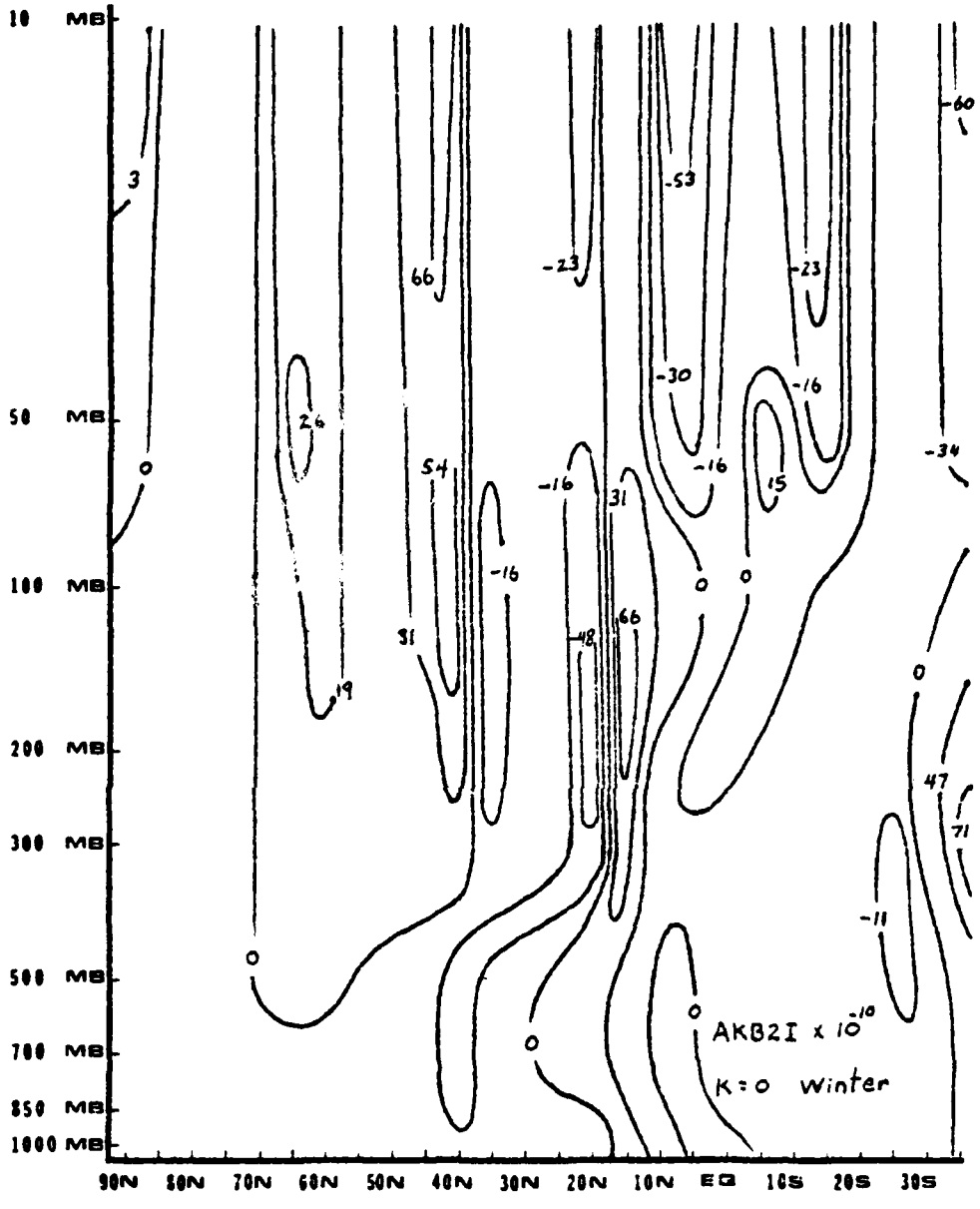


Figure 41. Distribution of vertical geopotential flux for wave number 0 averaged over the winter season ($m^2/sec^2/day$).

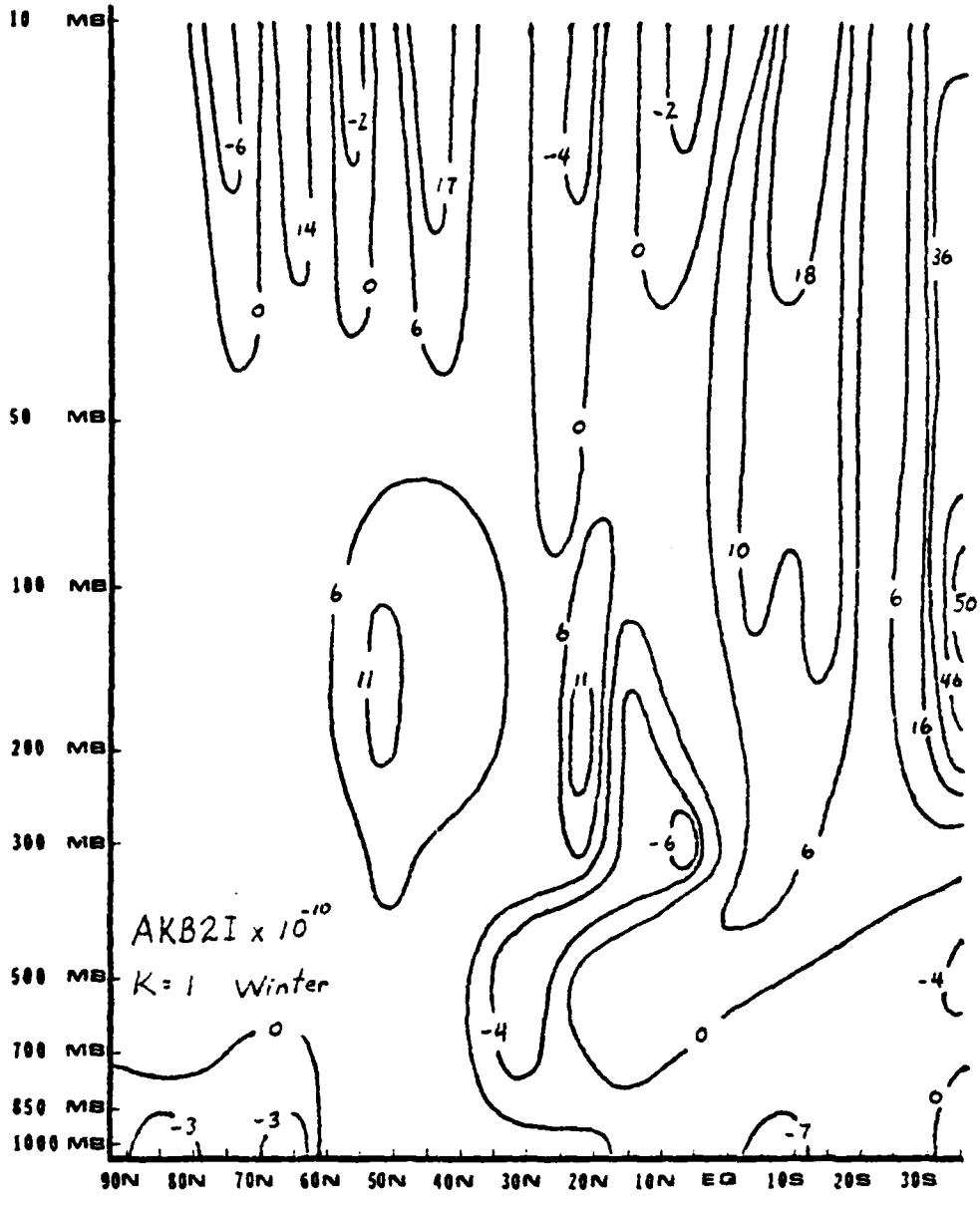


Figure 42. Distribution of vertical geopotential flux for wave number 1 averaged over the winter season ($m^2/sec^2/day$).

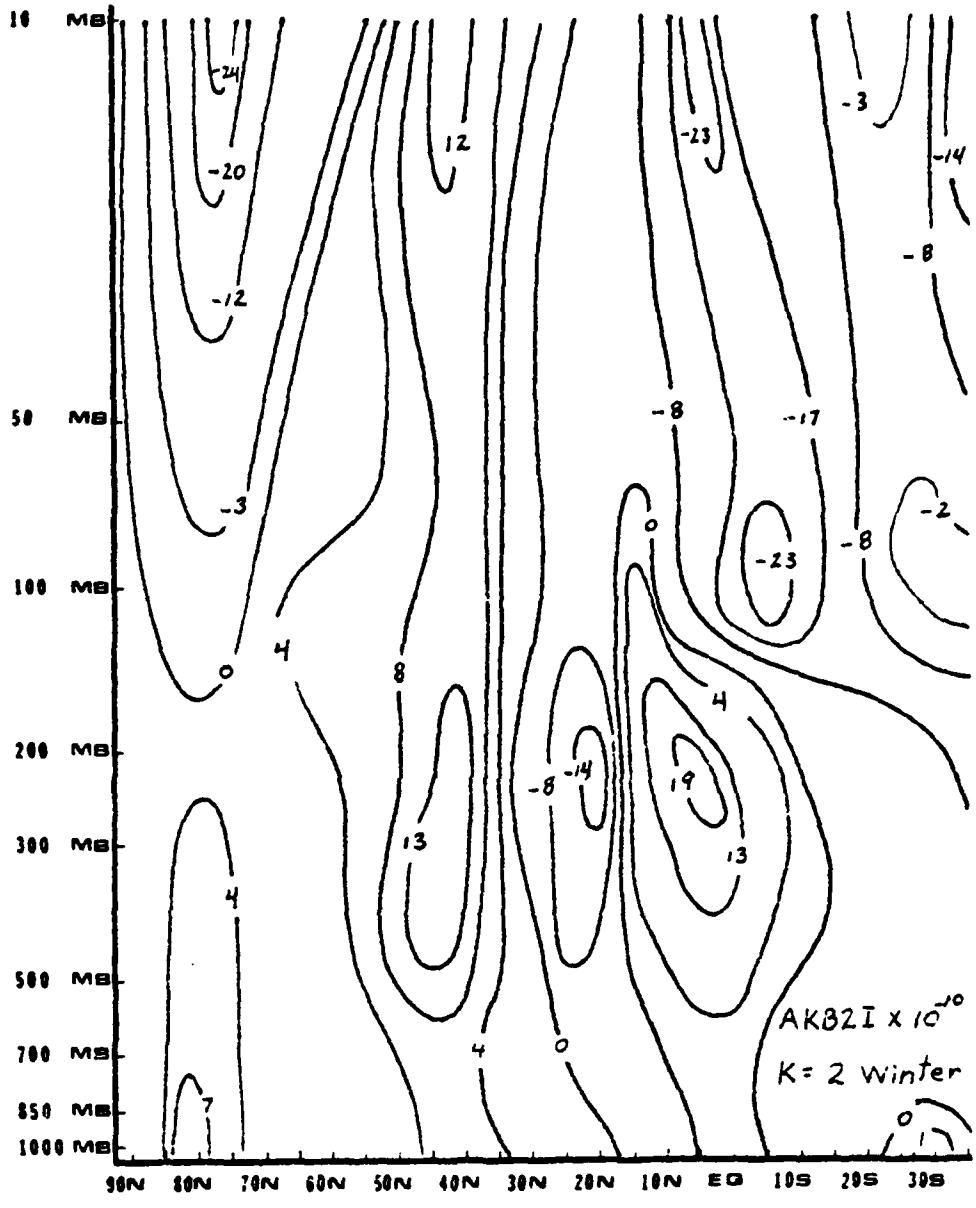


Figure 43. Distribution of vertical geopotential flux for wave number 2 averaged over the winter season ($m^2/sec^2/day$).

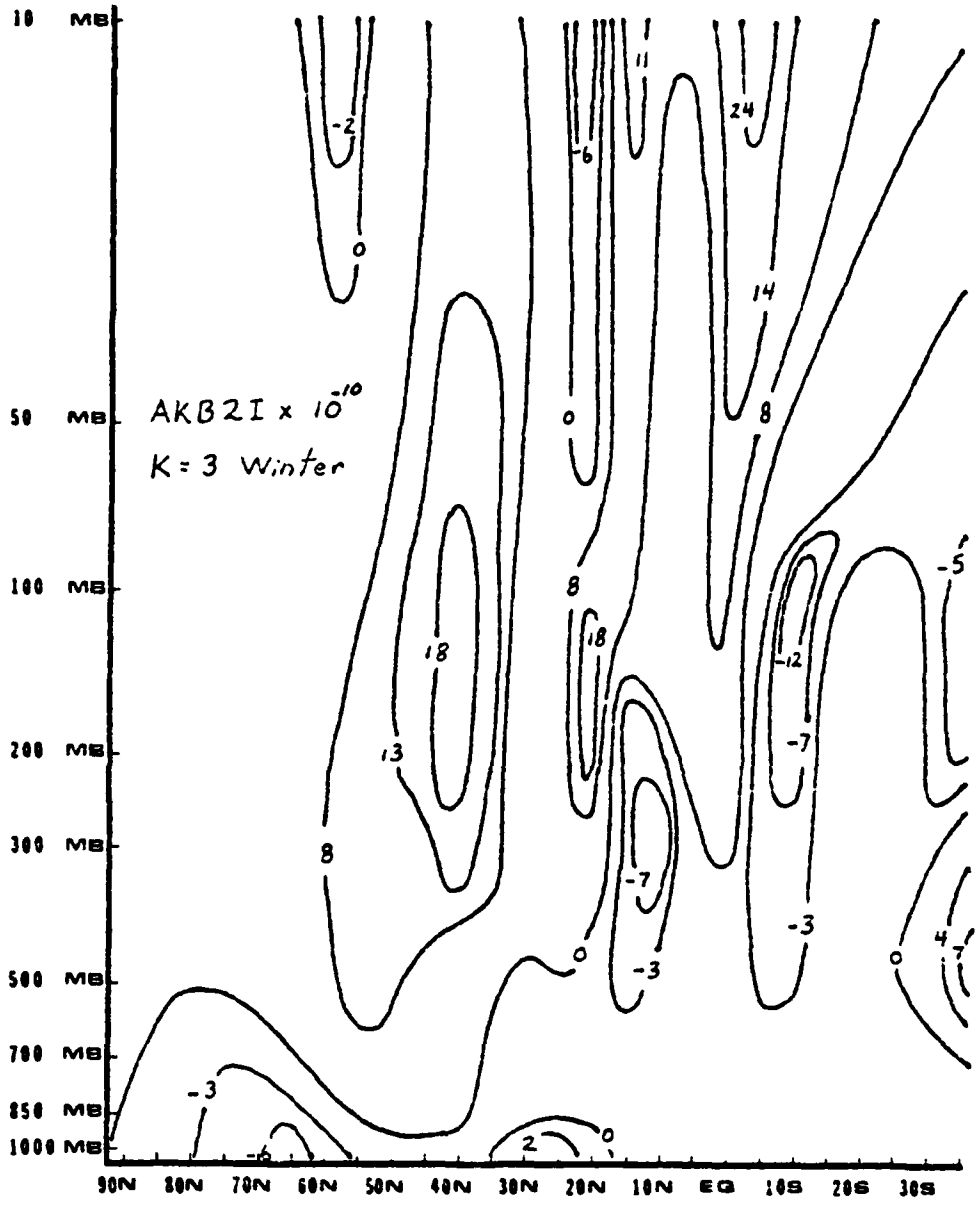


Figure 44. Distribution of vertical geopotential flux for wave number 3 averaged over the winter season ($m^2/sec^2/day$).

troposphere values of kinetic energy, as seen in Figure 28. Also, just below the centers of maximum kinetic energy, there are centers of negative AKB2I. This structure would indicate that AKB2 vertical transfer can act in a dispersive way, tending to spread high kinetic energy density from its maxima. On the other hand, the positive AKB2I center at 5°N and the associated neighboring negative centers at 10°S and 15°N do not correspond to kinetic energy maxima, but appear to be in response to the processes generating the maximum upward vertical velocities in the tropical region.

Vertical transfer of energy associated with the zonal mean flow, wave number 0 (Figure 41), shows moderately strong upward values over the middle latitudes at all levels above 700 mb. Again, extremely strong upward energy transfer is seen over the area of maximum heating. A narrow band of downward transfer values is seen to extend down from the stratosphere, to the north side of the maximum heating and around to the descent side of the most intense Northern Hemisphere direct circulation cell. Many major features of Figure 41 may also be seen in Figure 4 for the winter mean vertical velocity; however, some features, such as the upward transfer in the stratosphere at 60°N, would not be expected from Figure 4 alone. The AKB2 term is essentially given by $-\omega'Z'$. This means that descent (positive omega) through an area of Negative Z' can give positive upward values, and this is the case at 60°N in the stratosphere of Figure 41. Above 50 mb at 7°N, the reverse situation exists, with negative omega intersecting an area

positive Z'.

For waves of wave number 1, 2, and 3, Figures 42, 43, and 44 show upward energy transfer in most regions of the Northern Hemisphere; however, very strong downward propagation of energy is seen for wave number 2 (Figure 43) in the polar stratosphere. The strength of this feature may well determine the extent to which the tongue of maximum EK values seen in Figure 25 penetrates into the troposphere. The extremely strong wave number 2 upward transfer below 100 mb at the equator is also not seen for wave numbers 1 and 3. In fact, in equatorial regions at all levels, the energy propagation for wave numbers 1 and 3 is nearly opposite that seen for wave number 2. Note that upward propogation of energy for wave number 1 and 2 begins to become important at about 300 mb above the equator, just at the center of maximum wave number 2 upward transfer. In the stratosphere above this area, wave numbers 1 and 3 transfer strongly upward, while wave number 2 transfers strongly downward. It appears that wave number 2 will tend to concentrate energy near the tropical tropopause, while wave numbers 1 and 3 tend to be dispersive in this region. In summary, upward transfer is the general rule over must of the Northern Hemisphere, especially above areas of maximum kinetic energy. Note also that the maximum value of 91 $m^2/sec^2/day$ shown on Figure 40 is must greater than that obtained in summing the values for wave numbers 1 through 3. This indicates that the majority of upward energy transfer is generated by waves of wave number greater than 3. This is consistent with maximum value of the omega power

spectra being at or near wave number 7, as shown in Figures 10 and 13.

Meridionally integrated values of AKB1I are presented in Figures 45 through 49. The composite picture over wave numbers 1 through 20 is shown in Figure 45. In this figure, AKB1I appears to transfer southward at all latitudes north of 20°N in the middle and upper troposphere and in the lower stratosphere, and northward in these areas south of 20°N. This would certainly indicate strong convergence of energy between 10°N and 35°N near the tropopause. A second striking feature of Figure 45 is the general lack of meridional transfer in the upper stratosphere. AKB1I values for wave number 1 are given in Figure 47. A cellular pattern similar to that seen in Figure 45 is apparent, only now the transfer alternates from northward to southward. When Figures 47 and 24 are compared, we see that the positive cells of AKB1I (northward transfer) occur to the north of kinetic energy maxima, and that negative cells of AKB1I (southward transfer) occur to the south of kinetic energy maxima. Just as AKB2I could act to disperse regions of high kinetic energy in the vertical direction, so too is AKB1I acting to disperse energy centers in the meridional direction. Also note the large positive center at 10°N, 200 mb and the corresponding negative center at 17°S, 200 mb. These centers indicate strong meridional energy transfer from the tropical region into both the Northern Hemisphere and the Southern Hemisphere. Figure 48 presents the AKB1I plot for wave number 2. The most striking feature of this diagram is the strong, southward

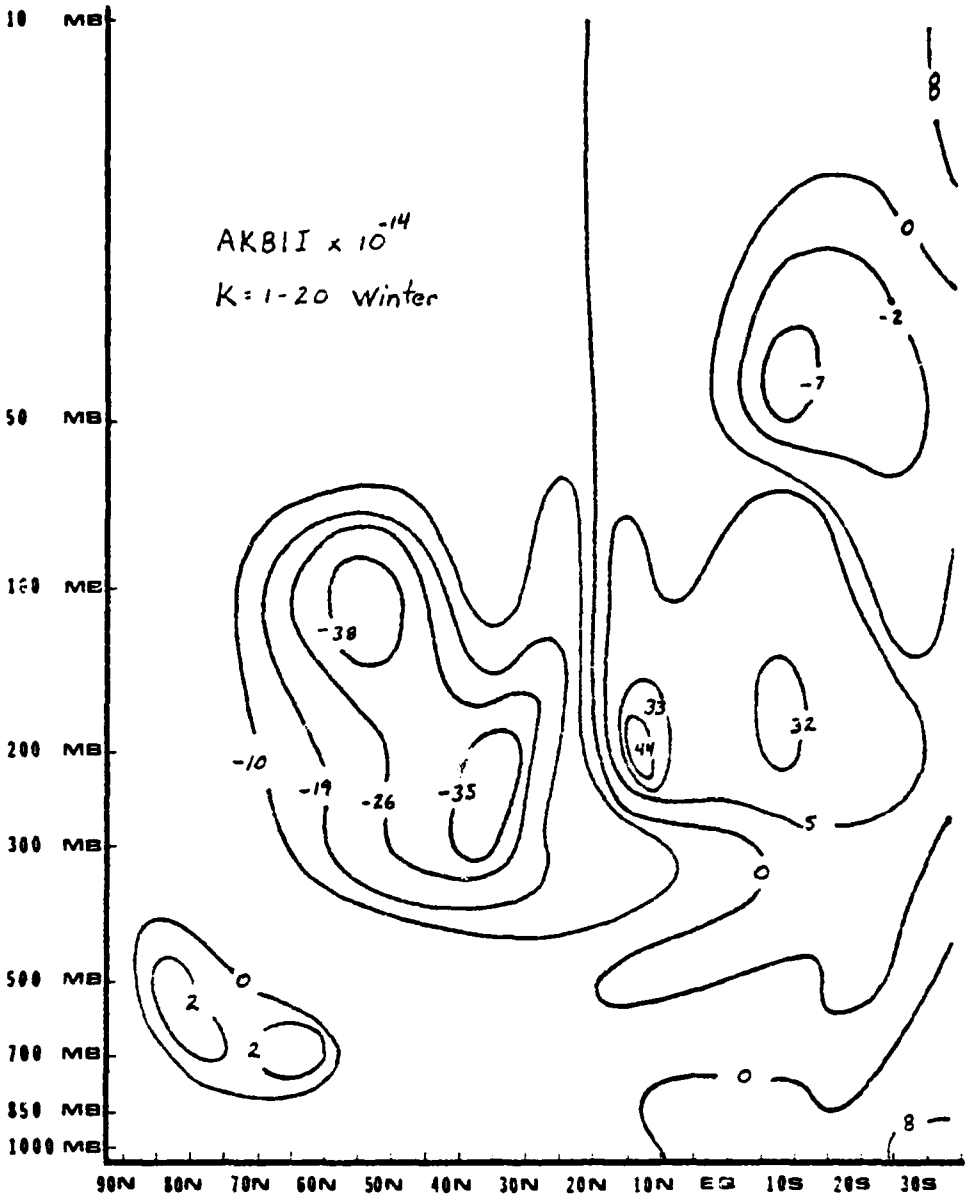


Figure 45. Distribution of meridional geopotential flux summed over wave numbers 1 - 20 and averaged over the winter season ($m^2/sec^2/day$).

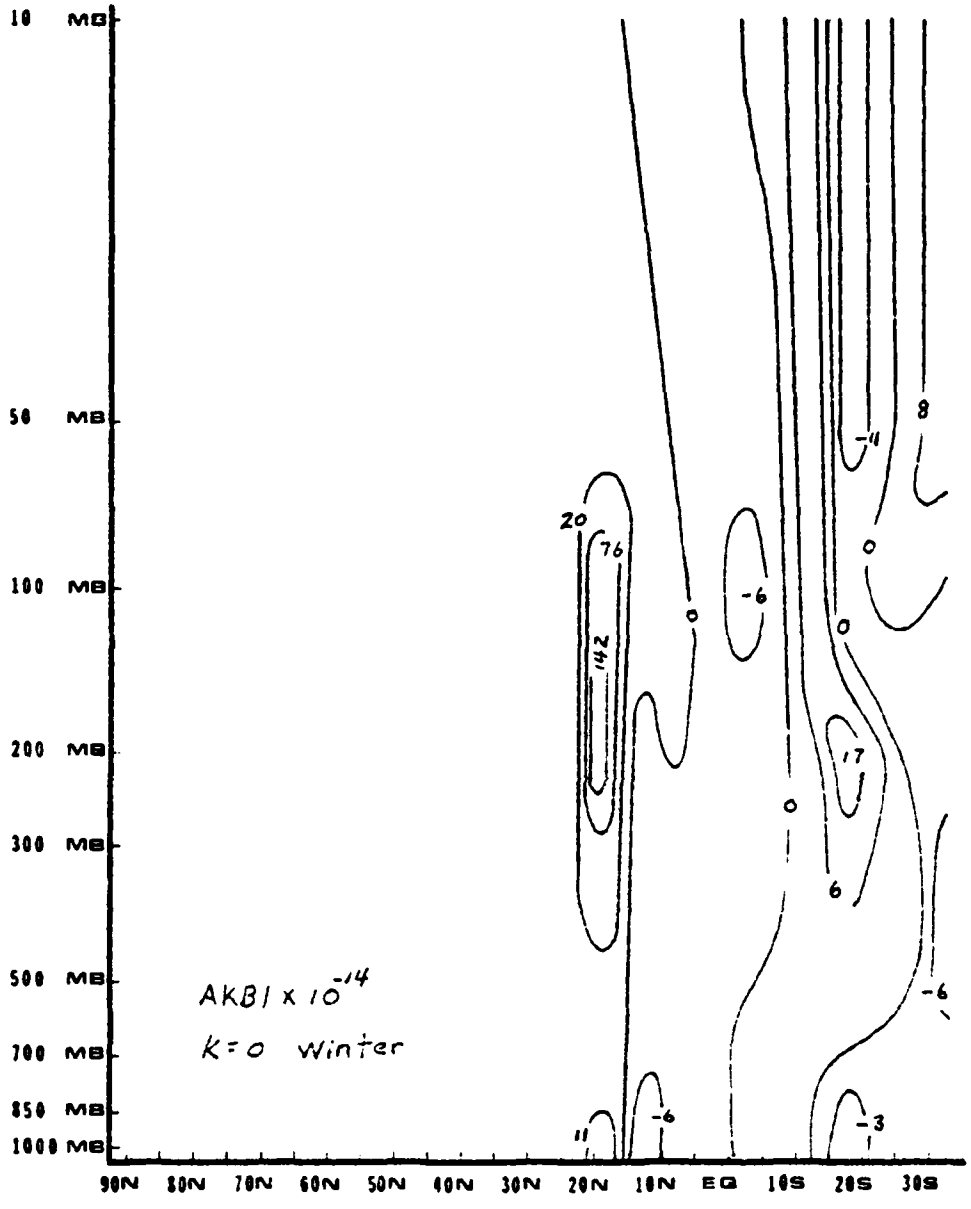


Figure 46. Distribution of meridional geopotential flux averaged over the winter season for wave number 0 ($m^2/sec^2/day$).

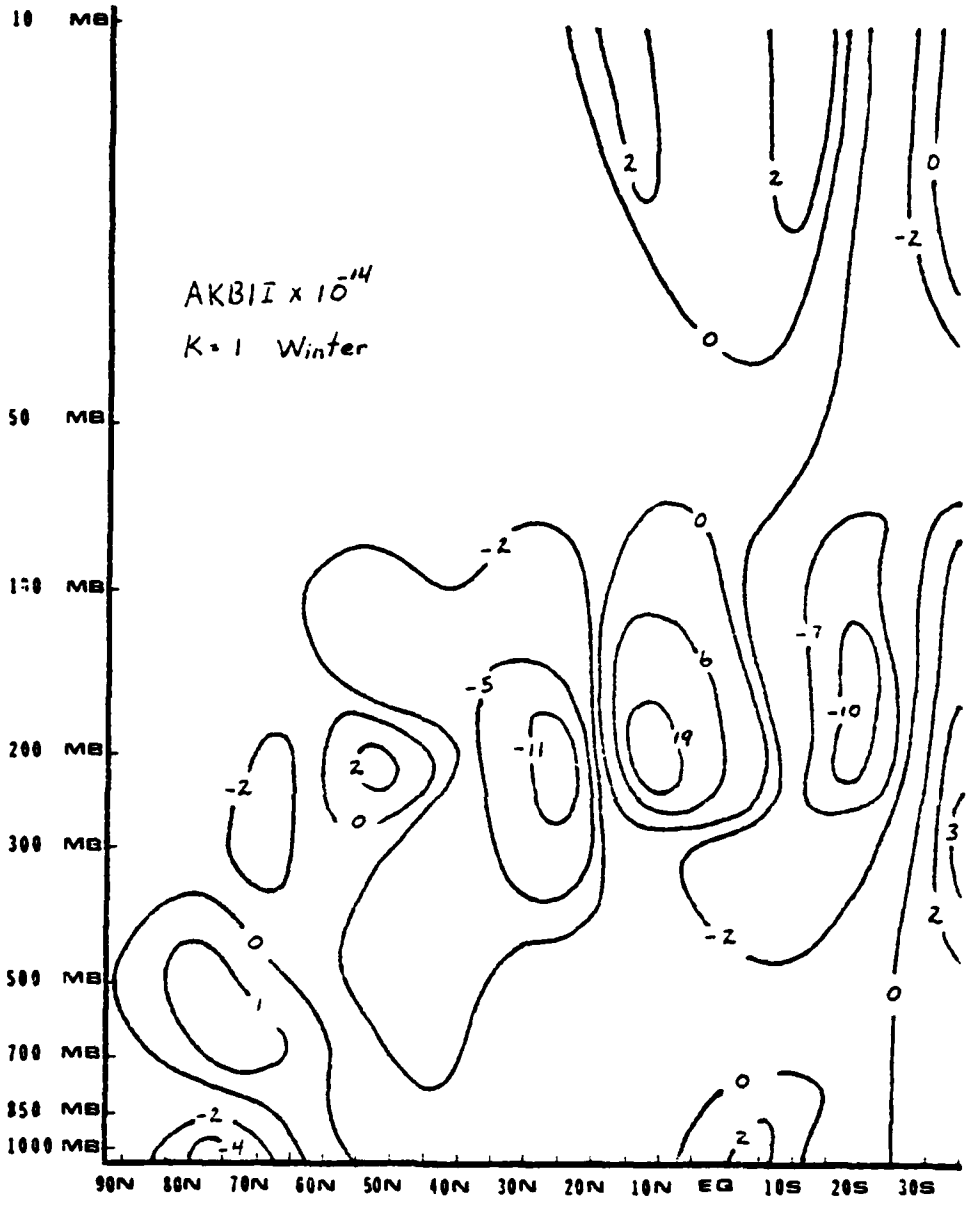


Figure 47. Distribution of meridional geopotential flux averaged over the winter season for wave number 1 ($m^2/sec^2/day$).

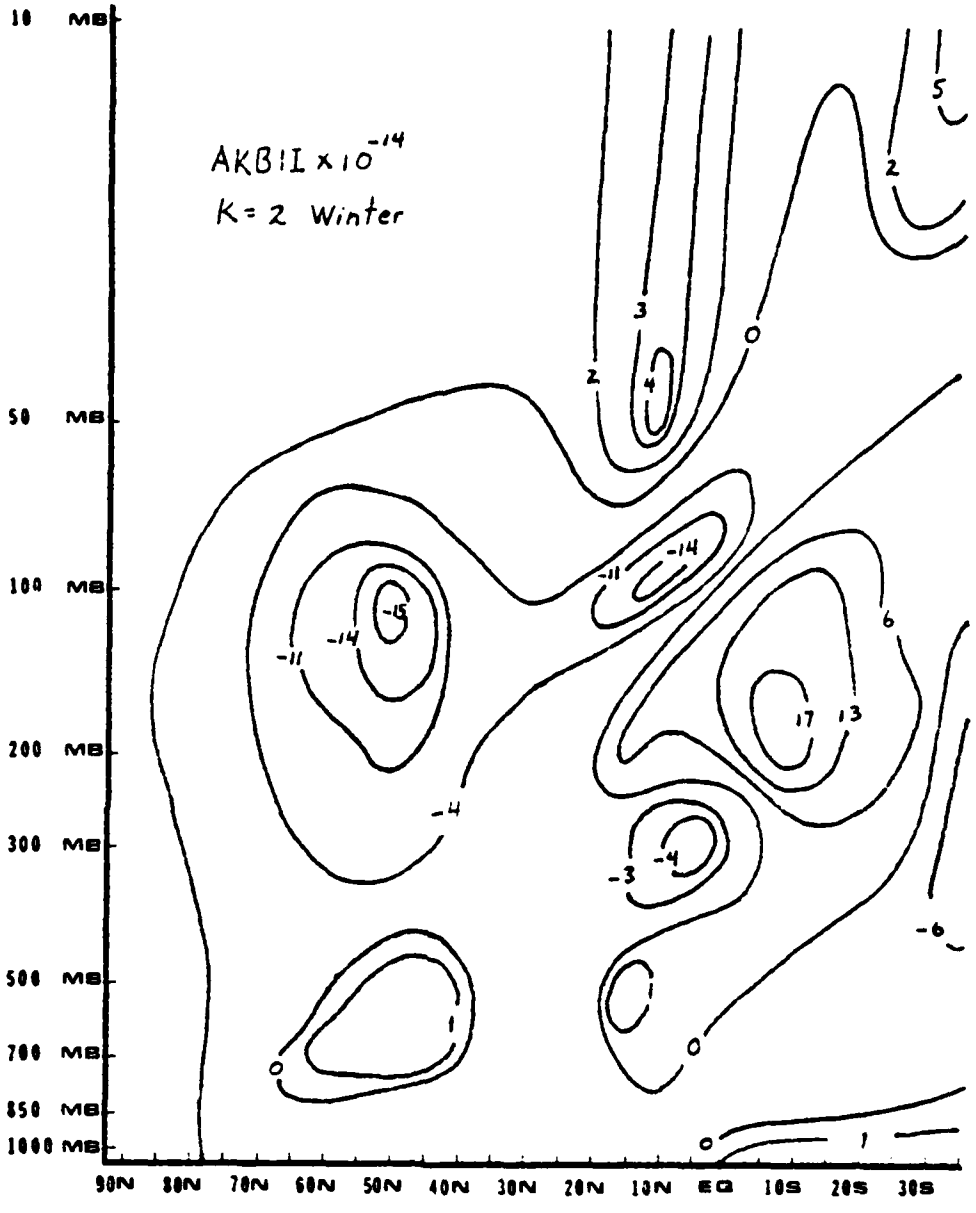


Figure 48. Distribution of meridional geopotential flux averaged over the winter season for wave number 2 ($m^2/sec^2/day$).

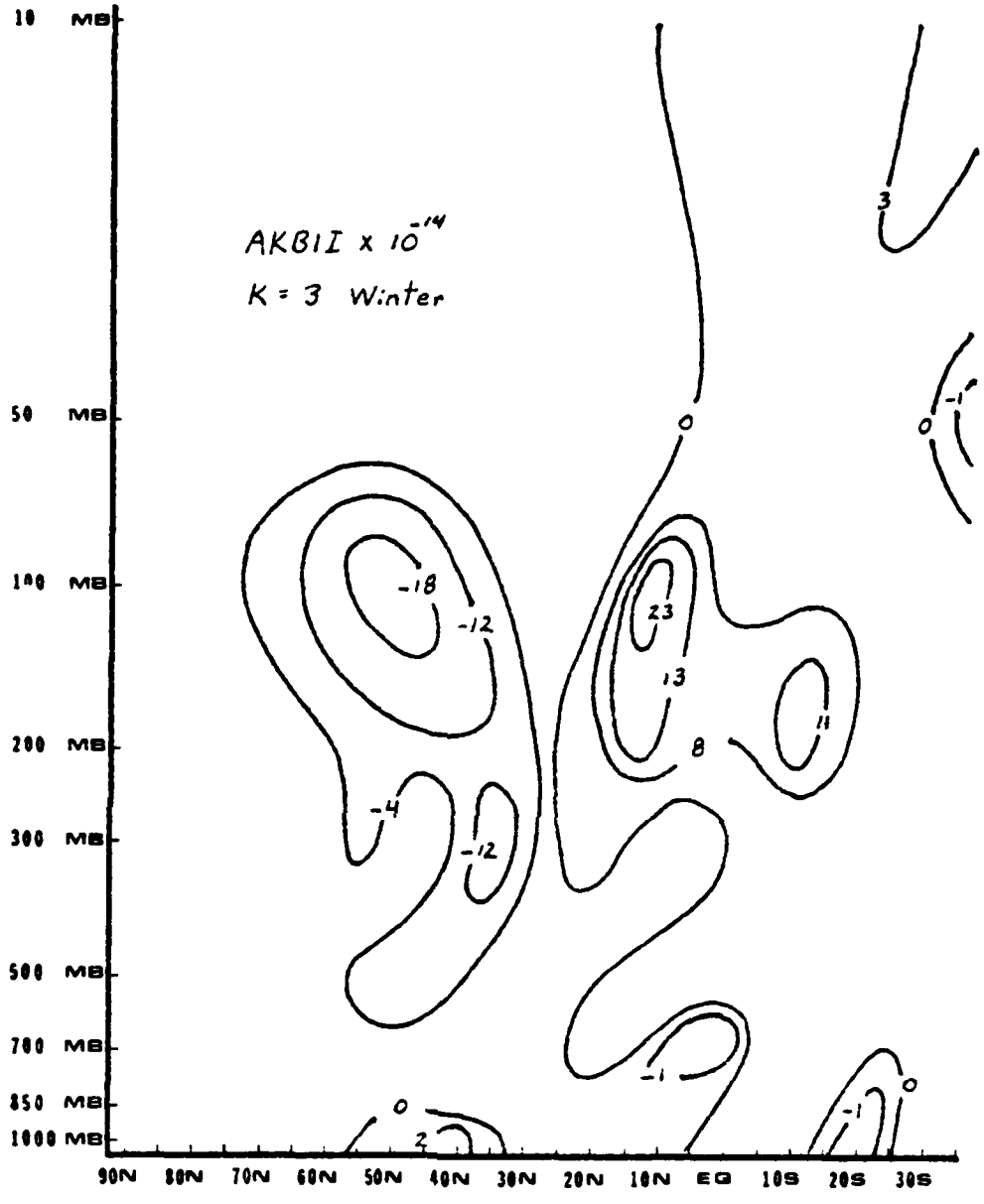


Figure 49. Distribution of meridional geopotential flux averaged over the winter season for wave number 3 ($m^2/sec^2/day$).

transfer maximum located above the area of maximum heating at 10°N and 100 mb, and an associated strong northward energy propagation region to the south at 5°S, 180 mb. This structure is similar to that observed for AKB2I for wave number 2, and it appears that AKB1I also tends to concentrate energy in the tropical region below the tropical tropopause for wave number 2. An additional strong negative center is seen at 50°N, 100 mb in Figure 48. This feature is closely linked to the wave number 2 kinetic energy maximum seen in this area in Figure 25. In areas of maximum EK, AKB1I appears to act to decrease intensity.

Figure 49 represents the cross section plot of AKB1I for wave number 3. Two features of this diagram are especially interesting. First, AKB1I for wave number 3 acts much like it does for wave numbers 1 and 2 in areas of maximum EK, and the strong negative center at 50°N, 100 mb will tend to decrease the intensity of the EK maximum for wave number 3 in that region. Second, AKB1I for wave number 3 acts much like it does for wave number 1 near the tropical tropopause, exhibiting strong northward porpagation of energy over this whole region. One final note concerning AKB1I. Note that the composite diagram, Figure 45, cannot be constructed entirely from the sun of wave numbers 1, 2, and 3; however, in some regions, it can be constructed almost completely from these first three wave numbers. For example, consider the two negative centers in Figure 45 at 100 mb, 50°N, and 250 mb, 35°N. The upper center can be constructed from wave numbers 1 through 3, but not the lower center. To understand this, the sequence of kinetic energy cross

sections (Figures 24 through 28) must be reviewed. It is seen that EK is maximum in the stratosphere for long waves, but maximum in the troposphere for shorter waves. The AKB1I term responds to this, and acts to decrease centers of maximum EK at all wave numbers. The upper negative center of AKB1I acts to disperse the low wave number, stratospheric, EK maximum, while the lower negative center acts to decrease the higher wave number, tropospheric, EK maximum.

The nonlinear horizontal boundary forcing term, NKB1I, differs markedly from AKB1I, in that stropospheric maxima in northern latitudes exist for all wave numbers presented (Figures 50 through 53). In the troposphere, NKB1I acts much like AKB1I, dispersing kinetic energy maxima, but in the stratosphere the sign of this transfer reverses, and NBK1I acts to reinforce high energy centers rather than to dissipate them. Note also that NKB1I exhibits strong northward transfer for all wave numbers shown in the region just below the tropical tropopause. We will return to this point again after briefly discussing NKB2I.

The vertical nonlinear transfer term, NKB2I, is presented in Figures 54 through 57. This figures do not exhibit well defined trends, except over the equatorial region. Here the transfer is upward and quite strong in the region of maximum upward vertical motion, and strongly downward both north and south of this region. Tropospheric transfer appears generally to be up on the poleward side of kinetic energy maxima and down on the side of the maxima nearest the equator. No general pattern for stratospheric transfer

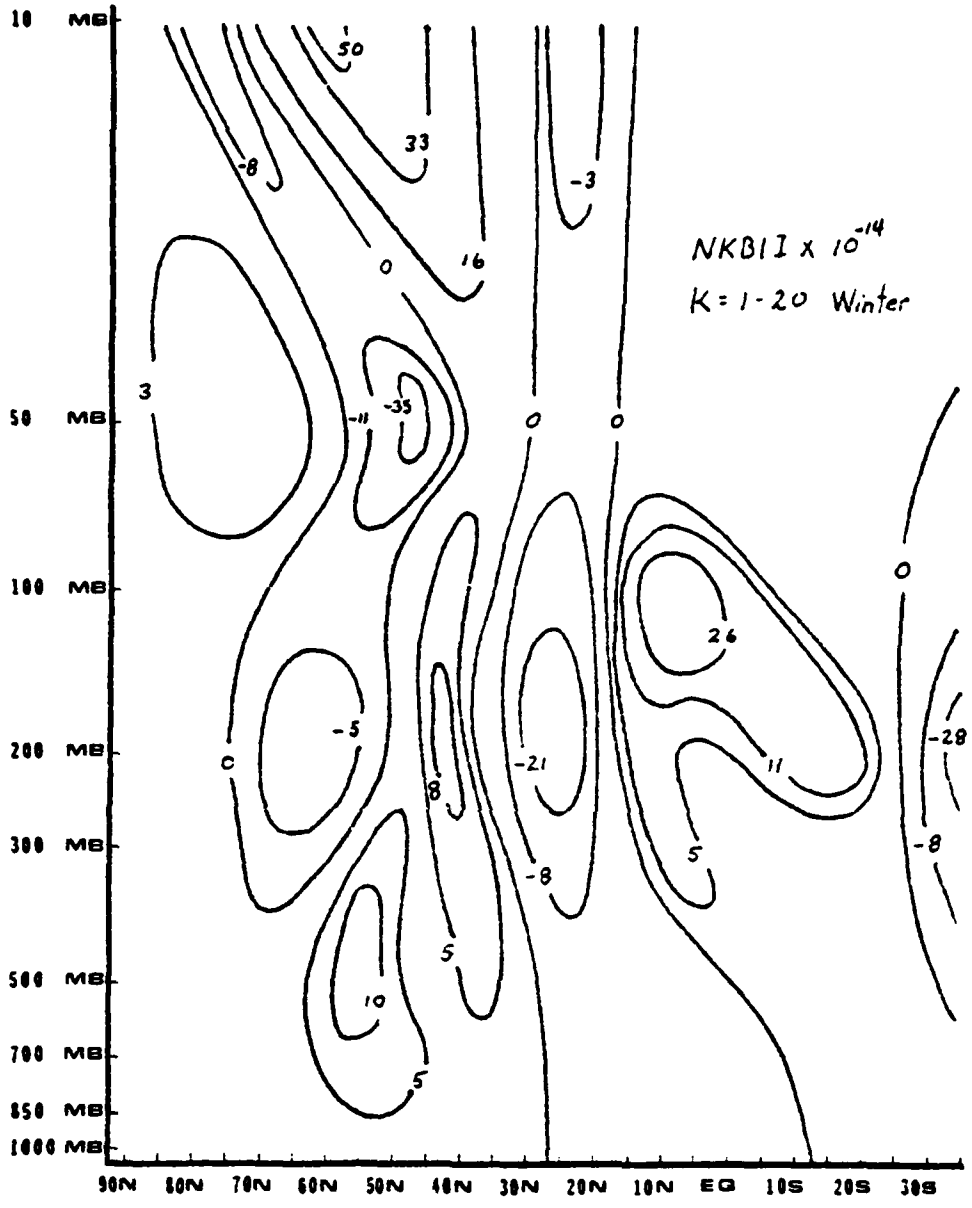


Figure 50. Distribution of NKBII summed over wave numbers 1 - 20 and averaged over the winter season ($m^2/sec^2/day$).

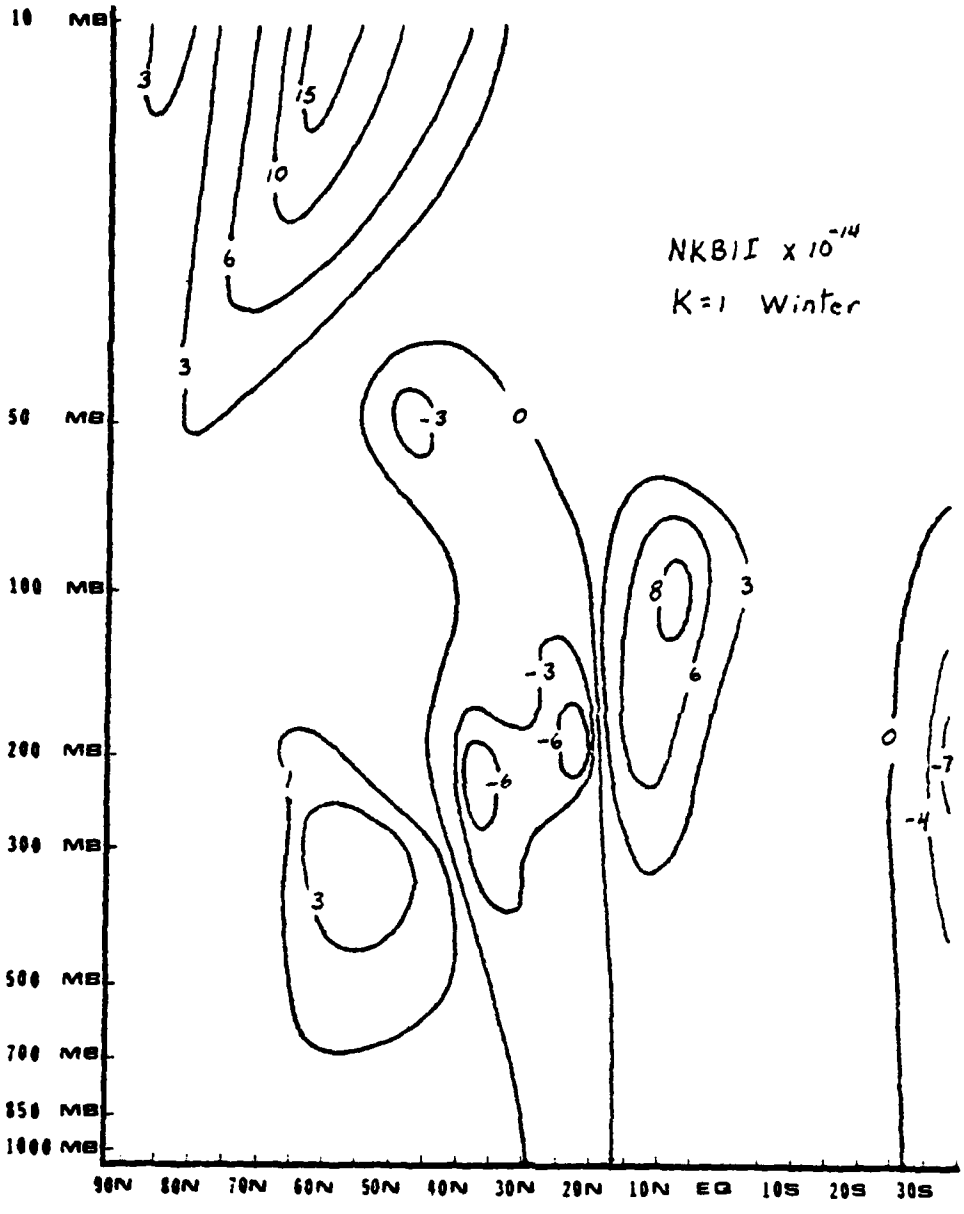


Figure 51. Distribution of NKB1I over the winter season for wave number 1 ($m^2/sec^2/day$).

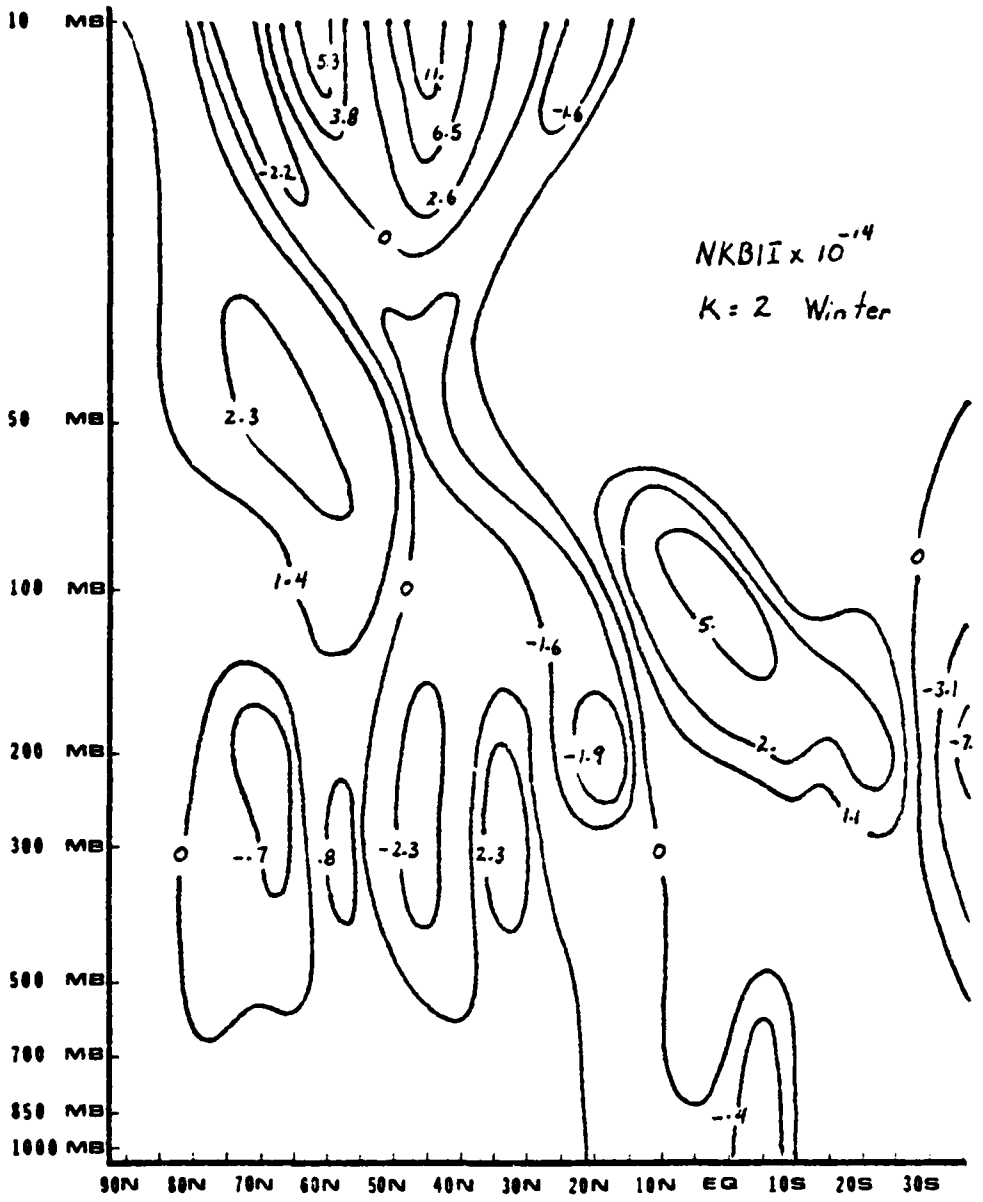


Figure 52. Distribution of NKB1I over the winter season for wave number 2 ($m^2/sec^2/day$).

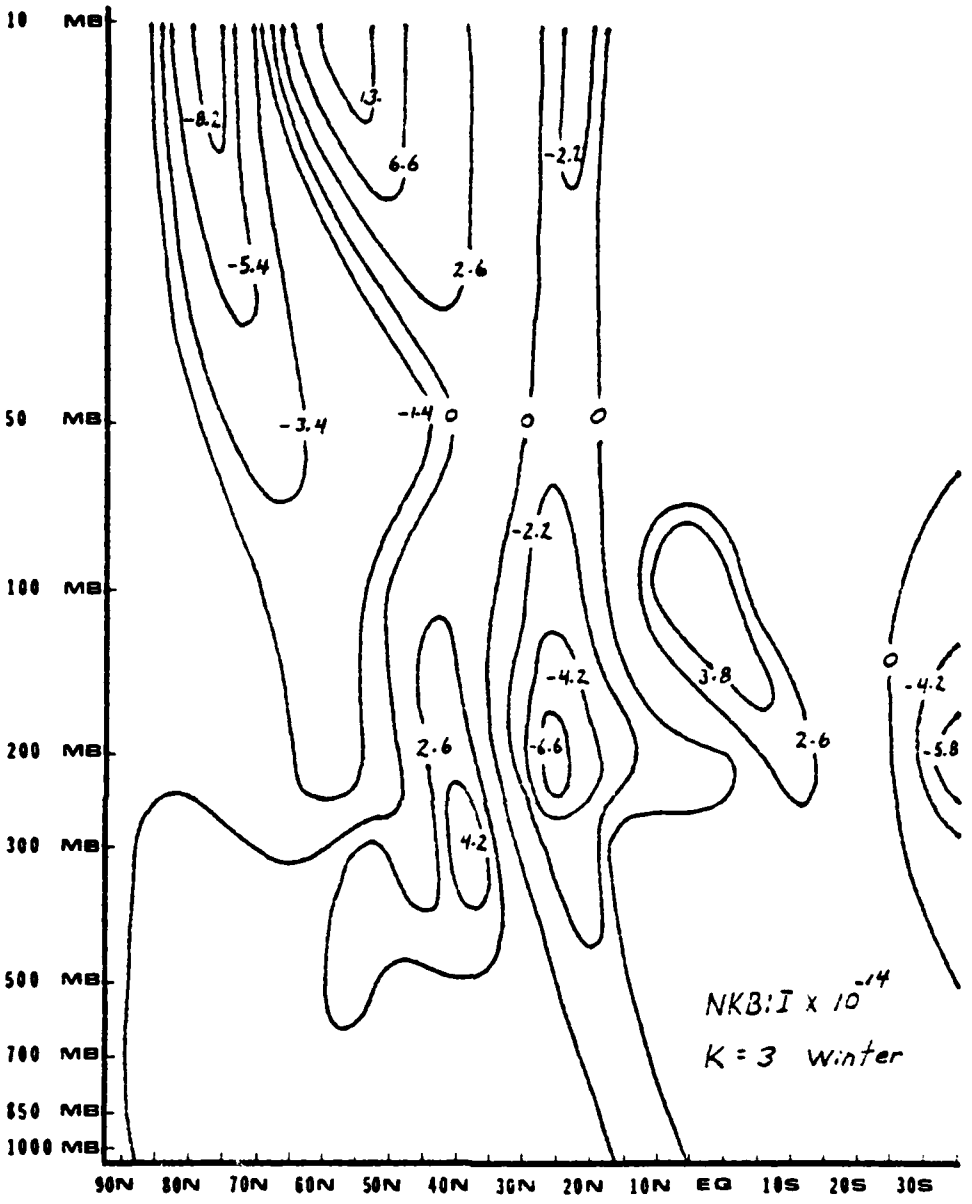


Figure 53. Distribution of NKB1I over the winter season for wave number 3 ($m^2/sec^2/day$).

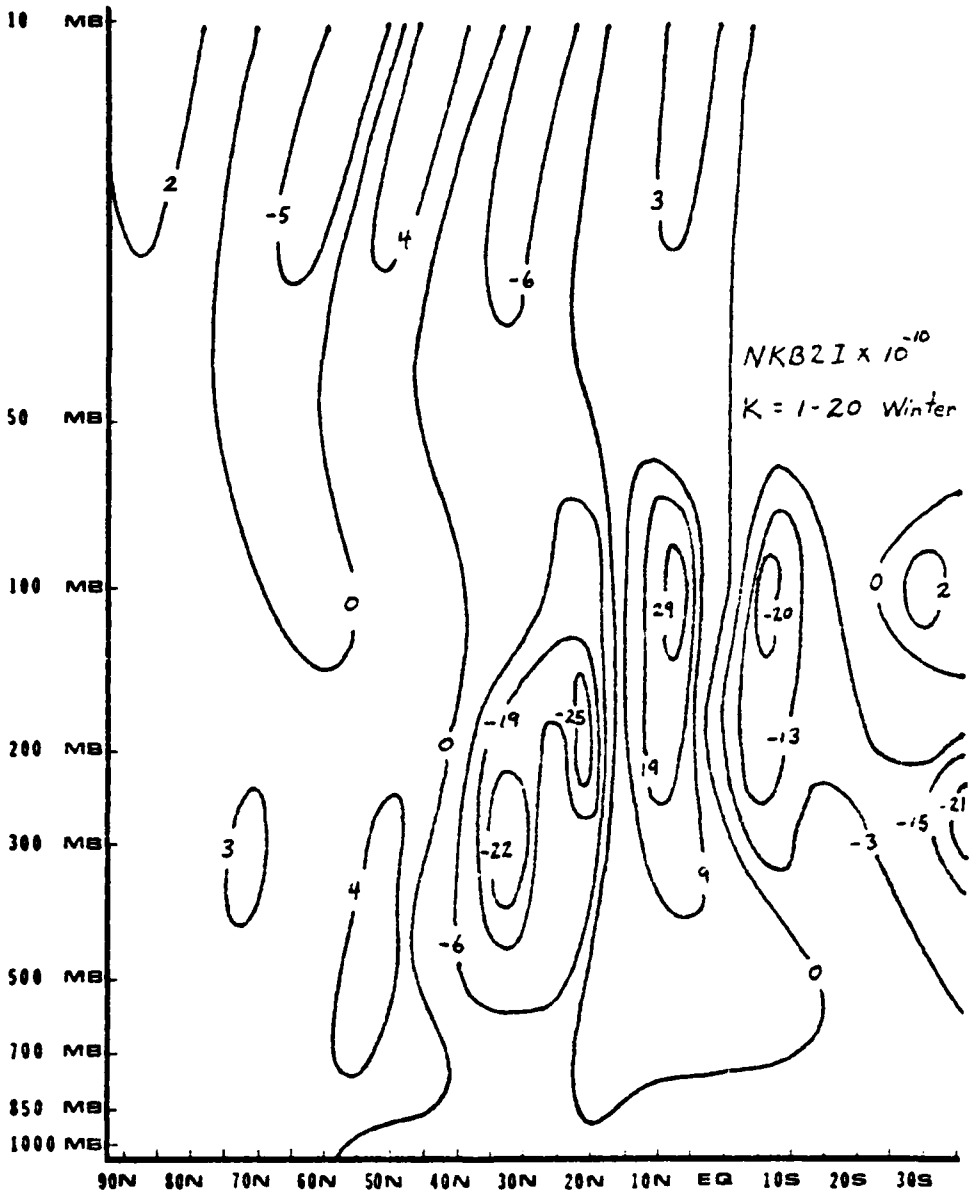


Figure 54. Distribution of NKB2I summed over wave numbers 1 - 20 and averaged over the winter season ($m^2/sec^2/day$).

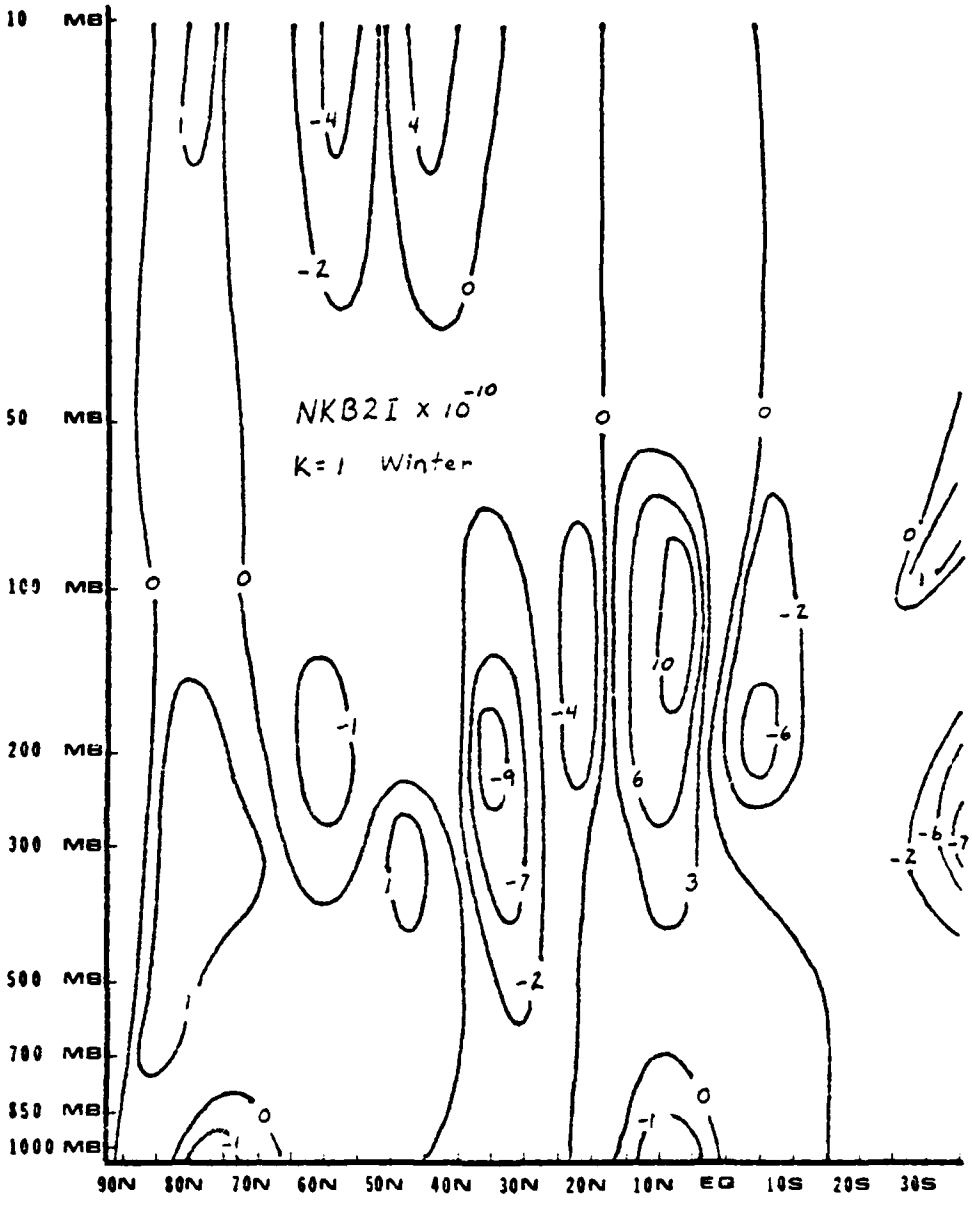


Figure 55. Distribution of NKB2I over the winter season for wave number 1 ($m^2/sec^2/day$).

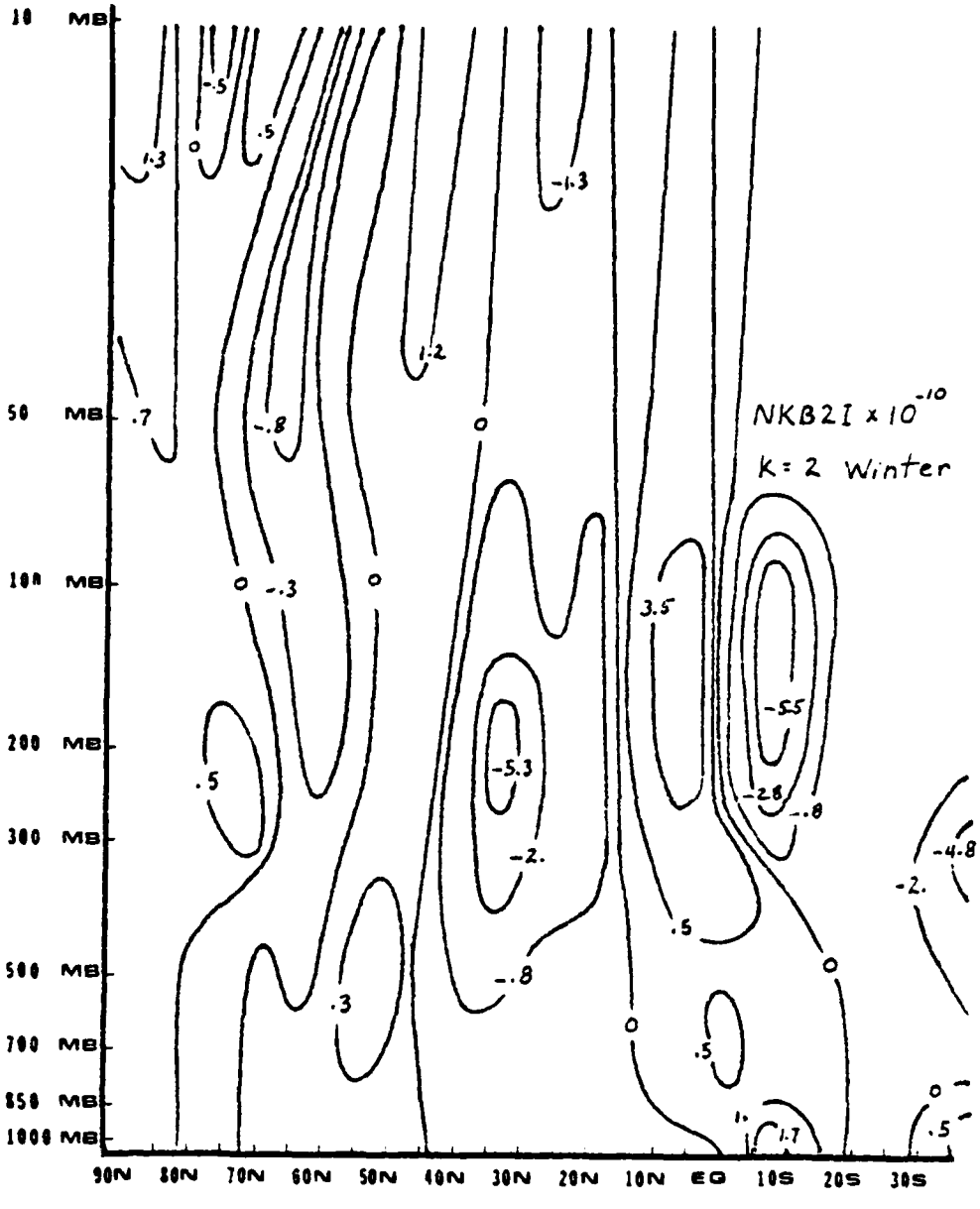


Figure 56. Distribution of NKB2I over the winter season for wave number 2 ($m^2/sec^2/day$).

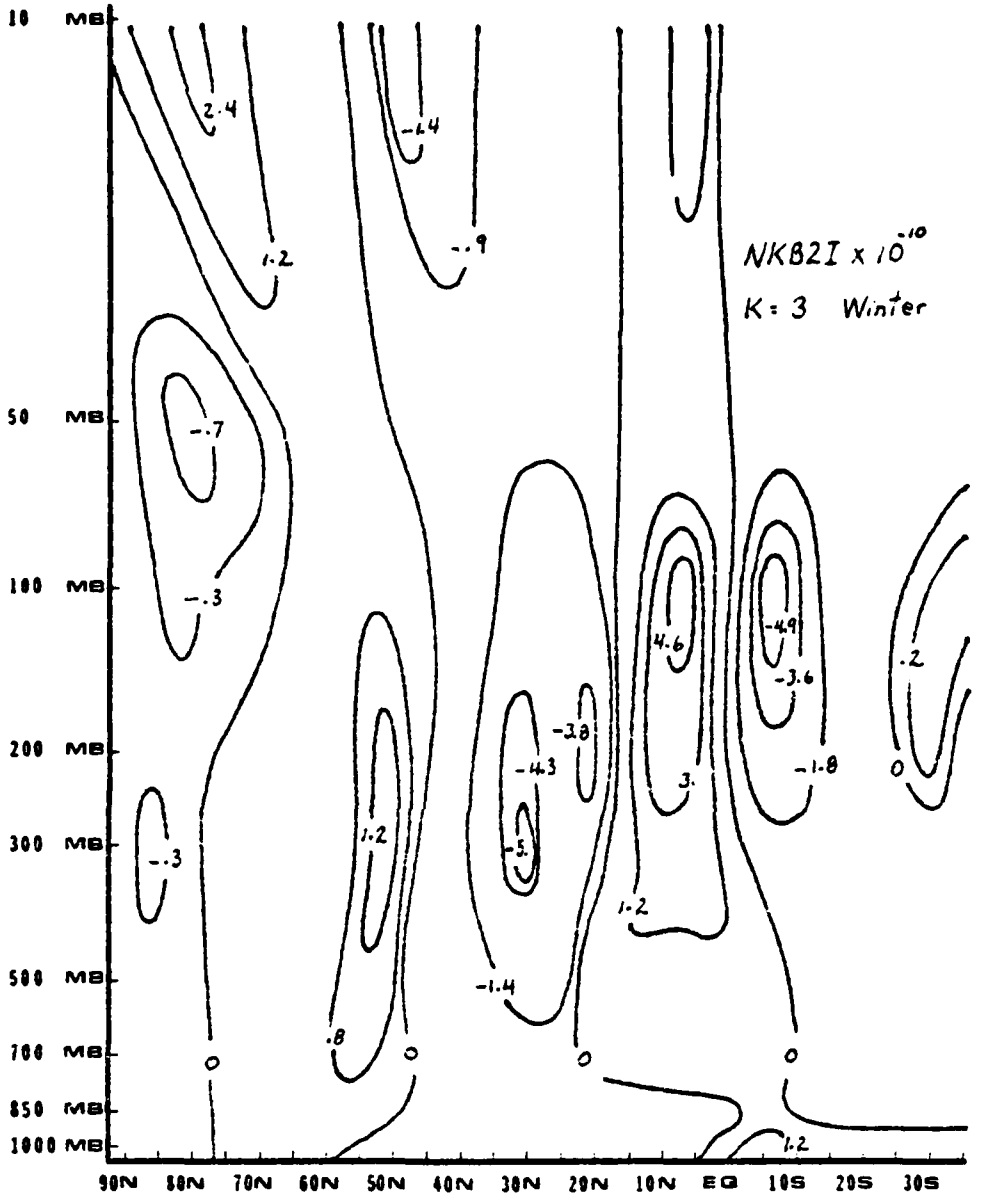


Figure 57. Distribution of NKB2I over the winter season for wave number 3 ($m^2/sec^2/day$).

is seen.

In summary, transfer terms associated with the kinetic energy equation (2.16) almost always act to decrease the intensity of kinetic energy maxima. There are, however, two very important exceptions to this. For wave number 2, both AKB1I and AKB2I act to concentrate energy in the region of the tropical tropopause. All other terms for all other wave numbers tend to transfer upward and northward from this region.

Figures 58 and 59 may depict an effect of this energy transfer. The solid lines in these figures represent observed values of EK during the winter, while the dashed lines represent values of EA. The location of the center of the EK peaks and the time intervals between peaks is plotted on the two arrows appearing above the peaks in each diagram. Each frame presented in Figures 58 and 59 represent a different level and/or latitude band. All values plotted in these figures were averaged by applying (4.3)

The three peaks of kinetic energy, shown in the upper portion of Figure 58, appear to move upward and northward with time, as might be expected from the wave number 1 forcing discussed above. The center peak, seen in the lower half of Figure 59, corresponds to the easterly flow associated with the minor stratospheric warming which began 30 Jan 1976 and reaches its maximum intensity 6 Feb 1976. The leading peak corresponds to a characteristic increase in the upper level westerlies prior to flow reversal to easterlies during the warming. Note that the three EK peaks are quite difficult to find at 50 mb in the 10°N to 20°N latitude band shown in

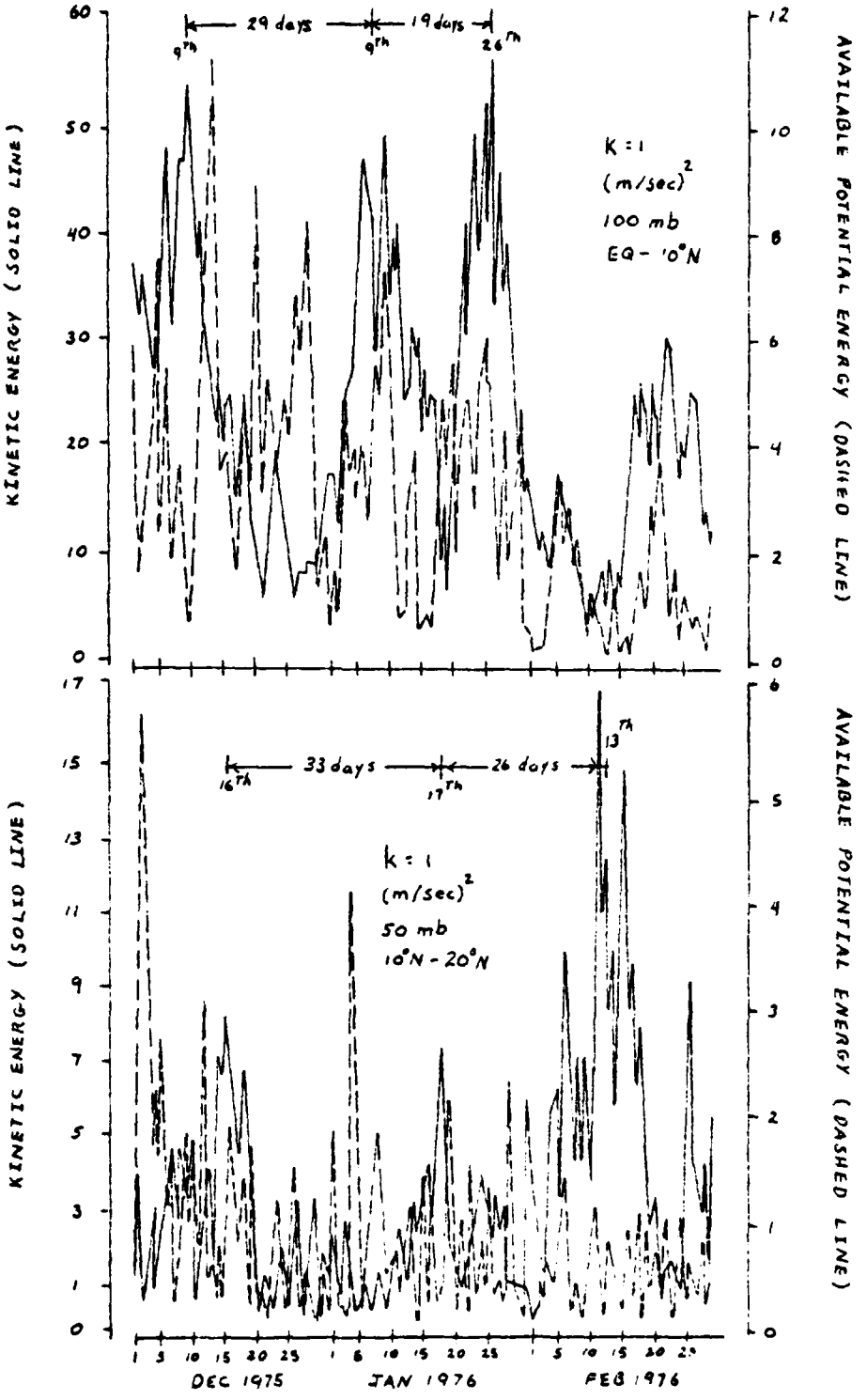


Figure 58. Daily values of EK and EA averaged over 0° - 10°N at 100 mb and 10°N - 20°N at 50 mb.

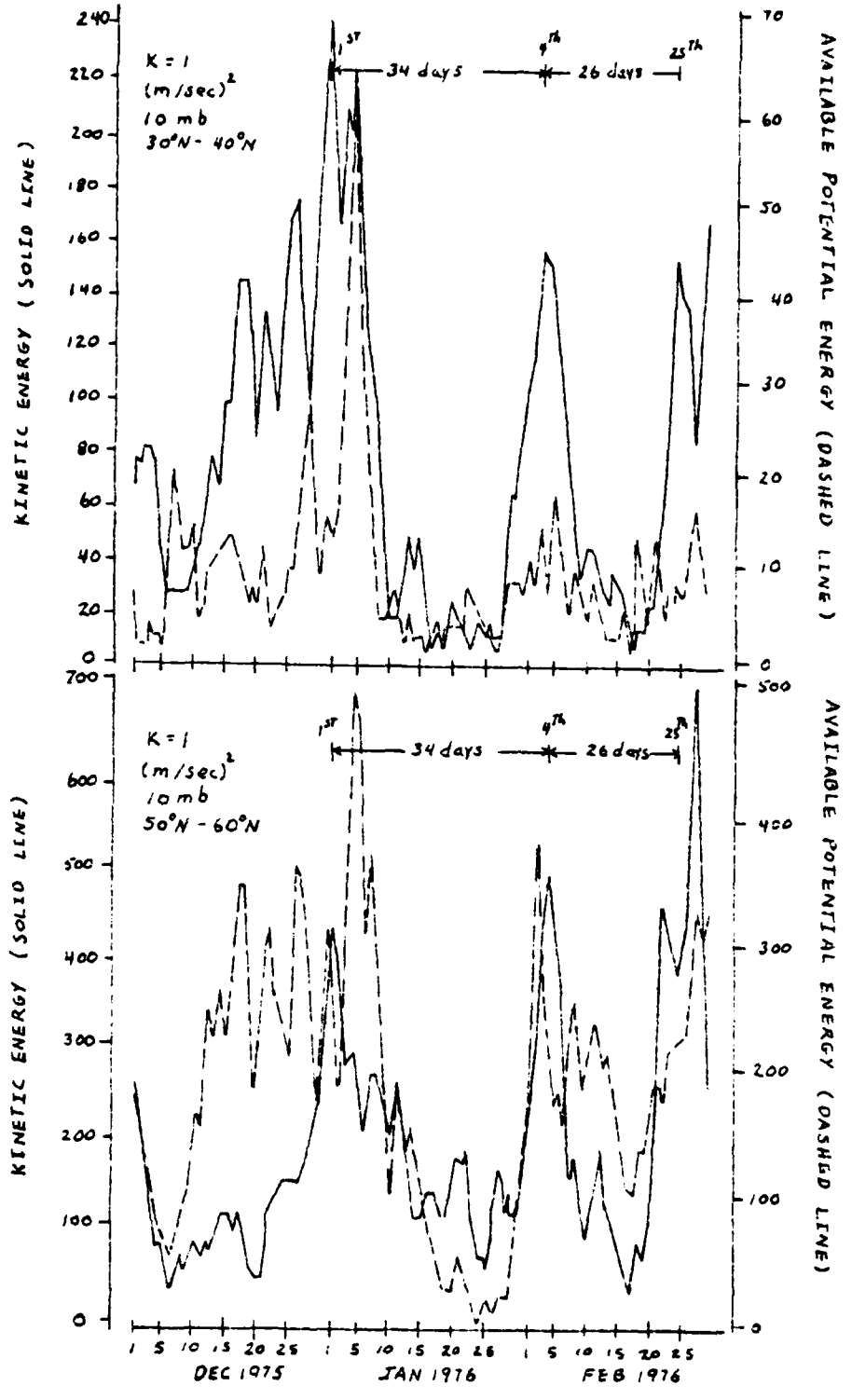


Figure 59. Daily values of EK and EA at 10 mb averaged over 30°N - 40°N and 50°N - 60°N.

the bottom half of Figure 58. As seen in Figure 5, the mean winter temperature cross section, this is an extremely stable area, where temperatures increase with height and are nearly isothermal meridionally. In all years studied, this region demonstrated strong damping of waves. Both frames presented in Figure 59 are for the 10 mb level. The upper frame represents the 30°N to 40°N latitude band, while the lower frame represents 50°N to 60°N. The major difference between these two frames is in the intensity of the waves, with the northward band showing considerably greater intensities for both EK and EA waves. This increasing energy per unit area is probably a result of the decreasing area contained within the northern band, more than an increase in the strength of the northward moving waves themselves.

If these waves are, in fact, moving upward and northward, a further question must be asked. What happens to the energy of the wave when it reaches the pole? No attempt will be made here to answer this question; however, note again that extremely strong downward energy transfer was observed in the stratospheric polar regions for AKB2I in wave number 2, a feature not seen for any other term or wave number.

Meridional transfer for available potential energy is depicted in Figures 60 through 63. The composite diagram, representing the sum of wave numbers 1 through 20, is Figure 60. On this figure, a large positive (northward energy transfer) tongue is seen centered on 68°N at 10 mb, and a secondary maximum is located near 15°N at 200 mb. Three negative centers are seen at 43°N, 700 mb;

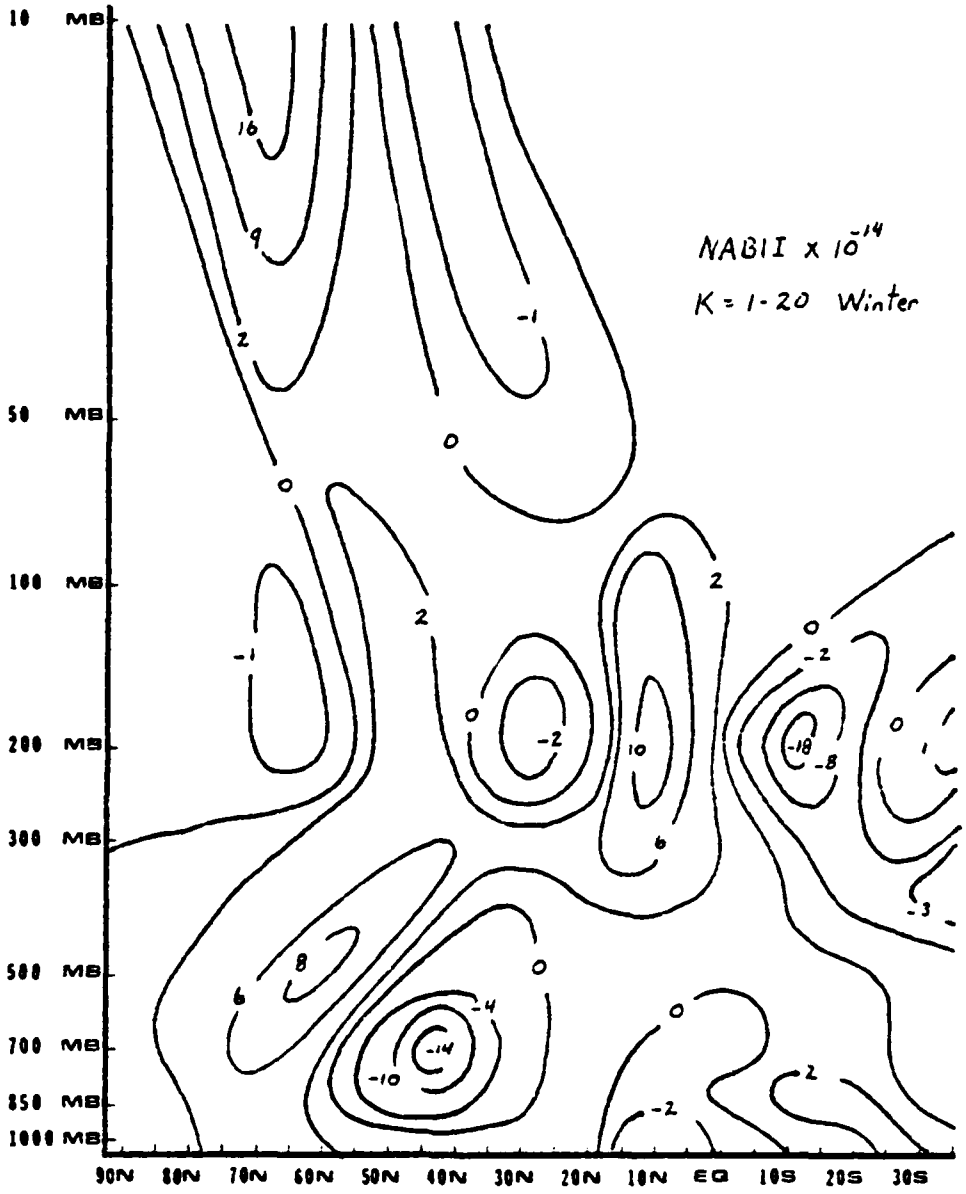


Figure 60. Distribution of NABlI summer over wave numbers 1 - 20 and averaged over the winter season ($m^2/sec^2/day$).

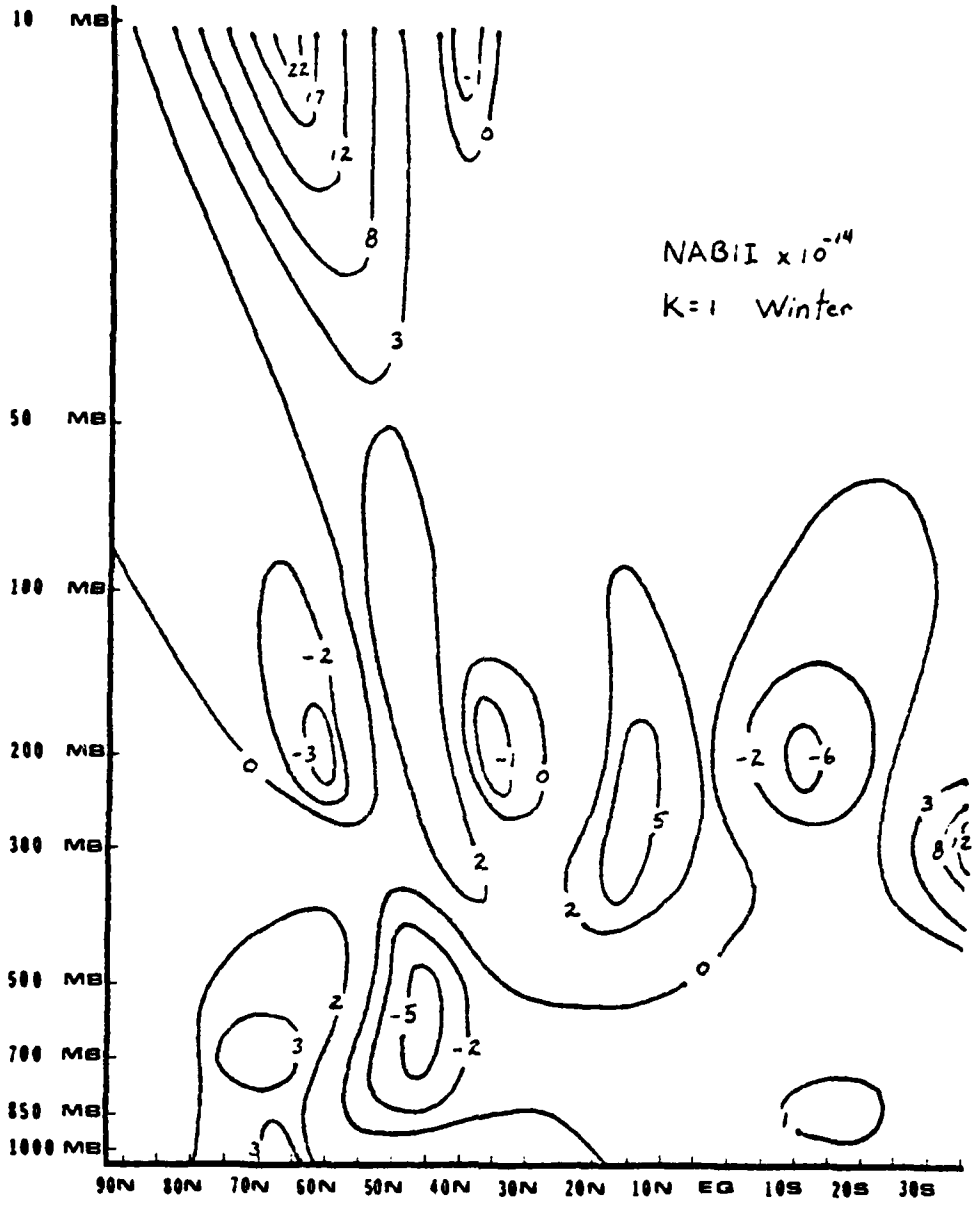


Figure 61. Distribution of NABlI over the winter season for wave number 1 ($m^2/sec^2/day$).

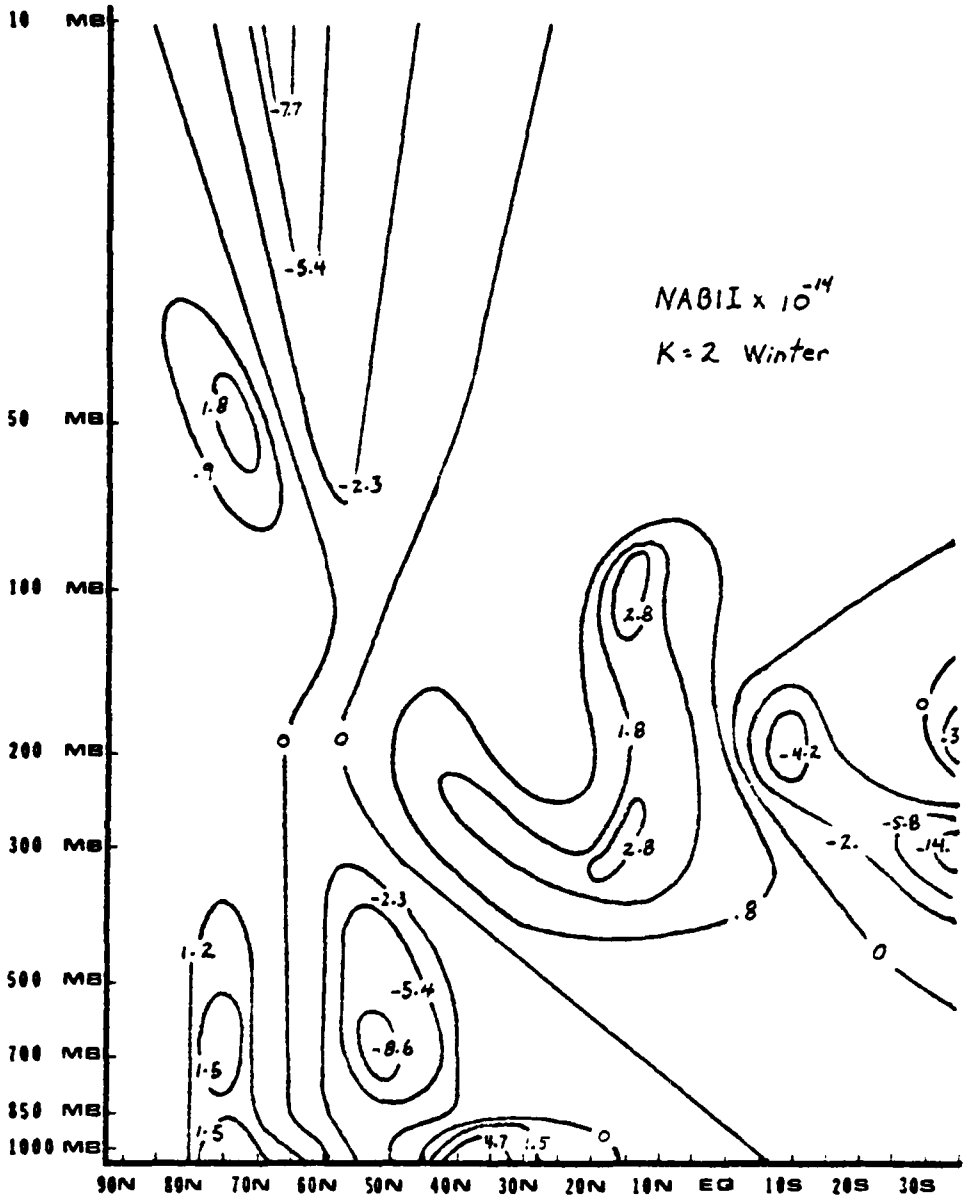


Figure 62. Distribution of NABlI over the winter season for wave number 2 ($m^2/sec^2/day$).

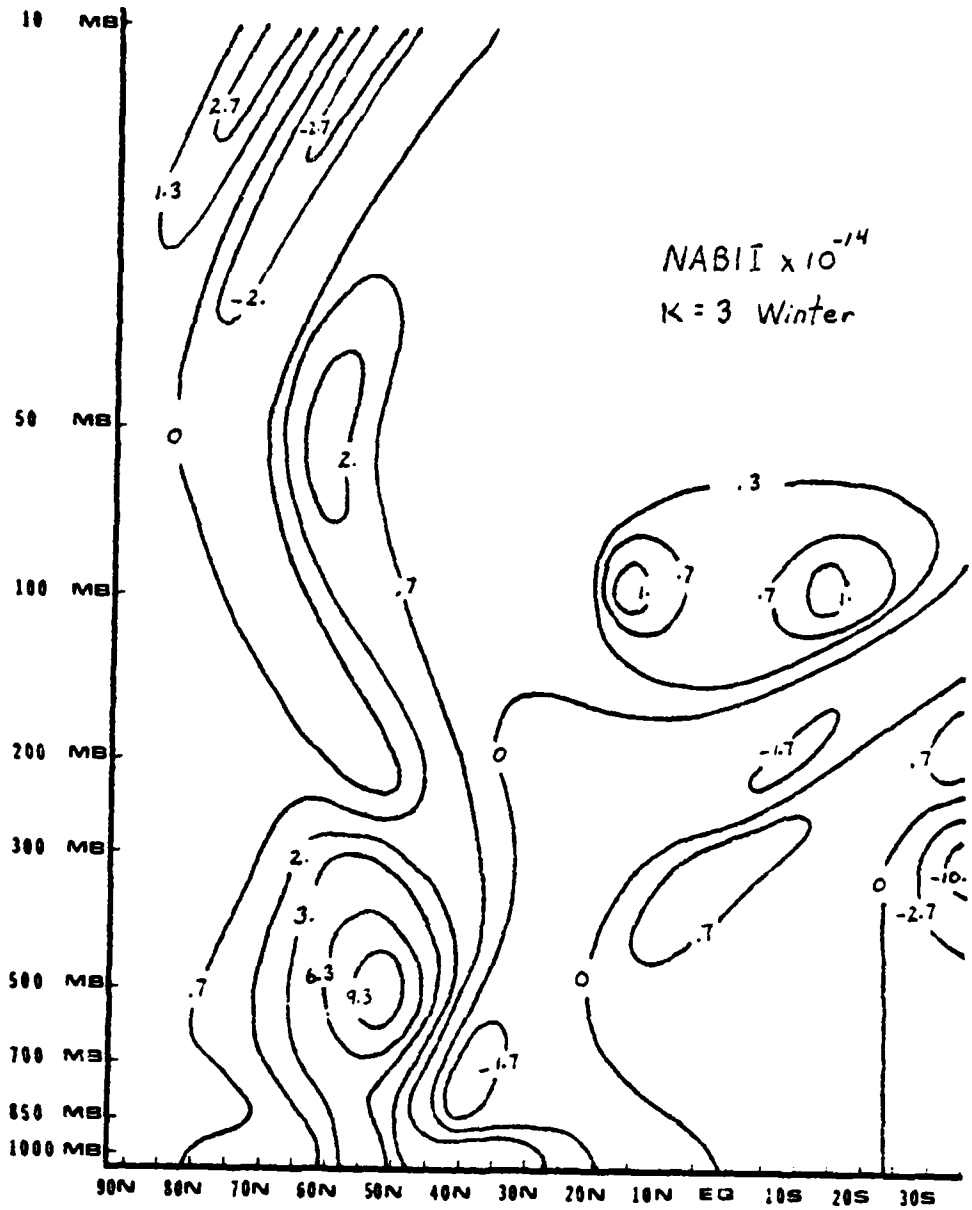


Figure 63. Distribution of NABII over the winter season for wave number 3 ($m^2/sec^2/day$).

30°N, 180 mb; and 10°S, 200 mb. The tropospheric centers correspond well with the composite available potential energy centers appearing in Figure 23, with northward transfer to the north of energy centers and southward transfer to the south of energy centers. It may also be pointed out that southward transfer is seen to the north of EA minimums and northward transfer is seen to the south. These patterns indicate that NAB1I is primarily dissipative in nature, operating to transfer energy away from large available potential energy centers and into regions of low available potential energy through nonlinear interaction. Three major features of NAB1I transfer by individual wave numbers may be pointed out. First, transfer is northward in the region of the tropical tropopause for all wave numbers shown in Figures 61 through 63. Second, transfer in the Northern Hemisphere troposphere is always dispersive as described for the composite figure above, but wave numbers 2 and 3 appear to concentrate energy in the region of Southern Hemisphere tropospheric maximum EA seen in Figures 21 and 22. The final important feature concerns the "decay" of the strong tongue of available potential energy seen in Figure 20, and discussed earlier in section 4.2.2 For wave number 1, this stratospheric feature is strongly supported by intense positive energy transfer due to NAB1I. For wave number 2 (Figure 21), the stratospheric tongue of available potential energy greatly decreased in intensity, and corresponding stratospheric transfer by NAB1I has turned strongly negative. For wave number 3, the stratospheric transfer is weak and both positive and negative.

Associated with this, the stratospheric maximum of available potential energy has completely disappeared. It would appear that transfer by NAB1I can be dramatic indeed.

Figures 64 through 67 display the vertical nonlinear transfer term, NAB2I, for the composite of wave numbers 1 through 20 and for wave numbers 1, 2, and 3. Figure 64, showing composite transfer by NAB2I, demonstrates the two major features seen on Figures 65, 66, and 67 as well. First, transfer by NAB2I in the stratosphere is almost nonexistent. Second, very strong upward vertical transfer exists in the area of maximum vertical velocity seen in Figure 4. Since NAB2I is a function of temperature and omega interactions, this term probably follows the area of maximum heating influence to a greater degree than do the other terms. The final feature of NAB2I forcing is evident only when Figures 65, 66, and 67 are compared with the associated available potential energy cross sections (Figures 21, 22, and 23). From this comparison, it is seen that NAB2I transfers upward to the north of available potential energy centers, and transfers downward to the south of these centers. In this light, the three cell mean circulation in the Northern Hemisphere troposphere can clearly be drawn directly from Figure 67, for wave number 3. This three cell circulation is not as obvious for wave numbers 1 or 2, indicating that wave number 3 transfer by NAB2I may be of significant importance in the maintenance of the Northern Hemisphere general circulation.

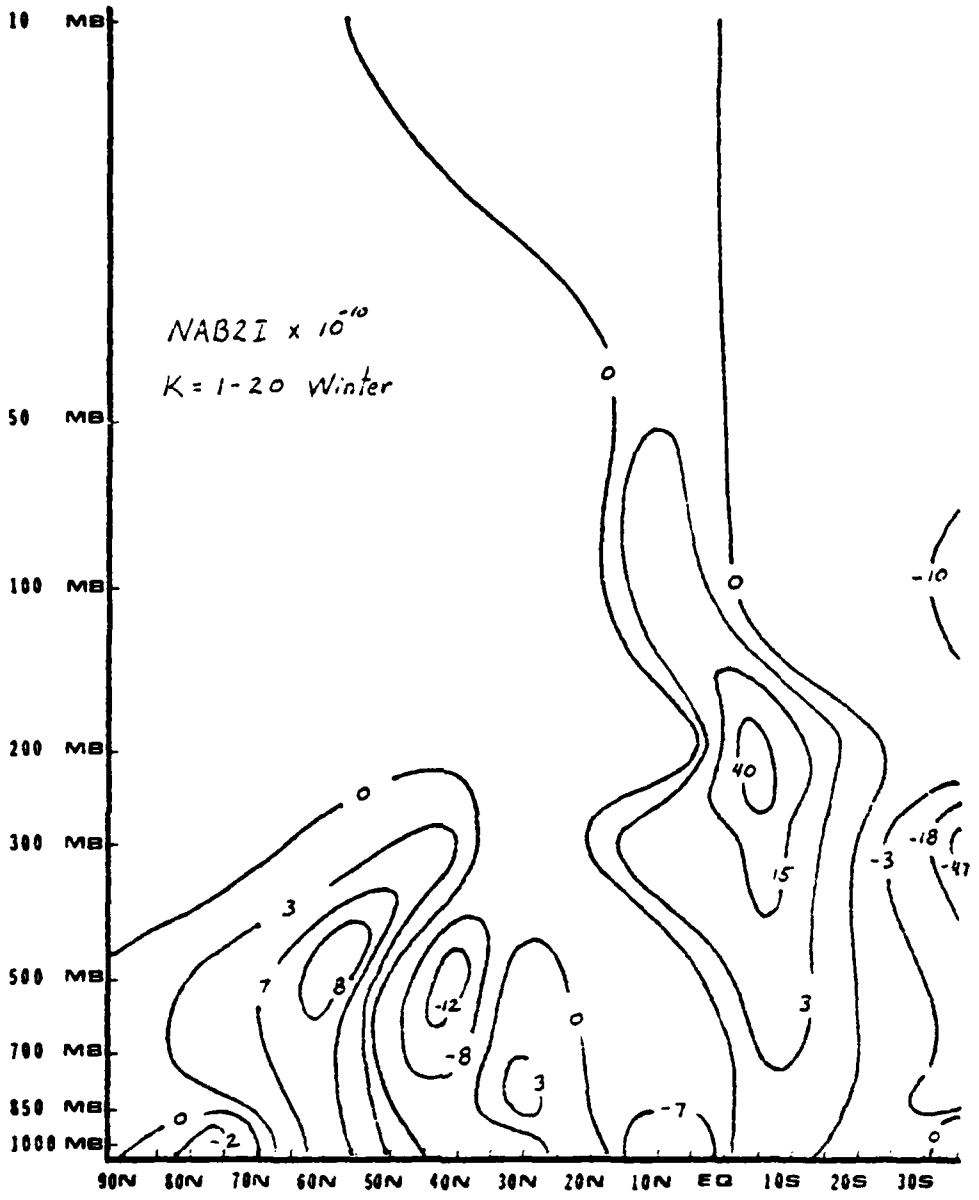


Figure 64. Distribution of NAB2I summer over wave numbers 1 - 20 and averaged over the winter season ($m^2/sec^2/day$).

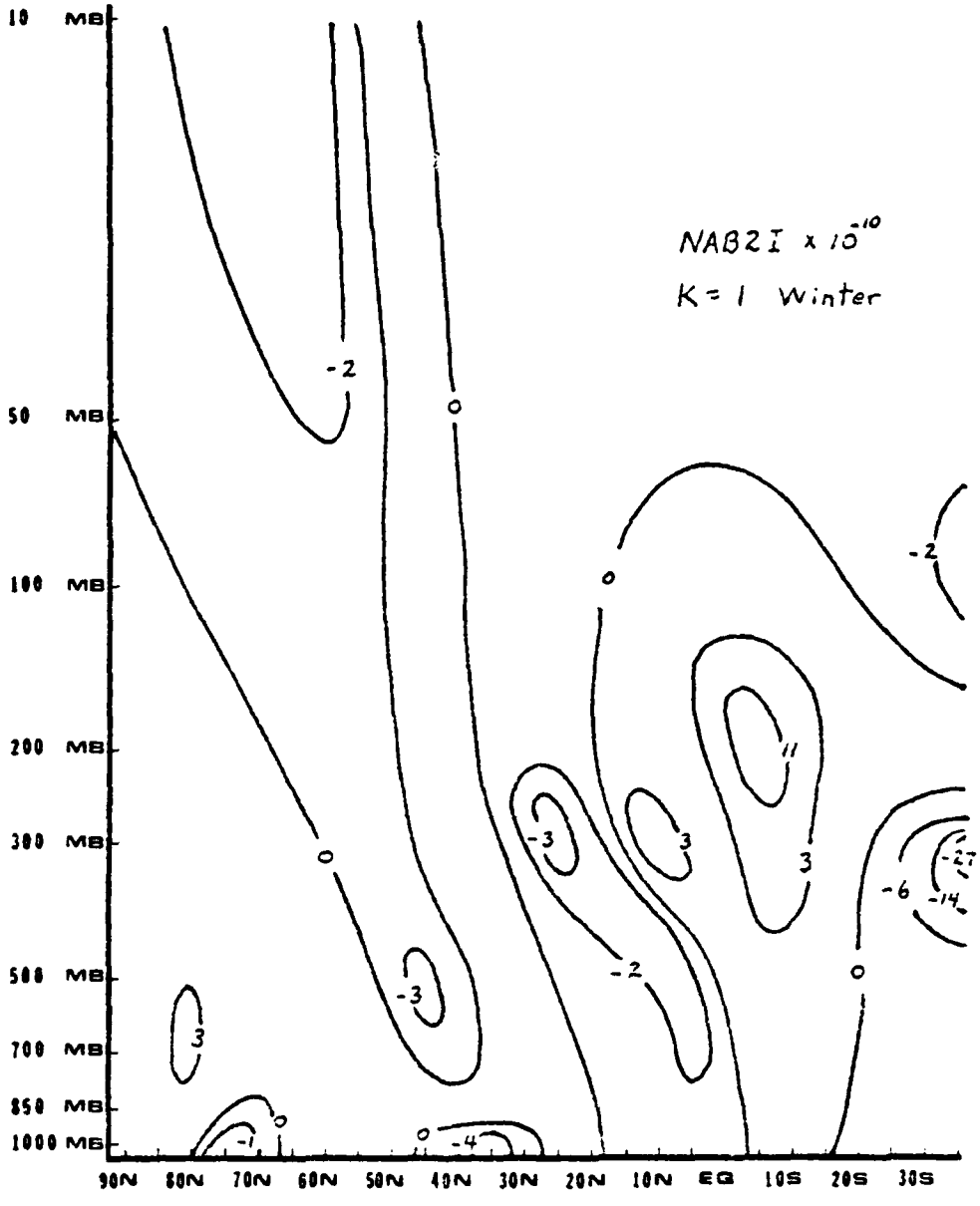


Figure 65. Distribution of NAB2I over the winter season for wave number 1 ($m^2/sec^2/day$).

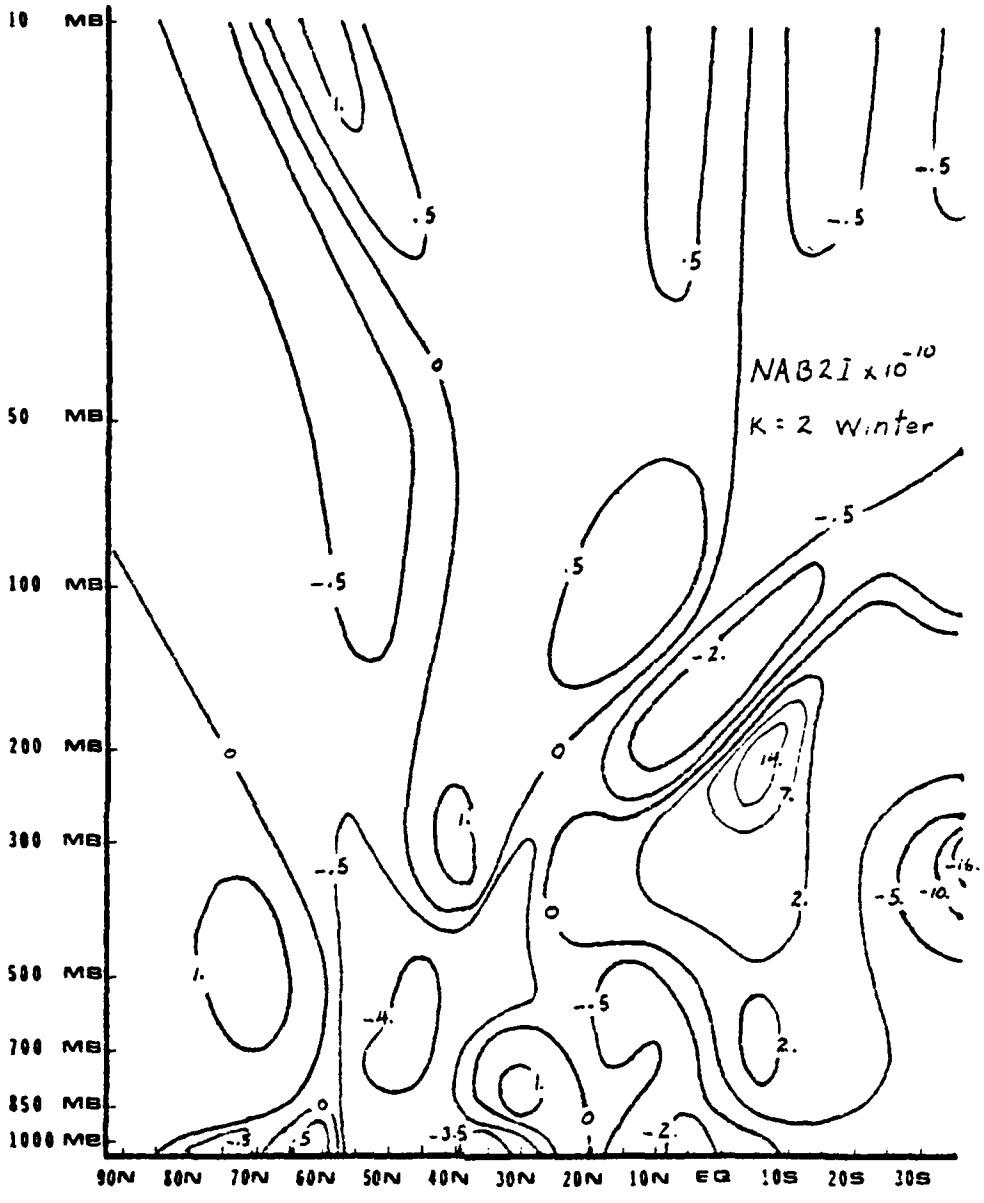


Figure 66. Distribution of NAB2I over the winter season for wave number 2 ($m^2/sec^2/day$).

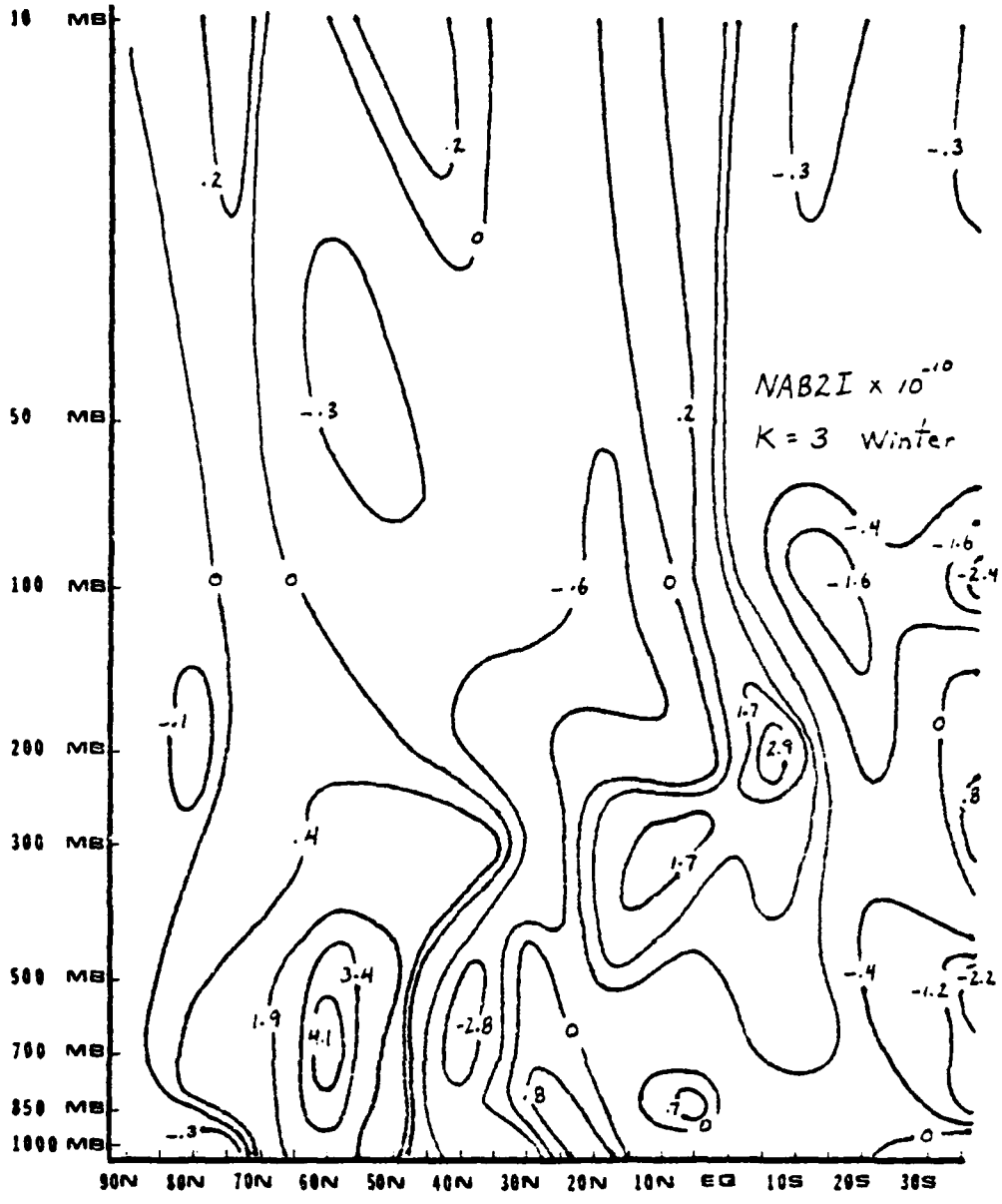


Figure 67. Distribution of NAB2I over the winter season for wave number 3 ($m^2/sec^2/day$).

# CHAPTER 5

# GROWTH AND DECAY OF LARGE SCALE ATMOSPHERIC WAVES

## 5.1 Physical Interpretation of Time Transforms

While study of mean seasonal conditions can produce many important features of energy exchanges operating in the atmosphere, this approach cannot bring to light any information concerning the sequence of events leading to the growth or decay of a wave in the atmosphere. To study the order of events leading to wave growth and decay, transforms in time must be done. As a result of the time transformed equations (2.30) and (2.31), phase angles may be derived which show the relative occurrence in time of each term in relation to all other terms.

Before discussing the results of any time transforms, a firm understanding of the physical meaning of the concept is required. The physical meaning of a transform in space is an appropriate place to begin. When a cyclic set of data is transformed, such as values of temperature around a complete latitude circle, the result is a single complex number for each "wave number" contributing to total wave pattern existing in the original data. The "wave number" is simply the number of cosine waves fitting the data around a latitude

circle. While data is not gererally cyclic in time, it can be made to appear cyclic by gradually tapering the beginning and ending of the sequence of data to be transformed to zero (cosine bell). The data may now be transformed in time just as it was in space, with the resultant single complex number associated with each "frequency" (rather than wave number). From the complex number associated with a given frequency, both the phase angle ($\theta = \tan^{-1} Q_i/Q_r$) and the magnitude ($\sqrt{Q_i^2 + Q_r^2}$) for that frequency can be obtained, and these are essentially the phase angles and magnitudes appearing in the figures to follow. Chapter 2 discusses the details of this process in a rigorous fashion.

## 5.2 Evolution of the Available and Kinetic Energy of the Large Scale Atmospheric Waves

Examining (2.30) and (2.31) we have found that the evolving kinetic and available potential energy depends primarily on the phase angle and amplitude of the terms on the right hand side of the equations. We shall now analyze the processes of the evolution of the kinetic and available potential energy associated with waves of various wavelengths and frequencies in the troposphere and stratosphere in the mid-latitudes and near the equator.

Figures 68 through 97 show the evolution of the kinetic and available potential energy at 500, 50, and 10 mb for wave numbers 0, 1, 2, 3, and 7. Area integration using (4.3) was carried out from 30°N to 60°N for winter and from 15°S to 15°N for summer. Terms with magnitudes of less than 10% of the magnitude of the largest term in each frame were not plotted. The periods of wave

growth or decay, i.e., the time for one complete cycle, were selected on the basis of having the largest amplitude of $\partial EK/\partial t$ for each wave number presented. The average periods for the largest value of $\partial EK/\partial t$ for the winter middle latitude troposphere and stratosphere are, respectively, 5.8 days and 7.5 days. For the summer tropical cases, the average corresponding periods are 4.0 days and 2.9 days, demonstrating that summer tropical disturbances are much shorter lived than winter middle latitude systems.

Before discussing Figures 68 through 97 in detail, it must be pointed out that the phase angles presented as "phase relative to $\partial EK/\partial t$" in the diagrams may equally well be considered as "relative phase between terms". The point is that $\partial EK/\partial t$ need not begin the process of wave growth simply because it occupies the central location on these phase diagrams.

Examining the mechanisms for the evolution of 500 mb winter tropospheric waves of wave number 1 through 7, as shown in Figure 68 through 72, it is seen that the growth and decay of waves are almost directly the response to the nonlinear interactions (NK1, NK2) and the vertical convergence of geopotential flux (AKB2). Consider first the evolution of waves of wave number 1 as shown in Figure 69. Beginning from NK1 and proceeding in cyclic manner through both plots of phase angle, the sequence of events would be NK1, NK2, AKB2, $EK_t$, HA, $EA_t$, MA, AK, NAB1, GK, NA1, NKB1, AKB, and finally, KA. This may be seen as an orderly sequence of events, starting with energy input by nonlinear interactions (NK1

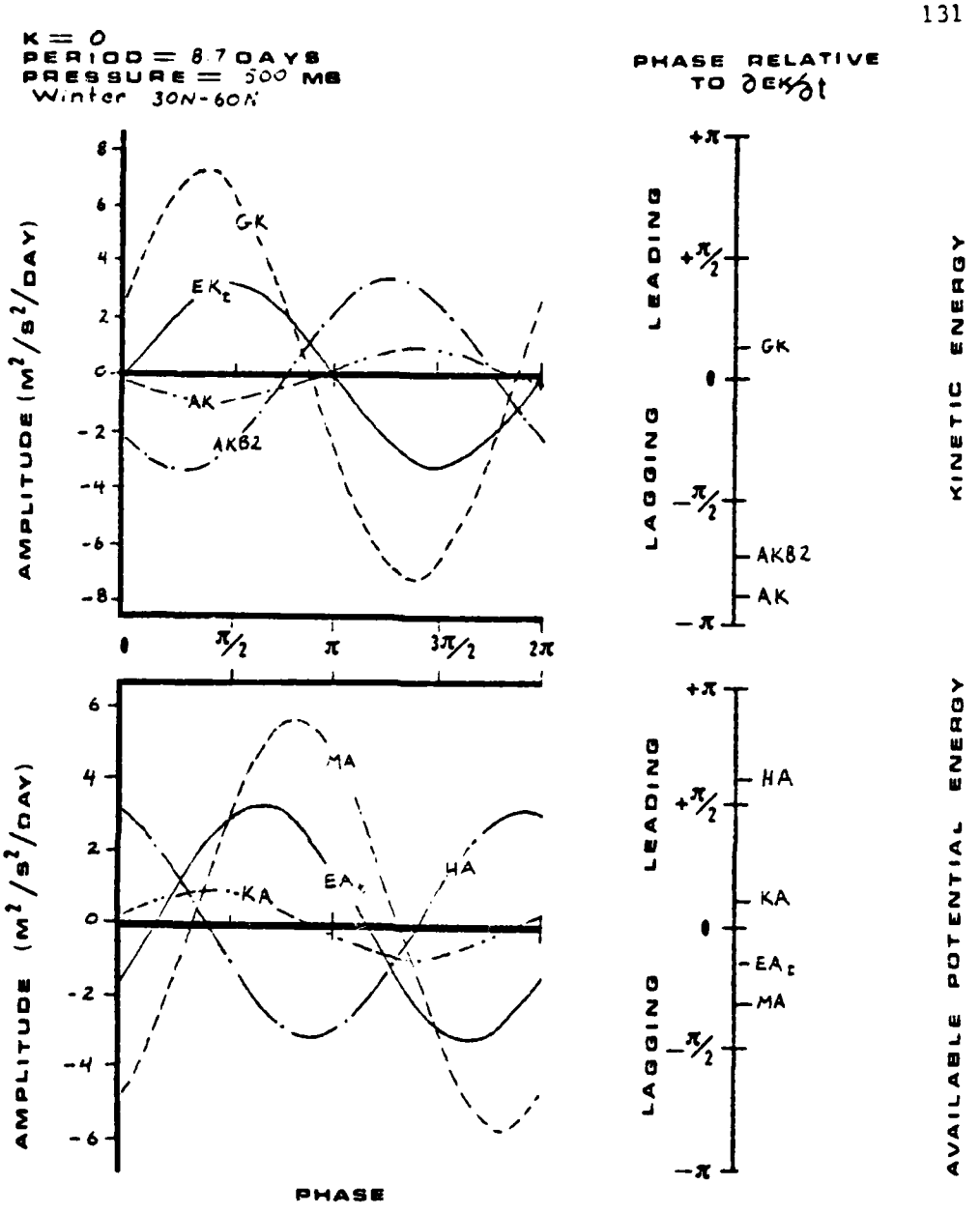


Figure 68. Winter variations of the kinetic and available potential energies in relation to the linear and nonlinear contributions to waves of wave number 0, period 8.7 days, averaged over 30°N - 60°N at 500 mb.

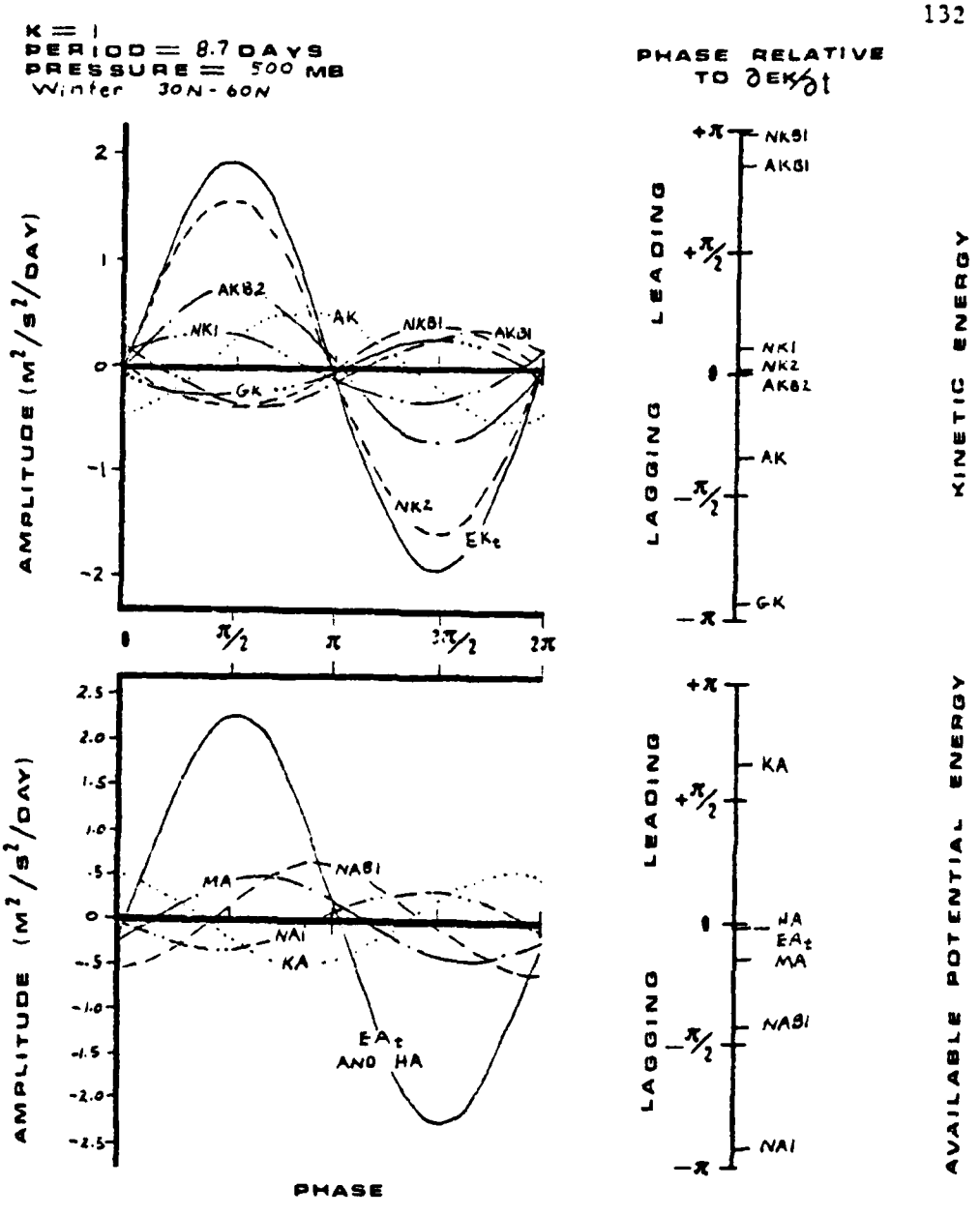


Figure 69. Winter variations of the kinetic and available potential energies in relation to the linear and nonlinear contributions to waves of wave number 1, period 8.7 days, averaged over 30°N - 60°N at 500 mb.

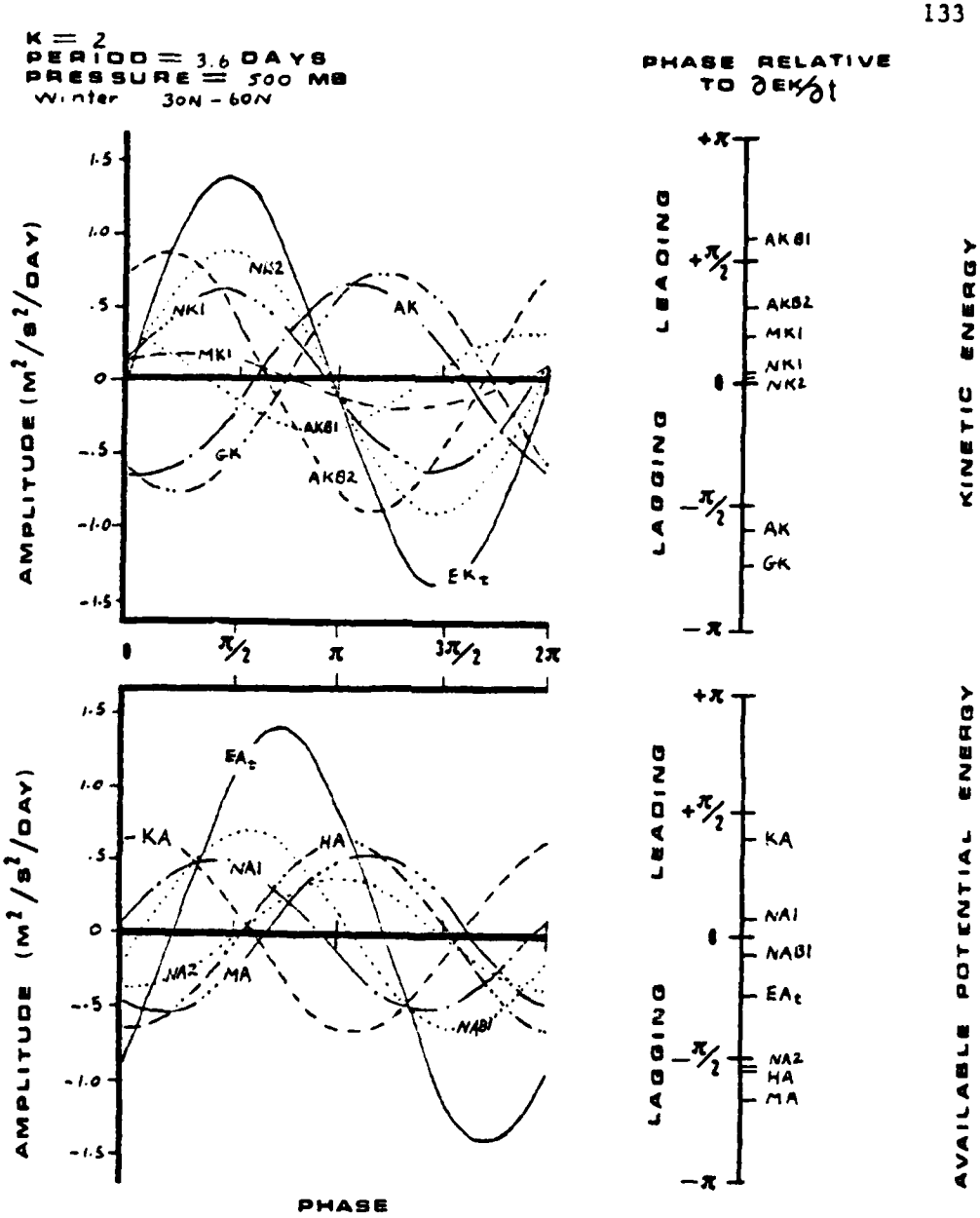


Figure 70. Winter variations of the kinetic and available potential energies in relation to the linear and nonlinear contributions to waves of wave number 2, period 3.6 days, averaged over 30°N - 60°N at 500 mb.

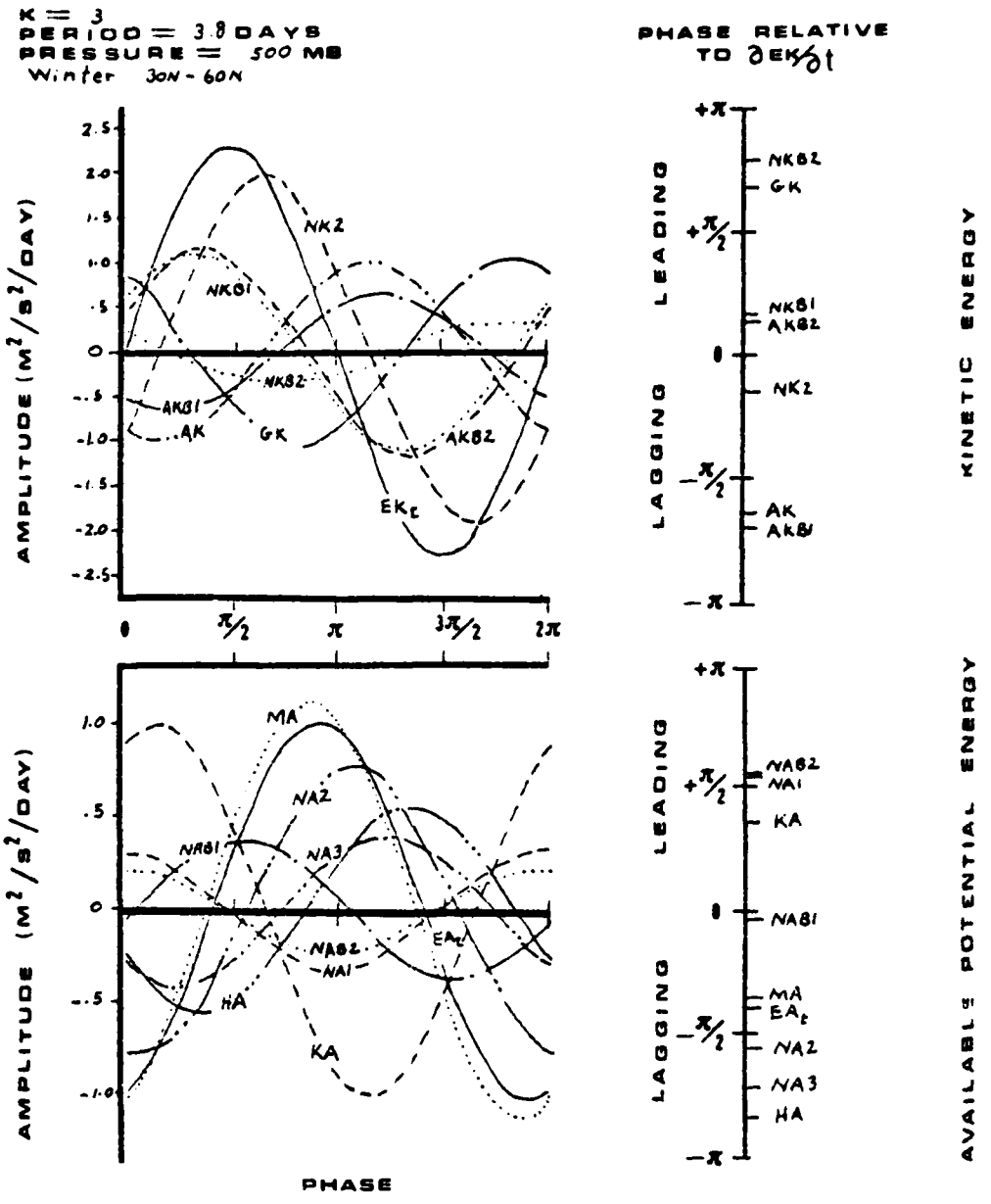


Figure 71. Winter variations of the kinetic and available potential energies in relation to the linear and nonlinear contributions to waves of wave number 3, period 3.8 days, averaged over 30°N - 60°N at 500 mb.

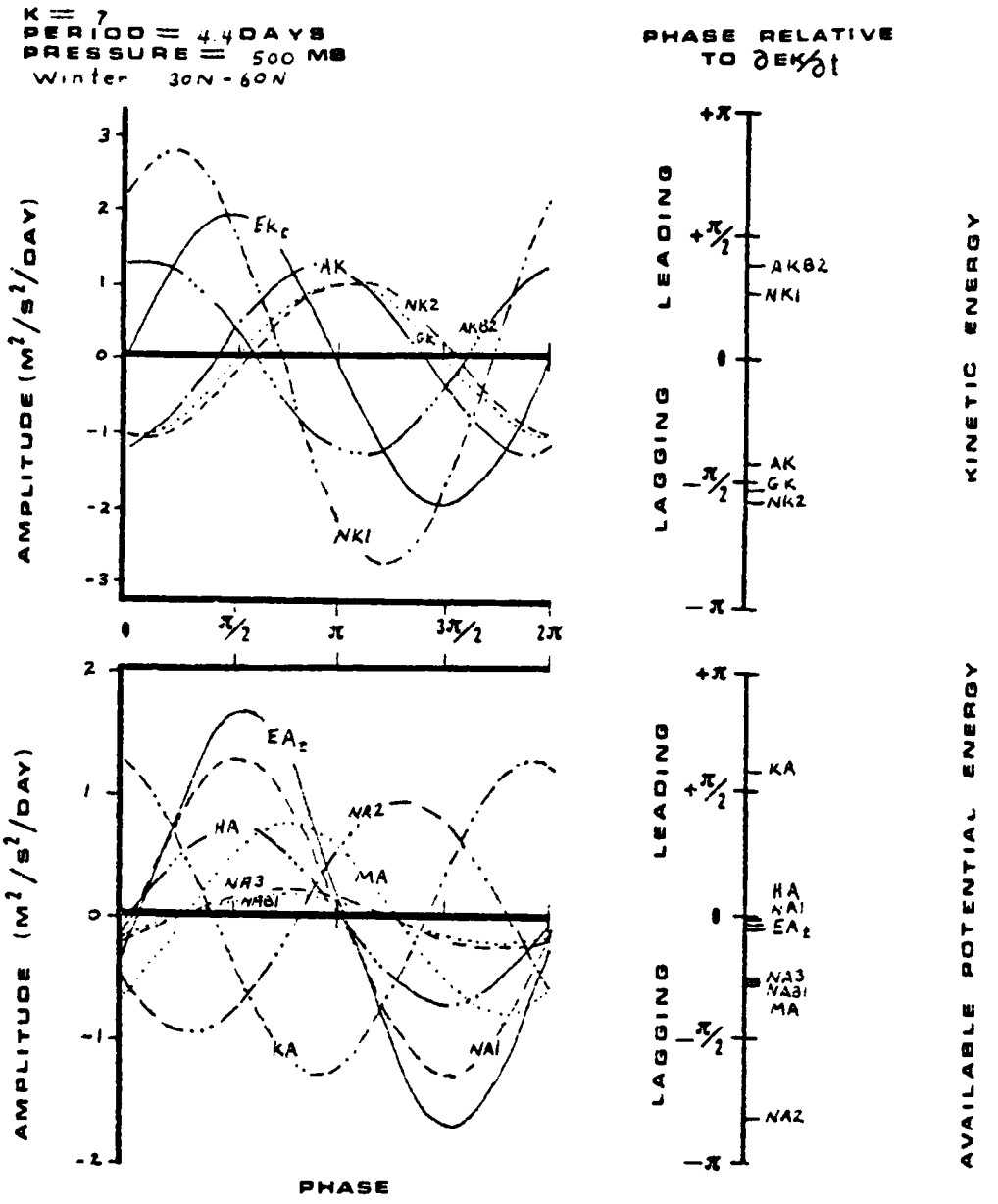


Figure 72. Winter variations of the kinetic and available potential energies in relation to the linear and nonlinear contributions to waves of wave number 7, period 4.4 days, averaged over 30°N - 60°N at 500 mb.

and NK2) and the vertical convergence of geopotential flux (AKB2). In response to these inputs, the kinetic energy of the wave begins to increase ($EK_t$). Meanwhile HA also increases, either due rectly to latent heat release or due to nonadiabatic heating (which may also have caused the height field to change). Changes in HA dictate changes in $EA_t$. As $EK_t$ is increasing, so too does MA, dependent primarily on V'T' interaction. AK may naturally begin its increase at this point for either of two reasons. First, if any shear in the wind is present, upward vertical velocity can develop by (3.2), and second, increasing MA generally implies warm air moving north or cold air moving south, both of which can cause the conversion of available potential energy to kinetic energy. Probably near this point, the wave begins to decay by energy extraction due to GK and the nonlinear interactions NKB1, and NA1, and loss of kinetic energy through KA.

For the evolution of waves of wave number 2, as shown in Figure 70, the sequence of events would be AKB2, MK1, NA1, NK1, NK2, $EK_t$, NAB1, $EA_t$, NA2, HA, AK, MA, GK, AKB1, and KA. For wave number 2, the vertical convergence of geopotential flux (AKB2) and the nonlinear interactions MK1, NK1, and NK2 preceded the increase in EK, while interactions NA1 and NAB1 preceded the increase in EA. These events were then followed by nonadiabatic heating (HA), the conversion of available potential energy to kinetic energy (AK), transfer of eddy kinetic energy to kinetic energy of the mean flow (MA), sub-scale wave interaction kinetic energy dissipation (GK), energy extraction due to horizontal forcing (AK31), and loss of kinetic

energy through conversion to available potential energy (KA).

It would first appear that changes in U' or V' are required before MK1 could correspondingly increase, but this is not necessarily true. The MK1 term can increase by changes in the mean flow, even if no changes in U' or V' occur in time. For wave number 2 then, it appears that pressure forcing, extraction of energy from the mean flow, and nonlinear contributions initiate the growth of kinetic energy, while nonlinear energy transfer from other waves and nonlinear horizontal forcing may cause the first increases in EA.

With remarkable similarity, the chain of events leading to wave growth and decay for wave numbers 3 and 7 (Figures 71 and 72) follow the same reasoning presented above. For completeness, the chain of events for wavenumber 3 would be AKB2, $EK_t$, NAB1, NK2, MA, $EA_t$, NA2, AK, AKB1, NA3, HA, NKB2, GK, NAB2, NA1, KA, and NKB1, while the events for wave number 7 are AKB2, NK1, $EK_t$, HA, NA1, $EA_t$, NA3, NAB1, MA, AK, GK, NK2, NA2, and KA.

Evolution of winter stratospheric waves is shown in Figures 73 through 82. At 50 mb and for wave numbers 3 and 7 at 10 mb, it is seen that the vertical pressure work term (AKB2) plays a dominant role. We will therefore select this term as the one which begins the wave growth-decay process, and apply the same general kind of logic to wave evolution in the winter stratosphere as was used in analyzing the winter troposphere. Consider now Figure 74 and assume some external upward forcing. The sequence of events in this diagram would be AKB2, KA, NKB2, NK2, NA1, $EK_t$, GK, $EA_t$,

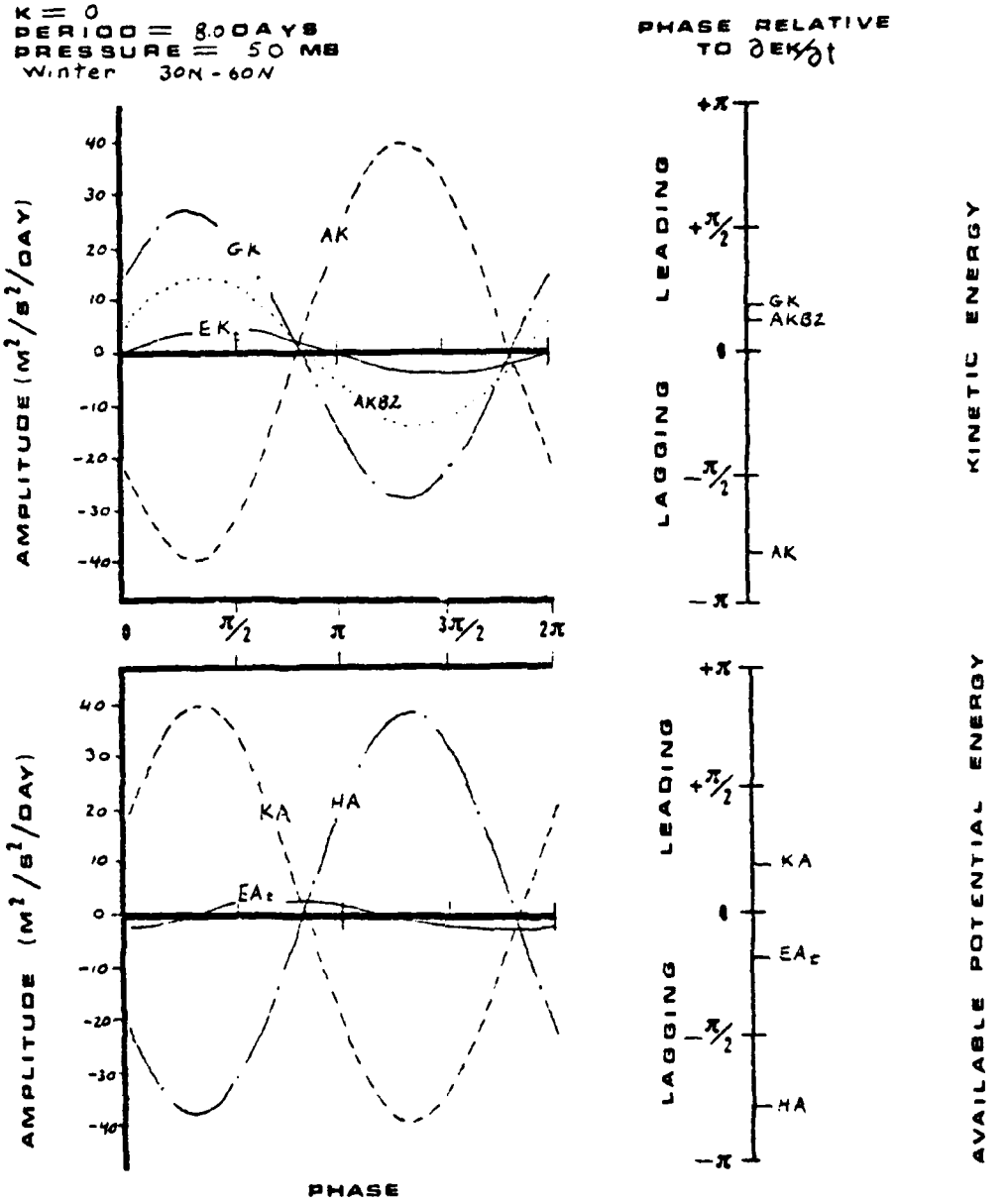


Figure 73. Winter variations of the kinetic and available potential energies in relation to the linear and nonlinear contributions to waves of wave number 0, period 8.0 days, averaged over 30°N - 60°N at 50 mb.

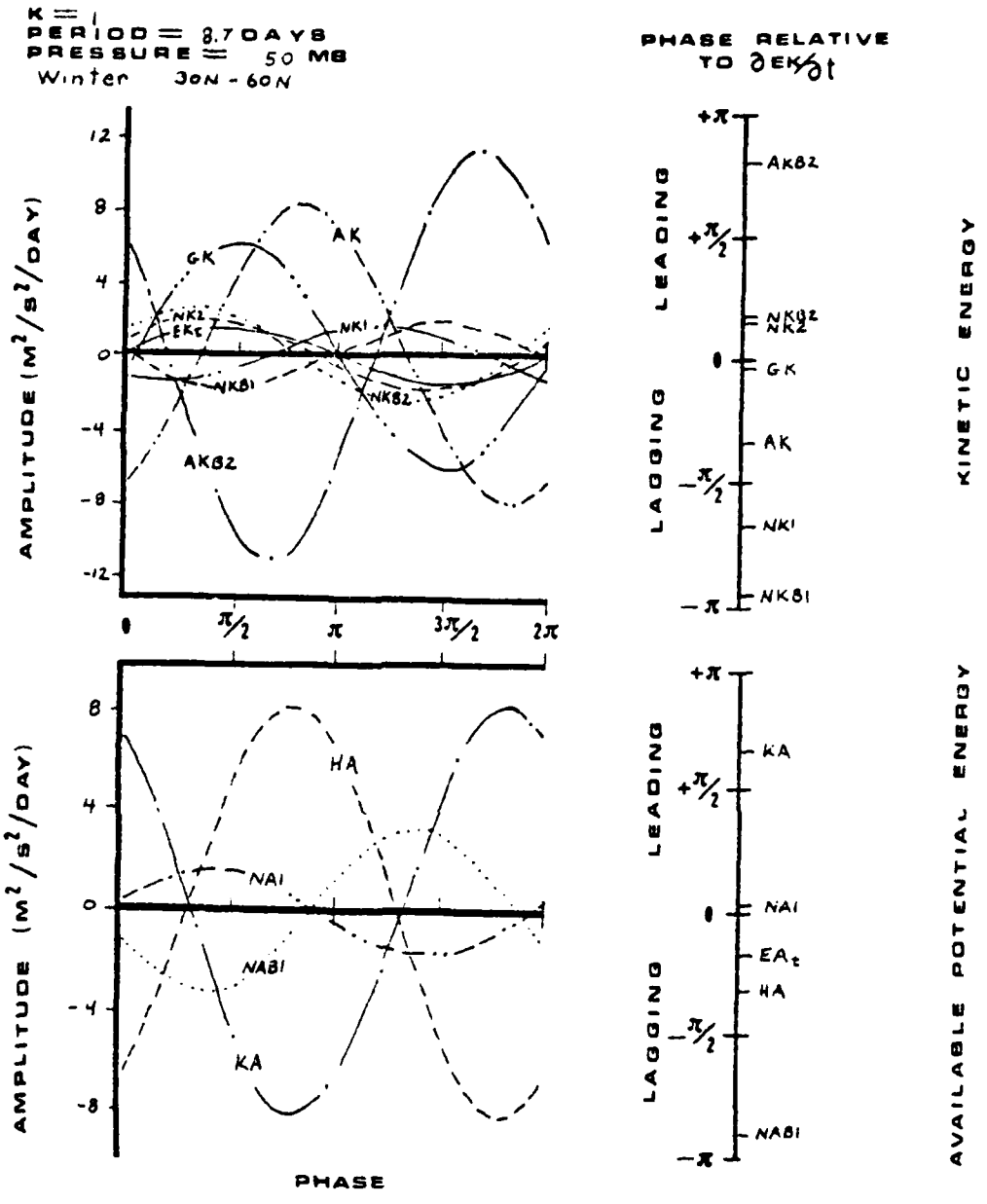


Figure 74. Winter variations of the kinetic and available potential energies in relation to the linear and nonlinear contributions to waves and wave number 1, period 8.7 days, averaged over 30°N - 60°N at 50 mb.

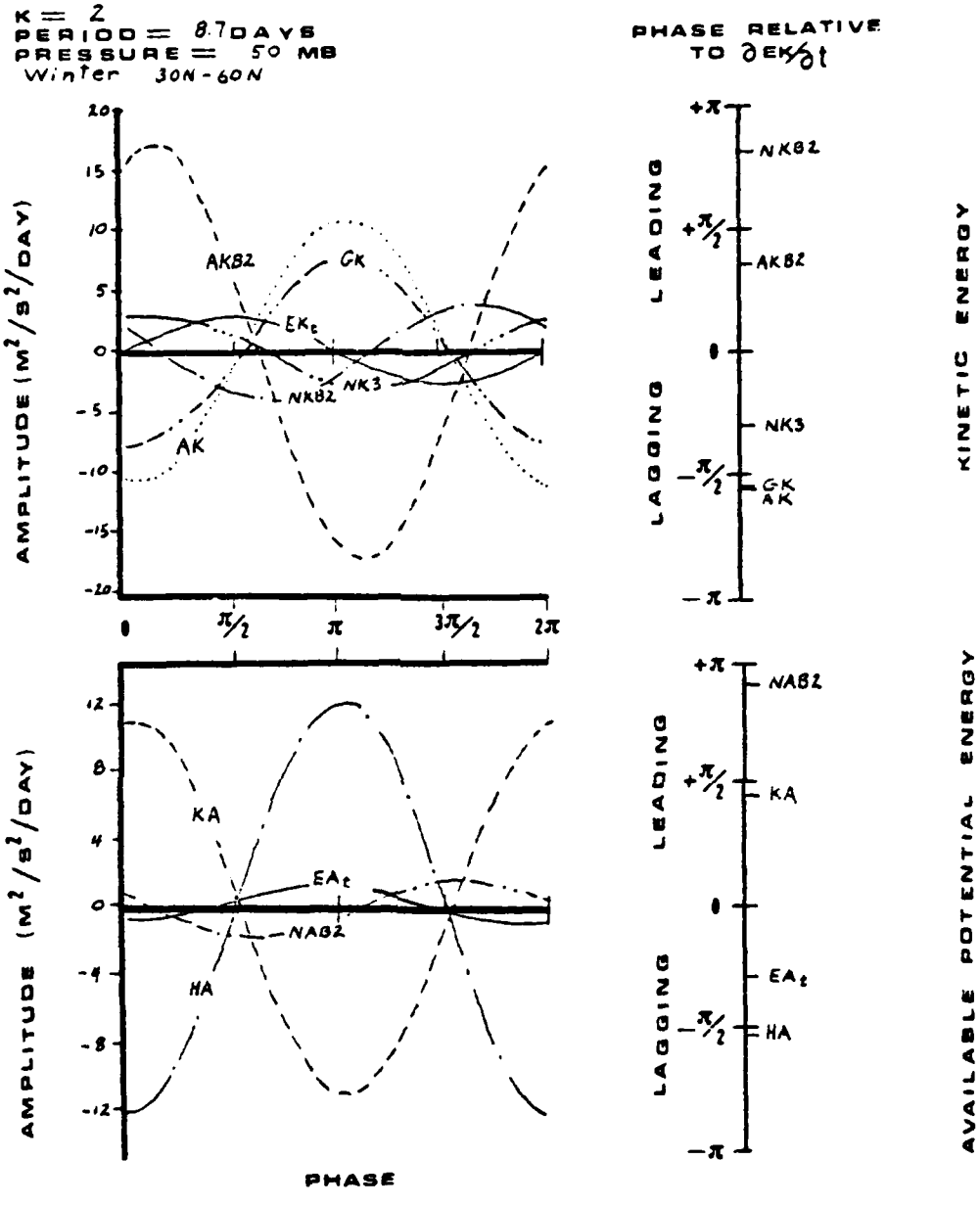


Figure 75. Winter variations of the kinetic and available potential energies in relation to the linear and nonlinear contributions to waves of wave number 2, period 8.7 days, averaged over 30°N - 60°N at 50 mb.

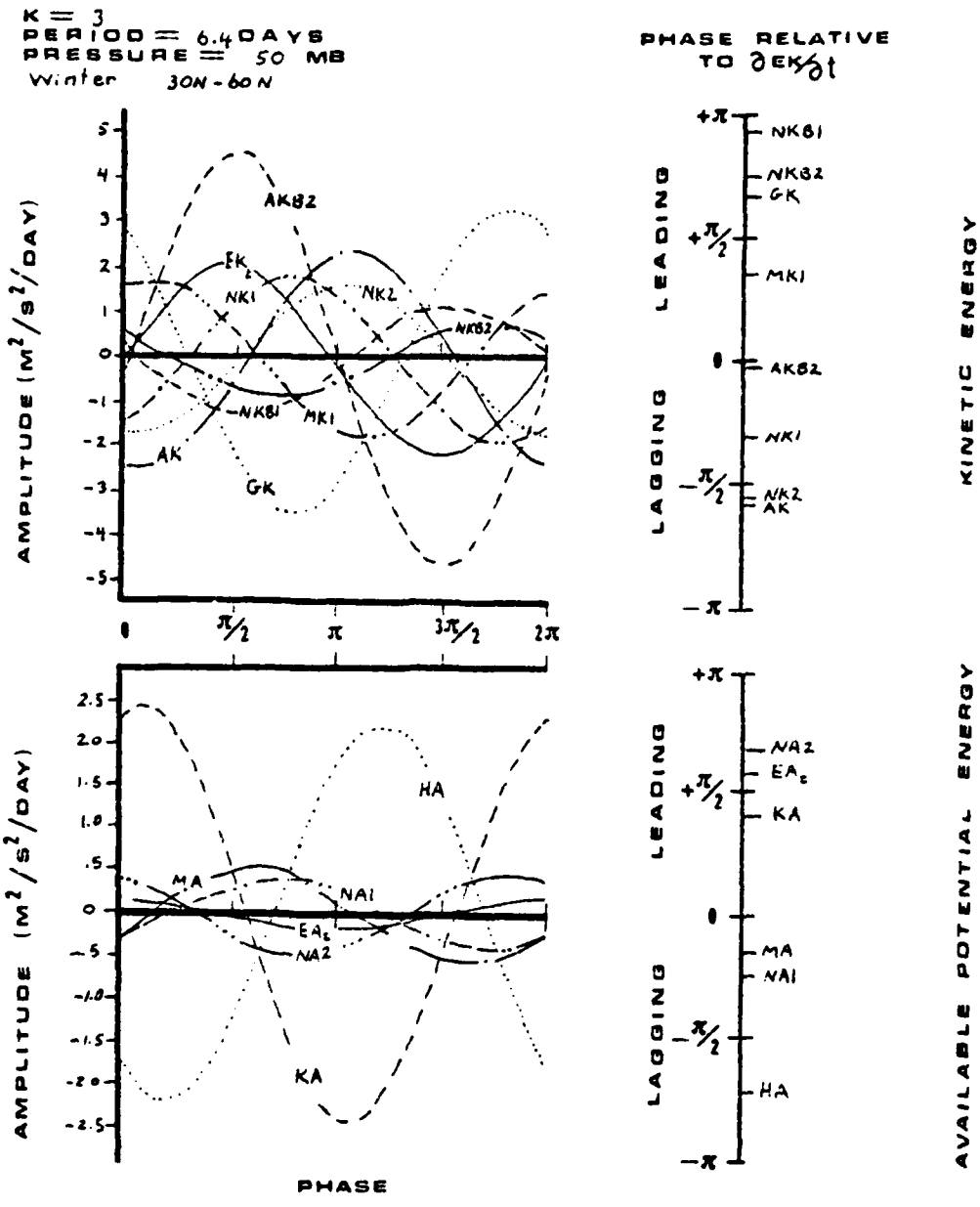


Figure 76. Winter variations of the kinetic and available potential energies in relation to the linear and nonlinear contributions to waves of wave number 3, period 6.4 days, averaged over 30°N - 60°N at 50 mb.

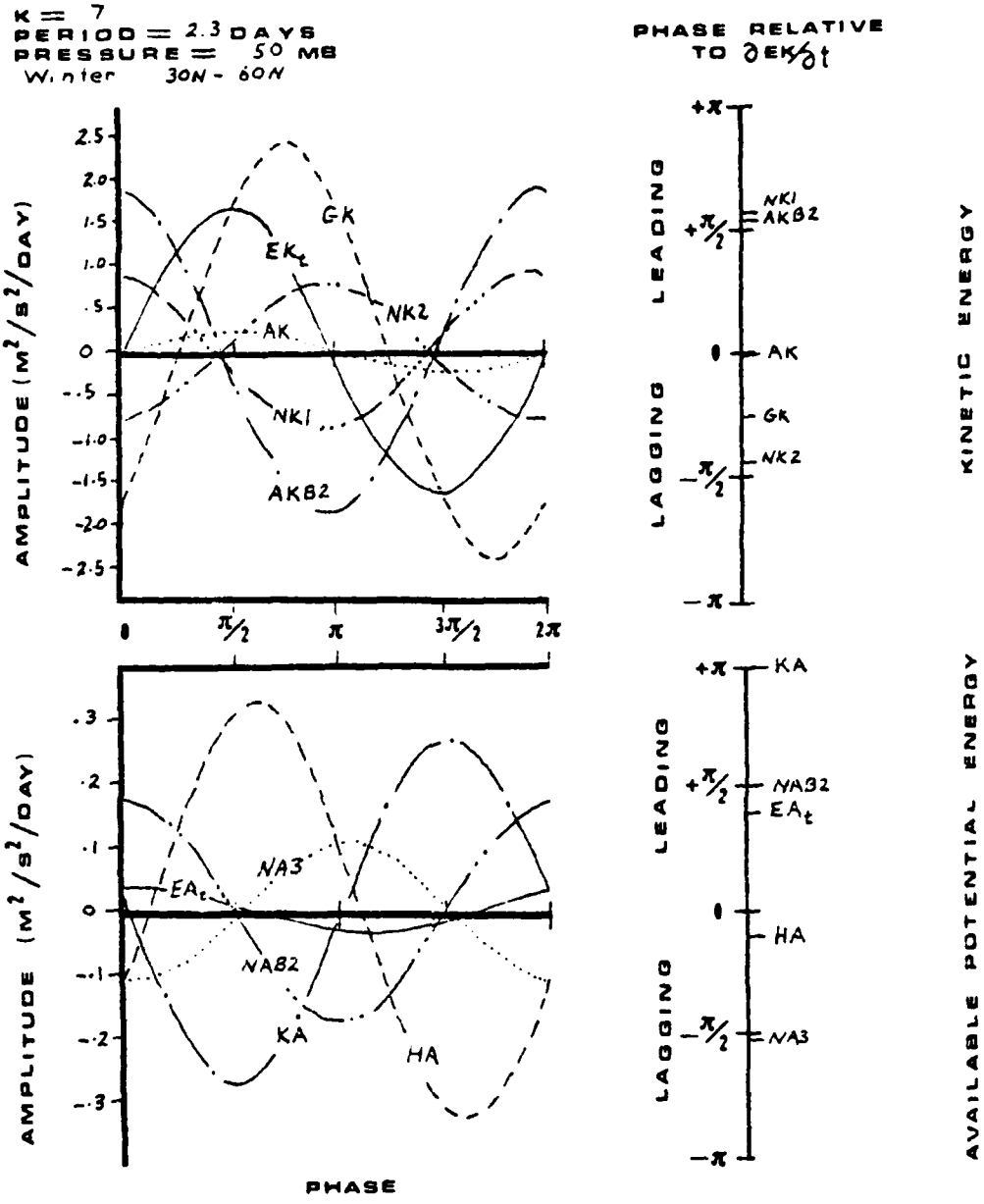


Figure 77. Winter variations of the kinetic and available potential energies in relation to the linear and nonlinear contributions to waves of wave number 7, period 2.3 days, averaged over 30°N - 60°N at 50 mb.

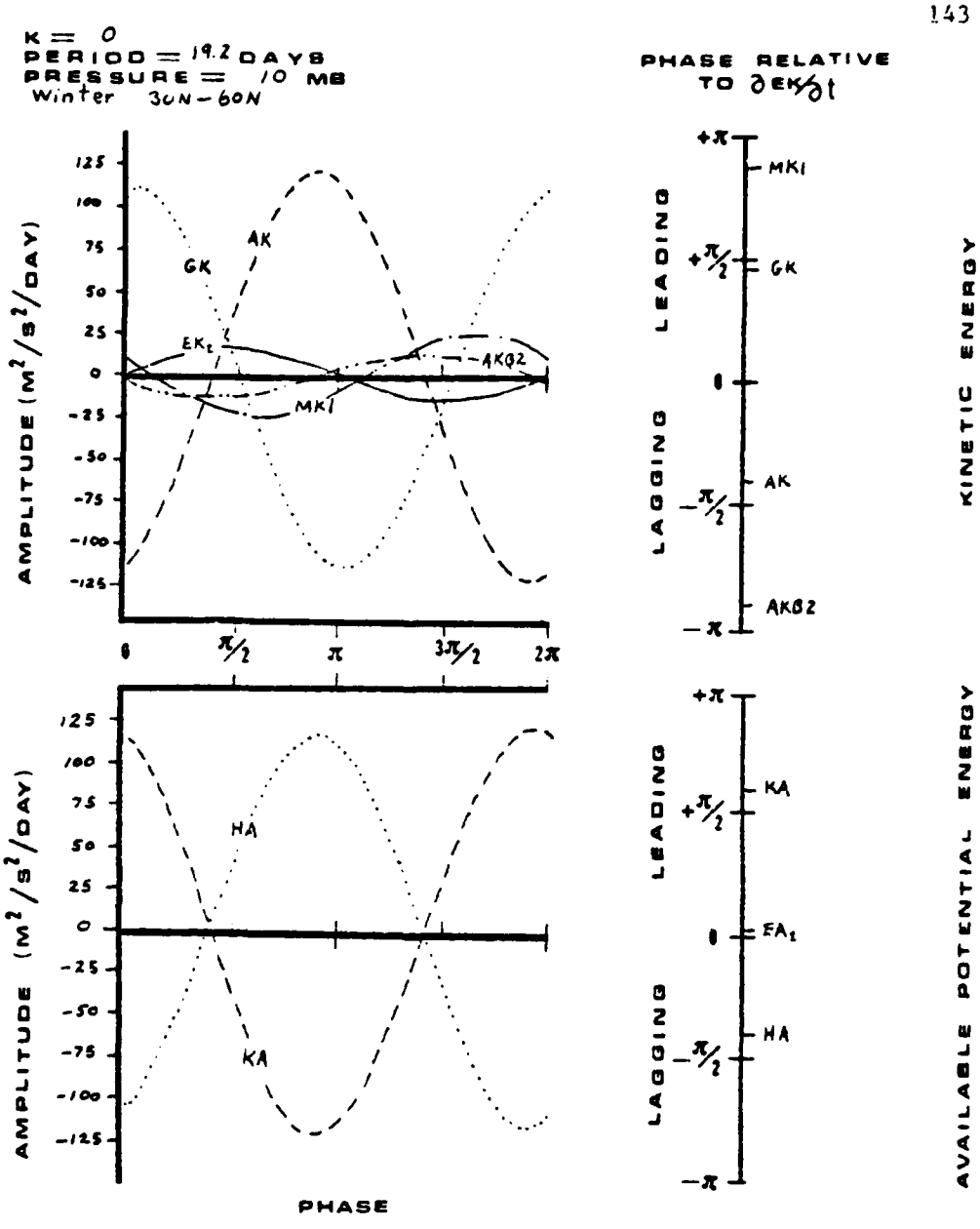


Figure 78. Winter variations of the kinetic and available potential energies in relation to the linear and nonlinear contributions to waves of wave number 0, period 19.2 days, averaged over 30°N - 60°N at 10 mb.

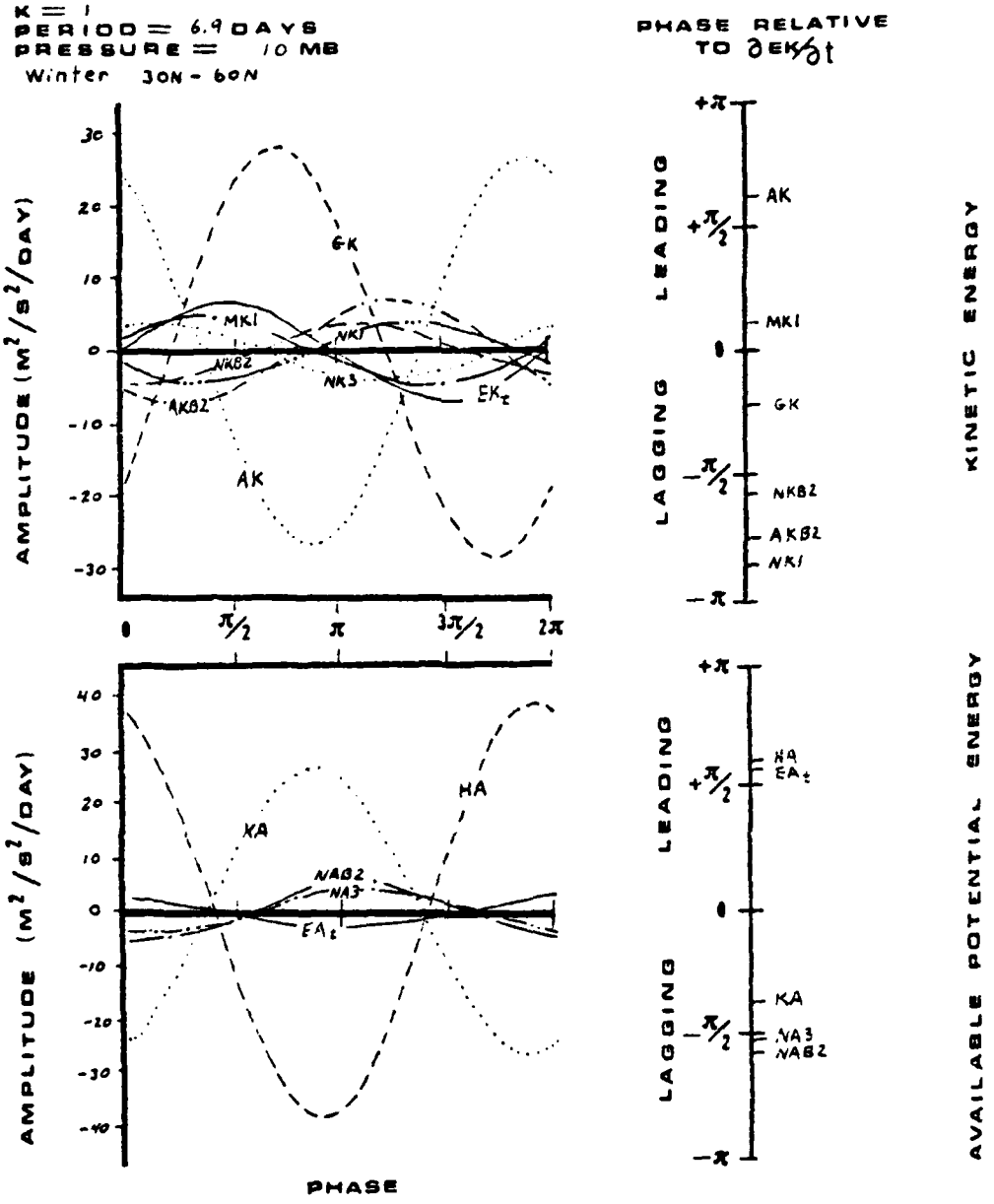


Figure 79. Winter variations of the kinetic and available potential energies in relation to the linear and nonlinear contributions to waves of wave number 1, period 6.9 days, averaged over 30°N - 60°N at 10 mb.

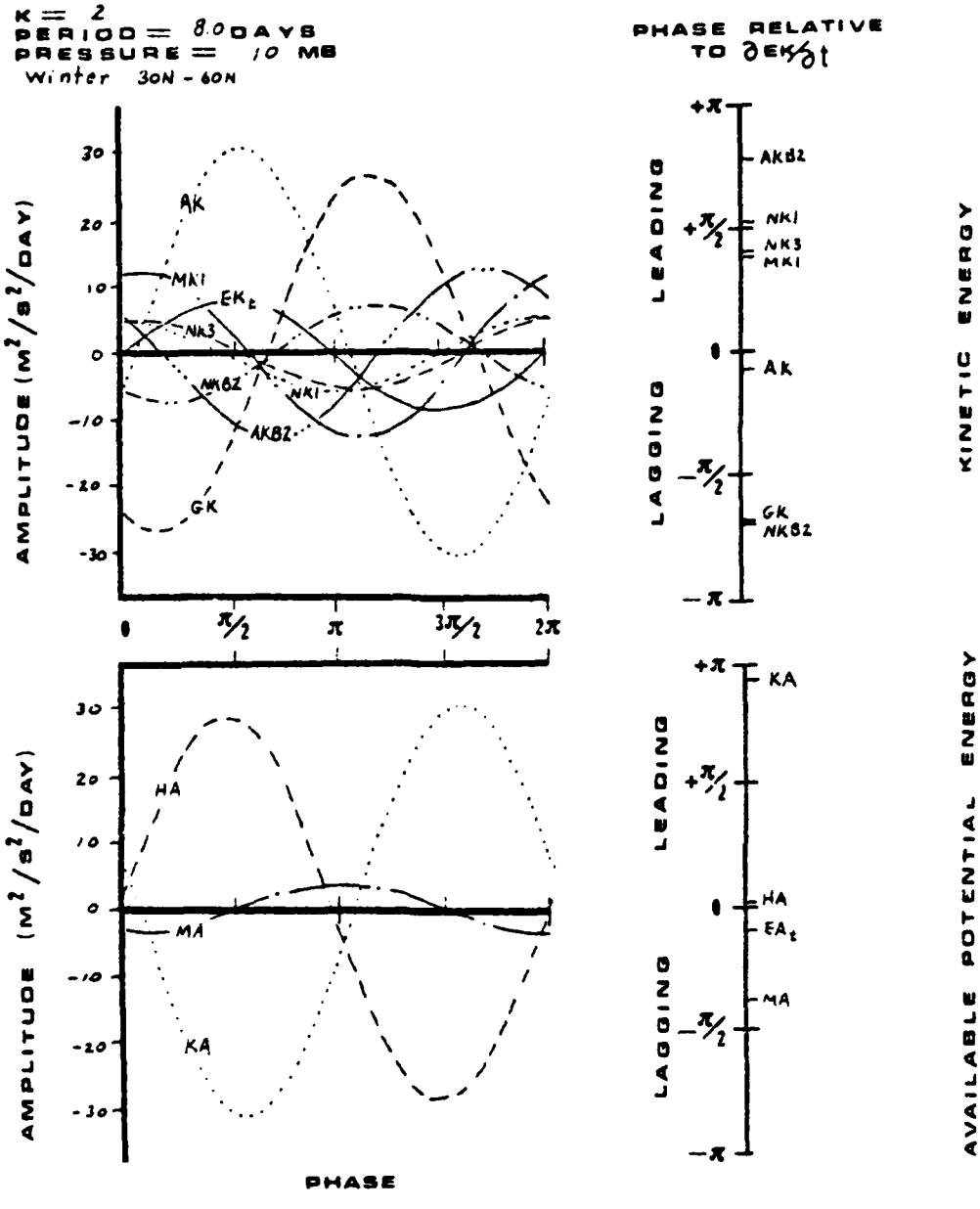


Figure 80. Winter variations of the kinetic and available potential energies in relation to the linear and nonlinear contributions to waves of wave number 2, period 8.0 days, averaged over 30°N - 60°N at 10 mb.

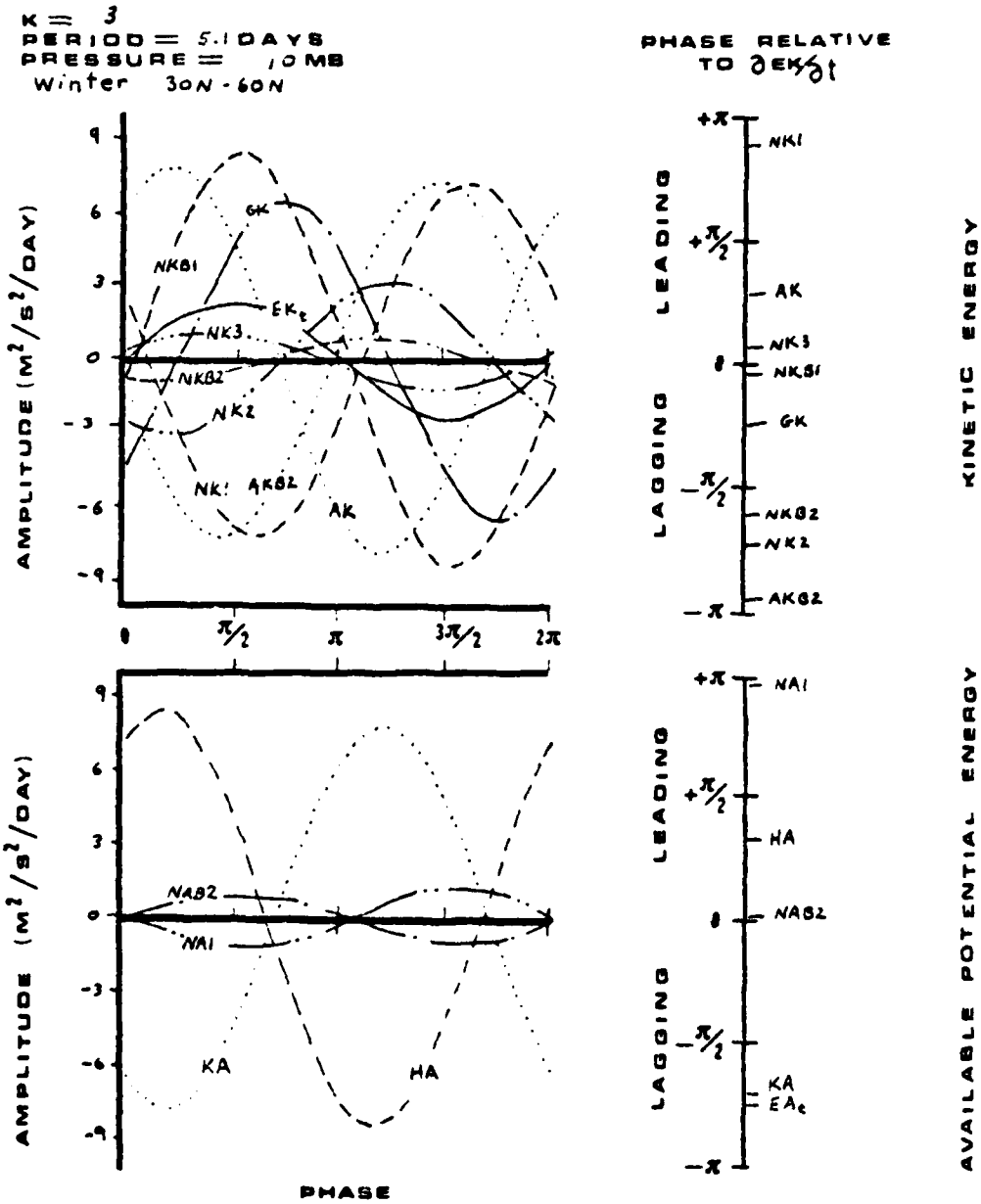


Figure 81. Winter variations of the kinetic and available potential energies in relation to the linear and nonlinear contributions to waves of wave number 3, period 5.1 days, averaged over 30°N - 60°N at 10 mb.

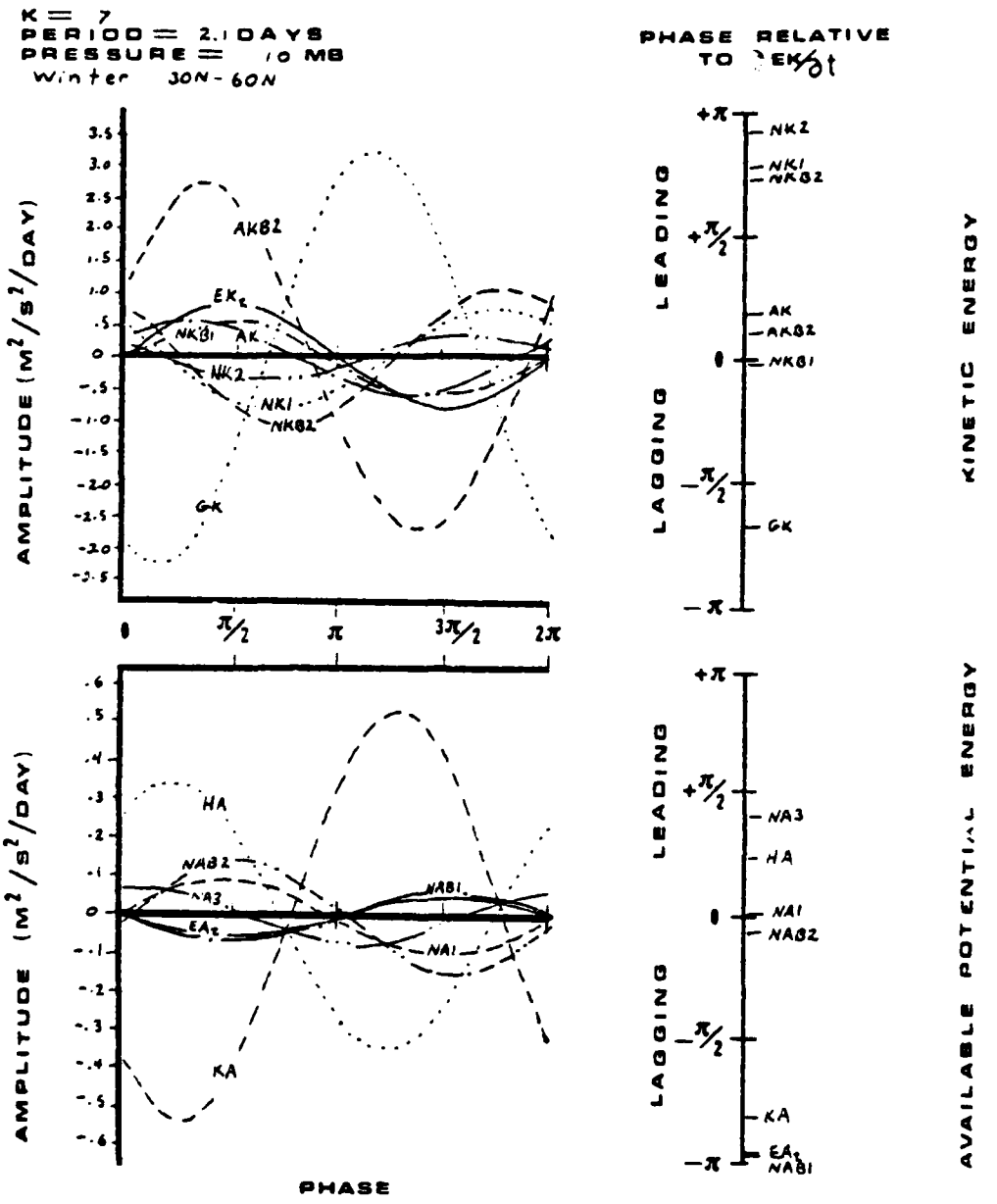


Figure 82. Winter variations of the kinetic and available potential energies in relation to the linear and nonlinear contributions to waves of wave number 7, period 2.1 days, averaged over 30°N-60°N at 10 mb.

HA, AK, NK1, NAB1, and NKB1. Now AKB2 and KA increase, as does NKB2, also reflecting the upward forcing. NK2 and NA1 act as energy sources in transferring energy from other waves, and $EK_t$ begins to increase. GK now usually acts as an energy source as well. The $EA_t$ curve begins to grow from input by NA1, but is followed closely by an increasing HA. The growing $EA_t$ wave is immediately stunted, however, as AK begins its rapid increase. This forces corresponding decrease in KA and completely cancels HA. In all stratospheric middle latitude figures, it will be seen that KA and HA are of equal magnitude and nearly 180° out of phase. This essentially leaves only the nonlinear terms, which are very weak in the stratosphere, to drive changes in $\partial EA/\partial t$. As a result, $\partial EA/\partial t$ curves in the stratosphere are very weak indeed.

At 10 mb for wave numbers 0, 1, and 2 (Figures 78, 79, and 80), the dominant term is not AKB2. Rather, the diabatic effect HA, the action of energy conversion AK, and sub-scale wave interactions embodied in GK dominate the evolution of the kinetic and available potential energy. In these cases, the energy transfer cycle generally follows as HA, AK, $EK_t$, $EA_t$, and GK.

Analysis of other wave numbers in the middle latitudes would follow similar lines to those above; however, it is more important to present the general features of the overall wave growth and decay process in the mid-latitude troposphere and lower stratosphere.

(1) Vertical forcing due to the vertical convergence of geopotential flux provides an important mechanism for

wave evolution in both the middle latitude troposphere and lower stratosphere.

(2) Nonlinear interaction provides a more effective mechanism for wave evolution in the troposphere, whereas vertical forcing (AKB2) and energy conversion (AK) provide an effective mechanism for wave evolution in the lower and middle stratosphere, respectively.

(3) Horizontal forcing terms nearly always act out of phase with $EK_t$, and may be generally considered as energy sinks.

(4) Final decay of waves is indicated by an increasing conversion of kinetic energy to available potential energy (KA), and the increasing effect of sub-scale interactions.

(5) Increasing kinetic energy nearly always precedes increases in available potential energy.

At 10 mb in middle latitudes for wave numbers 0, 1, and 2, we conclude the following:

(1) AKB2 is small in magnitude and always out of phase with $EK_t$.

(2) Maximum wave amplitudes of all waves shown are approximately three times greater than for 50 mb, reflecting the stronger winds and temperature gradients at 10 mb.

(3) HA and KA are nearly the same magnitude and out of phase. Perhaps the large values of HA reflect the increasing diabatic effects of the ozone layer.

(4) GK and KA are nearly the same magnitude and out of phase.

(5) The overall balance between HA, KA, and GK essentially determines wave evolution at 10 mb.

Figures 68, 73, and 78 for the mean flow are considerably more difficult to understand. In both the troposphere and the stratosphere it appears the nonadiabatic heating (HA) and sub-scale interactions through GK are the major ingredients. At 500 mb, GK is balanced by AKB2 and AK (two pressure gradient forces), and $EK_t$ increases or decreases as a result of this balance. For the available potential energy, HA is nearly balanced by MA, and $EA_t$ seems to be controlled by KA. Perhaps this is due to the general lowering of the northern troposphere during winter?

As seen in Figures 83 through 97, the evolution of kinetic energy waves in the tropical troposphere and stratosphere is dominated by conversions of available potential and kinetic energies (AK,KA), sub-scale wave interactions and Reynolds and molecular stresses (GK), and vertical and meridional convergence of geopotential flux (AKB1, AKB2). The major terms operating in the evolution of EA waves are interconversions of available potential and kinetic energies (AK,KA), and sub-scale wave actions and diabatic heating or cooling (HA). From these figures, it also appears that any of the major terms contributing to the life cycle of kinetic energy waves can initiate the growth cycle. That is, AK is the leading term in Figures 85, 88, 91, 95, and 96; GK appears to start the evolution process in Figures 83, 84, 89, 93, 94, and 97; AK32 initiates the cycle in Figures 87, 90, and 92;

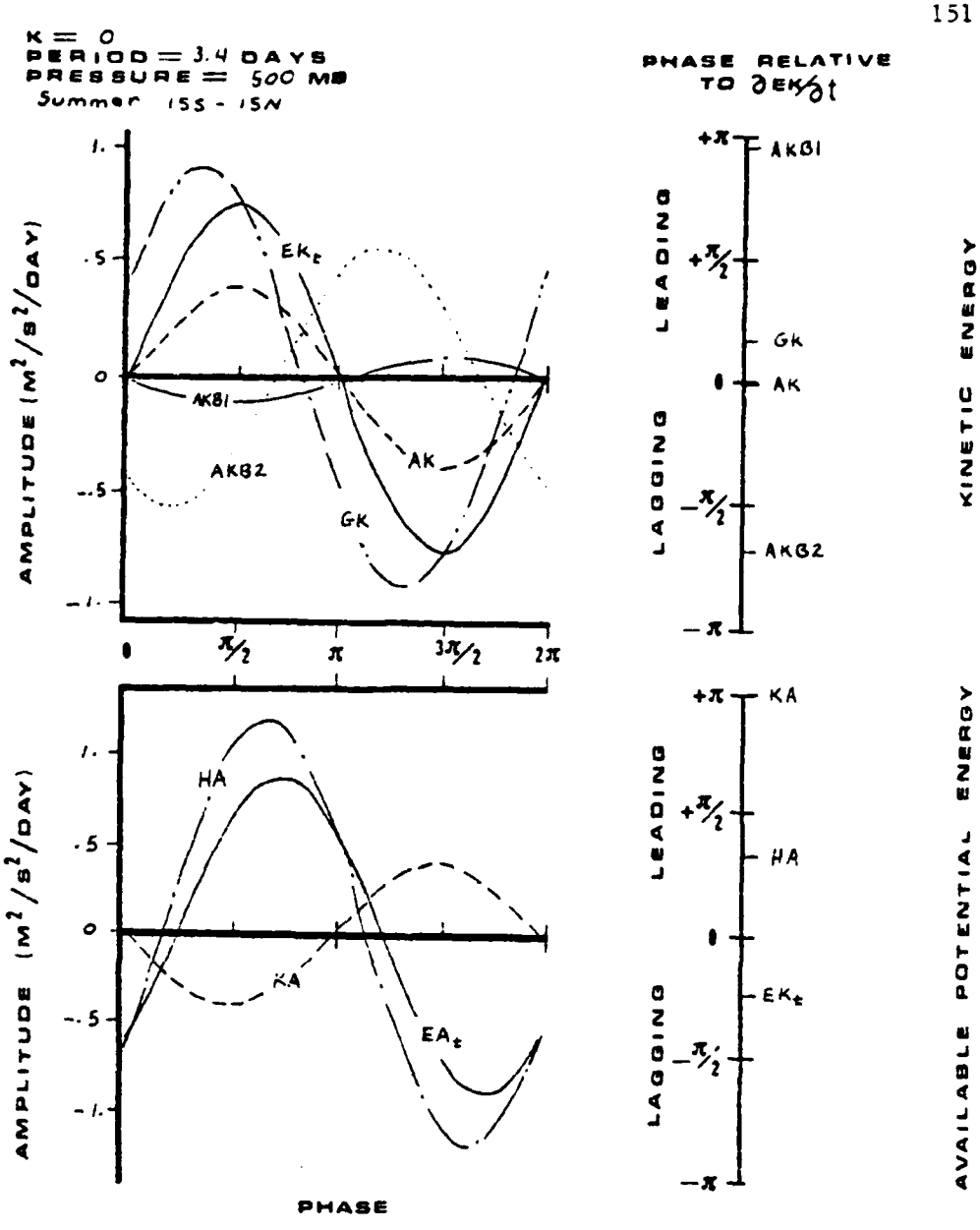


Figure 83. Summer variations of the kinetic and available potential energies in relation to the linear and nonlinear contributions to waves of wave number 0, period 3.4 days, averaged over 15°S - 15°N at 500 mb.

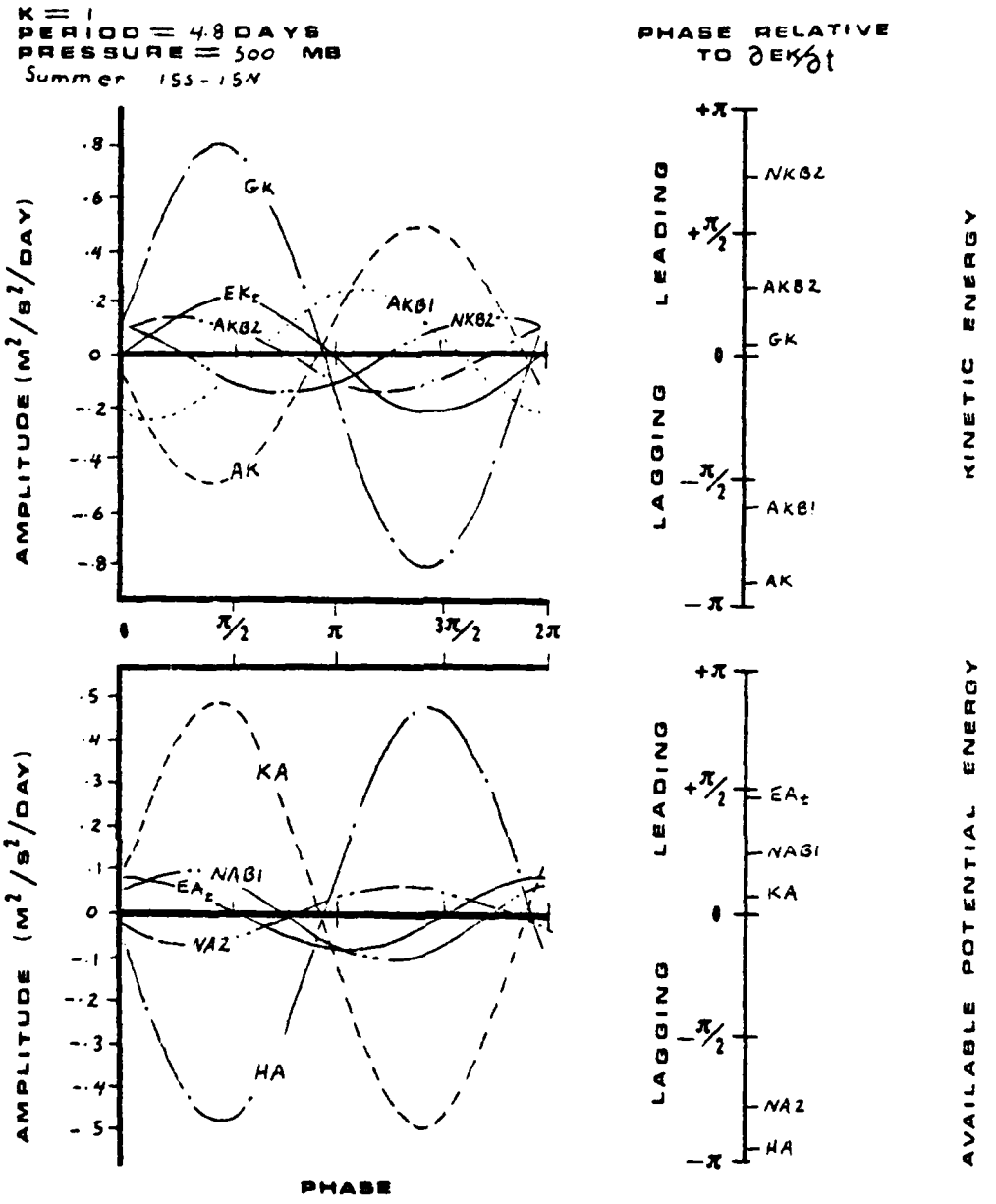


Figure 84. Summer variations of the kinetic and available potential energies in relation to the linear and nonlinear contributions to waves of wave number 1, period 4.8 days, averaged over 15°S - 15°N at 500 mb.

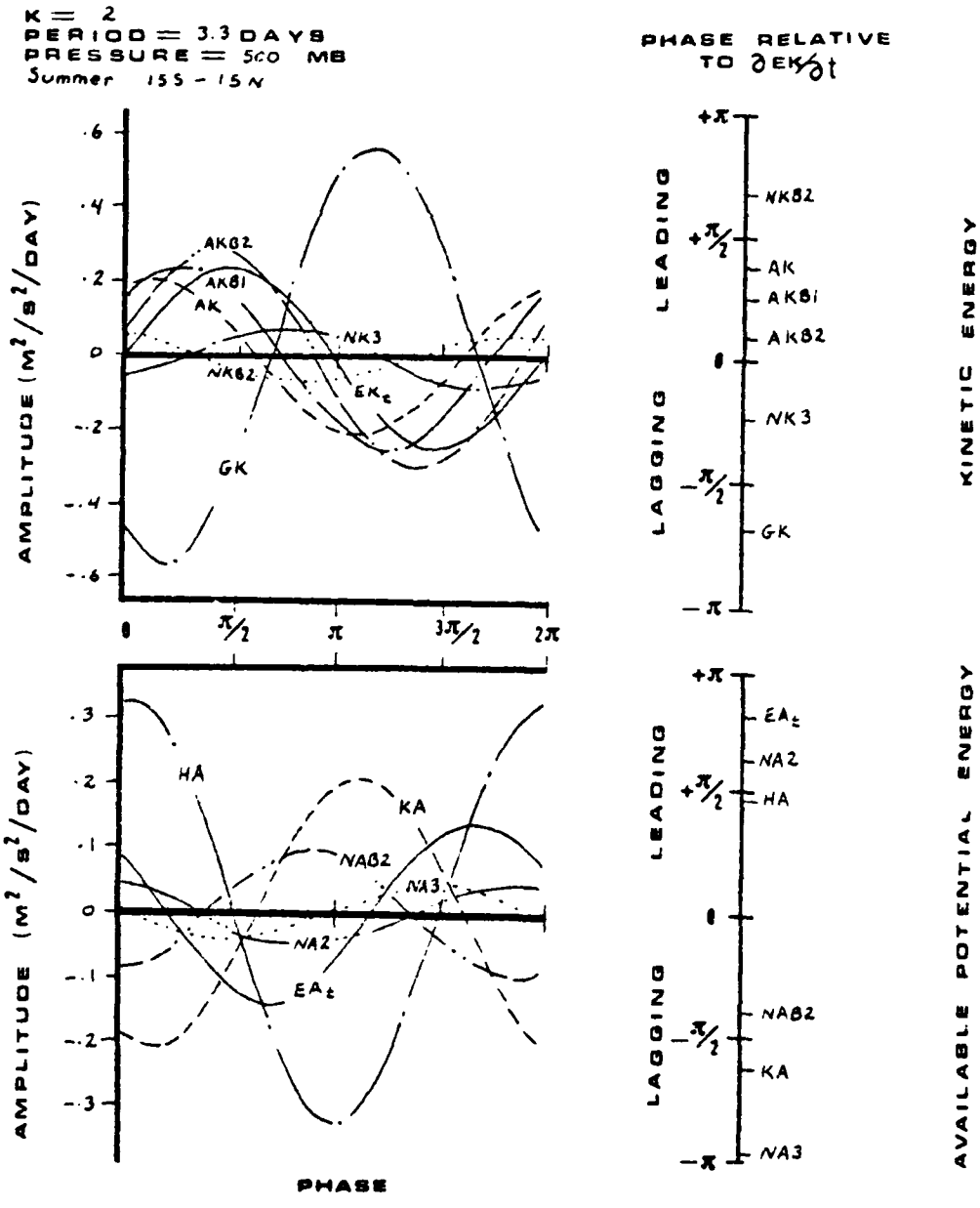


Figure 85. Summer variations of the kinetic and available potential energies in relation to the linear and nonlinear contributions to waves of wave number 2, period 3.3 days, averaged over 15°S - 15°N at 500 mb.

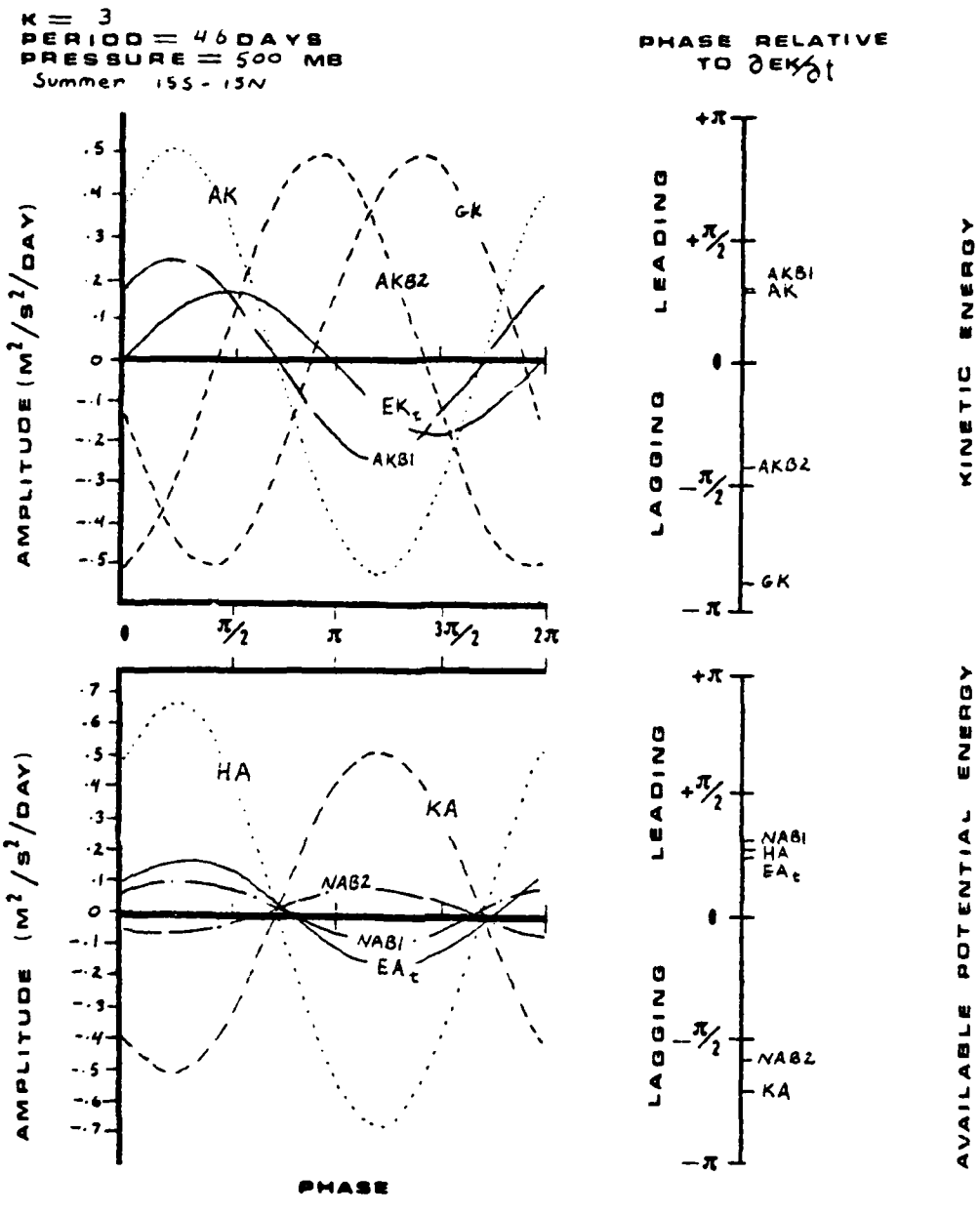


Figure 86. Summer variations of the kinetic and available potential energies in relation to the linear and nonlinear contributions to waves of wave number 3, period 4.6 days, averaged over 15°S - 15°N at 500 mb.

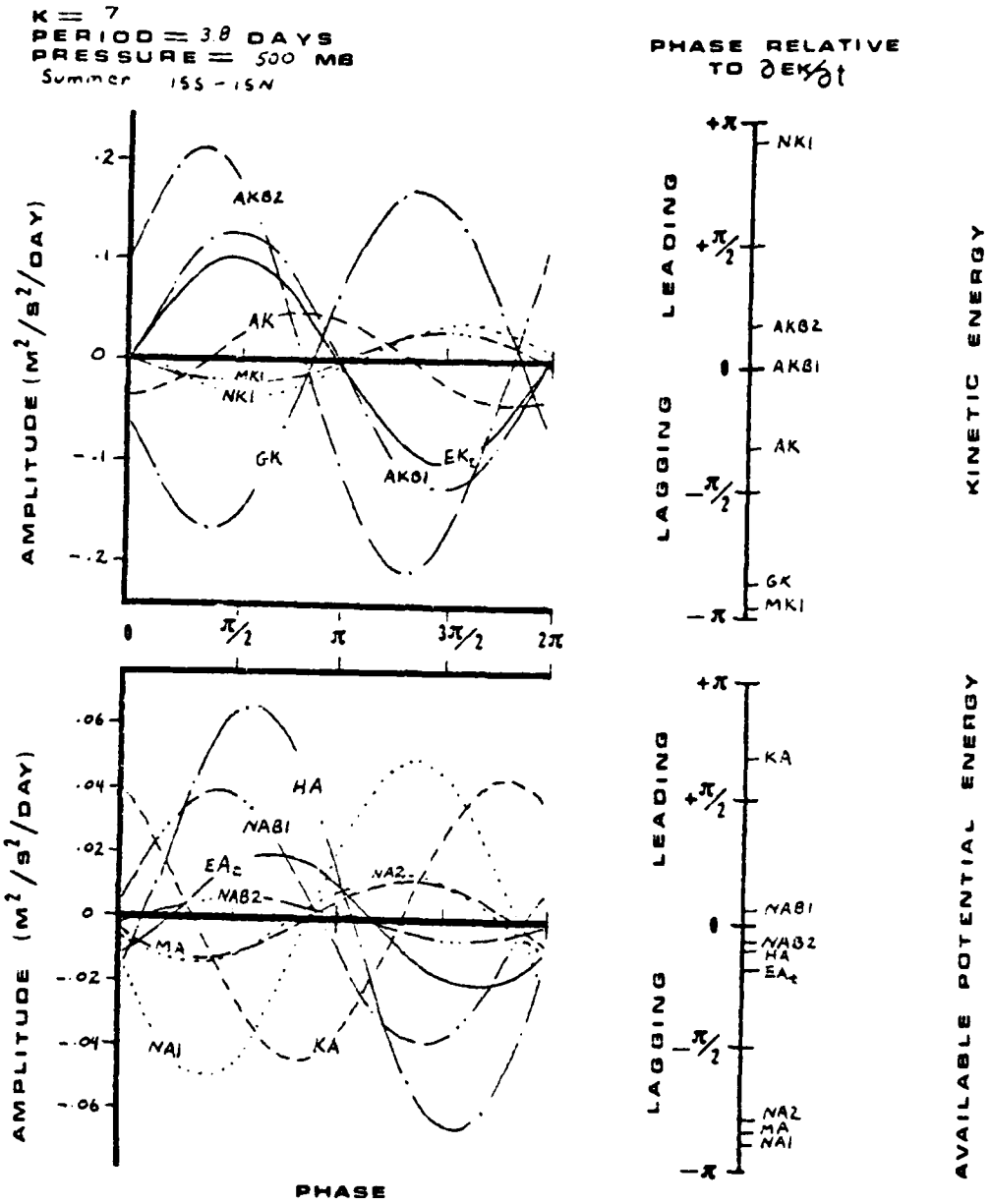


Figure 87. Summer variations of the kinetic and available potential energies in relation to the linear and nonlinear contributions to waves of wave number 7, period 3.8 days, averaged over 15°S - 15°N at 500 mb.

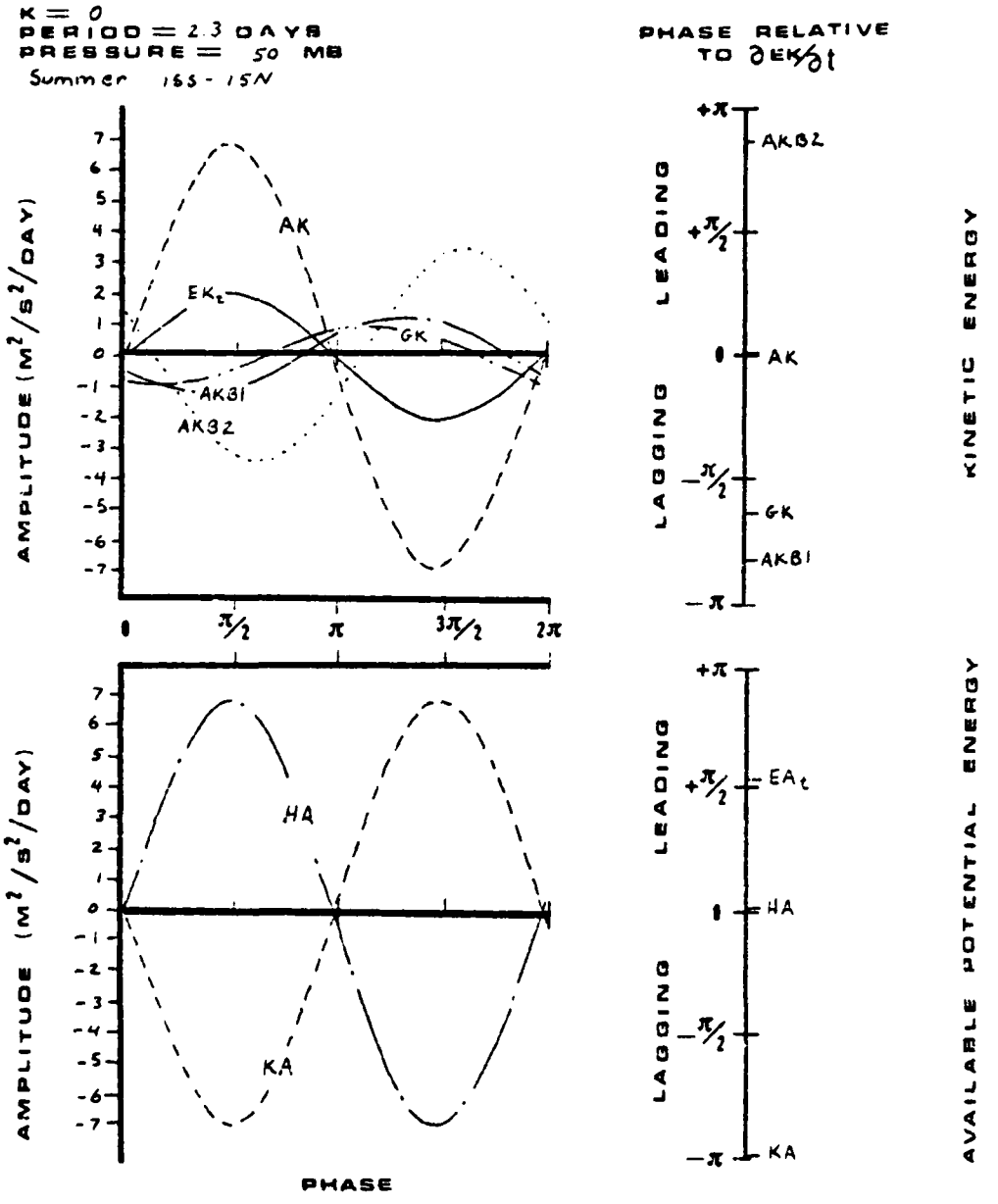


Figure 38. Summer variations of the kinetic and available potential energies in relation to the linear and nonlinear contributions to waves of wave number 0, period 2.3 days, averaged over 15°S - 15°N at 50 mb.

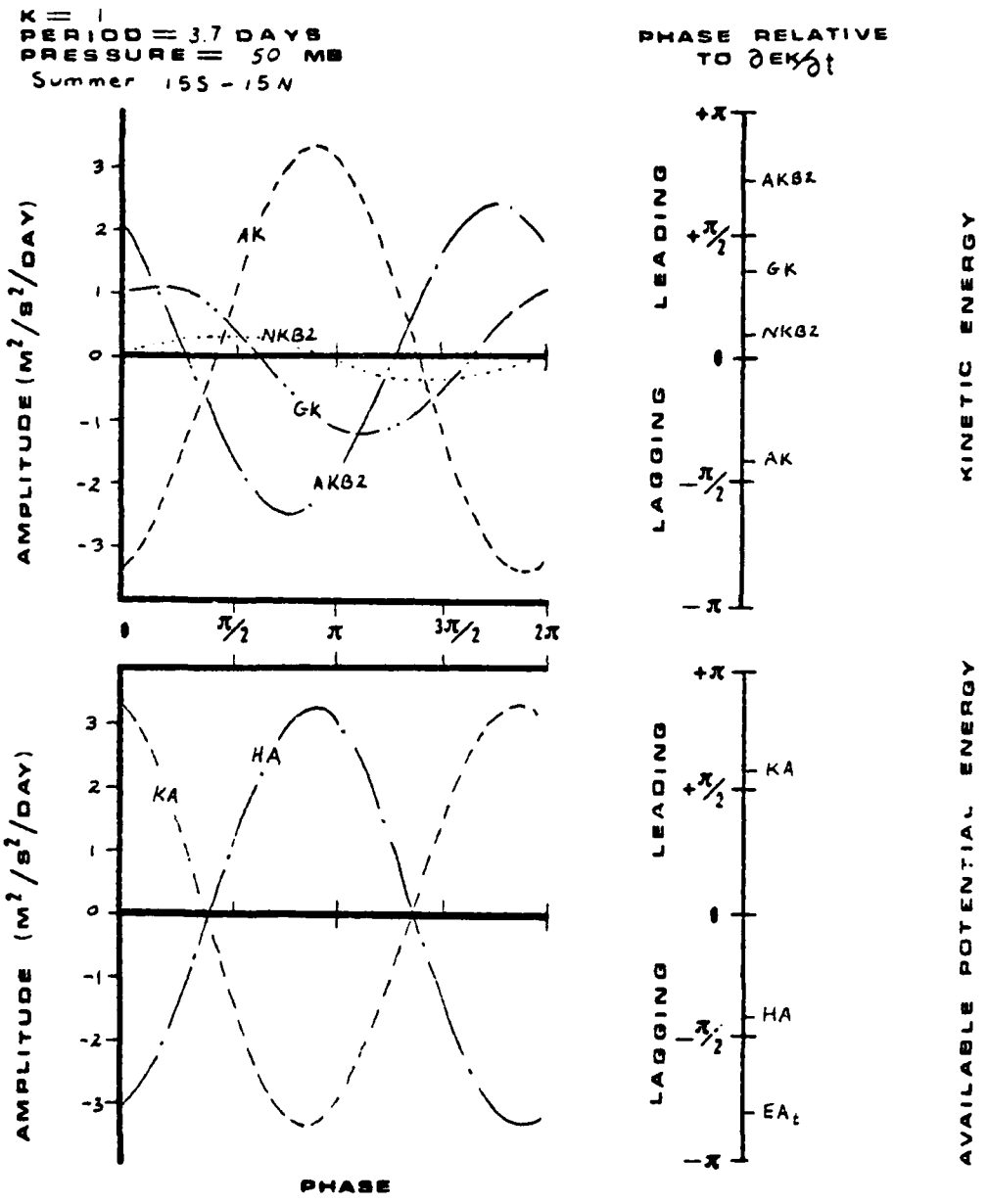


Figure 89. Summer variations of the kinetic and available potential energies in relation to the linear and nonlinear contributions to waves of wave number 1, period 3.7 days, averaged over 15°S - 15°N at 50 mb.

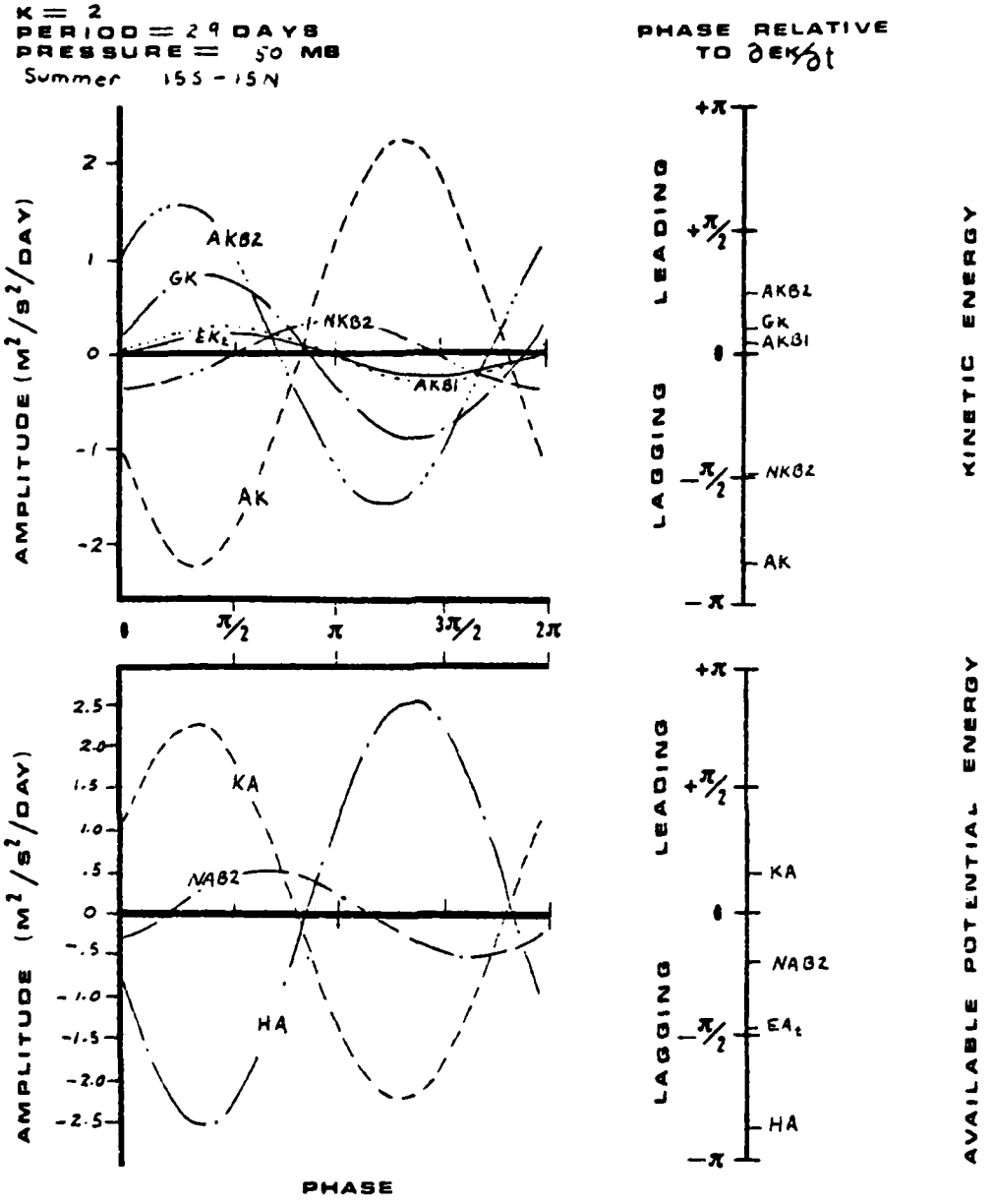


Figure 90. Summer variations of the kinetic and available potential energies in relation to the linear and nonlinear contributions to waves of wave number 2, period 2.9 days, averaged over 15°S - 15°N at 50 mb.

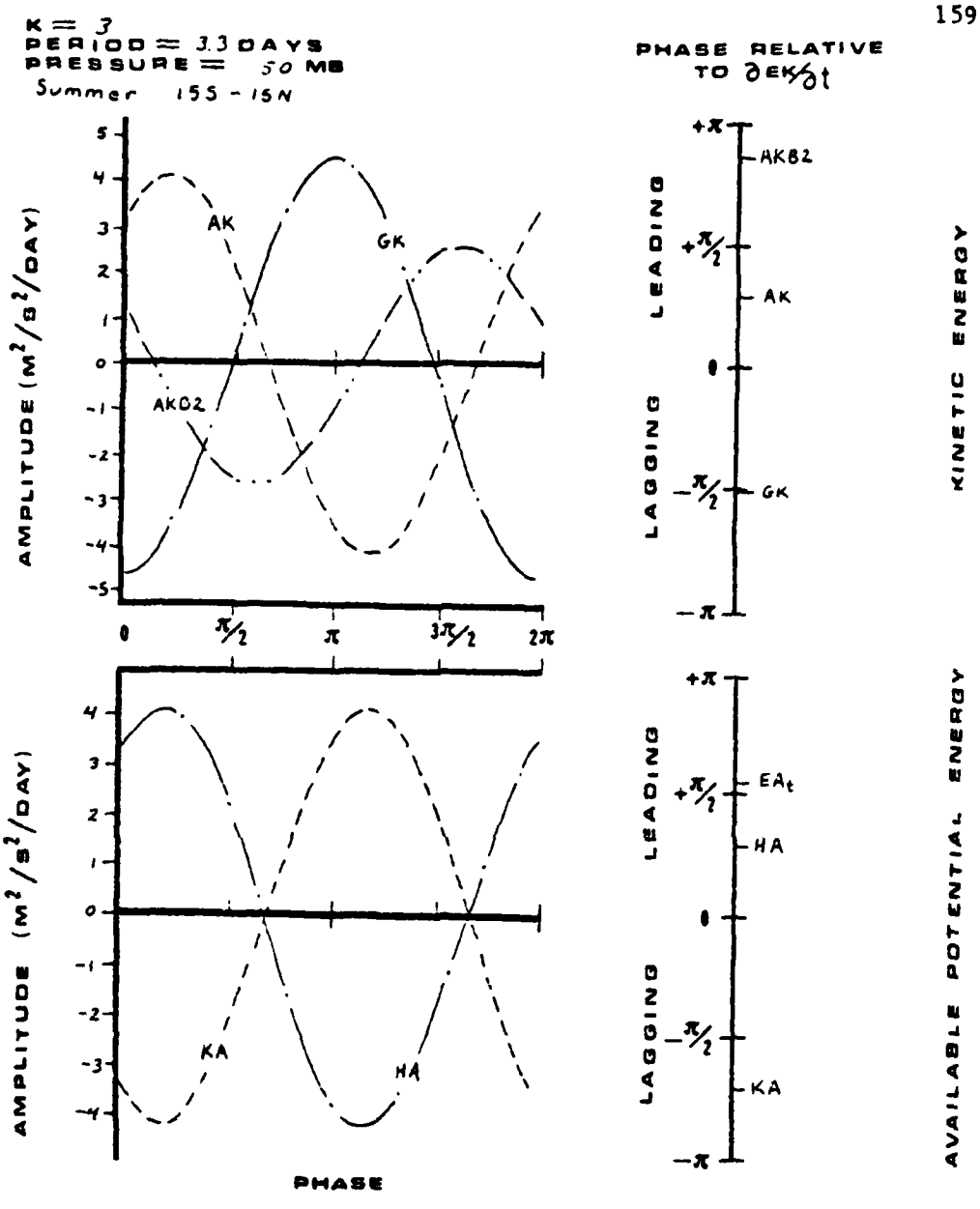


Figure 91. Summer variations of the kinetic and available potential energies in relation to the linear and nonlinear contributions to waves of wave number 3, period 3.3 days, averaged over 15°S - 15°N at 50 mb.

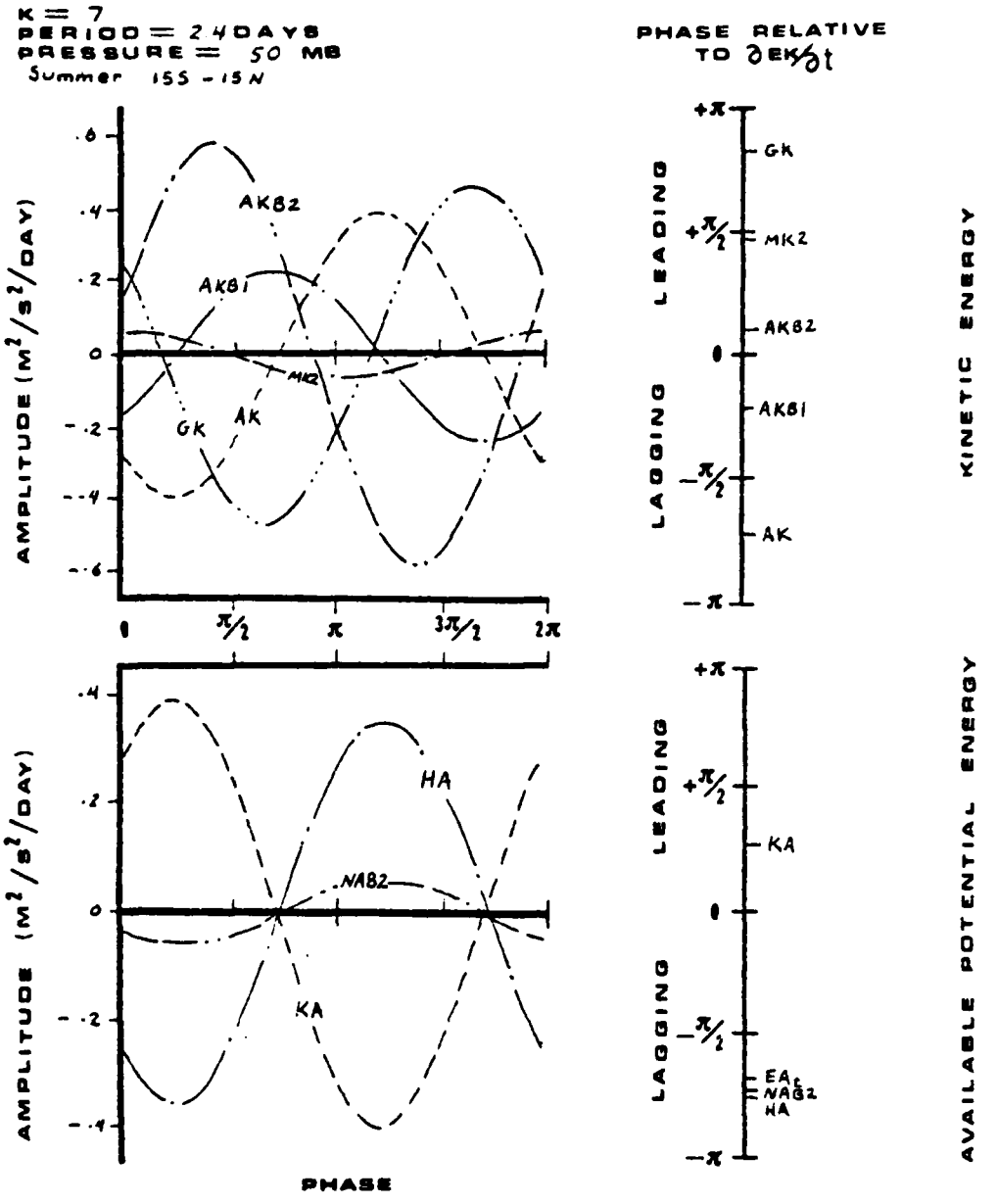


Figure 92. Summer variations of the kinetic and available potential energies in relation to the linear and nonlinear contributions to waves of wave number 7, period 2.4 days, averaged over 15°S - 15°N at 50 mb.

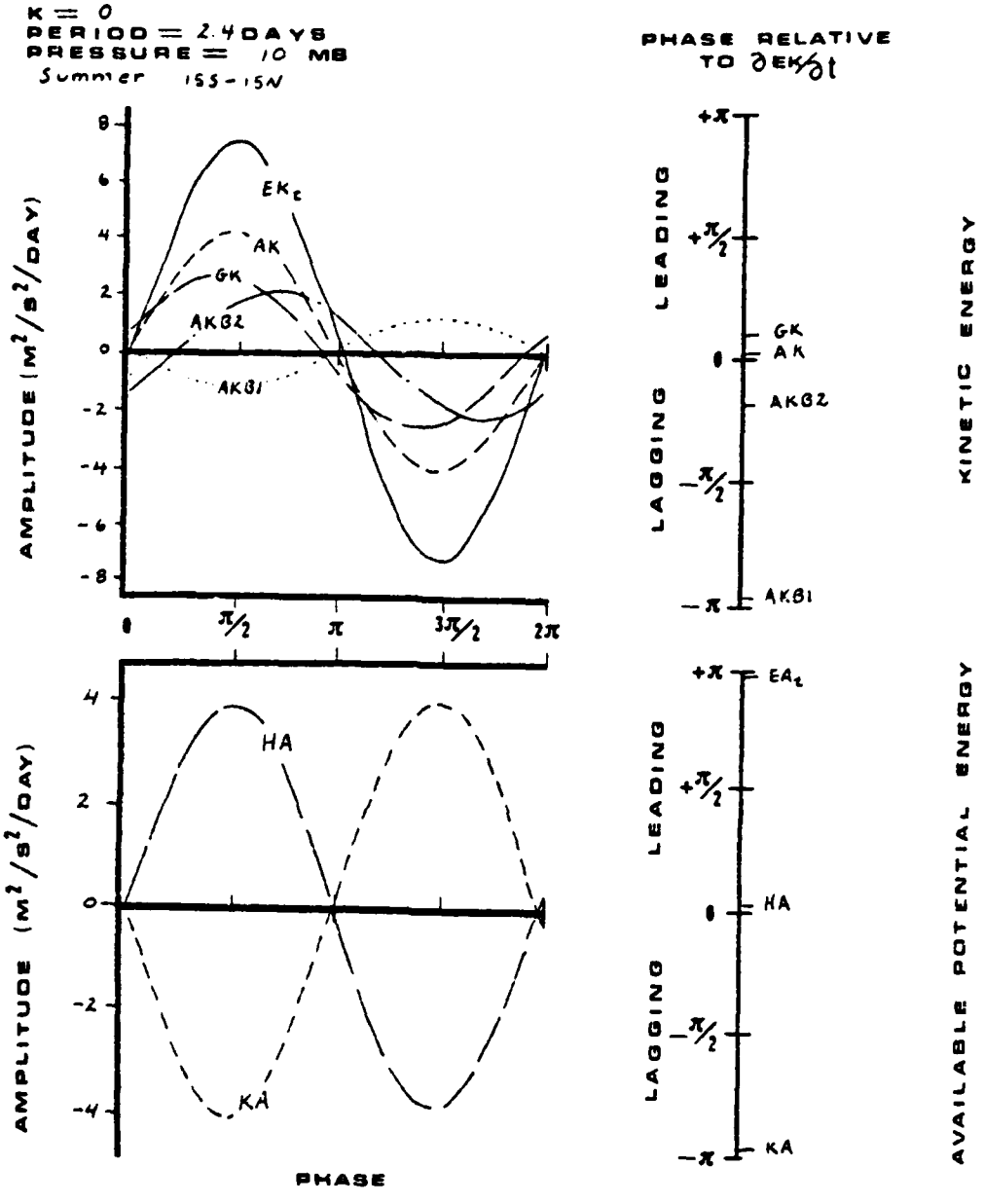


Figure 93. Summer variations of the kinetic and available potential energies in relation to the linear and nonlinear contributions to waves of wave number 0, period 2.4 days, averaged over 15°S - 15°N at 10 mb.

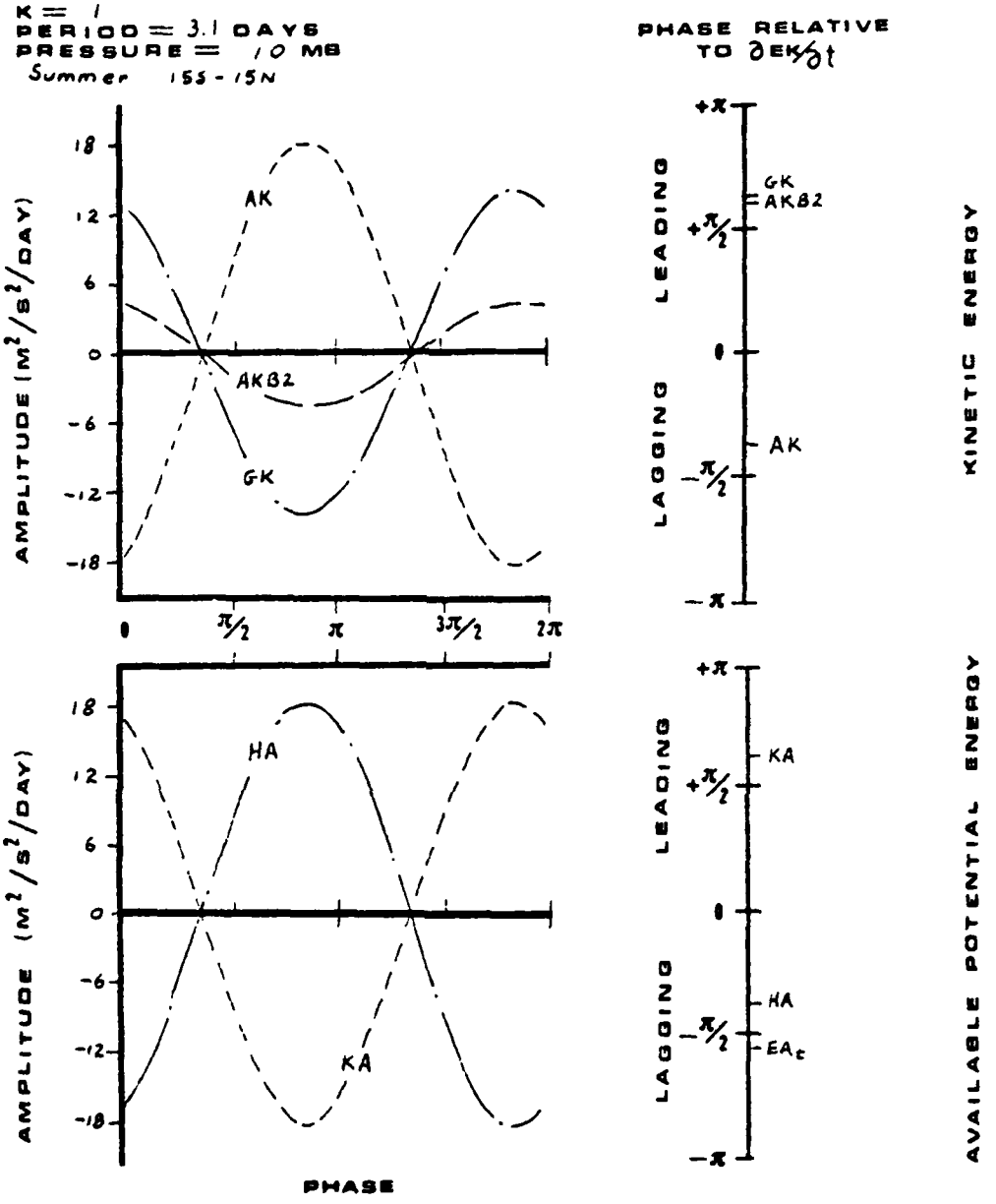


Figure 94. Summer variations of the kinetic and available potential energies in relation to the linear and nonlinear contributions to waves of wave number 1, period 3.1 days, averaged over 15°S - 15°N at 10 mb.

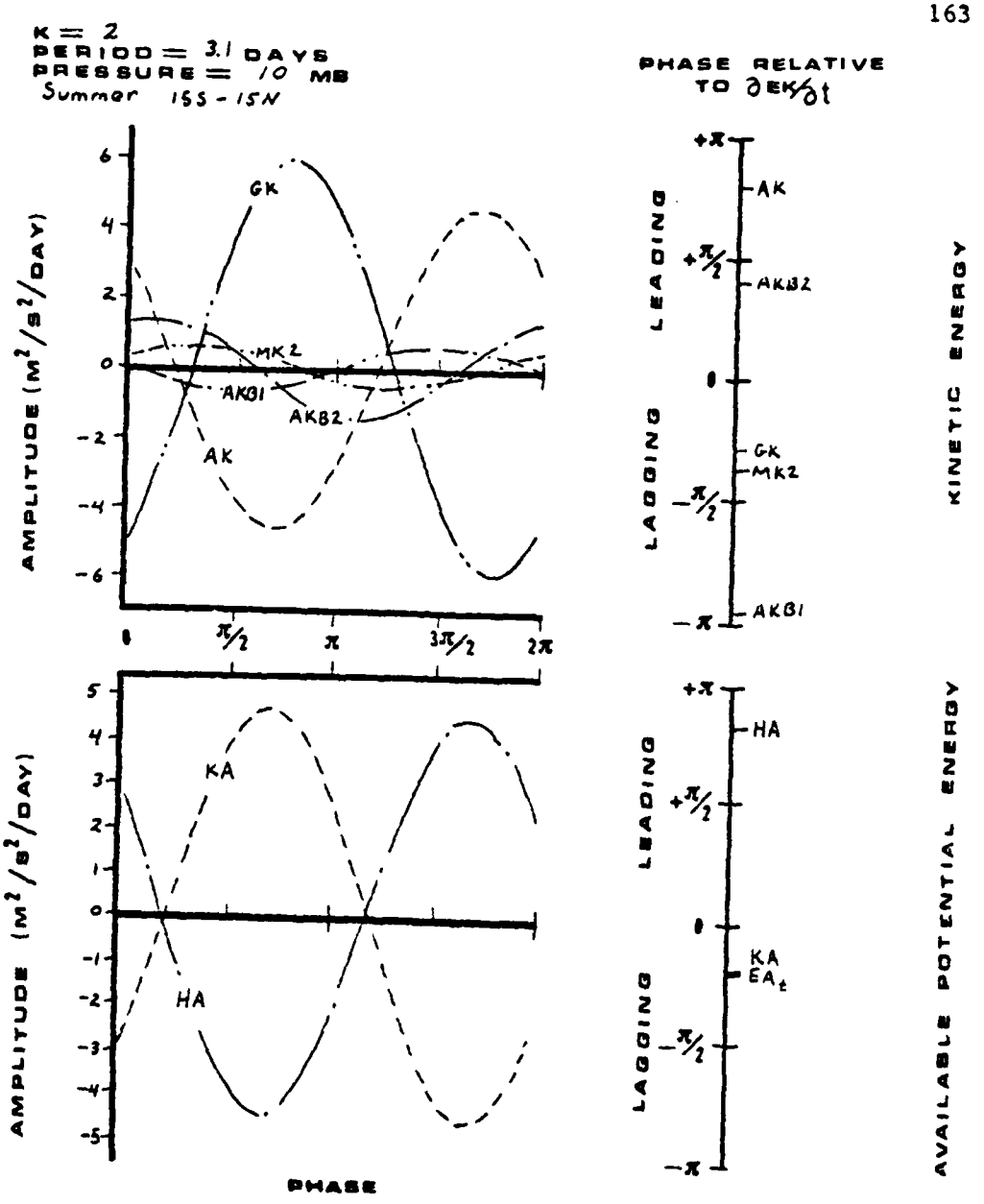


Figure 95. Summer variations of the kinetic and available potential energies in relation to the linear and nonlinear contributions to waves of wave number 2, period 3.1 days, averaged over 15°S - 15°N at 10 mb.

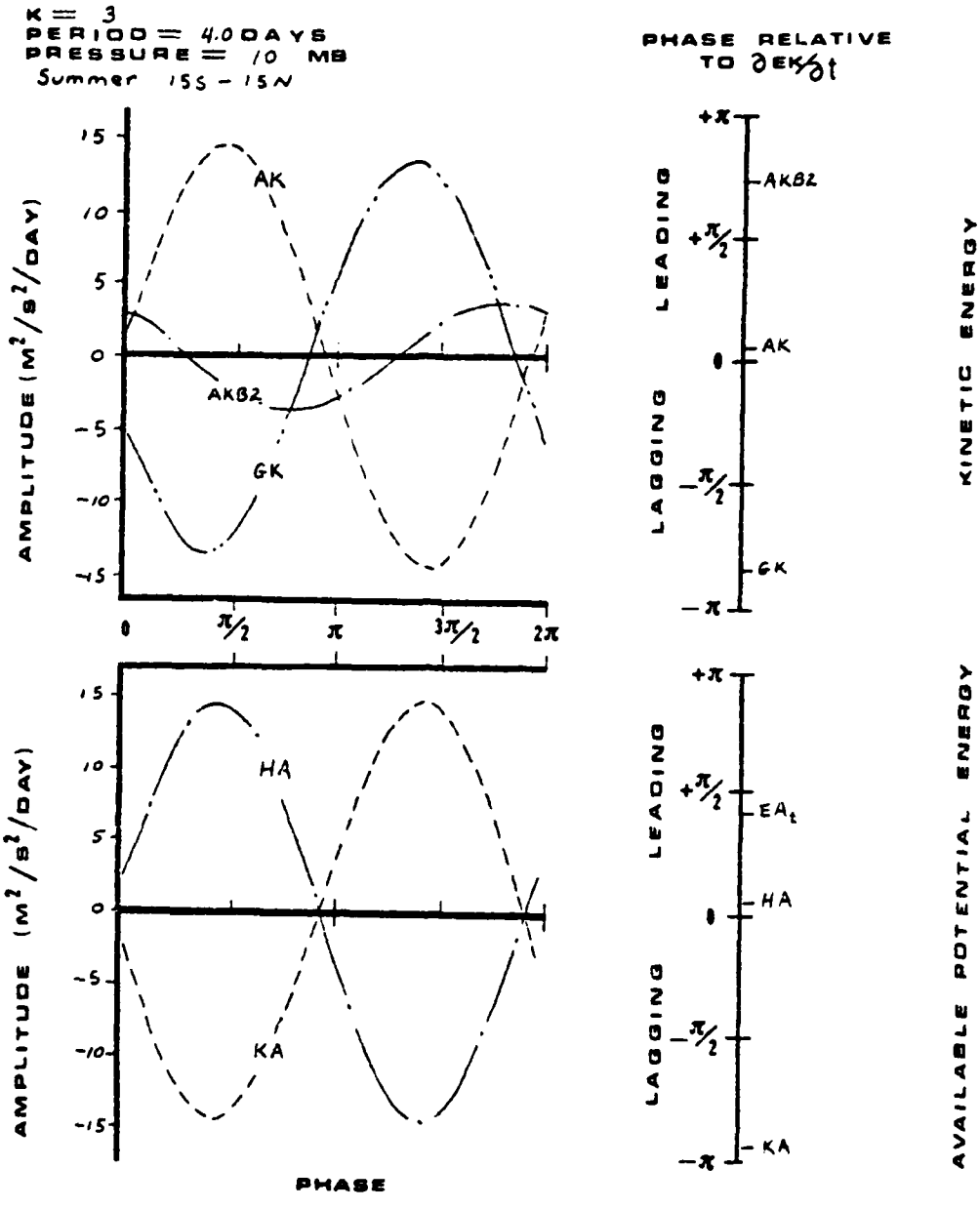


Figure 96. Summer variations of the kinetic and available potential energies in relation to the linear and nonlinear contributions to waves of wave number 3, period 4.0 days, averaged over 15°S - 15°N at 10 mb.

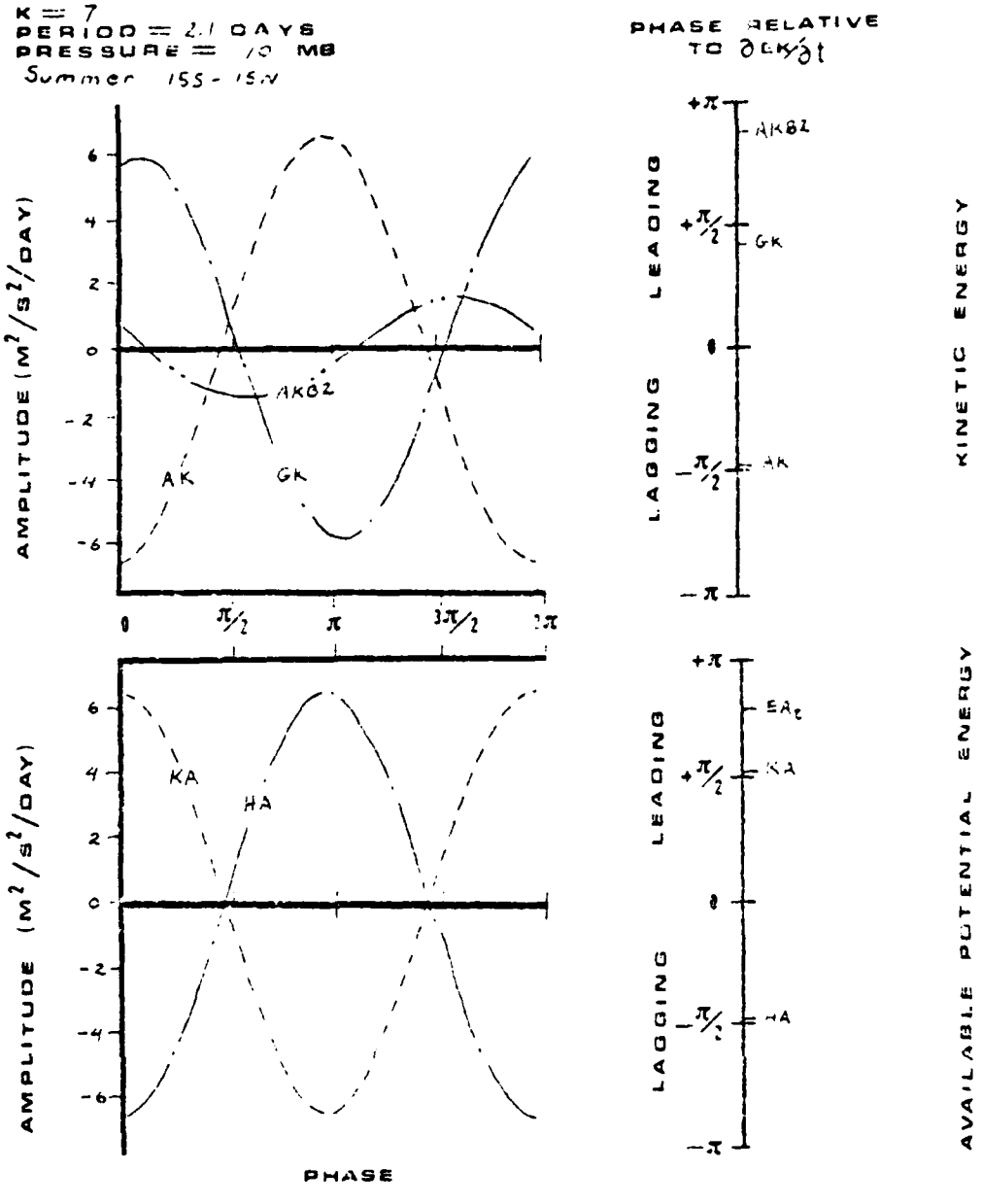


Figure 97. Summer variations of the kinetic and available potential energies in relation to the linear and nonlinear contributions to waves of wave number 7, period 2.1 days, averaged over 15°S - 15°N at 10 mb.

while AKB1 may begin the process shown in Figure 86. In most cases, vertical and meridional convergence of geopotential flux (AKB2, AKB1), or energy conversion (KA or AK) appear to be the major factors initiating wave evolution. It should be pointed out that, as for the stratosphere in general, nonlinear terms are almost never significant in the tropics.

Because of the great variability seen in tropical wave evolution, it is probably not meaningful to discuss specific cases of development and decay. Some general conclusions about the summer tropical troposphere and stratosphere may be stated as follows:

(1) In the tropical troposphere (500 mb) and lower stratosphere (50 mb), most wave evolution is initiated by the vertical and meridional convergence of geopotential flux (AKB2, AKB1) and energy conversion (AK). At 10 mb, subscale interaction (GK) almost balances the diabatic heating (HA).

(2) In the tropical atmosphere in general, nonlinear terms are less important than for winter, middle latitude evolution.

(3) Conversion of available potential energy to kinetic energy (AK) is almost always close to 180° out of phase with GK.

(4) Conversion of kinetic energy to available potential energy (KA) is almost always close to 180° out of phase with HA.

(5) For wave number 0 only, meridional energy transfer (AKB1)

opposes wave development, and therefore, may be thought of as an energy sink.

(6) In the tropical stratosphere, terms AK, GK, and AKB2 almost always balance each other, therefore ∂EK/∂t is generally small.

(7) In the tropical stratosphere, terms HA and KA generally balance each other, and therefore ∂EA/∂t is usually small.

AD-A107 964 AIR FORCE INST OF TECH WRIGHT-PATTERSON AFB OH F/G 9/2
AN INVESTIGATION OF THE INTERACTION, EVOLUTION AND MAINTENANCE --ETC(U)
MAR 79 J L HATCH
UNCLASSIFIED AFIT-CI-79-2930-S NL

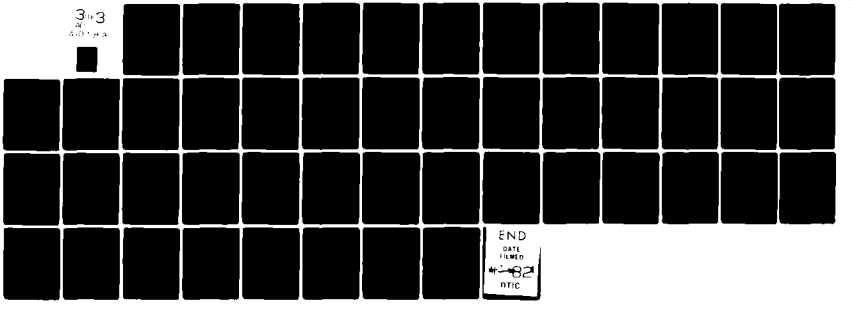

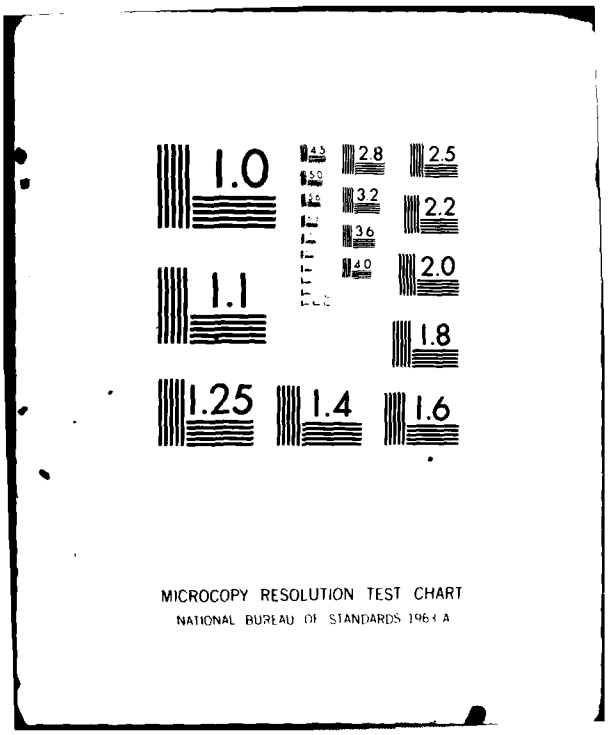
1.0
1.1
1.25
1.4
1.6
1.8
2.0
2.2
2.5
2.8
3.2
3.6
4.0
MICROCOPY RESOLUTION TEST CHART
NATIONAL BUREAU OF STANDARDS 1963 A

# CHAPTER 6

## SUMMARY AND CONCLUSIONS

Analyses of the distribution, maintenance and evolution of the available potential and kinetic energy in the Northern Hemisphere, winter 1975-76 indicate that the kinetic energy per unit mass of both the zonal mean flow and wave motion shows a primary maximum near 65°N, 10 mb in the stratosphere and a secondary maximum at 35°N, near the tropopause. The specific kinetic energy of the wave motion in the stratosphere is essentially contributed by the extra-long waves (k = 1, 2, 3), whereas that in the troposphere is contributed by both the long and synoptic scale waves. The available potential energy per unit mass associated with the zonal mean flow has a primary maximum near 23°N in the lower troposphere, whereas that associated with the large-scale waves has two maxima of almost equal strength, one in the stratosphere near 10 mb at 63°N, and the other in the lower troposphere near 53°N. The specific available potential energy associated with the extra-long waves shows a transition of an intense maximum for wave number 1 in the high-latitude stratosphere, to two weak maxima in the high-latitude stratosphere and the lower troposphere for wave number 2, and to a weak maximum in the mid-latitude troposphere for wave number 3.

The maintenance of the energetics in the troposphere and

stratosphere appears to follow a definite cycle. For the winter season from 90°N to 20°N, nonadiabatic processes supplied available potential energy to the stratosphere zonal mean flow. The majority of this energy was seen to convert to mean kinetic energy, and then was removed from the system through the Reynolds and molecular stresses. Energy input to the tropospheric mean available potential energy by the nonadiabatic processes was primarily transferred first to the tropospheric eddy available potential energy through interactions of waves and the meridional gradient of the zonal mean temperature, second to tropospheric eddy kinetic energy through conversion, third to stratospheric eddy kinetic energy by vertical convergence of geopotential flux, fourth to stratospheric eddy available potential energy through conversion processes, and finally, out of the system by diabatic cooling and sub-scale wave interactions. Northern Hemisphere integration for the summer season showed a modified, more complicated structure. Energy supplied to the mean stratospheric available potential energy is first converted to mean stratospheric kinetic energy, transfers to mean tropospheric kinetic energy, and finally is removed from the system. In the troposphere, energy is input to the mean available potential energy by diabatic heating. The mean energy subsequently transfers to tropospheric eddy available potential energy, then to tropospheric eddy kinetic energy, and finally is transferred out of the system. Stratospheric eddy kinetic energy is primarily supplied by sub-scale interactions, then converts to stratospheric eddy available potential energy,

and is finally removed from the system by diabatic cooling.

Analysis of energy transfer at boundaries indicated that boundary terms act principally to decrease centers of high kinetic or available potential energy or to increase energy in areas of relative minimum kinetic or available potential energy. Upward energy transfer was the general rule over most of the Northern Hemisphere with a maximum near the tropopause at 45°N, just above the location of the maximum kinetic energy of the wave motion. Major meridional energy transfer was seen to be southward north of 20°N and northward south of 20°N, with maximum values occurring in the vicinity of the tropical tropopause. Also in the region of the tropical tropopause, vertical transport of energy for wave number 2 acted to concentrate energy, while other boundary terms tended to transfer energy upward and northward. The sudden stratospheric warming, which may be an effect of this boundary energy transfer, was suggested to be a wave originating in the region of the tropical tropopause and moving upward and northward. Since the area of northern regions is considerably less than the area of tropical regions, the energy per unit area of the wave was seen to grow dramatically as it appeared to move northward.

An analysis of the mechanism for the evolution of the large scale atmospheric waves in the mid-latitudes, winter 1975-1976, indicates that the vertical convergence of geopotential flux provides a substantial mechanism for kinetic energy evolution in both the mid-latitude troposphere and stratosphere. While nonlinear interaction provides a more effective mechanism for wave evolution

in the troposphere, the vertical pressure work term is effective in affecting wave evolution in the stratosphere. The vertical convergence of geopotential flux, which is found generally in phase with the rate of change in kinetic energy, would enhance the wave growth; whereas the meridional pressure work term, which is generally out of phase from the rate of kinetic energy change, would act as an energy sink. The evolution of kinetic energy is found generally to precede that of available potential energy associated with the waves. In the equatorial region, most wave evolution was initiated by the vertical and meridional convergence of geopotential flux, although energy conversion could frequently begin the process. At all levels, nonlinear terms were less important in the tropics than for the middle latitudes. In general, summer tropical wave evolution was found to be far more variable and less well defined than for the middle latitudes in winter.

# APPENDIX A

## DISTRIBUTION OF AK, MK, NK, MA, AND NA AVERAGED OVER THE 1975-76 WINTER SEASON FOR VARIOUS WAVE NUMBERS

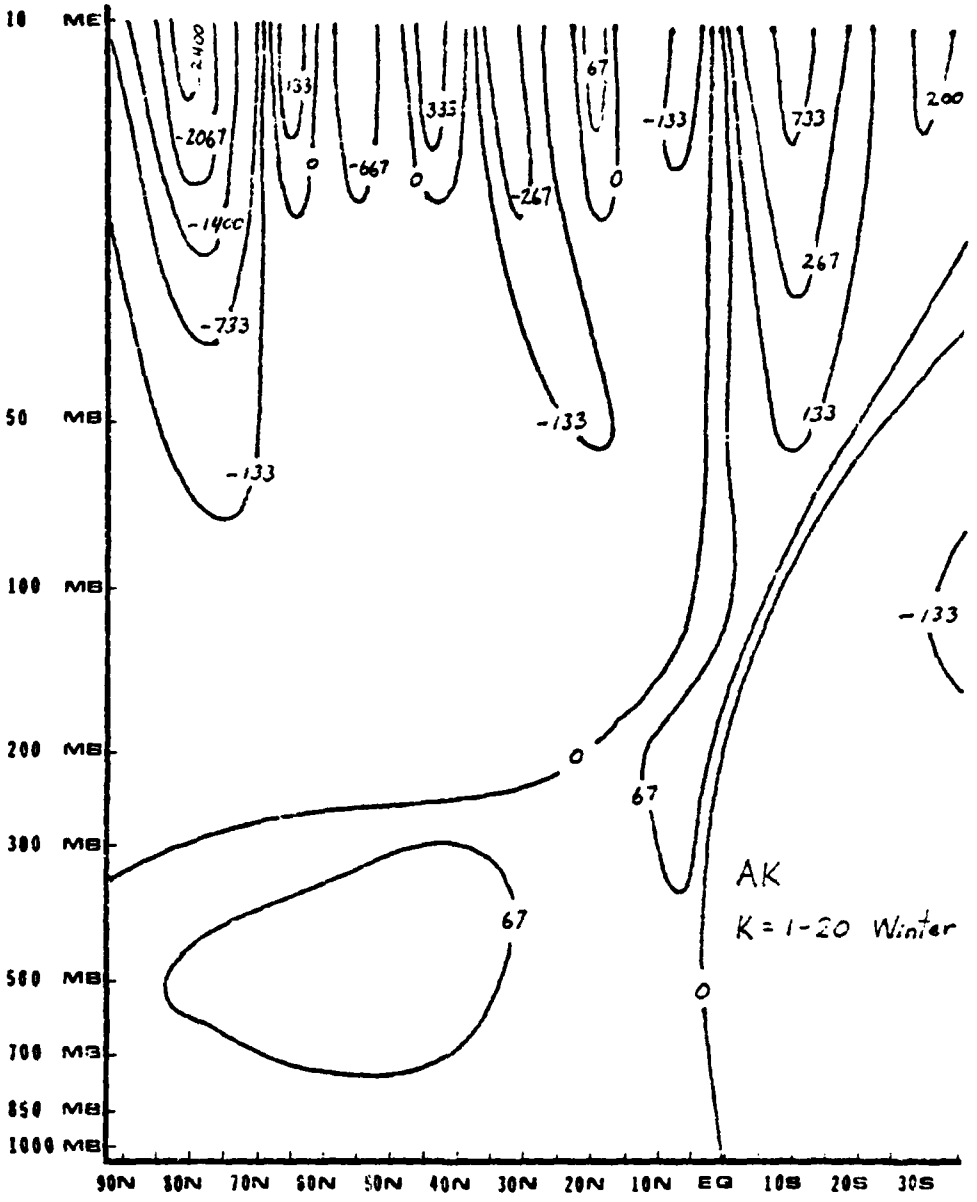


Figure 98. Distribution of AK summer over wave numbers 1 - 20 and averaged over the winter season ($m^2/sec^2/day$).

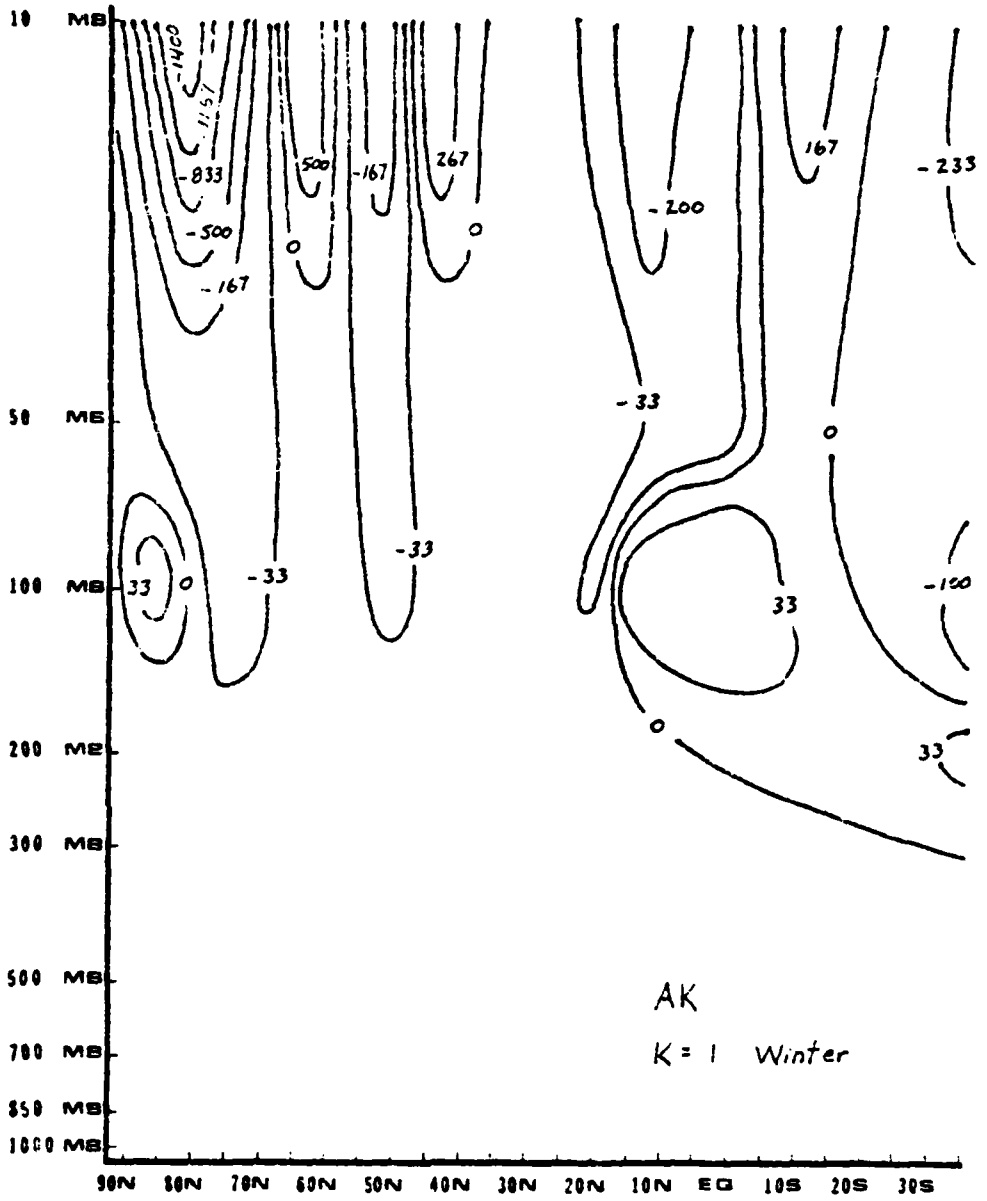


Figure 99. Distribution of AK over the winter season for wave number 1 ($m^2/sec^2/day$).

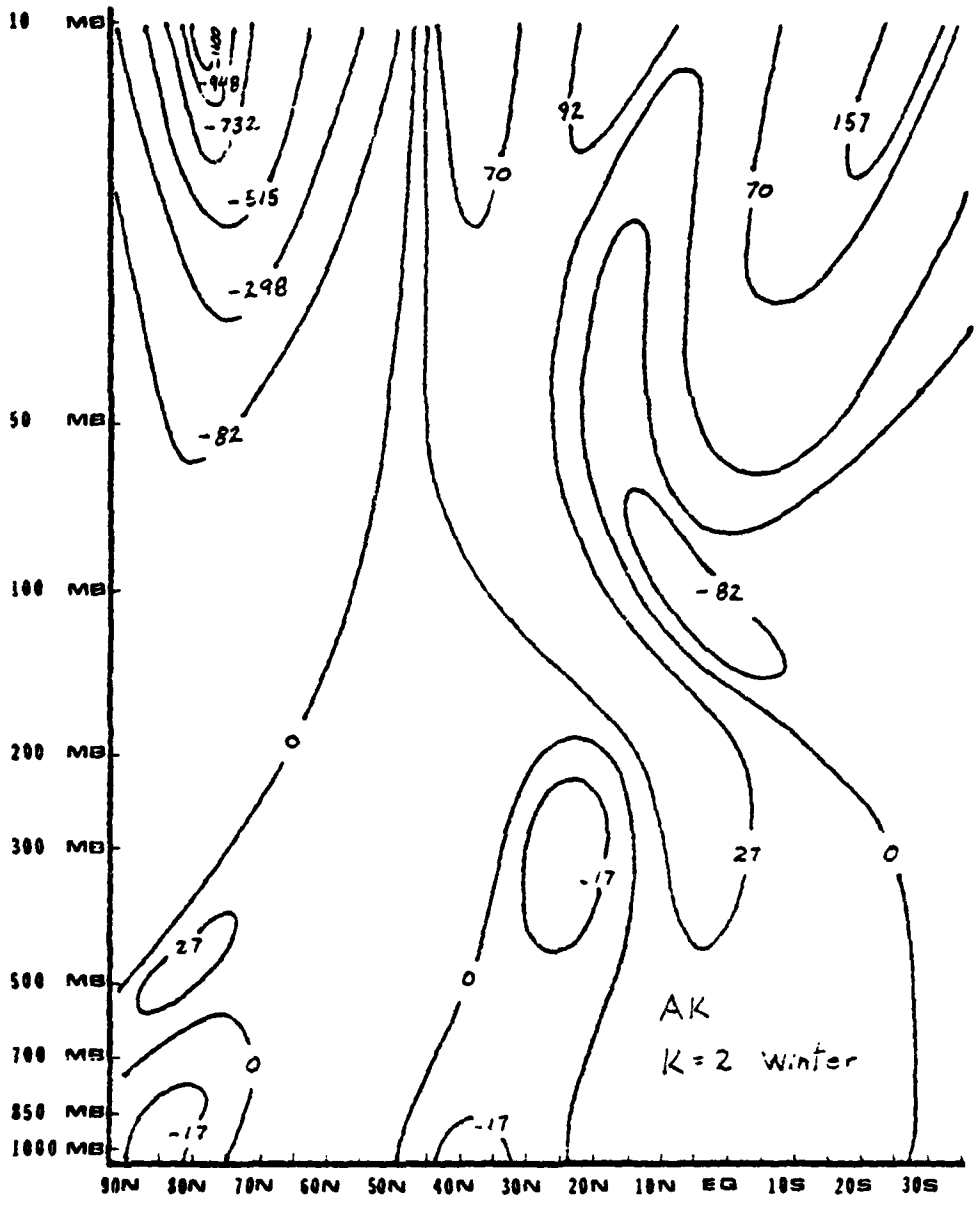


Figure 100. Distribution of AK over the winter season for wave number 2 ($m^2/sec^2/day$).

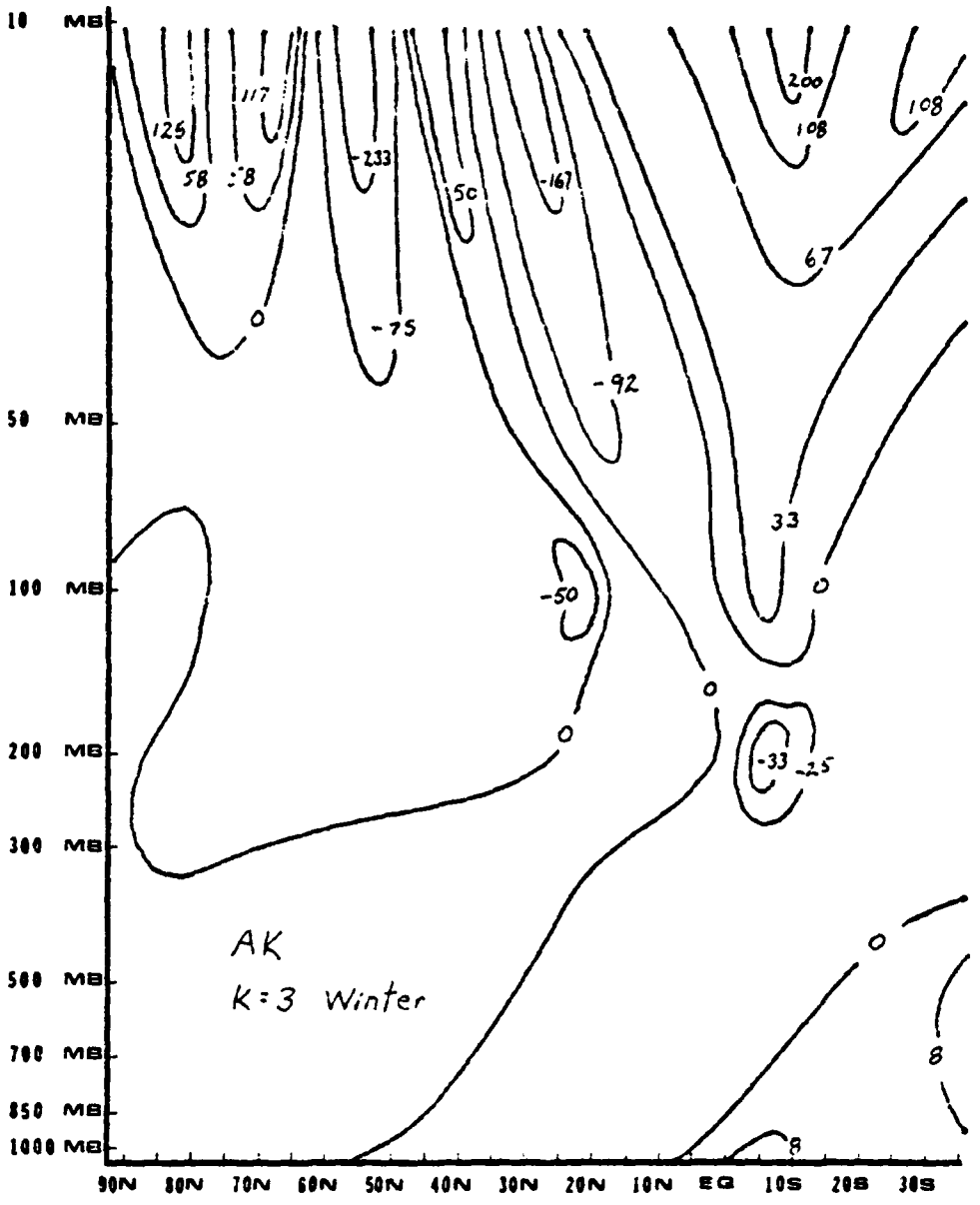


Figure 101. Distribution of AK over the winter season for wave number 3 ($m^2/sec^2/day$).

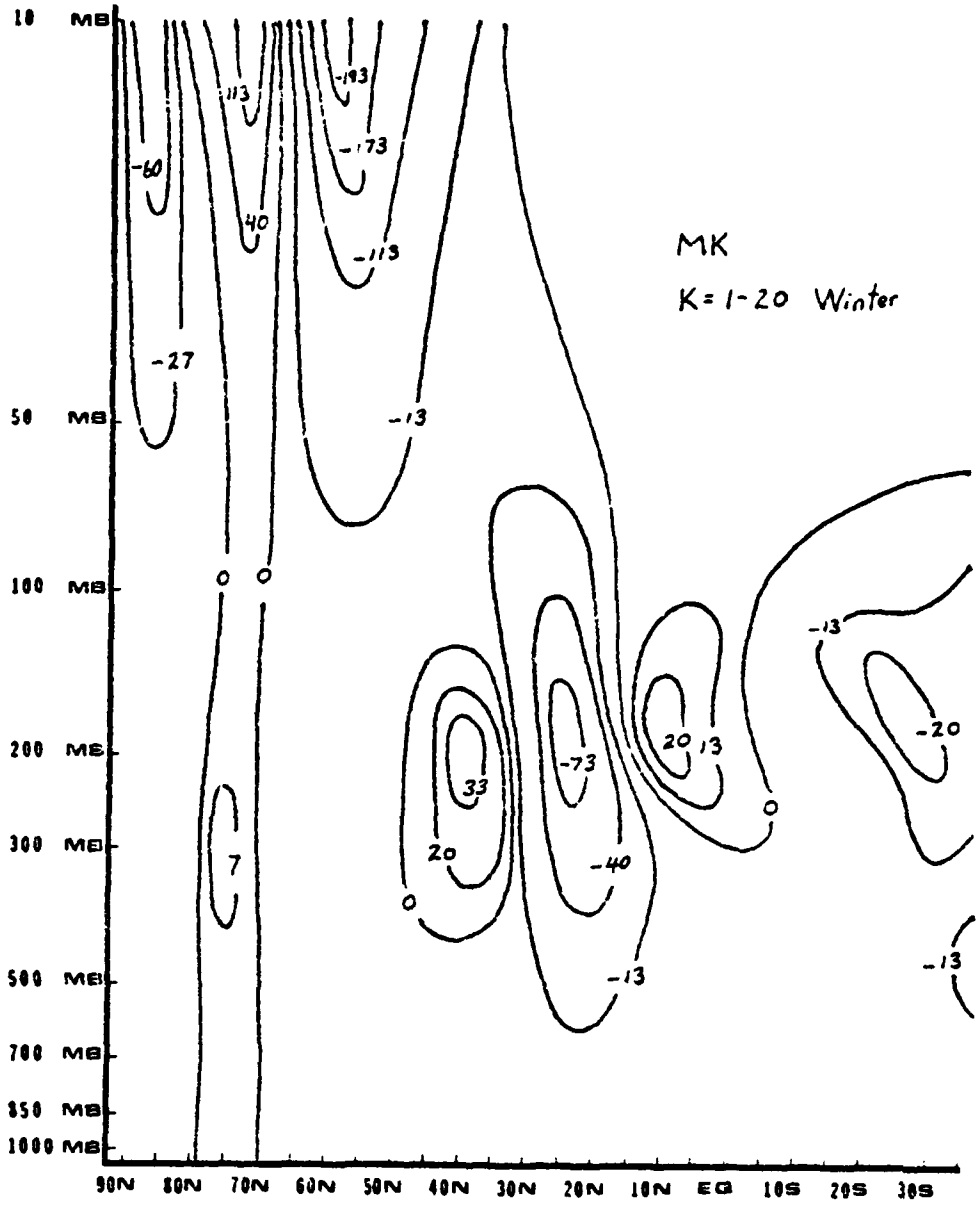


Figure 102. Distribution of MK summed over wave numbers 1 - 20 and averaged over the winter season ($m^2/sec^2/day$).

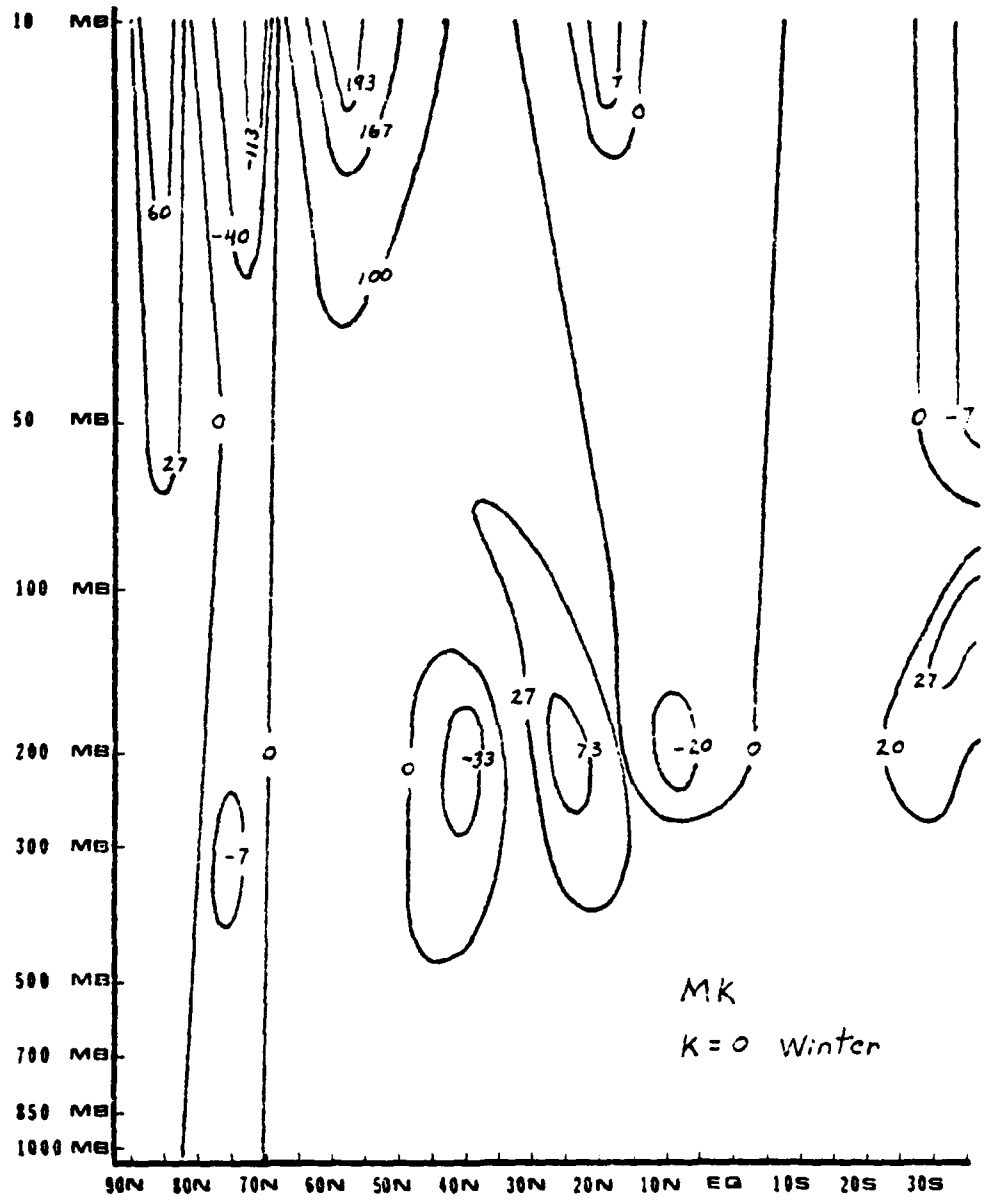


Figure 103. Distribution of MK over the winter season for wave number 0 ($m^2/sec^2/day$).

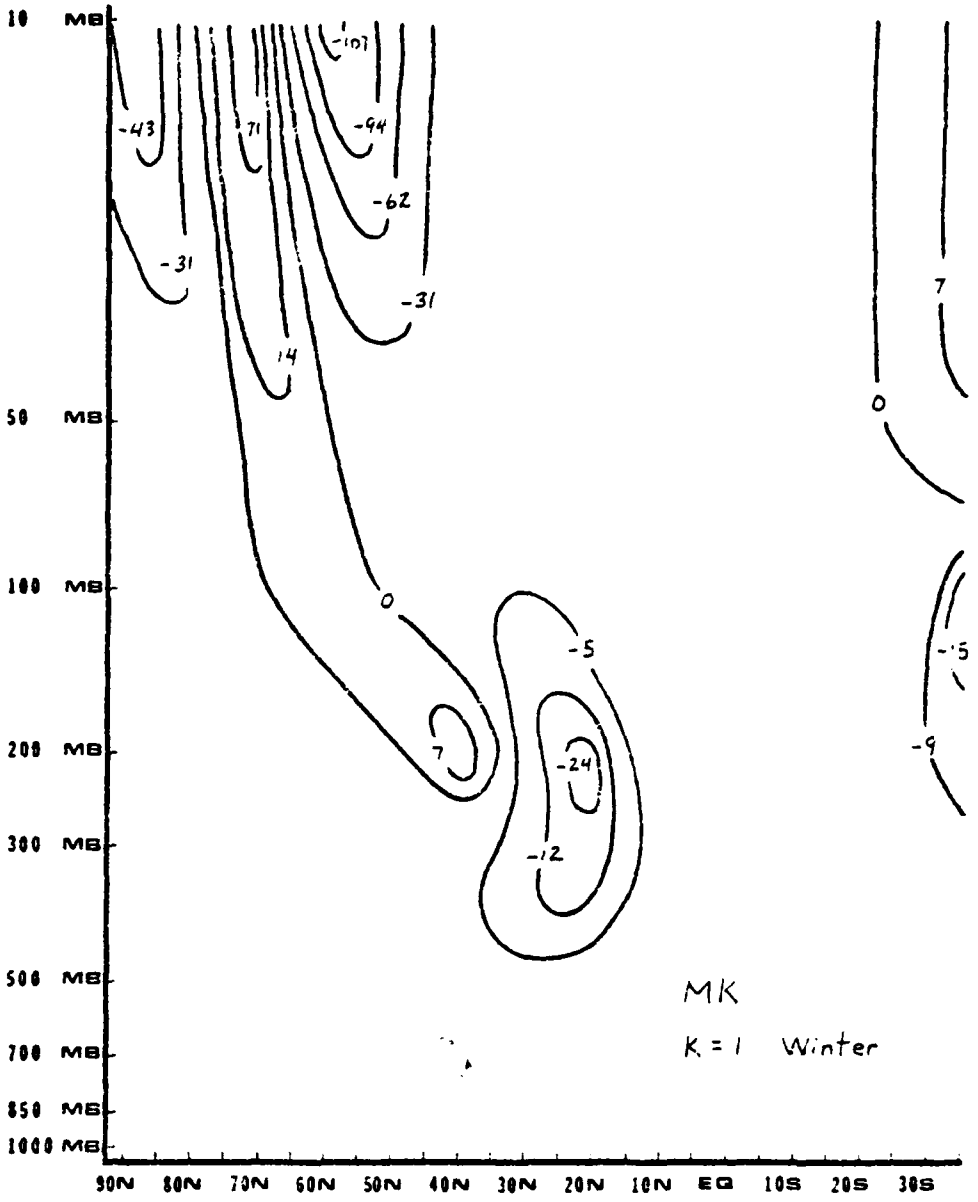


Figure 104. Distribution of MK over the winter season for wave number 1 ($m^2/sec^2/day$).

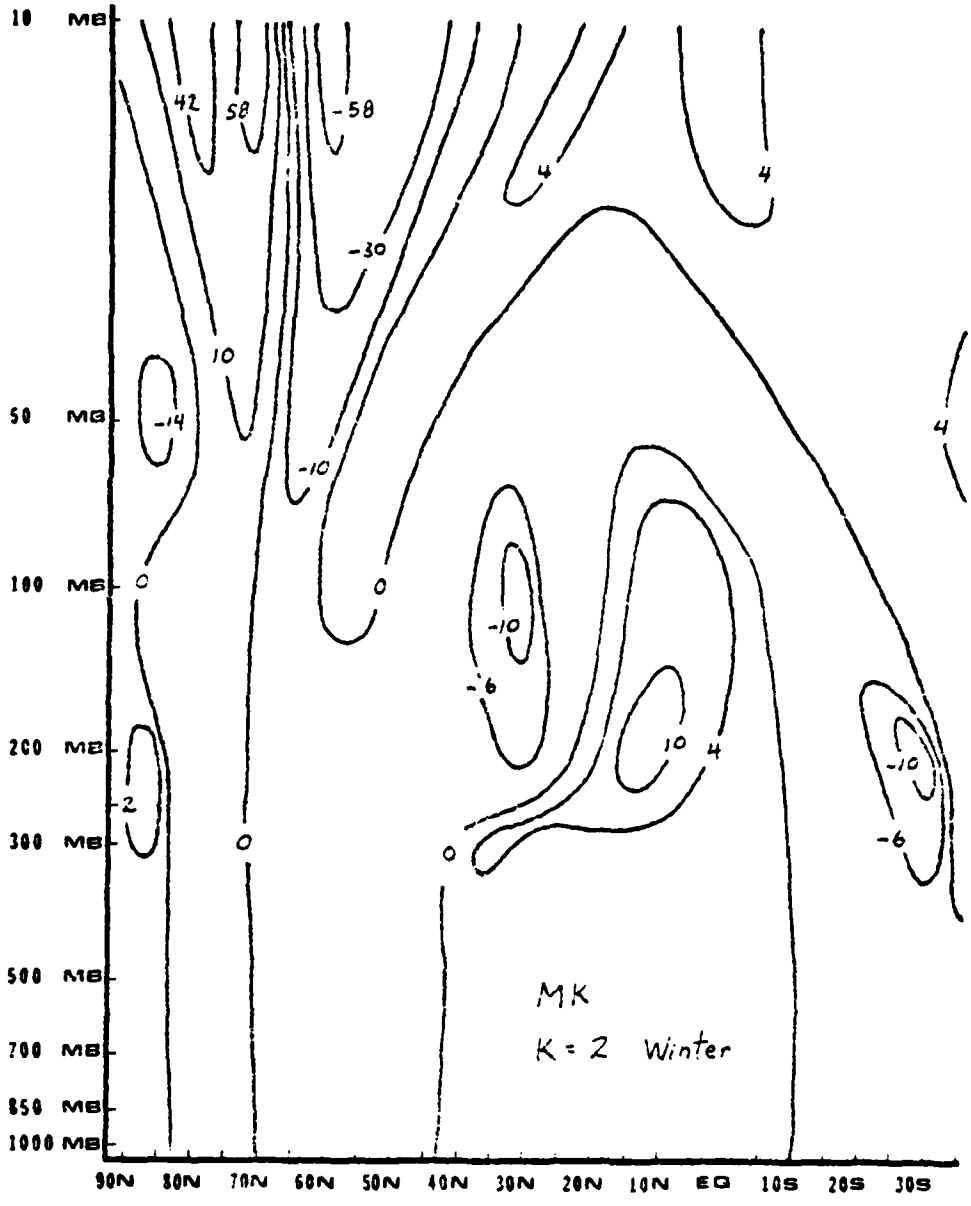


Figure 105. Distribution of MK over the winter season for wave number 2 ($m^2/sec^2/day$).

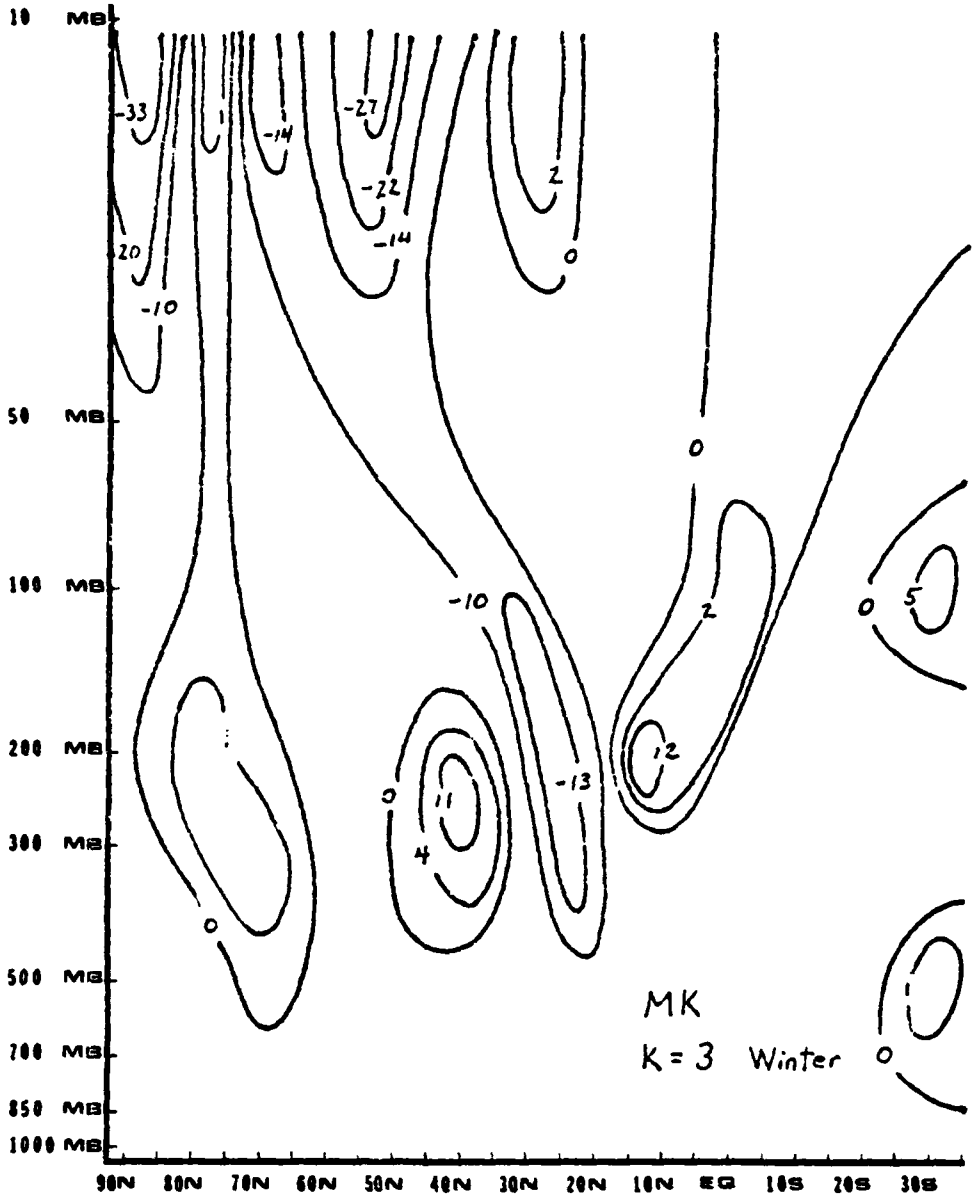


Figure 106. Distribution of MK over the winter season for wave number 3 ($m^2/sec^2/day$.)

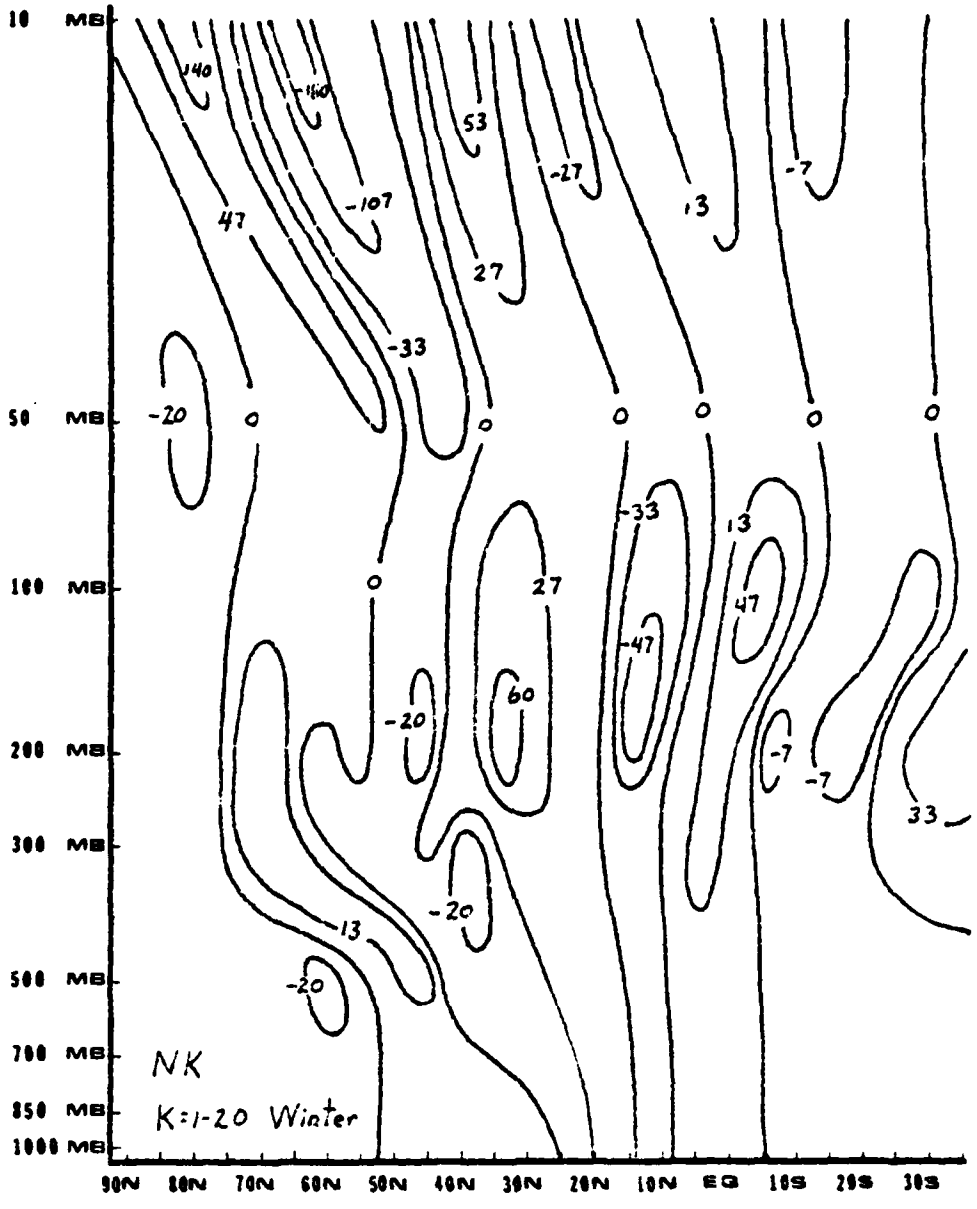


Figure 107. Distribution of NK summed over wave numbers 1 - 20 and averaged over the winter season ($m^2/sec^2/day$).

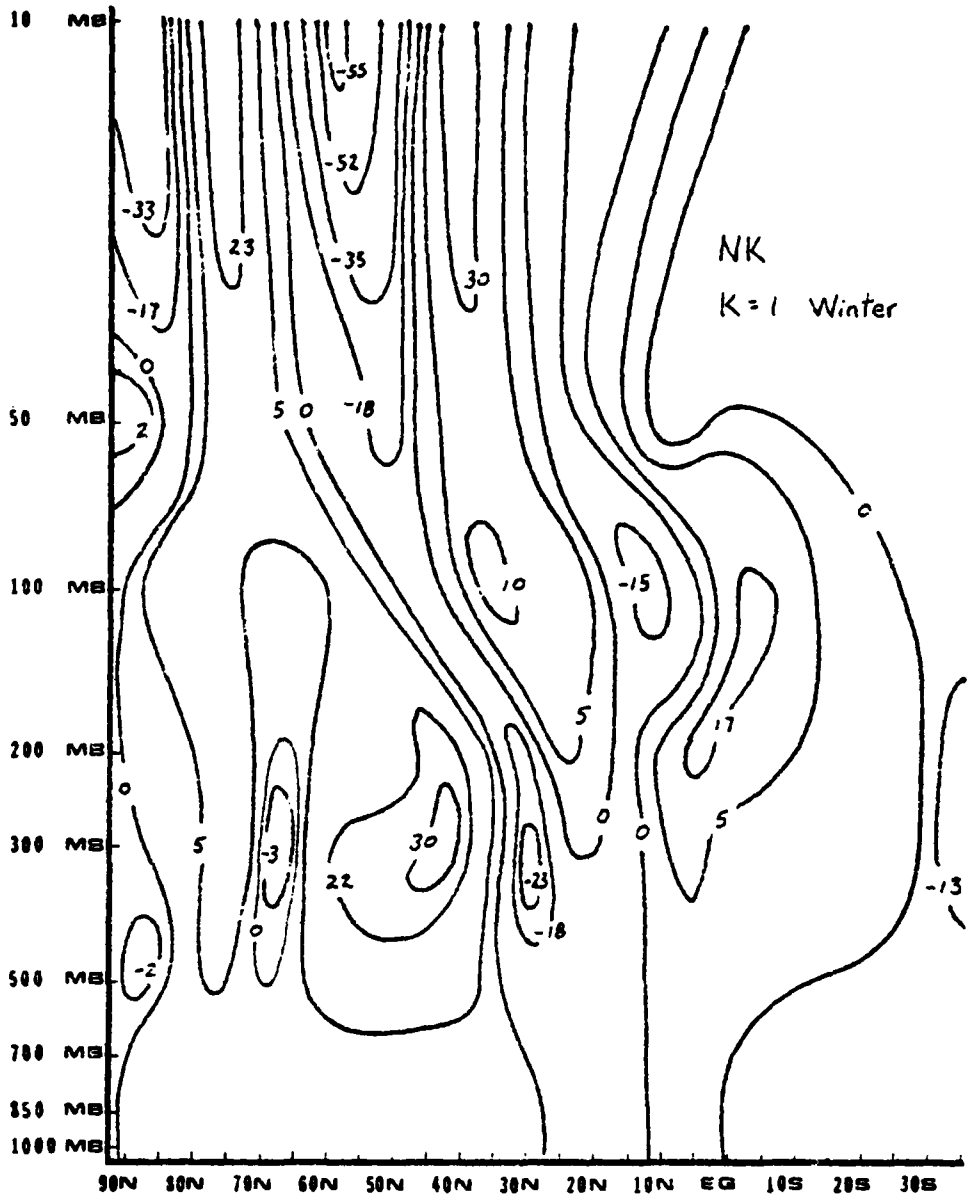


Figure 108. Distribution of NK over the winter season for wave number 1 ($m^2/sec^2/day$).

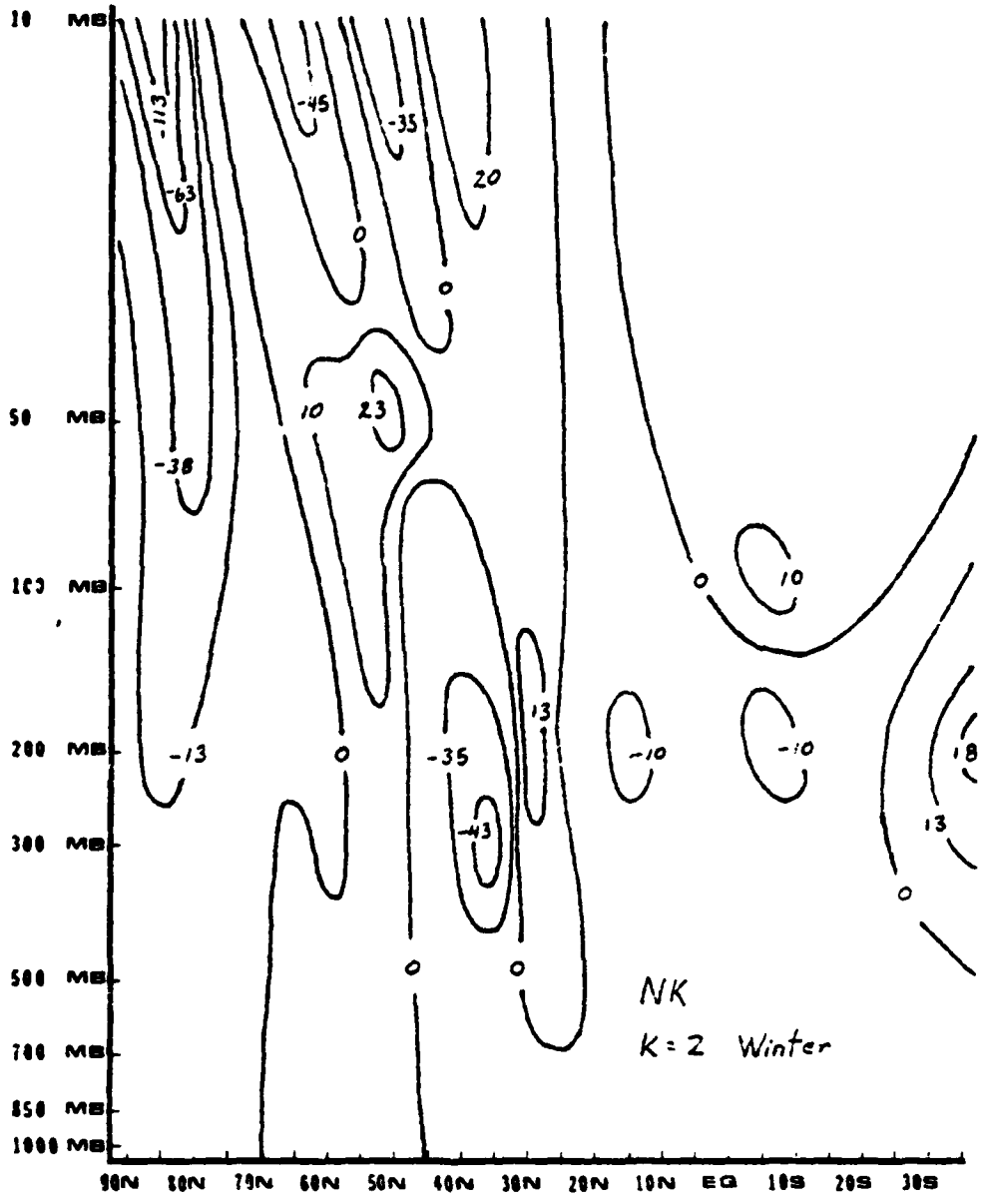


Figure 109. Distribution of NK over the winter season for wave number 2 ($m^2/sec^2/day$).

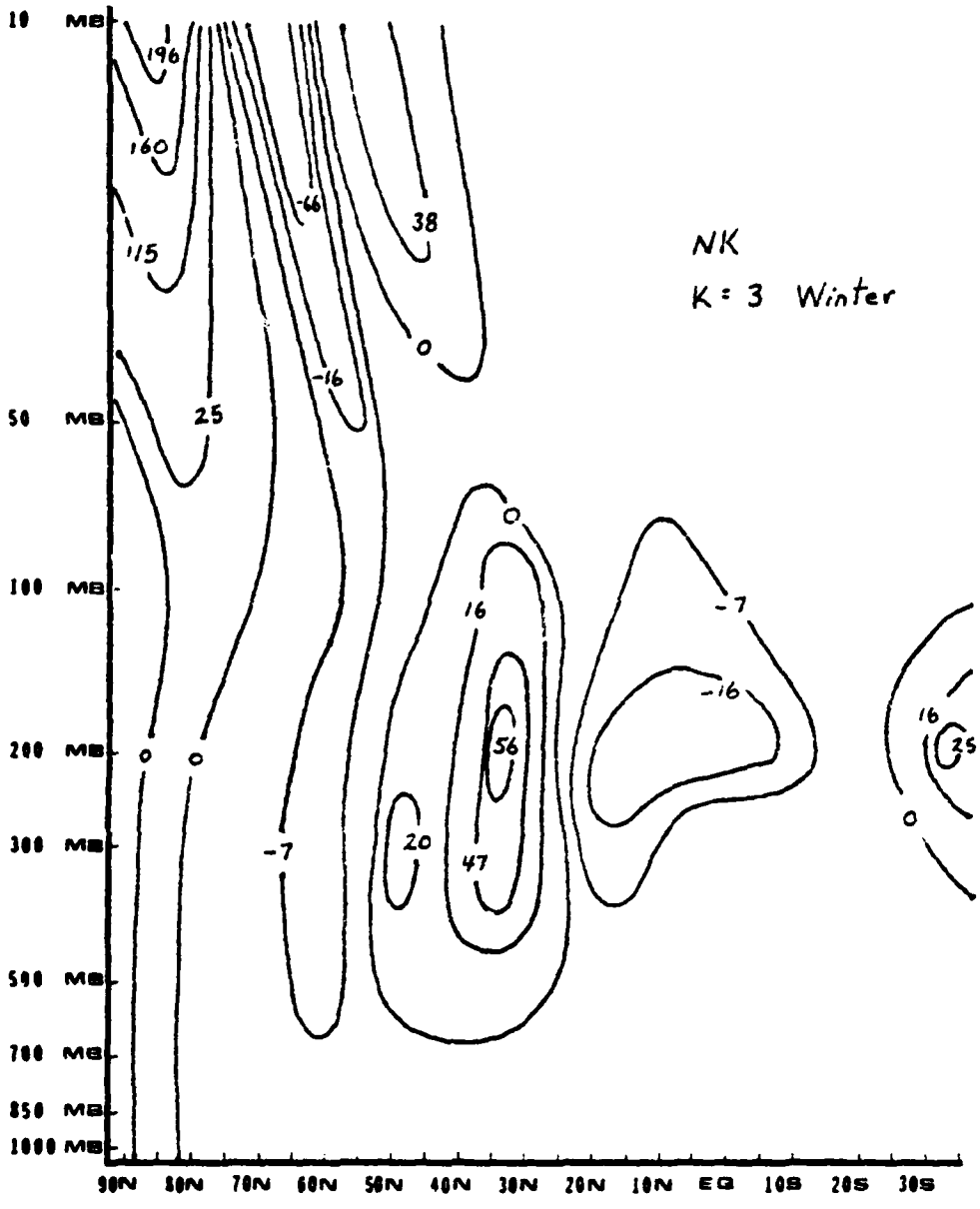


Figure 110. Distribution of NK over the winter season for wave number 3 ($m^2/sec^2/day$).

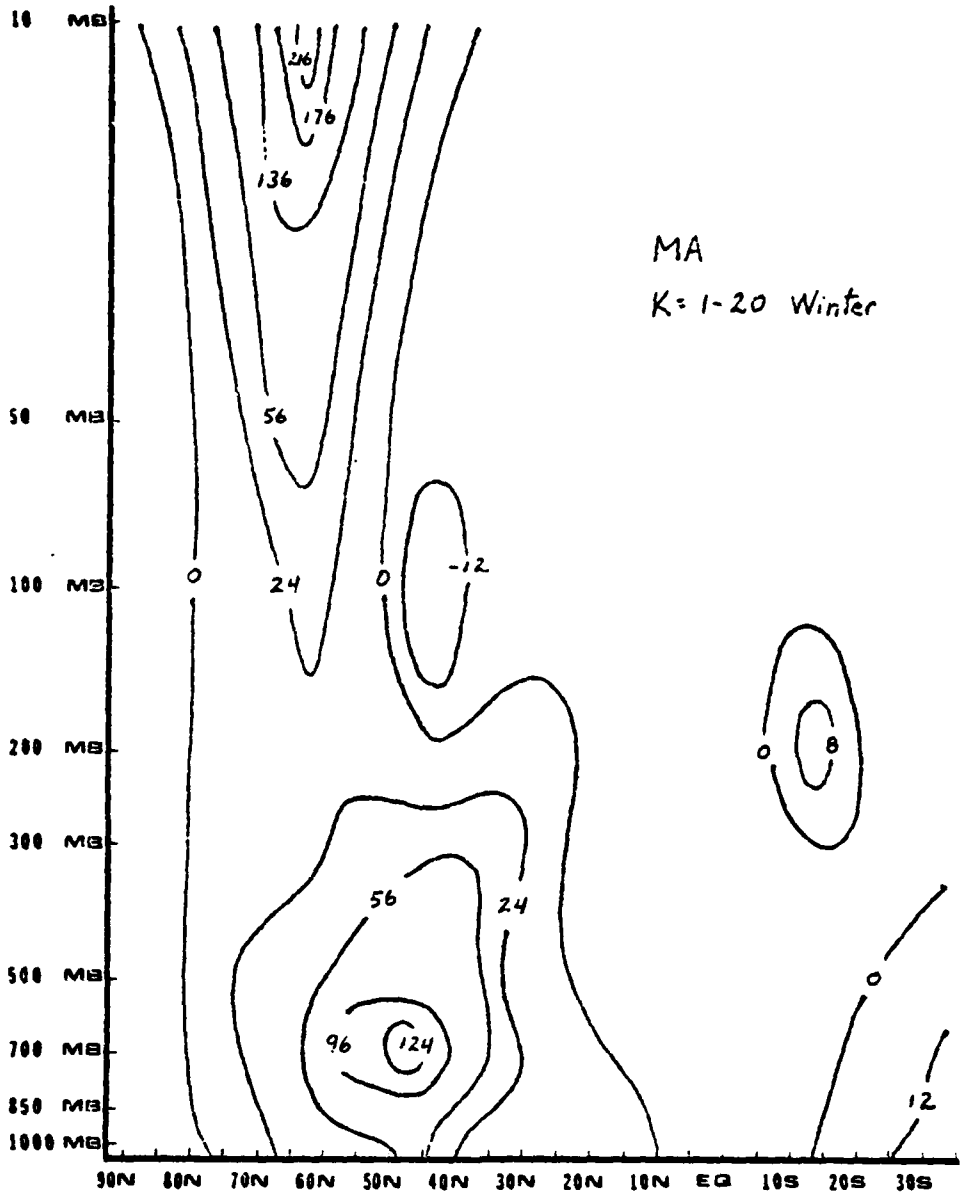


Figure 111. Distribution of MA summed over wave numbers 1 - 20 and averaged over the winter season ($m^2/sec^2/day$).

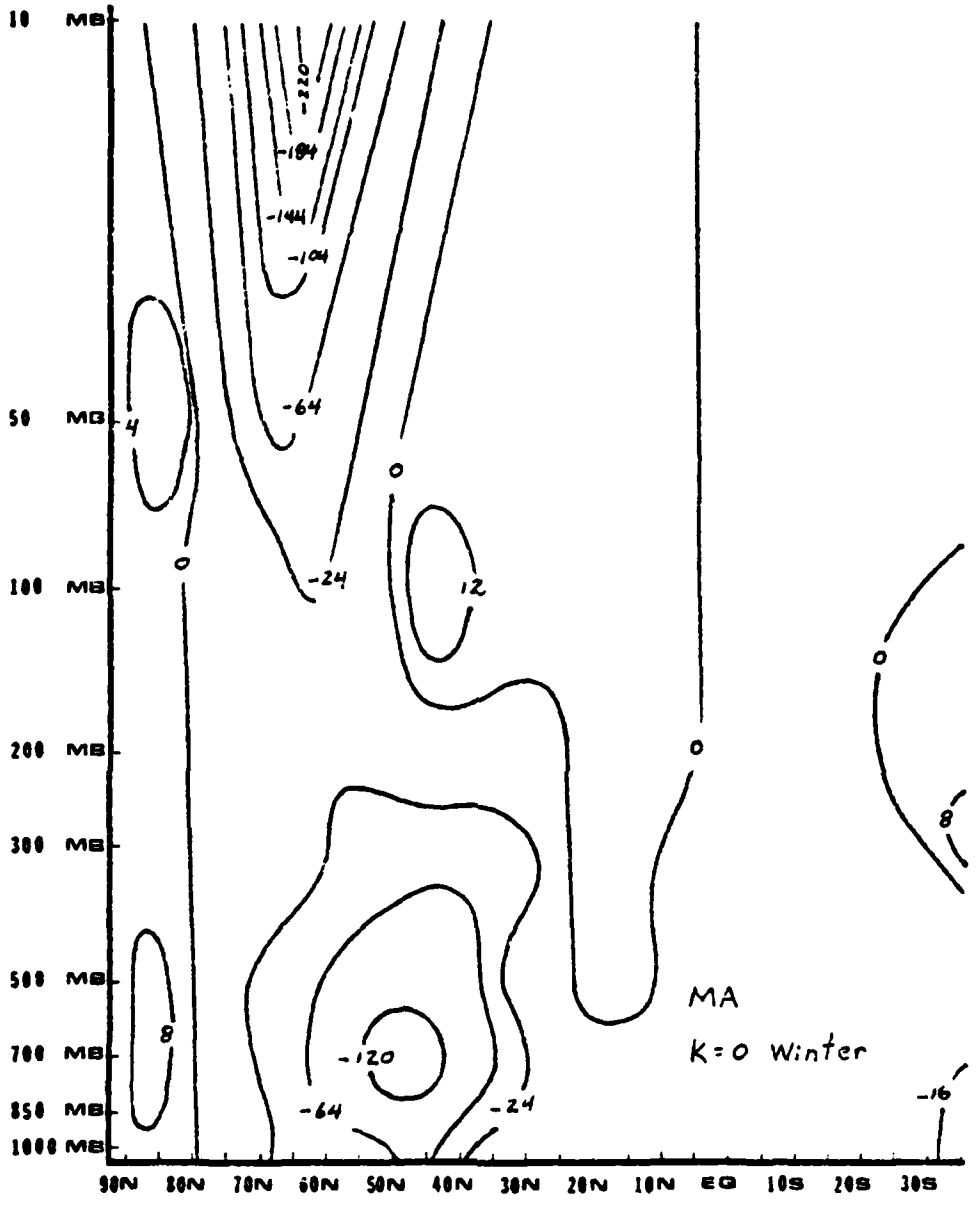


Figure 112. Distribution of MA over the winter season for wave number 0 ($m^2/sec^2/day$)

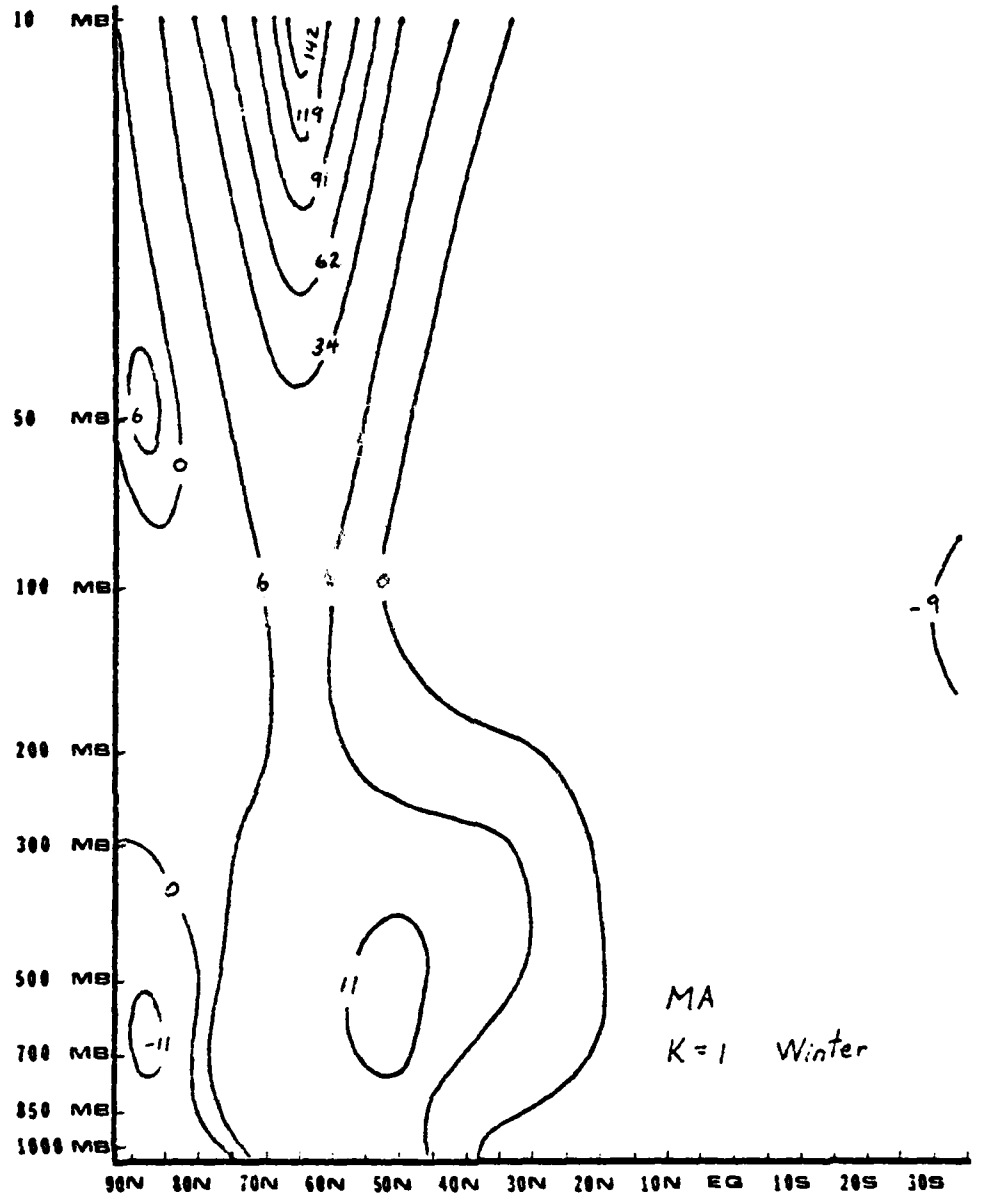


Figure 113. Distribution of MA over the winter season for wave number 1 ($m^2/sec^2/day$).

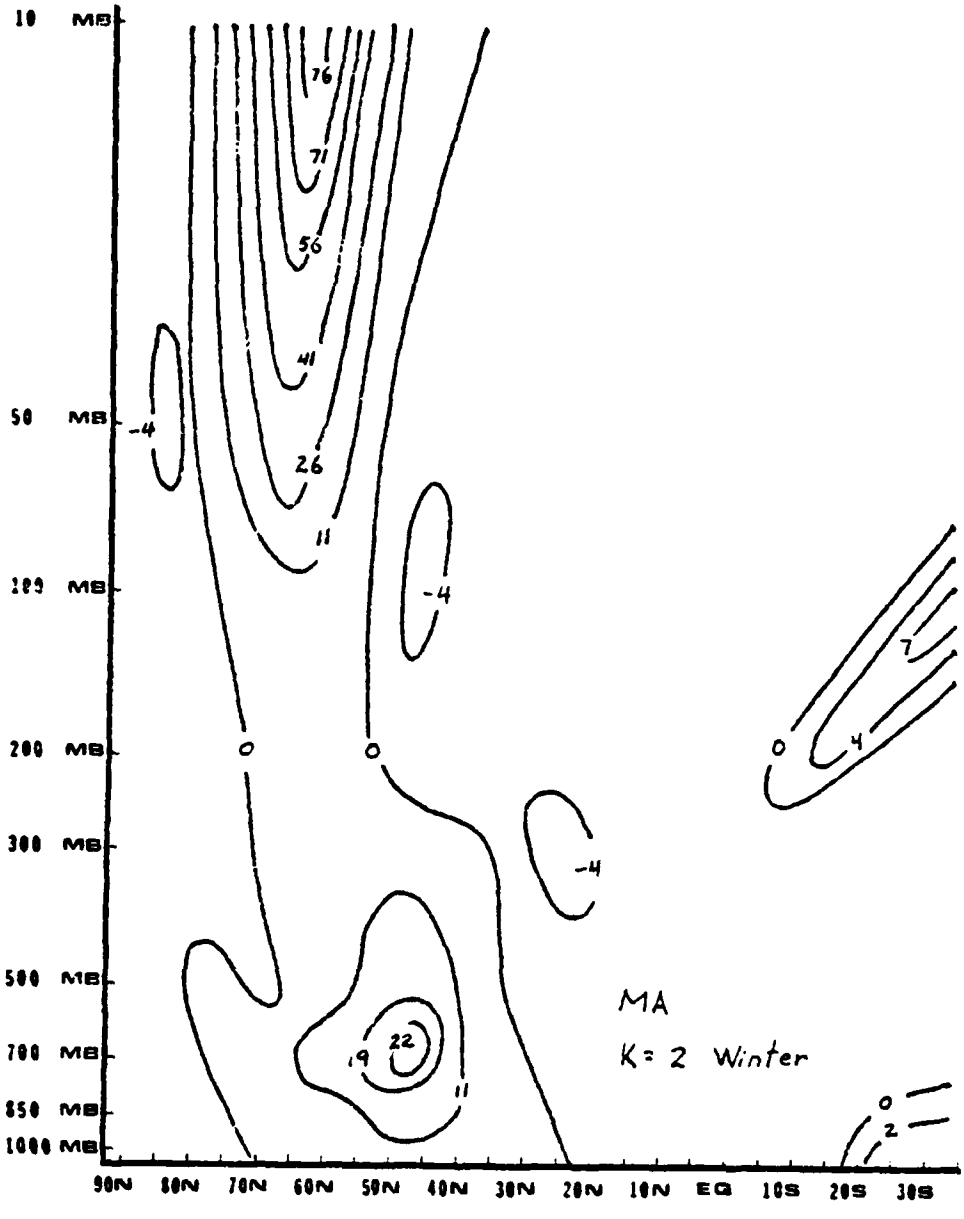


Figure 114. Distribution of MA over the winter season for wave number 2 ($m^2/sec^2/day$)

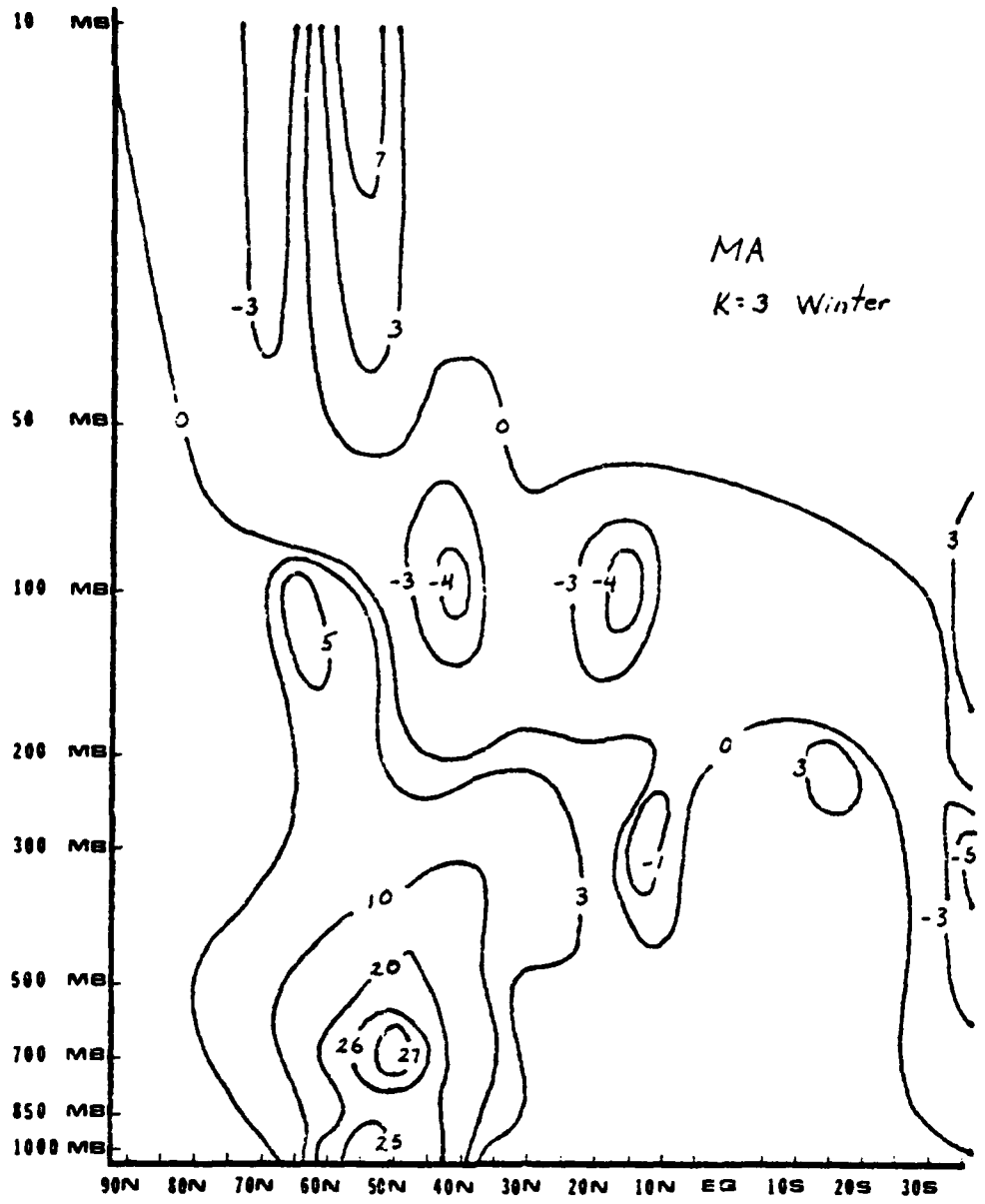


Figure 115. Distribution of MA over the winter season for wave number 3 ($m^2/sec^2/day$).

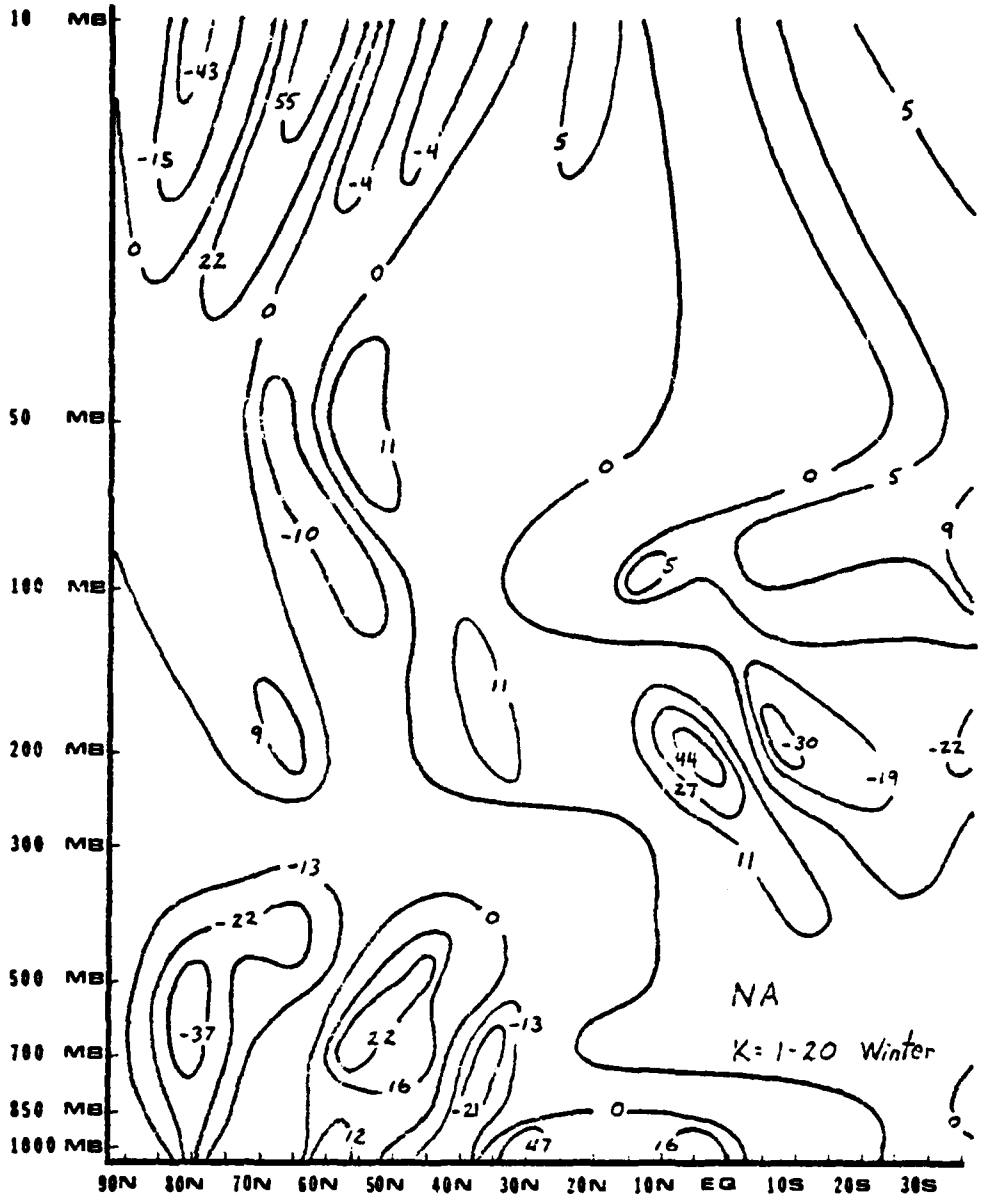


Figure 116. Distribution of NA summed over wave numbers 1 - 20 and averaged over the winter season ($m^2/sec^2/day$).

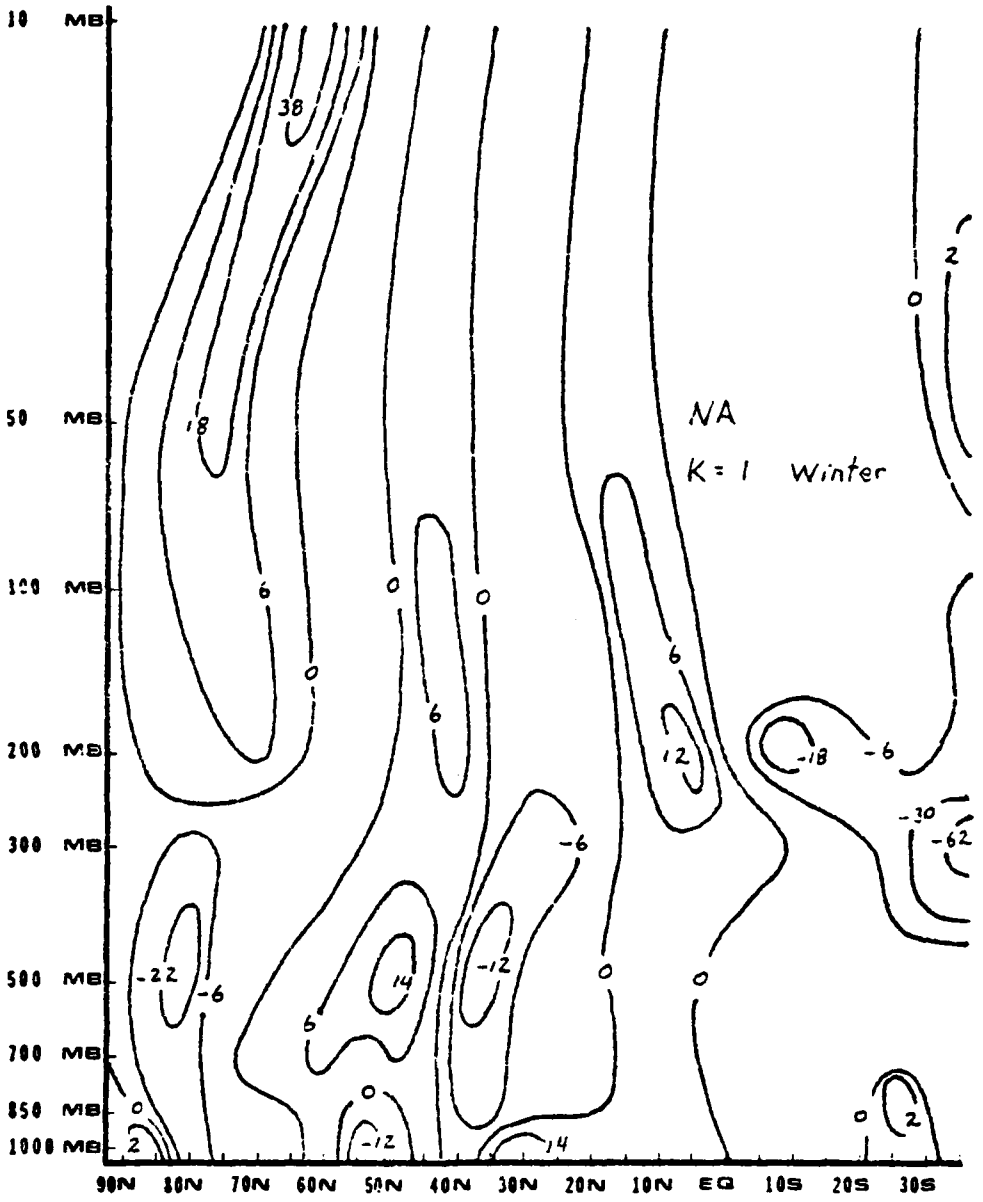


Figure 117. Distribution of NA over the winter season for wave number 1 ($m^2/sec^2/day$).

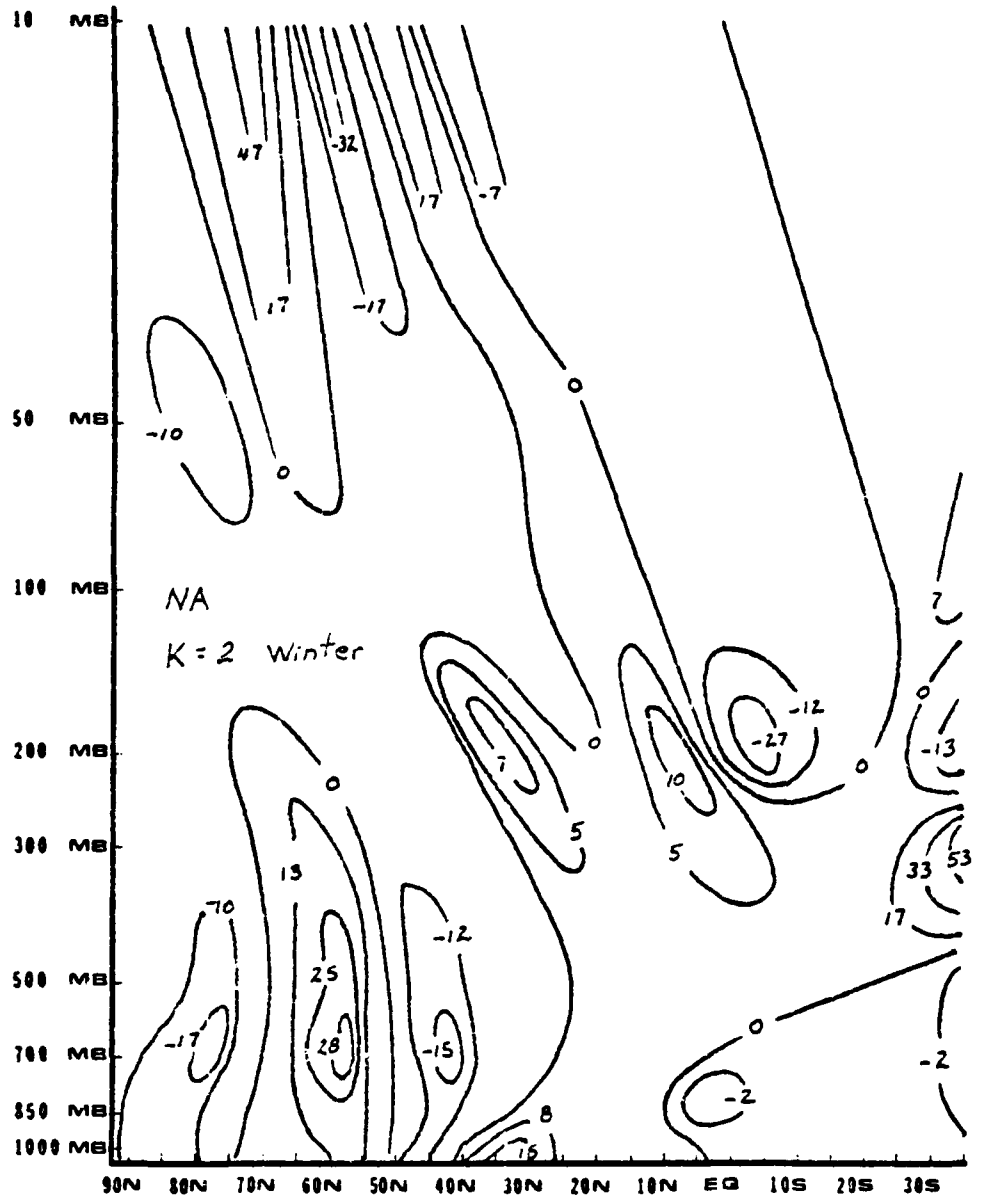


Figure 113. Distribution of NA over the winter season for wave number 2 ($m^2/sec^2/day$).

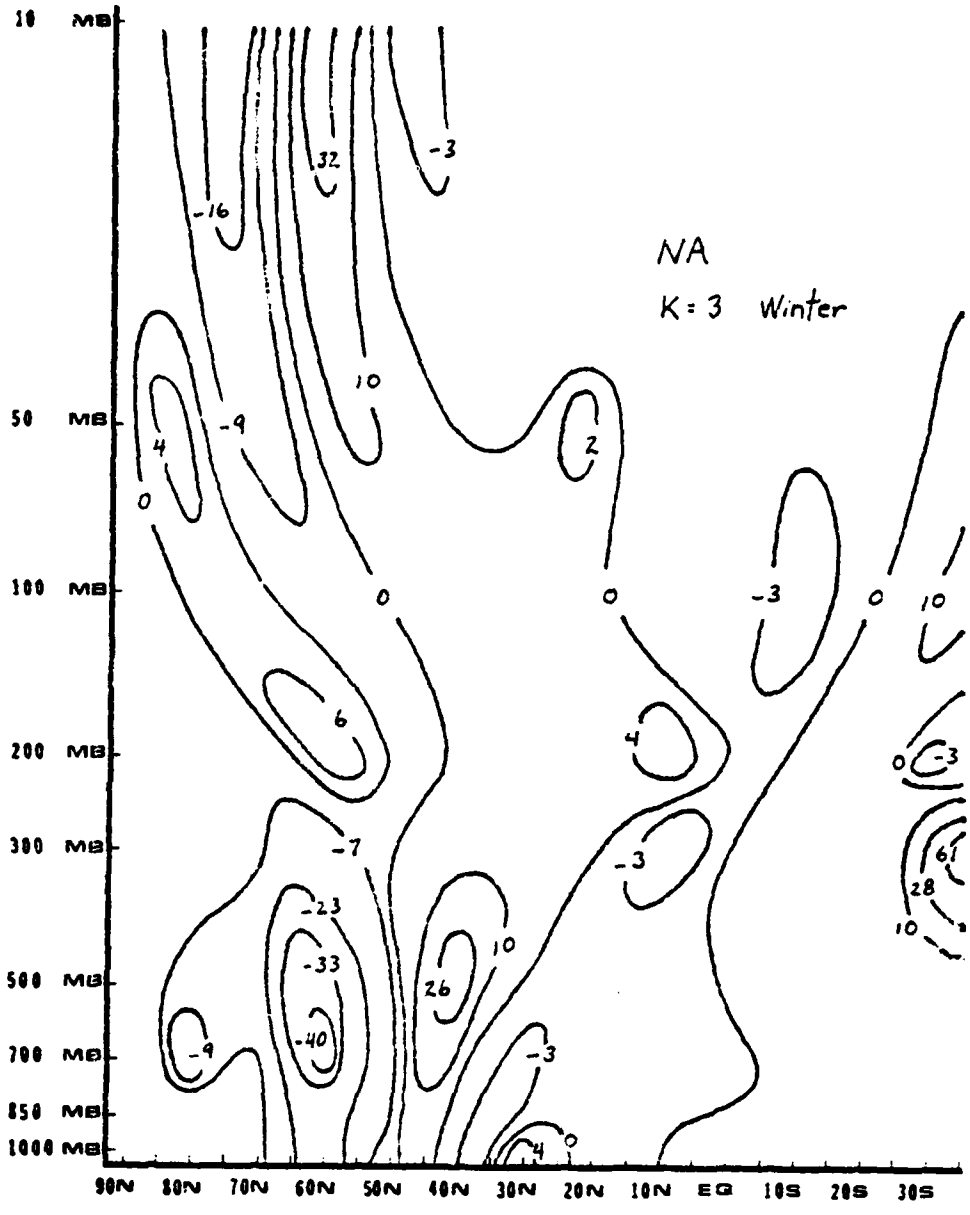


Figure 119. Distribution of NA over the winter season for wave number 3 ($m^2/sec^2/day$).

# APPENDIX B

## ENERGY TRANSFER DIAGRAMS FOR WINTER AND SUMMER AVERAGED OVER VARIOUS LATITUDE BANDS FOR WAVE NUMBERS 0 THROUGH 10

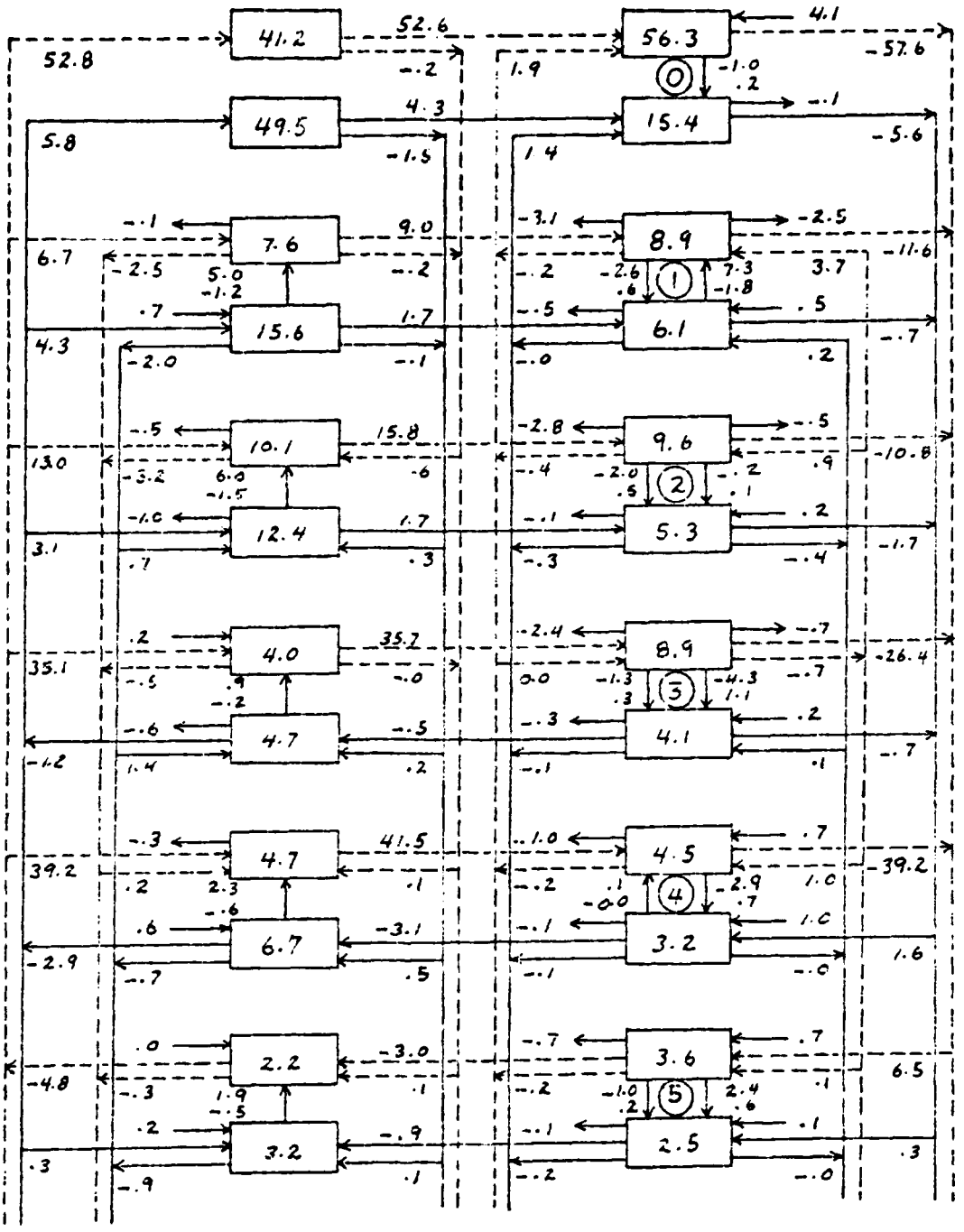


Figure 120. Transfer diagram of atmospheric energy for winter average conditions for wave numbers 0 - 5 over 30°S to°0. Energy fluxes are in $m^2/sec^2/day$, while EK and EA within the boxes are $m^2/sec^2$.

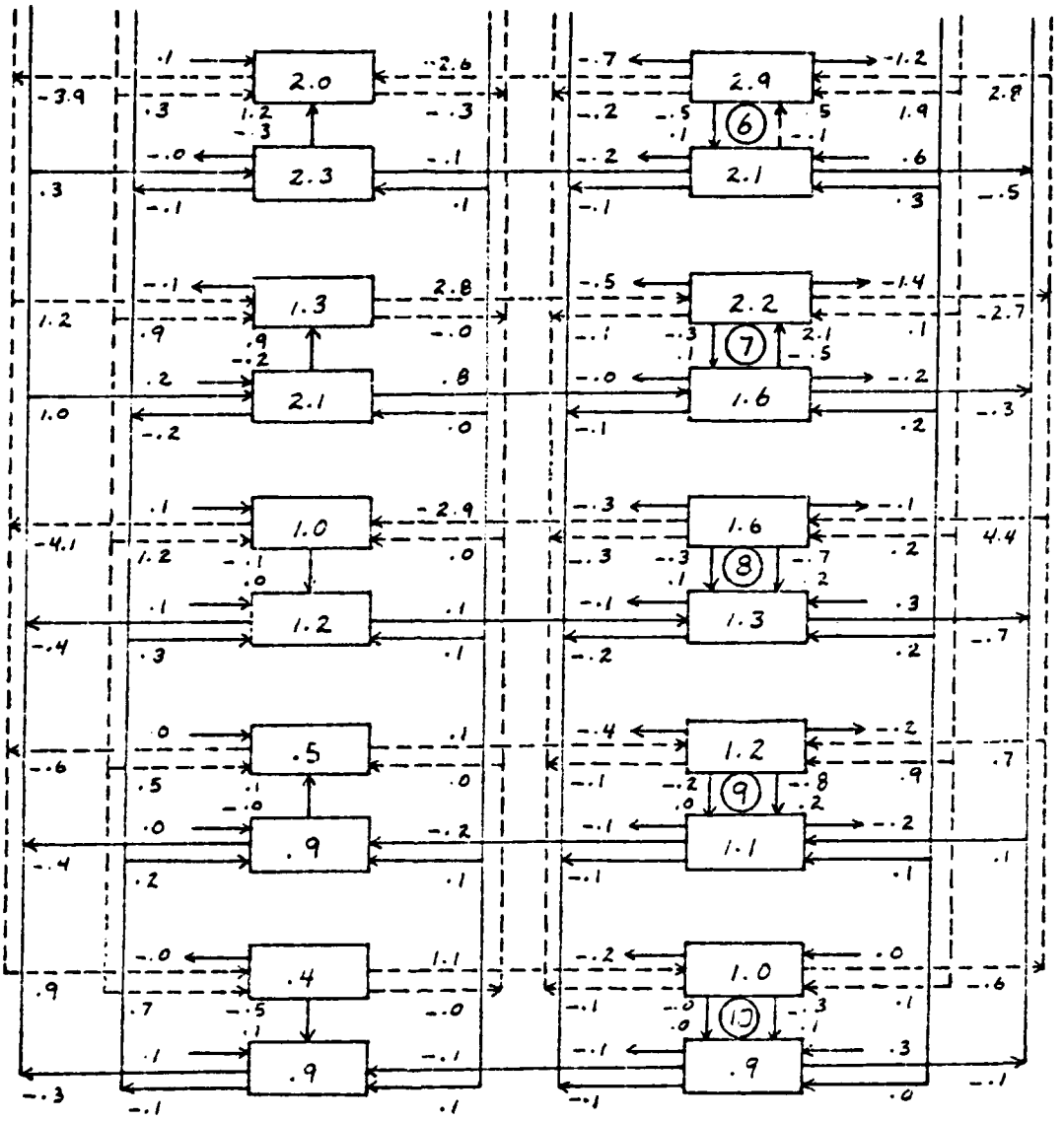


Figure 121. Transfer diagram of atmospheric energy for winter average conditions for wave numbers 6 - 10 over 30°S to°0. Energy fluxes are in $m^2/sec^2/day$, while EK and EA within the boxes are $m^2/sec^2$.

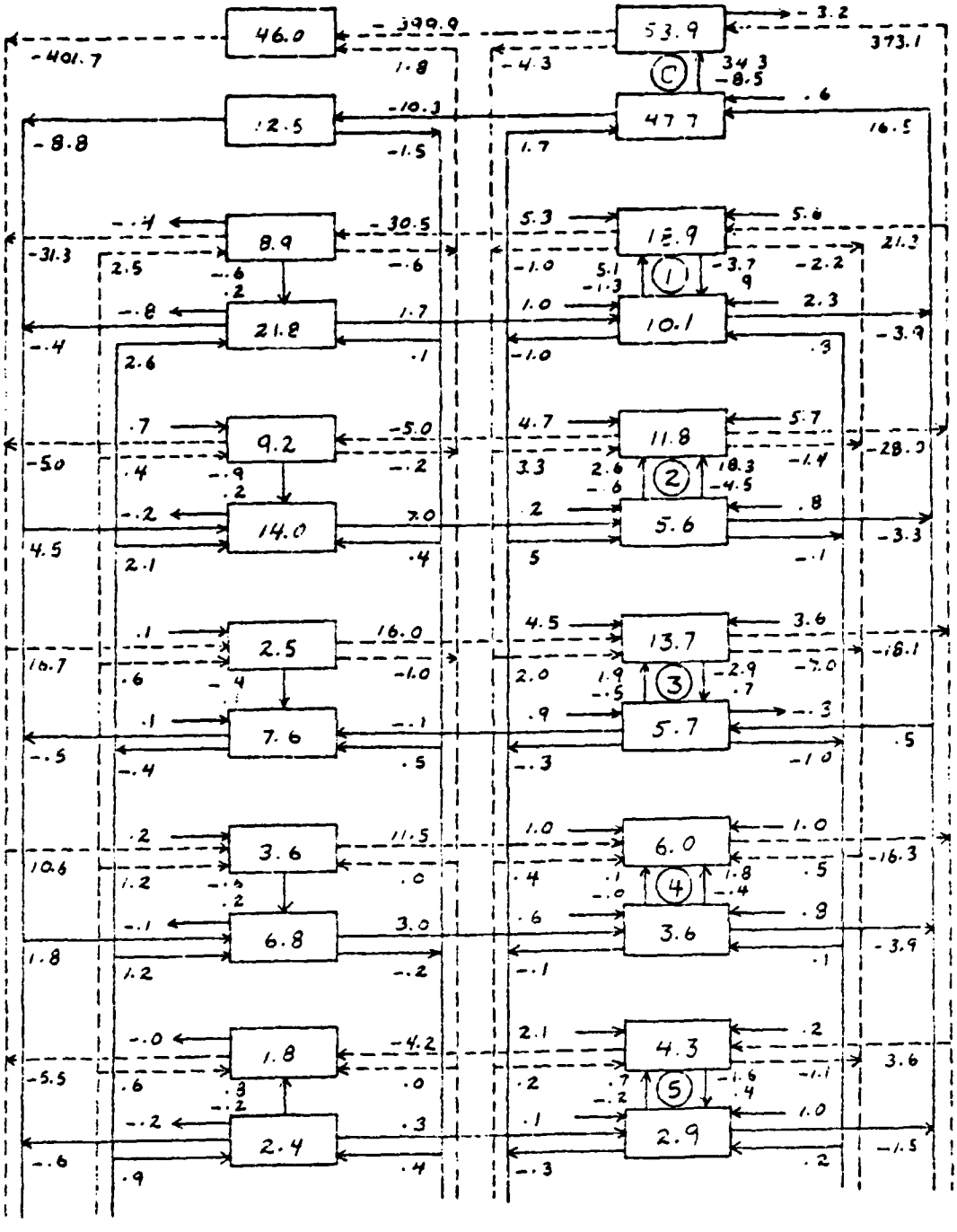


Figure 122. Transfer diagram of atmospheric energy for winter average conditions for wave numbers 0 - 5 over 0° to 20°N. Energy fluxes are in $m^2/sec^2/day$, while EK and EA within the boxes are $m^2/sec^2$.

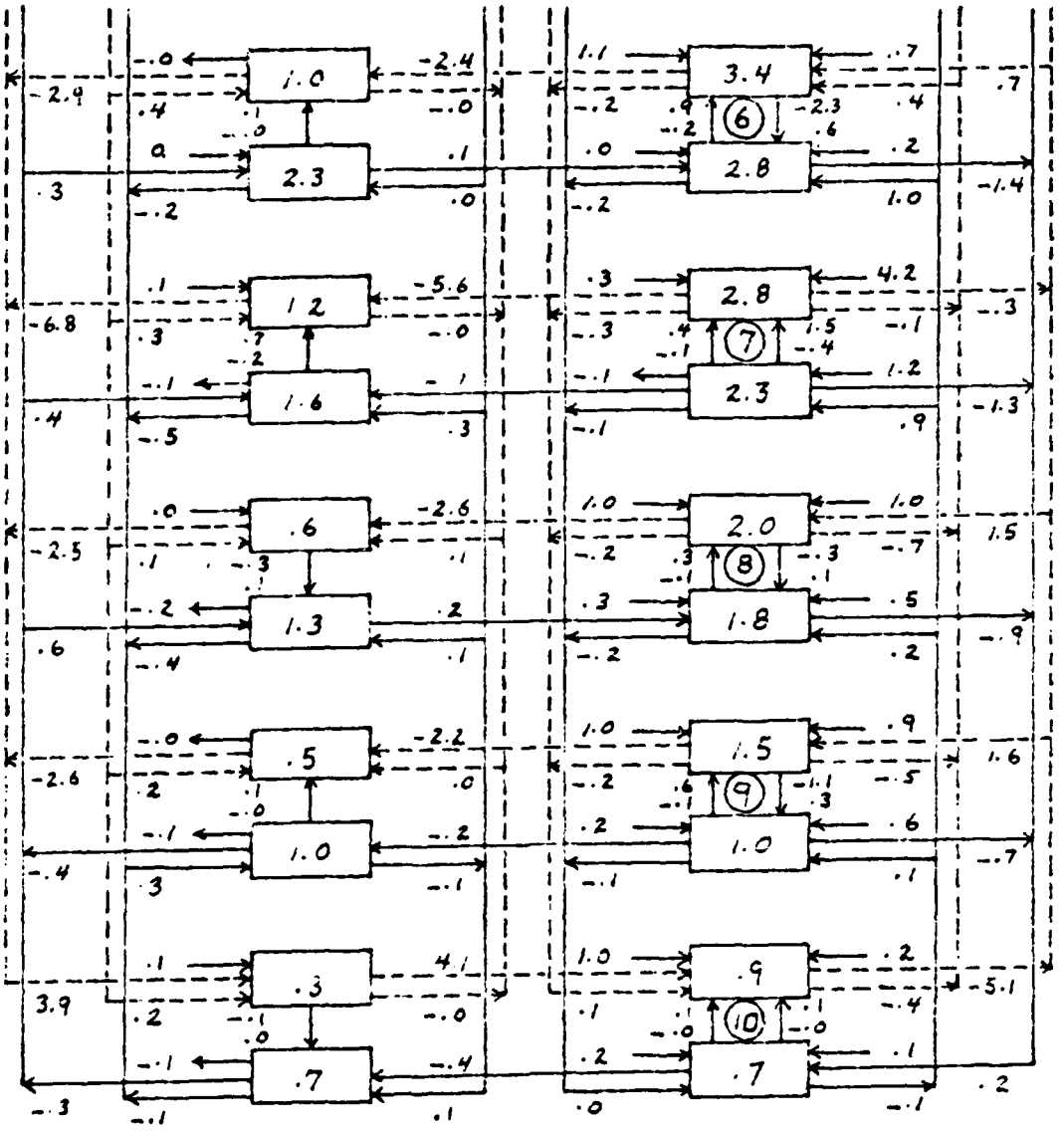


Figure 123. Transfer diagram of atmospheric energy for winter average conditions for wave numbers 6-10 over 0° to 20°N. Energy fluxes are in $m^2/sec^2/day$, while EK and EA within the boxes are $m^2/sec^2$.

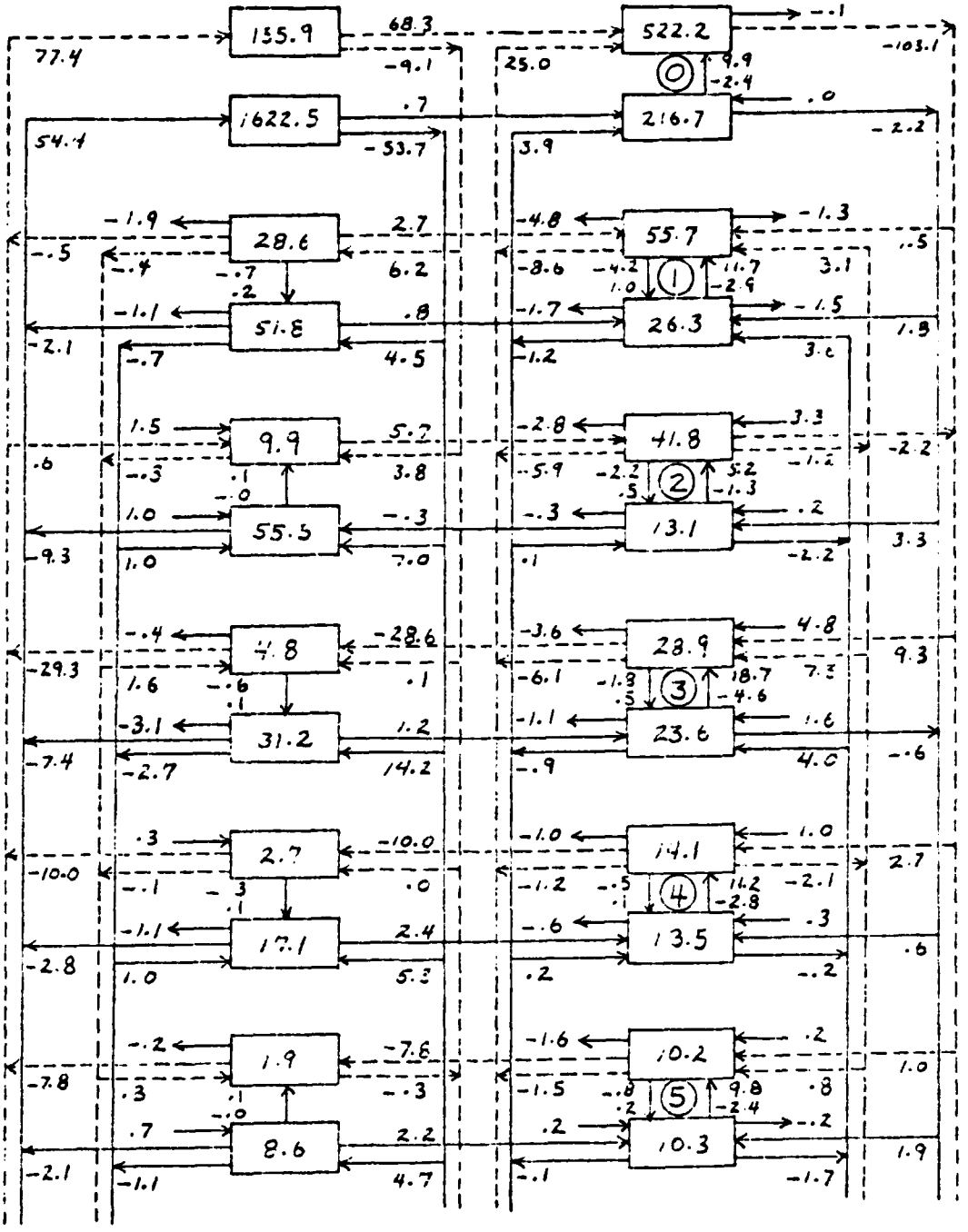


Figure 124. Transfer diagram of atmospheric energy for winter average conditions for wave numbers 0 - 5 over 20°N to 60°N. Energy fluxes are in $m^2/sec^2/day$, while EK and EA within the boxes are $m^2/sec^2$.

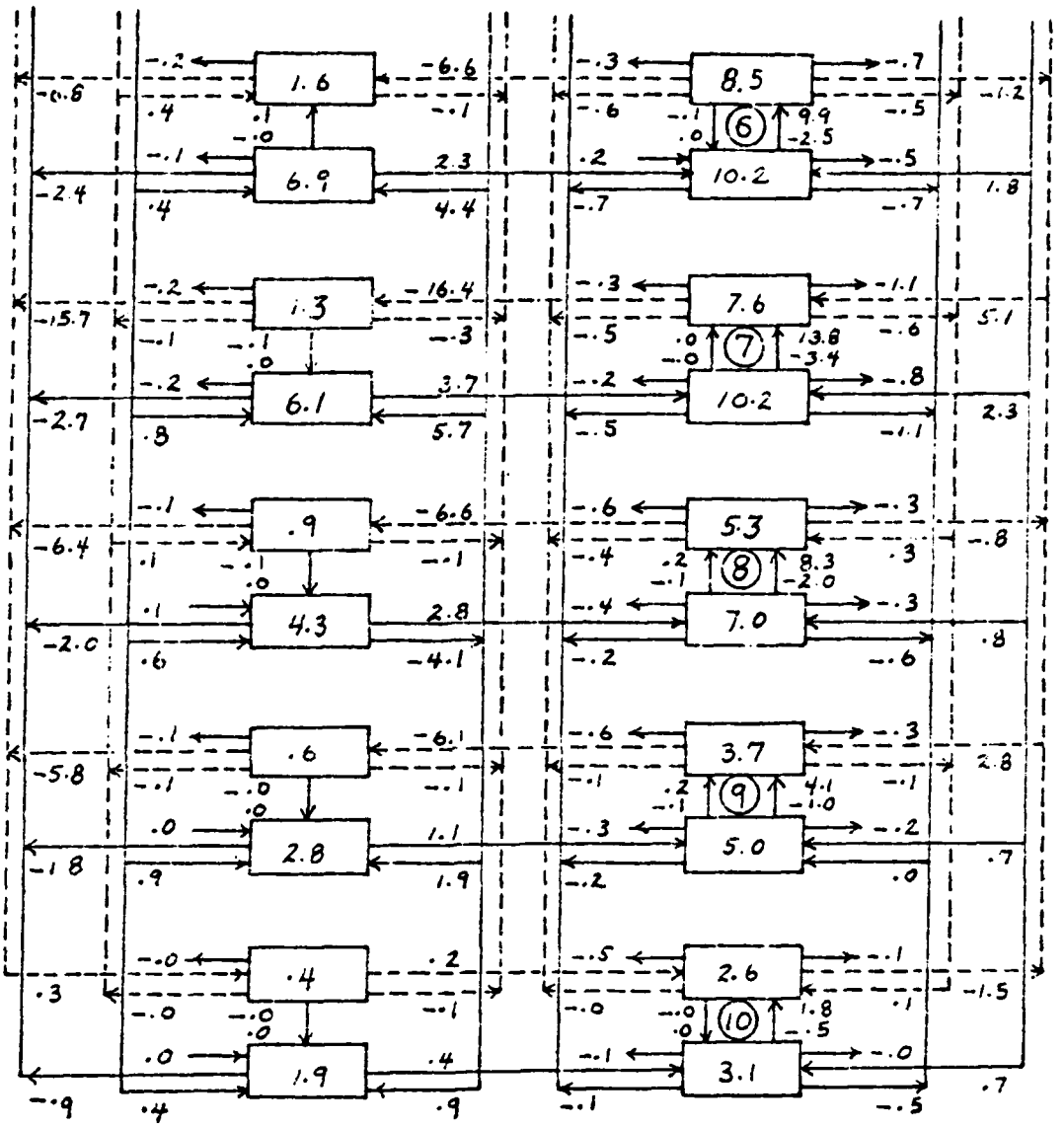


Figure 125. Transfer diagram of atmospheric energy for winter average conditions for wave numbers 6 - 10 over 20°N to 60°N. Energy fluxes are in $m^2/sec^2/day$, while EK and EA within the boxes are $m^2/sec^2$.

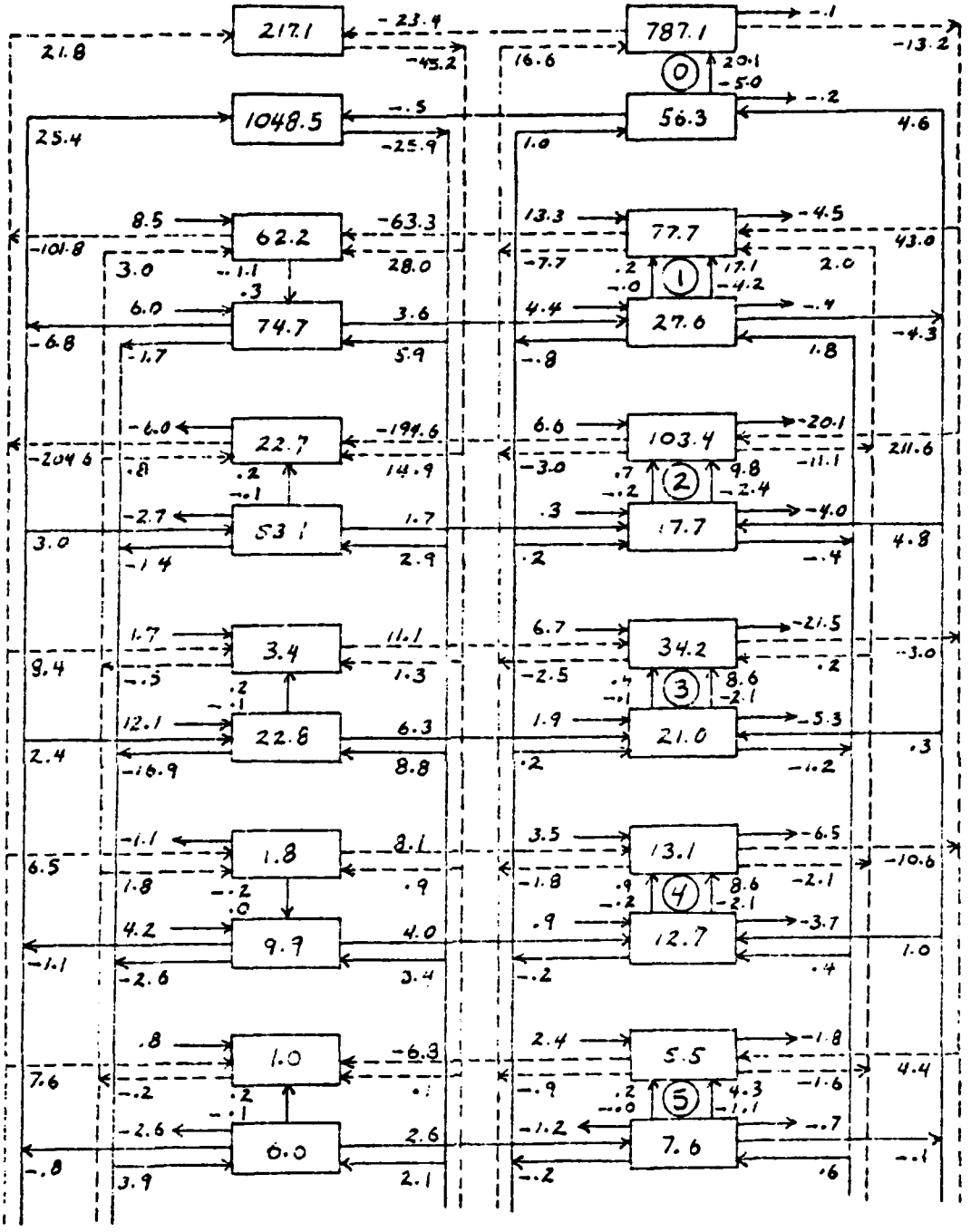


Figure 126. Transfer diagram of atmospheric energy for winter average conditions for wave numbers 0 - 5 over 60°N to 90°N. Energy fluxes are in $m^2/sec^2/day$, while EK and EA within the boxes are $m^2/sec^2$.

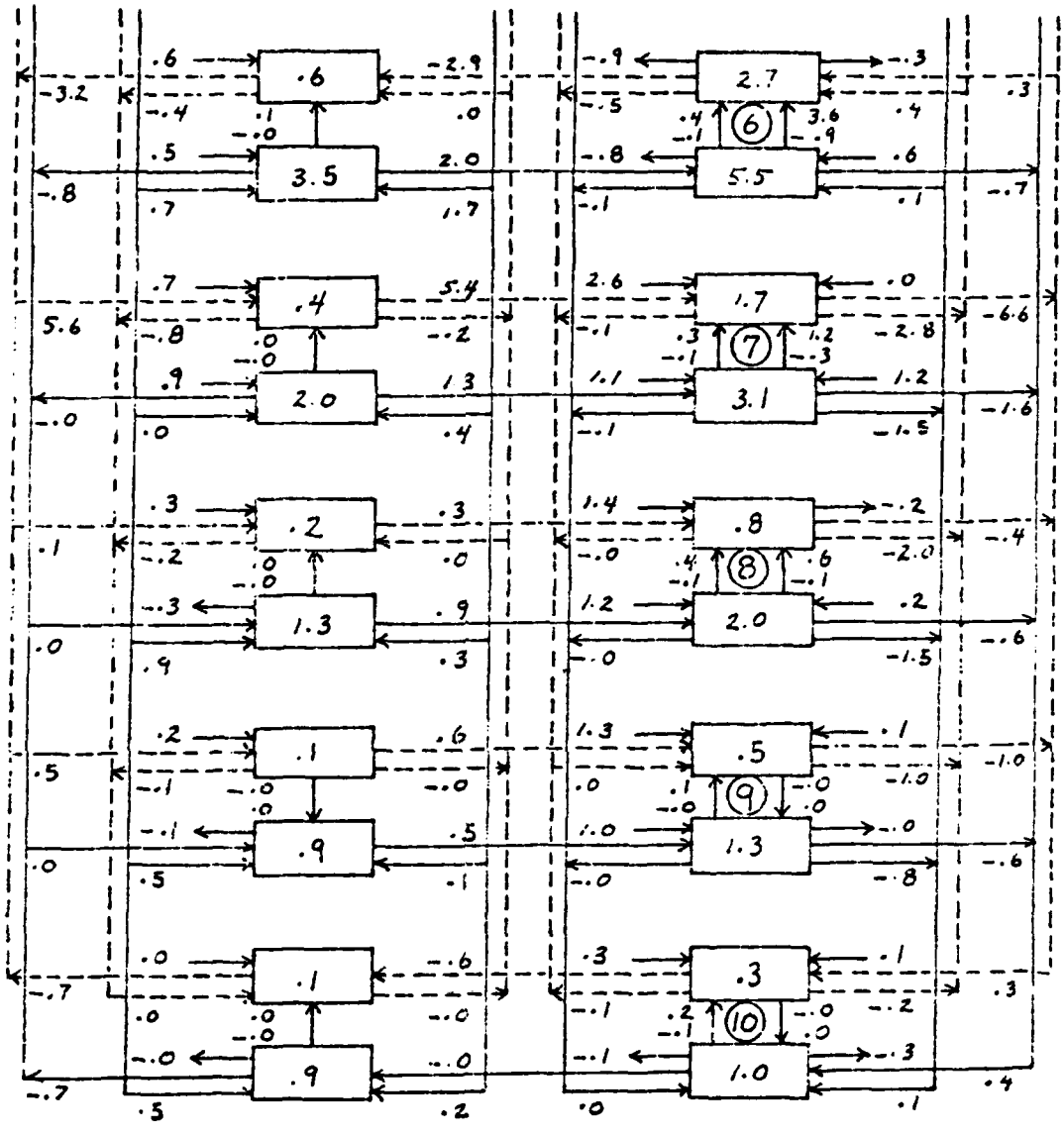


Figure 127. Transfer diagram of atmospheric energy for winter average conditions for wave numbers 6 - 10 over 60°N to 90°N. Energy fluxes are in $m^2/sec^2/day$, while EK and EA within the boxes are $m^2/sec^2$.

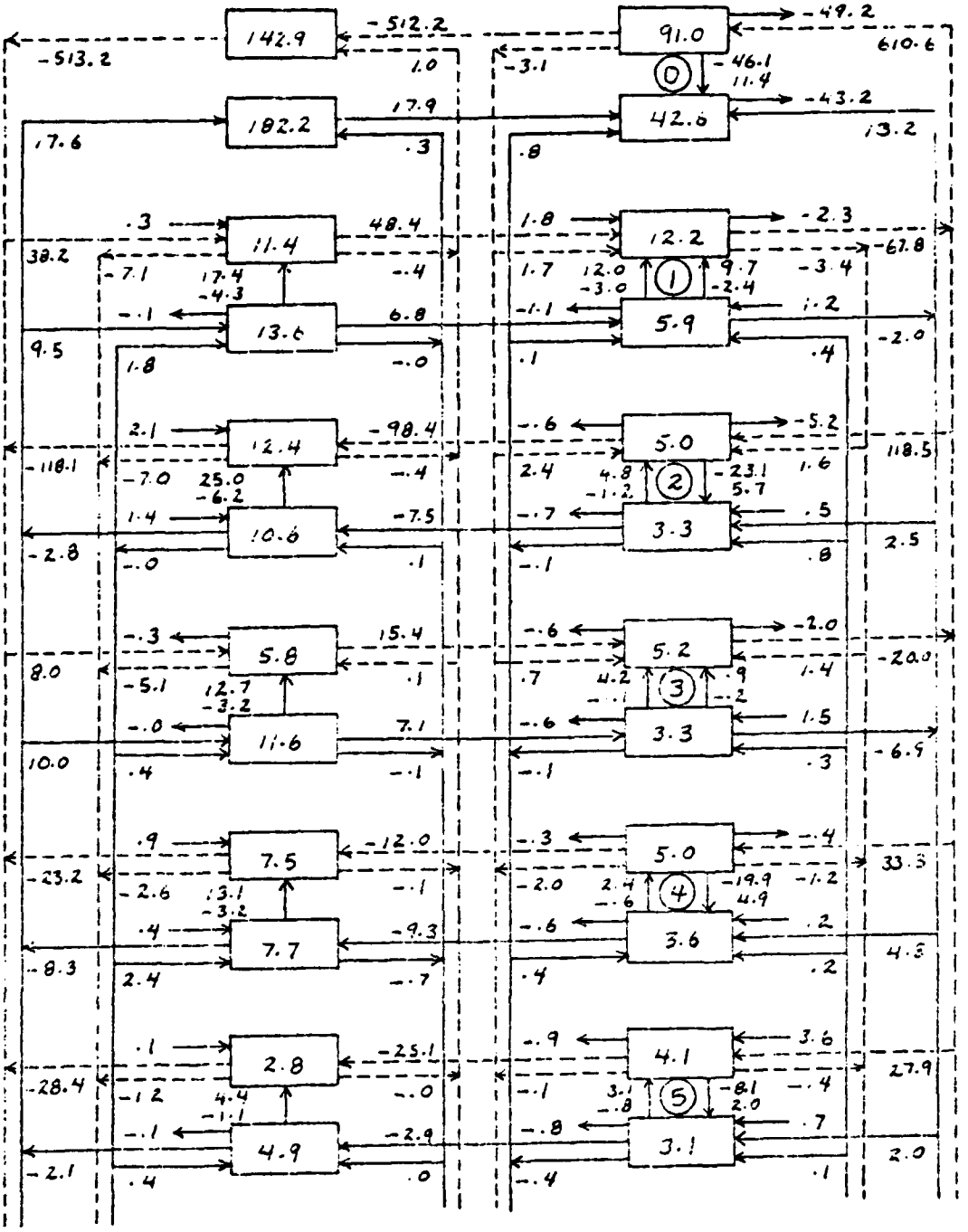


Figure 128. Transfer diagram of atmospheric energy for summer average conditions for wave numbers 0 - 5 over 20°S to 0°. Energy fluxes are in $m^2/sec^2/day$, while EK and EA within the boxes are $m^2/sec^2$.

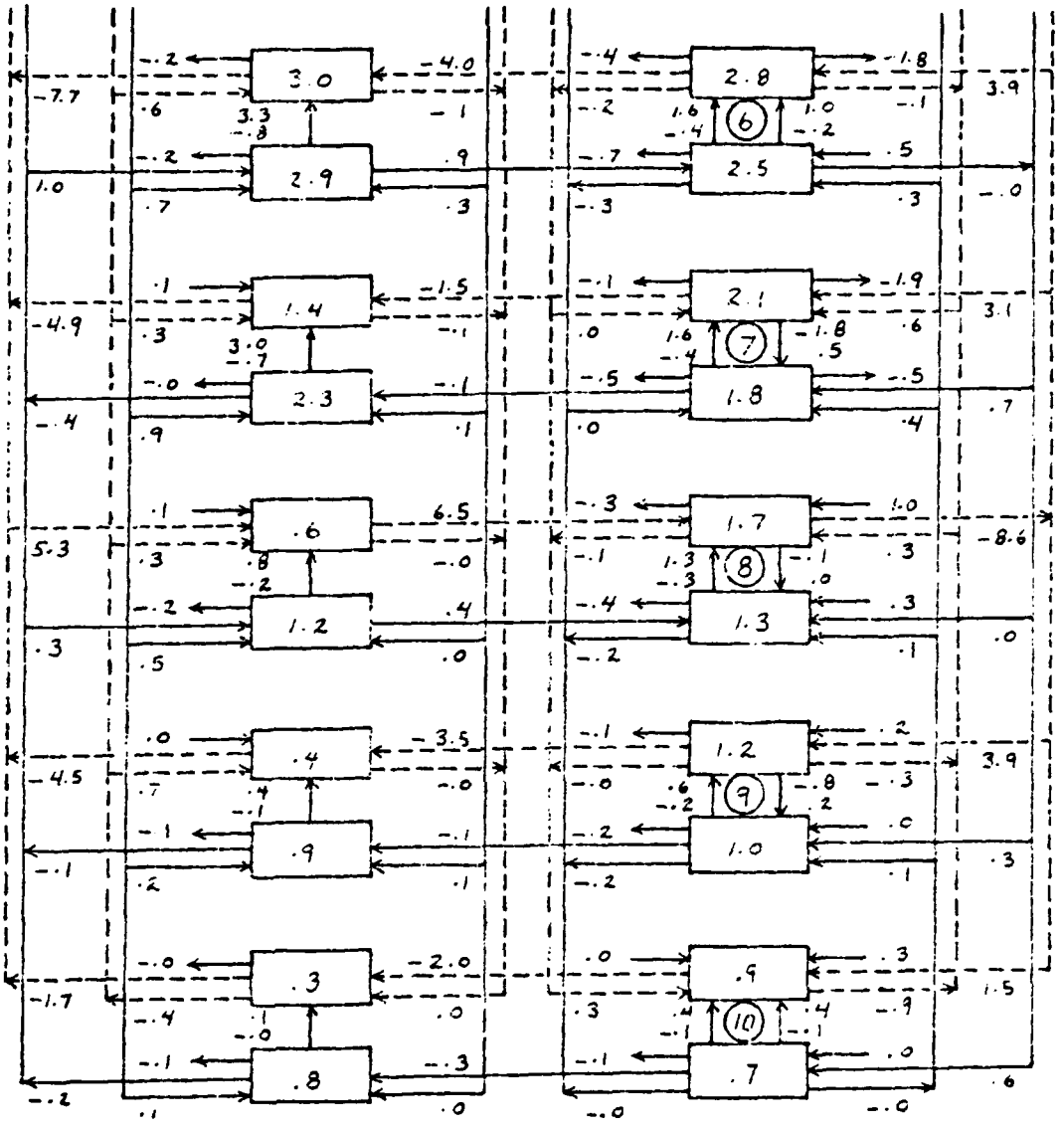


Figure 129. Transfer diagram of atmospheric energy for summer average conditions for wave numbers 6 - 10 over 20°S to 0°. Energy fluxes are in $m^2/sec^2/day$, while EK and EA within the boxes are $m^2/sec^2$.

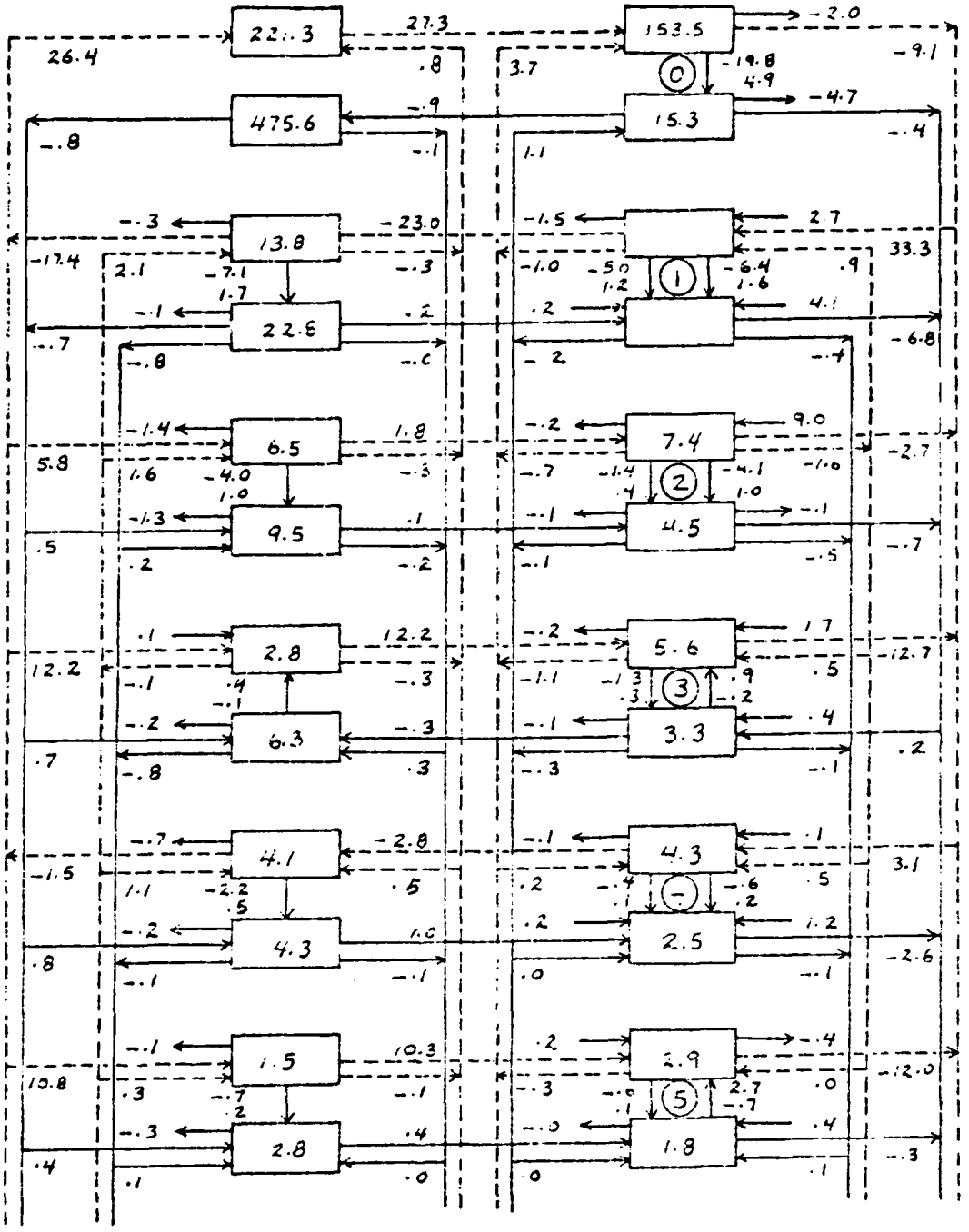


Figure 130. Transfer diagram of atmospheric energy for summer average conditions for wave numbers 0 - 5 over 0° to 30°N. Energy fluxes are in $m^2/sec^2/day$, while EK and EA within the boxes are $m^2/sec^2$.

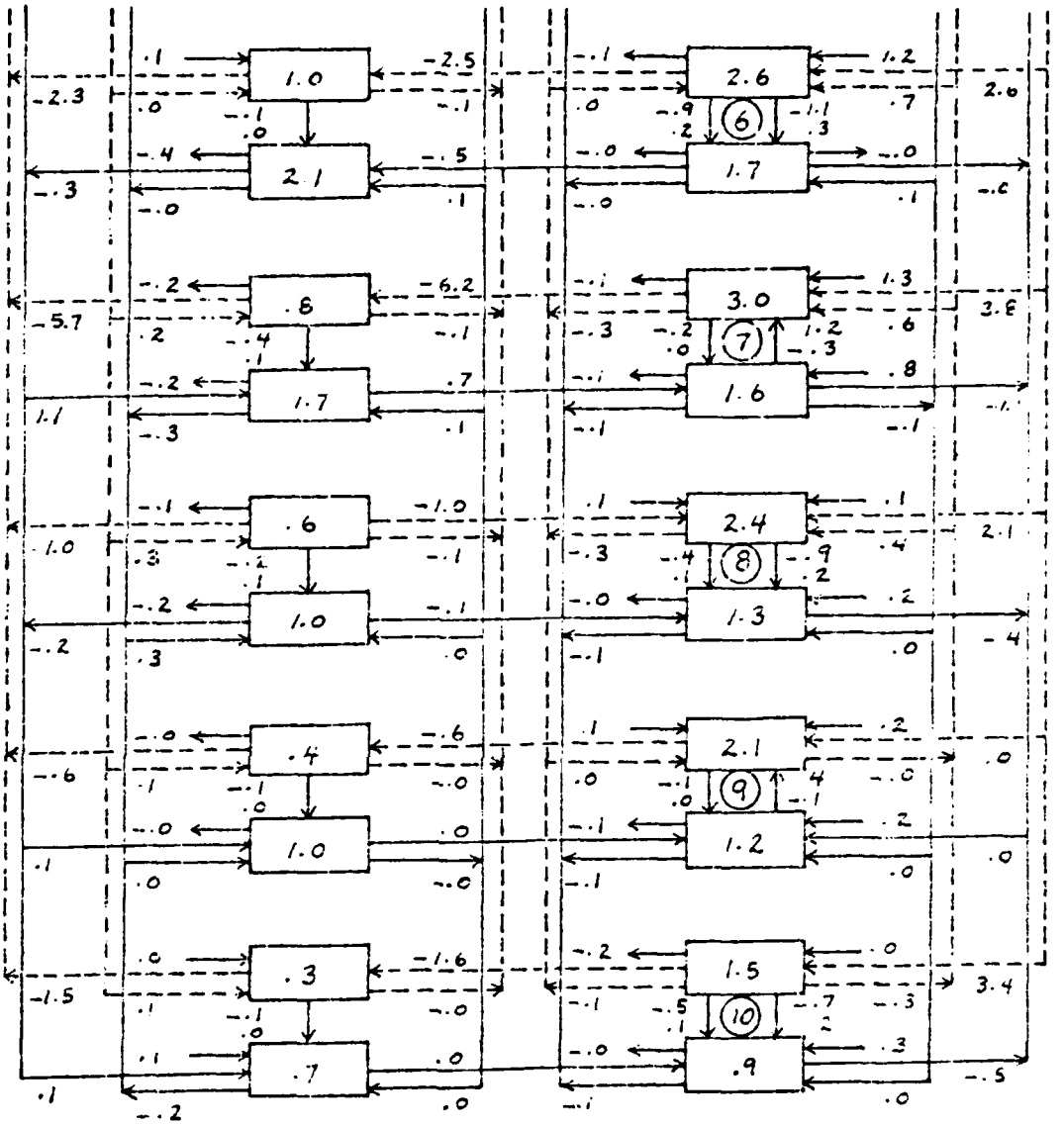


Figure 131. Transfer diagram of atmospheric energy for summer average conditions for wave numbers 6 - 10 over 0° to 30°N. Energy fluxes are in $m^2/sec^2/day$, while EK and EA within the boxes are $m^2/sec^2$.

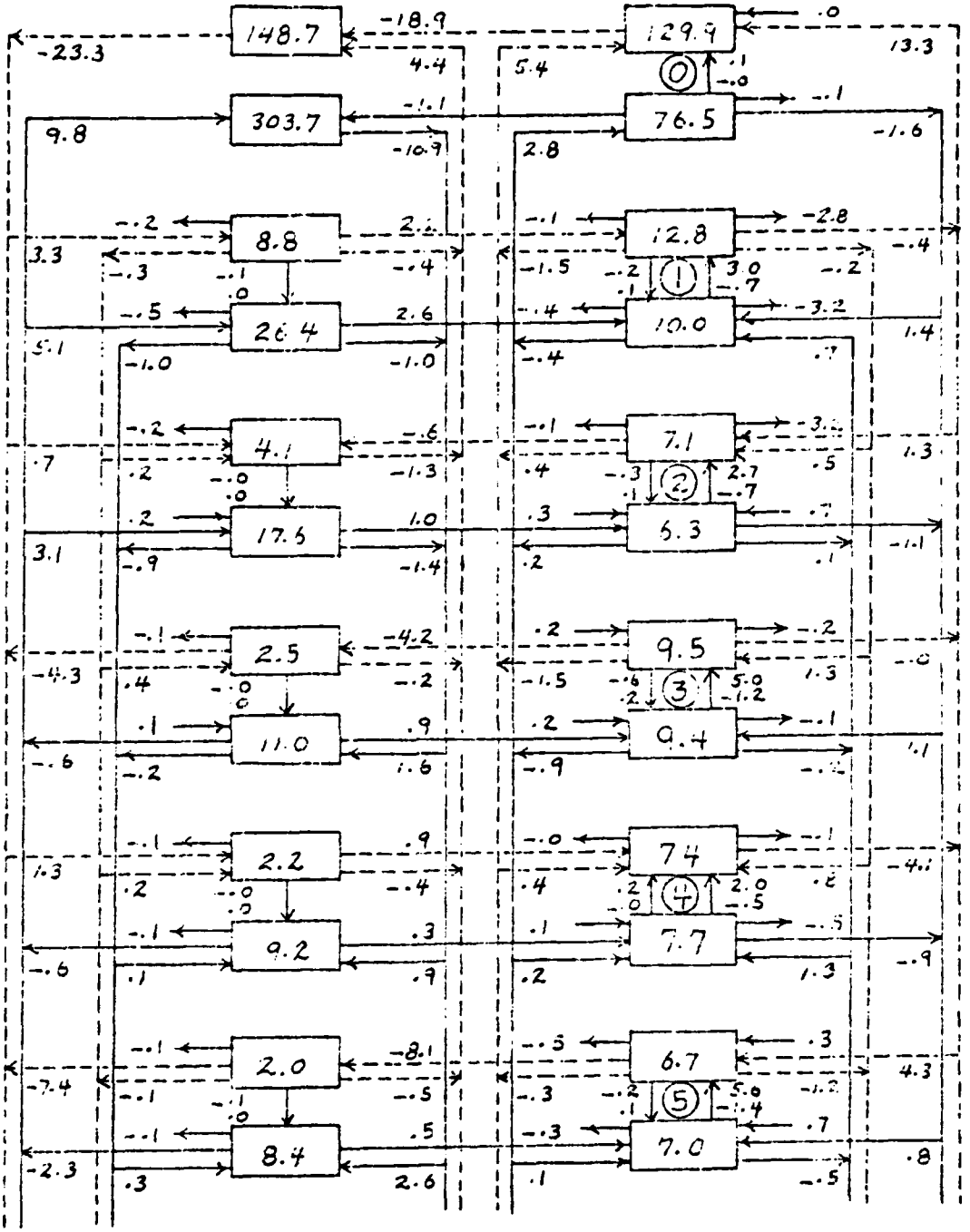


Figure 132. Transfer diagram of atmospheric energy for summer average conditions for wave numbers 0 - 5 over 30°N to 60°N. Energy fluxes are in $m^2/sec^2/day$, while EK and EA within the boxes are $m^2/sec^2$.

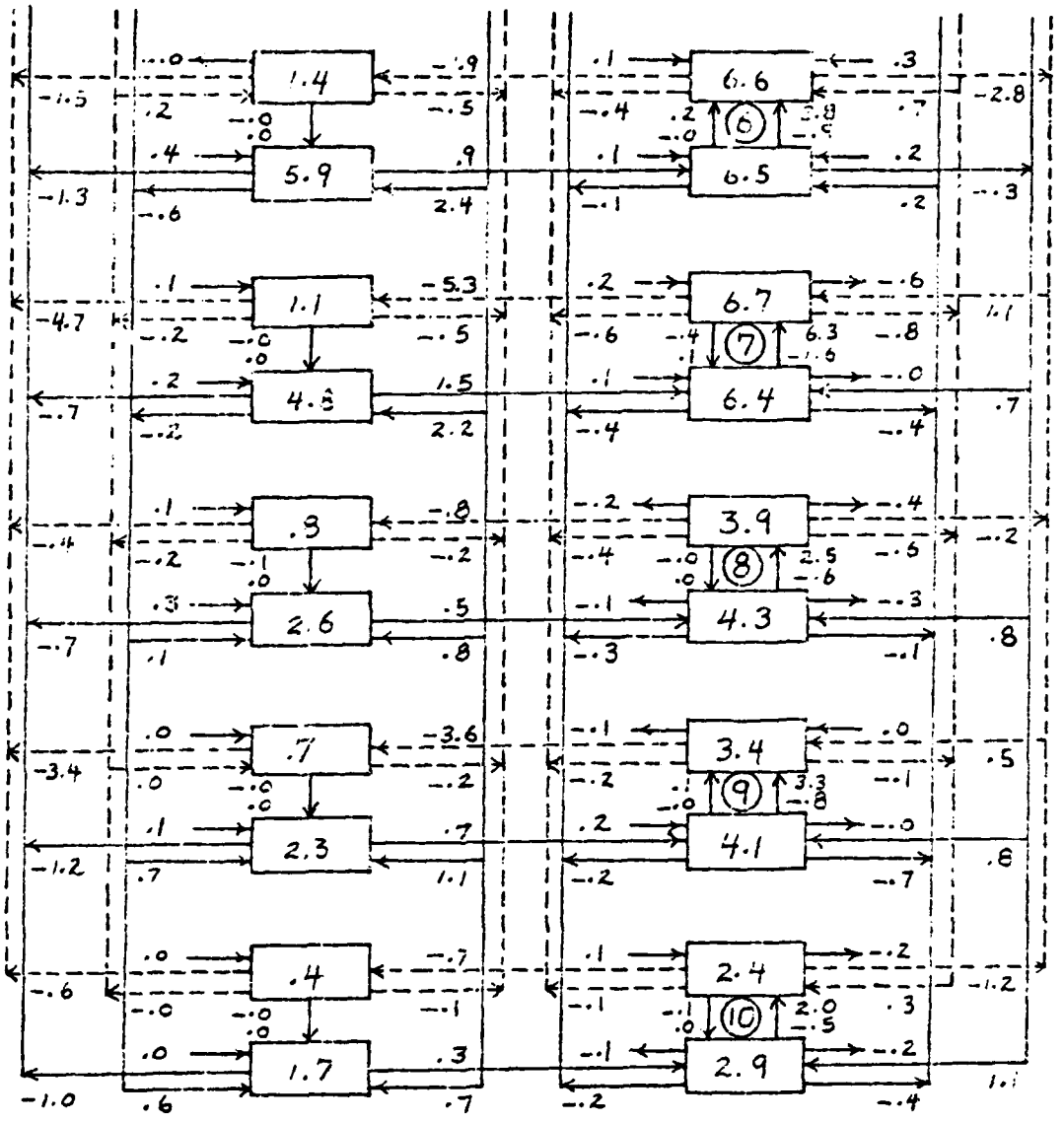


Figure 133. Transfer diagram of atmospheric energy for summer average conditions for wave numbers 6 - 10 over 30°N to 60°N. Energy fluxes are in $m^2/sec^2/day$, while EK and EA within the boxes are $m^2/sec^2$.

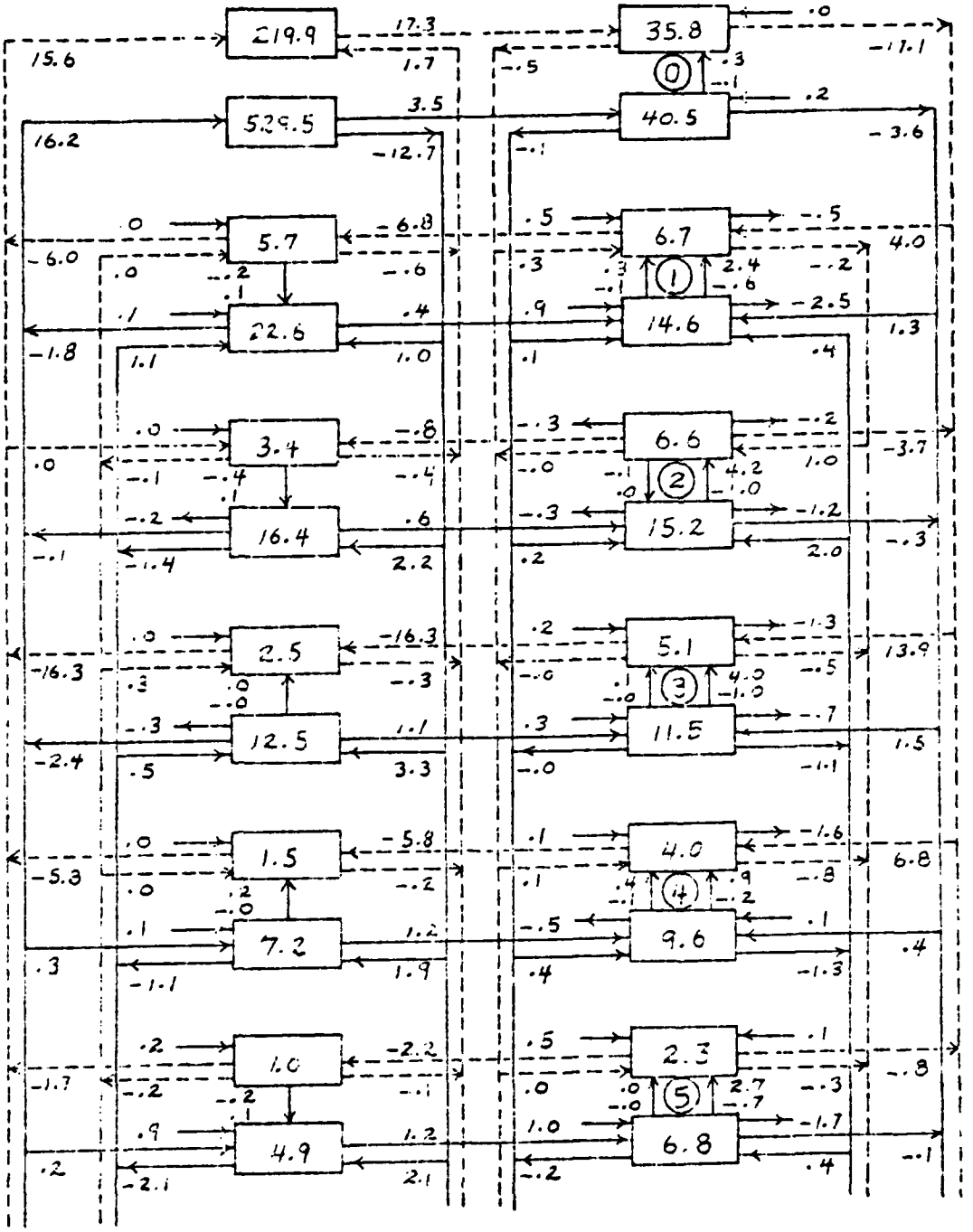


Figure 134. Transfer diagram of atmospheric energy for summer average conditions for wave numbers 0 - 5 over 60°N to 90°N. Energy fluxes are in $m^2/sec^2/day$, while EK to EA within the boxes are $m^2/sec^2$.

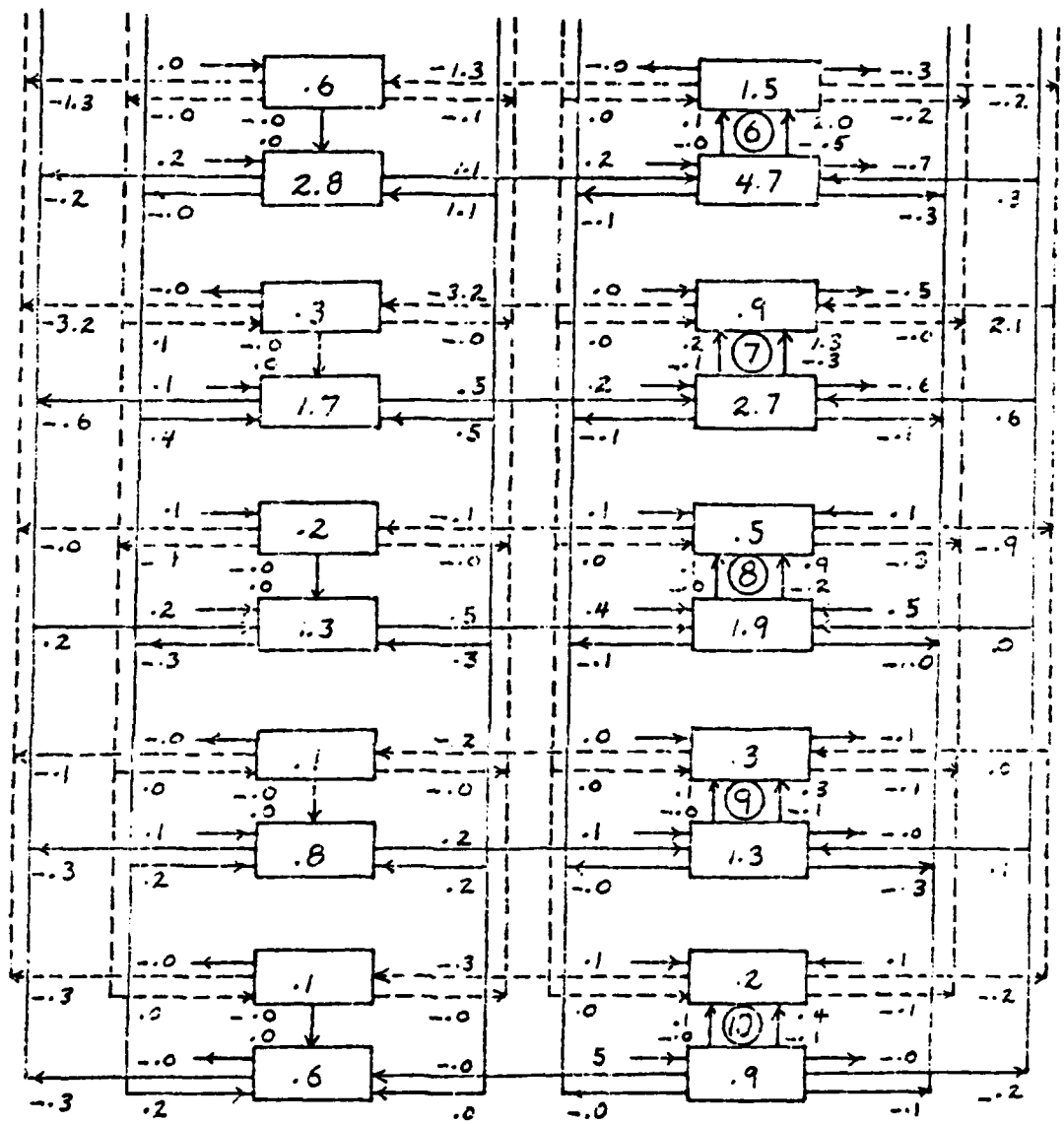


Figure 135. Transfer diagram of atmospheric energy for summer average conditions for wave numbers 6 - 10 over 60°N to 90°N. Energy fluxes are in $m^2/sec^2/day$, while EK to EA within the boxes are $m^2/sec^2$.

## REFERENCES


Bingham, D., M. D. Godfrey, and V. W. Tukey, 1967: Modern techniques of power spectrum estimation. IEEE Trans. Audio Electroacoustics, Au-15, 56-66.

Burrows, W. R., 1976: A diagnostic study of atmospheric spectral kinetic energetics. J. Atmos. Sci., 33, 2308-2321.

Conte, S. D., and C. deBoor, 1972: Elementary Numerical Analysis: An Algorithmic Approach. McGraw-Hill Book Company, 396 pp.

Dutton, J. A., and D. R. Johnson, 1967: The theory of available potential energy and a variational approach to atmospheric energetics. Advan. Geophys., 12, 333-343.

Fjørtoft, R., 1953: On the changes in the spectral distribution of kinetic energy for two-dimensional, non-divergent flow. Tellus, 5, 255-231.

Flattery, T. W., 1967: Hough functions. Tech. Rep. No. 21, Dept. of Geoph. Sci., Univ. of Chicago, 175 pp.

Fröberg, C. -E., 1969: Introduction to Numerical Analysis. Addison-Wesley Publishing Company, Inc., 340 pp.

Gruber, A., 1975: The wave number-frequency spectra of the 200 mb wind field in the tropics. J. Atmos. Sci., 32, 1615-1625.

Kao, S. -K., 1968: Governing equations and spectra for atmospheric motion and transports in frequency wave number space. J. Atmos. Sci., 25, 32-38.

————, 1970: Wave number-frequency spectra of temperature in the free atmosphere. J. Atmos. Sci., 27, 1000-1007.

————, 1977: Equations of the kinetic and available potential energies in the wave number-frequency space. Sci. Rep. NSF Grant ATM-73-00188, Dept. of Meteorology, University of Utah.

————, C. -Y. Tsay, and L. L. Wendell, 1970: The meridional transport of angular momentum in wave number frequency space. J. Atmos. Sci., 27, 614-626.

———— and L. L. Wendell, 1970: The kinetic energy of the large-scale atmospheric motion in wave number frequency space: I. Northern Hemisphere. J. Atmos. Sci., 27, 359-375.

———— and H. -N. Lee, 1977: The nonlinear interactions and maintenance of the large-scale moving waves in the atmosphere. J. Atmos. Sci., 34, 471-485.

———— and C. N. Chi, 1978: Mechanism for the growth and decay of long- and synoptic-scale waves in the mid-troposphere. J. Atmos. Sci., 35, 1375-1387.

King, E. C., 1967: Diurnal and long-term variations of the kinetic energy generation and dissipation for a five-year period. Mon. Wea. Rev., 95, 593-606.

Lorenz, E. N., 1955: Available potential energy and the maintenance of the general circulation. Tellus, 7, 157-167.

————, 1960: Maximum simplification of the dynamic equations. Tellus, 12, 243-254.

————, 1967: The nature and theory of the general circulation of the atmosphere. WMO No. 218, TP. 115, 161 pp.

Miyakoda, 1963: Some characteristic features of winter circulation in the troposphere and lower stratosphere. Tech. Rept. No. 14, Dynamical Prediction Group, Department of the Geophysical Sciences, University of Chicago, 93 pp.

Muench, H. S., 1965: On the dynamics of the wintertime stratospheric circulation. J. Atmos. Sci., 22, 349-360.

O'Brien, J. J., 1970: Alternative solutions to the classical vertical velocity problem. J. Appl. Meteor., 9, 197-203.

Oort, A. H., 1964: On estimates of the atmospheric energy cycle. Mon. Wea. Rev., 92, 483-493.

Perry, J. S., 1967: Long-wave energy processes in the 1963 sudden stratospheric warming. J. Atmos. Sci., 24, 539-550.

Pratt, R. W., 1976: The interpretation of space-time spectral quantities. J. Atmos. Sci., 33, 1060-1066.

Reed, R. J., J. L. Wolfe, and H. Nishimoto, 1963: A spectral analysis of the energetics of the stratospheric sudden warming of early 1957. J. Atmos. Sci., 20, 256-275.

Saltzman, B., 1957: Equations governing the energetics of the large scales of atmospheric turbulence in the domain of wave

number. J. Meteor., 14, 513-523.

————————, 1970: Large-scale atmospheric energetics in the wave number domain. Rev. Geophys. Space Phys., 8, 289-302.

———————— and A. Fleisher, 1960: The exchange of kinetic energy between larger scales of atmospheric motion. Tellus, 12, 374-377.

————————————————, 1961: Further statistics on the modes of release of available potential energy. J. Geophys. Res., 66, 2271-2273.

————————————————, 1962: Spectral statistics of the wind at 500 mb. J. Atmos. Sci., 19, 195-204.

Steinberg, H. L., A. Wiin-Nielsen, and C. -H. Yang, 1971: On nonlinear cascades in large-scale atmospheric flow. J. Geophys. Res., 76, 3629-8640.

Teweles, S., 1963: Spectral aspects of the stratospheric circulation during the IGY. M. I. T. Report No. 8, M. I. T. Cambridge, Mass., 191 pp.

Tenenbaum, J., 1976: Spectral and spatial energetics of the GISS model atmosphere. Mon. Wea. Rev., 104, 15-30.

Tsay, C. -Y., and S. -K. Kao, 1978: Linear and nonlinear contributions to the growth and decay of the large-scale atmospheric waves and jet stream. Tellus, 30, 1-14.

Van Mieghem, J., 1961: Zonal harmonic analysis of the Northern hemisphere geostrophic wind field. UGGI, Monograph 8, 57 pp.

Wendell, L. L., 1969: A study of the large-scale atmospheric turbulent kinetic energy in wave number-frequency space. Tellus, 21, 760-788.

Winn-Nielsen, A., 1959: A study of energy conversion and meridional circulation for the large-scale motion in the atmosphere. Mon. Weather Rev., 87, 319-332.

————————, 1968: On the intensity of the general circulation of the atmosphere, Rev. Geophys., 6, 559-579.

Yang, C. -H., 1967: Nonlinear aspects of the large-scale motion in the atmosphere. Univ. Mich. Tech. Rept., 08759-1-T, 173 pp.

VITA

| | |
|---|---|
| Name | James Larrien Hatch |
| Birthdate | December 15, 1943 |
| Birthplace | Spokane, Washington, |
| High School | Everett High School<br>Everett, Washington |
| College | Everett Junior College<br>Everett, Washington<br>1961 |
| Universities | The University of Washington<br>Seattle, Washington<br>1962-1966 |
| | The University of Texas<br>Austin, Texas<br>1967-1968 |
| | Texas A&M University<br>College Station, Texas<br>1971-1972 |
| Degrees | B. A. 1966<br>The University of Washington<br>Seattle, Washington |
| | M. S. 1972<br>Texas A&M University<br>College Station, Texas |
| Professional Position | Major, United States Air Force |


8
DTIC